CHARACTERISATION OF FLOW, MIXING AND CHANGEOVER IN SMX STATIC MIXERS

BY

OLGA MIHAILOVA

A thesis submitted to
The University of Birmingham
For the degree of
DOCTOR OF ENGINEERING

School of Chemical Engineering
College of Physical and Engineering Sciences
The University of Birmingham

September 2016

UNIVERSITY OF
BIRMINGHAM

University of Birmingham Research Archive

e-theses repository

This unpublished thesis/dissertation is copyright of the author and/or third parties. The intellectual property rights of the author or third parties in respect of this work are as defined by The Copyright Designs and Patents Act 1988 or as modified by any successor legislation.

Any use made of information contained in this thesis/dissertation must be in accordance with that legislation and must be properly acknowledged. Further distribution or reproduction in any format is prohibited without the permission of the copyright holder.

ABSTRACT

This thesis pursues an enhanced understanding of the dynamics of flow and mixing within Sulzer SMX static mixers, a popular in-line mixing solution across many industries. The concept of the thesis was conceived from an industrial need to develop a better understanding of the processing equipment and the unique position of the University of Birmingham, having access to a number of unique and powerful characterisation techniques. This thesis applies these techniques, in particular Positron Emission Particle Tracking (PEPT) and Particle Image Velocimetry (PIV), to study flow and mixing dynamics within SMX mixers.

To carry out this work a proof of concept study was conducted first, where PEPT, the main characterisation technique used in this research, was compared with a well-established Magnetic Resonance Imaging (MRI) technique. This study illustrated that the PEPT tracer location data can be processed in a way which provides results comparable to those obtained using MRI. PEPT, however, offers more flexibility compared to MRI, allowing a wider range of properties, such as occupancies, local velocities and mixing dynamics to be extracted from the experimental data.

MATLAB algorithms were developed to process PEPT location data allowing the derivation of properties such as local velocity fields, mixing efficiencies, occupancies and changeover efficiencies, for a number of model Newtonian and non-Newtonian fluids, under industrially relevant flow conditions. This work demonstrated that the velocity fields within SMX mixers are not adversely affected by the fluids rheological properties and the occupancies for all fluids demonstrate similar trends, with a sharp breakthrough front, reminiscent of plug flow in empty pipes.

The assessment of the mixing patterns provided evidence of the effects of the feed orientation at the mixer entry on the mixing efficiency, with a concentric feed providing the fastest reduction in variance across the mixer cross-section, when compared to side-by-side feed patterns.

PEPT tracer data also provided insight into the fluid changeover within the DN25 SMX mixers, which is important not only for processing, but also for cleaning of industrial systems containing in-line mixers. The assessment of the changeover patterns further emphasised the resemblance to plug flow within the mixer, with dependence on the fluid rheology. A model was developed that allows predicting the time required to achieve a desired level of changeover within a system for a fluid with known rheological properties.

In addition to PEPT, PIV was used for velocity field characterisation, using transparent 3D printed mixer elements to track the tracer particles using an optical approach. The 2D velocity maps obtained using PIV were shown to correlate well with equivalent slices of PEPT data. This allowed to illustrate, for the first time, that 3D printing can be used to manufacture transparent geometries for use in PIV.

The final measure of an in-line mixers performance which was assessed was pressure drop across the mixer assembly, which was studied at the P&G pilot plant facility in Brussels Innovation Centre. The study enabled pressure drop and velocity measurements to be made which were impossible under laboratory conditions. It was demonstrated, that for fluid exhibiting complex rheological phenomena, such as shear banding, the pressure drop can be predicted across multiple mixer geometries of various diameters. This can be achieved by assuming a constant average shear rate across the mixer cross-section and estimating the pressure drop based on the corresponding complex viscosity of the fluid, thus negating the shear banding effects.

ACKNOWLEDGEMENTS

I would like to express my gratitude to my academic supervisors, Prof. Serafim Bakalis and Dr. Andy Ingram, as well as my industrial supervisor, Dr. Denis O'Sullivan, for providing me with this opportunity, helping me make the most of my time on the project and lending their insights into my work. I would also like to thank Dr. Richard Greenwood for his support throughout the project and for his inputs and corrections on this thesis. Furthermore, I am very grateful for all the help I received from Dr. Thomas Leadbeater on PEPT tracer preparations and data acquisition, and to Prof. Kathryn McCarthy and Prof. Michael McCarthy at UC Davis, for providing the opportunity for an interesting collaboration.

I would further like to thank the EPSRC and Procter & Gamble for sponsoring the project and allowing me the freedom to explore the different techniques and methods used in this research and for permitting me to present my work at major conferences.

To my parents, Anna and Sergej, goes out my sincerest thanks for their love and constant encouragement and support, despite the geographical distance. And to my husband, Jon, I want to say thank you for always being there for me, not allowing me to lose sight of what is important and making the EngD even more enjoyable.

And to all the friends that I have made during my EngD, thanks for making it a fun ride!

Я хочу поблагодарить моих родителей, Анну и Сергея, за их любовь и постоянную поддержку и заботу, которые я всегда чувствую, несмотря на расстояние.

TABLE OF CONTENTS

LIST OF FIGURES

LIST OF TABLES

NOMENCLATURE

a	Transmission constant	(-)
A	Area	m^3
a, b, c	Polynomial constants	(-)
$a_1, a_2,$ $b_1, b_2,$ c_1, c_2	Universal changeover constants for changeover time prediction	(-)
C	Concentration	(-)
C_o	Initial concentration	(-)
CV	Coefficient of Variance	(-)
D	Mixer/mixer containing pipe diameter	m
D_1	Larger pipe diameter	m
D_2	Smaller pipe diameter	m
d_p	Pore diamater	m
f	Fraction of events used in triangulation	(-)
F	Total flux across cross-section	$m^{-2}\ s^{-1}$
f_d	Darcy friction coefficient	(-)
f_i	Flux across grid element	$m^{-2}\ s^{-1}$
f_i	Volumetric flux	$m\ s^{-1}$
G^*	Complex modulus	(-)
i	Directional component (x, y or z)	(-)
I	Emerging γ-ray intensity	keV
I_f	Flux weighted intensity of segregation	(-)
i_n	Pixel number	(-)

I_o	Initial γ-ray intensity	keV
k	Coefficient defining the “plunges” of a changeover front	(-)
K_e	Coefficient for fittings with expanding diameter	(-)
K_r	Coefficient for fittings with reducing diameter	(-)
L	Mixer length	m
L_m	Thickness of the medium	cm
m	Power law consistency coefficient	$Pa.s^n$
n	Polynomial exponent	(-)
N	Number of mixer elements	(-)
N_e	Number of grid elements	(-)
N_p	Number of points separated by radius r	(-)
n_p	Power law index	(-)
N_R	Number of locations per slice	(-)
N_{slice}	Number of events used per tracer location	(-)
n_y	Carreau-Yasuda index	(-)
Q	Flowrate	$m^3\ s^{-1}$
r	Radius between position A and B	mm
Re	Reynolds number	(-)
Re_p	Pore Reynolds number	(-)
s	Standard deviation signal intensity	(-)
S_F	Flux weighted variance	(-)
S_L	Length scale	mm
s_o	Standard deviation signal intensity at mixer entry	(-)
t	Time	ms
T	Transmission	(-)

t_{50}	Time taken for half of the original fluid to be displaced at a cross-section	ms
U	Overall fluid velocity from PEPT	m s^{-1}
U_i	Velocity in the direction *i* from PEPT	m s^{-1}
V	Average velocity in the mixer from flowrate	m s^{-1}
V_f	Average velocity in a fitting	m s^{-1}
X_A	Concentration at position A	(-)
X_B	Concentration at position B	(-)
X_i	Concentration in a grid element	(-)
$\bar{X}$	Mean signal intensity	(-)
ΔP	Pressure drop across the SMX mixer	Pa
ΔP_f	Pressure drop in fittings	Pa
$\dot{\gamma}_{SMX}$	Average shear rate in an SMX mixer based on Carreau-Yasuda	s^{-1}
$\dot{\gamma}$	Shear rate	s^{-1}
μ	Viscosity	Pa.s
μ_a	Apparent viscosity from pressure drop	Pa.s
μ_{ac}	Attenuation coefficient	cm^{-1}
μ_c	Complex viscosity	Pa.s
μ_{eff}	Effective viscosity	Pa.s
μ_{inf}	Infinite viscosity	Pa.s
μ_o	Viscosity at zero shear	Pa.s
ε	Porosity	(-)
ρ	Density	kg m^{-3}
τ	Tortuosity	(-)
ω	Angular frequency	Hz

CHAPTER 1. INTRODUCTION

1.1 BACKGROUND

Personal and home care products have seamlessly incorporated into our everyday lives decades, if not centuries, ago. As far back as ancient Egypt humans have learned to combine simple ingredients, such as fats and ash to produce a crude multipurpose cleaning product, which was refined across the ages and a similar process is still used today in the production of soap bars (Spitz, 2016), one variant of which is shown in Figure 1.1.

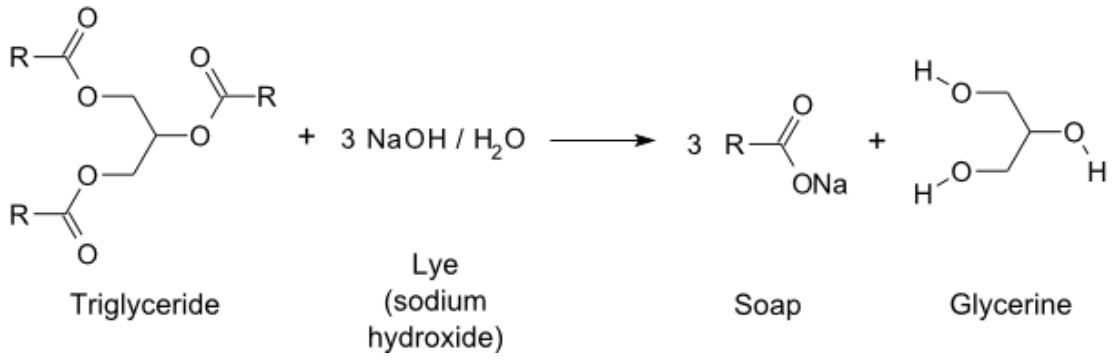

Figure 1.1. Simple saponification process used to this day in soap bar production (Spitz, 2016)

However, with the advancements in the chemical industry a broad range of alternatives to solid soaps have been developed, including products containing liquid surfactants, such as sodium lauryl sulphate (SLS), sodium lauryl ether sulphate (SLES) and Cocamidopropyl betaine (CAPB), to name a few most frequently used (Tai, 2000). In addition to surfactants, which deliver the core cleaning consumer benefit of home and personal care products, such as shampoo, toothpaste, dishwashing liquid and laundry detergent, a whole range of other ingredients is added to such products. These can boost stability, improve texture, smell or appearance of the products and deliver additional functional and consumer benefits, such as softening of hard water, deposition of fragrances and surface modifiers (Yu et al., 2008). Furthermore, the continued innovation and competition in the field is leading to the development of products containing complex

microstructures, such as surfactant micelle networks, emulsions and other colloid systems, which allow delivery of new technologies to the consumers (Lai, 1996).

With the advancements in product formulations, the manufacturing processes have also developed additional complexity, where simple combination of ingredients is insufficient to deliver a product with the desired functionality, physical and sensory properties. Products can be sensitive to the process temperatures, order of ingredient addition, energy dissipation rates and mixing times (Watson and Showell, 2006). For example, products containing emulsions will be processed under strict conditions, ensuring the correct droplet size distribution is achieved. Similar concerns arise when dispersing or dissolving solids and blending liquids, with the aim of achieving a homogenous product (Rhein et al., 2006).

In order to address the complexity of these products, a wide range of manufacturing processes has been developed across the industry, including both commercially available and proprietary process designs. The majority of the products are formulated using either batch or semi-continuous processes, where batch traditionally offers more flexibility in choice of the process conditions, as different process parameters such as shear and temperature can be applied at different stages of the process. However, batch processes lead to long equipment down time for cleaning and changeover and result in significant volumes of waste, when entire failed batches can be discarded. Conversely, continuous processing, such as high pressure homogenisation, as well as application of in-line dynamic and static mixers, allow for closer quality control and real time process adjustments, leading to reduced waste and more consistent product quality (Paul et al., 2004). However, the design of continuous processes can be more challenging than that of batch processes, as all process steps are usually single pass and therefore need to be well understood in order to deliver the necessary degree of mixing, heat transfer and shear.

Therefore, a strong research effort has been devoted to understanding of the dynamics within continuous processing equipment. However, the opaque construction materials, usually stainless steel, and the complex flow dynamics, which rely on either high turbulence (high pressure homogenisers and dynamic mixers) or complex stream recombination (static mixers) make many characterisation methods unsuitable for such systems (Bakalis et al., 2006). As the result, the dynamics within such equipment can be poorly understood, preventing manufacturers of complex personal and home care fluids from developing efficient processes. An understanding of the dynamics of mixing would allow for a step change in process development and enhance the efficiency of the manufacturing process in terms of energy consumption and waste generation.

1.2 OBJECTIVES

Given the process complexity described above, development of reliable characterisation techniques is crucial for the understanding of the dynamics within continuous processing equipment. More specifically the current work focuses on developing an understanding of flow and mixing within Sulzer SMX static mixers, which are widely used in continuous processes across many industries, including personal and home care. The complex geometry of SMX mixers makes it difficult to apply traditional techniques for characterisation of internal fluid dynamics, therefore the majority of current research in the area focuses on reporting results inferred from the mixer outlet stream composition, rather than the internal dynamics, or derived using CFD, which is difficult to validate, due to the abovementioned limitations (Das et al., 2013a; Legrand et al., 2001; Li et al., 1997).

Summarised the objectives of the work presented are as follows

- Develop an understanding of fluid behavior in SMX static mixers

  - Velocity fields
  - Mixing patterns
  - Fluid changeover
- Understand the effect of mixer size on fluid behaviour
- Understand the effect of fluid rheology on velocity fields, mixing and changeover
  - Newtonian fluids
  - Non-Newtonian fluids

Several techniques were applied to assess the fluid dynamics within the mixers, with the main focus around Positron Emission Particle Tracking (PEPT). This technique allows to address a number of system properties through the analysis and agglomeration of individual tracer particle pass data (Rafiee et al., 2011). Properties such as occupancies, local velocities, mixing efficiencies and product changeover times were derived using PEPT tracer data and correlated with a range of system properties, such as flowrate, rheology and mixer geometry. Other characterisation methods used included high speed image capture and Particle Image Velocimetry (PIV), to address the changeover process and local velocity fields. In addition, pressure drop studies at P&G pilot plant facilities were conducted, which allowed the derivation of correlations between pressure drop across a range of mixer element diameters and lengths, and fluid properties.

Furthermore, the wide range of rheological properties displayed by consumer products currently on the market has been addressed by using both model Newtonian and non-Newtonian model fluids in the studies, as well as consumer products provided by P&G.

This work provides the information needed to fill the knowledge gap that exists in the understanding of SMX mixers and paves the way for future studies of similar difficult to characterise systems.

1.3 RELEVANCE TO PROCTER & GAMBLE

Procter & Gamble Co. (P&G) was the industrial sponsor of the research presented in this thesis, with the aims of the project directly targeted at tackling manufacturing challenges faced by the company. P&G is a large multinational player in the fast moving consumer goods (FMCG) industry, mainly focusing on household and personal care products, with the portfolio including such popular brands as Ariel, Pampers, Head & Shoulders, Fairy and Gillette, among others. P&G was founded by William Procter, a candle maker, and James Gamble, a soap maker, in 1837 in Cincinnati, USA, where the corporate headquarters are located to this date. Today P&G is the largest personal care and household consumer goods manufacturer in the world, reporting net earnings at $11.64 billion in 2015. Distributing products in over 180 countries and with on the ground operations in over 70 countries worldwide, P&G employs over 118,000 people globally within four major divisions

1. Baby, feminine and family care
2. Beauty
3. Fabric and home care
4. Health and grooming (P&G, 2015).

Within all major divisions of P&G many products rely on processing of liquids with varying rheological complexity, including blending of fluids using continuous equipment, such as static mixers. The type of static mixer frequently used in P&G liquid processes is the SMX mixer in a range of lengths and diameters. The ability to predict the mixing quality and the required number of mixer elements to achieve the desired degree of mixing is crucial for improving any process that involves static mixers. A better understanding of the energy dissipated within the mixer, i.e. local velocities and velocity gradients is

integral when processing shear sensitive materials, such as structured fluids, where the microstructure of the fluid can be developed by the means of high-shear (Cardiel et al., 2013). Furthermore, an understanding of changeover dynamics allows cutting down cleaning and changeover times, leading to reduced waste and higher process efficiency (A. Yang et al., 2008), providing the necessary tools to support the P&G mission statement:

"We will provide branded products and services of superior quality and value that improve the lives of the world's consumers. As a result, consumers will reward us with leadership sales, profit, and value creation, allowing our people, our shareholders, and the communities in which we live and work to prosper."

1.4 THESIS LAYOUT

This thesis is composed of 7 chapters, an introduction, a literature survey and four results chapters, followed by a conclusions and future work chapter.

- Chapter 1 is the introduction of the current work, including industrial relevance and the rationale behind the work carried out.
- Chapter 2 contains the literature survey describing mixing equipment frequently used in FMCG industries, focusing on SMX mixers. It further provides an account of several non-invasive flow tracking techniques, such as Particle Image Velocimetry (PIV) and Computer Aider Radioactive Particle Tracking (CARPT), with a particular focus on Positron Emission Particle Tracking (PEPT) technique, which is the technique used for the data acquisition and analysis carried out in the current work.
- Chapter 3 is the proof of concept chapter, applying an established technique, MRI, to validate the PEPT results for a Newtonian fluid, and combining the results of the two techniques to assess the mixing efficiency.

- Chapter 4 is the first results chapter, based on the study of velocity distribution within the SMX static mixers using PEPT for Newtonian and non-Newtonian fluids.
- Chapter 5 is the second results chapter, based on the study of mixing dynamics and the changeover patters within the SMX static mixers using PEPT for Newtonian and non-Newtonian fluids.
- Chapter 6 is the third results chapter, based on a case study, carried out at the P&G pilot plant facility in Brussels, focusing on pressure drop prediction for a range of relevant commercial products.
- Chapter 7 is the conclusions chapter summarising the work done and outlining the future work recommendations.
- The Appendix is the summary of the proof of principle work carried out on 3D printed SMX mixers using Particle Image Velocimetry.

1.5 PUBLICATIONS AND CONFERENCES

Results presented in this thesis have been published in the flowing journals and presented at the following conferences

1.5.1 PUBLICATIONS

Mihailova, O., O'Sullivan, D., Ingram, A., Greenwood, R., Bakalis, S. (submitted). Characterisation of changeover in SMX static mixers. *Chemical Engineering Journal.*

Mihailova, O., D., Ingram, A., Greenwood, R., Bakalis, S. (submitted). Evaluation of fluid velocity inside SMX mixers using PIV. *Journal of Visualization.*

Mihailova, O., O'Sullivan, D., Ingram, A., Bakalis, S. (2016). Velocity Field Characterisation of Newtonian and Non-Newtonian Fluids in SMX Mixers Using PEPT. *Chemical Engineering. Research & Design,* **108**, 126–138

Mihailova, O., Lim, V., McCarthy, M.J., McCarthy, K.L., Bakalis, S., (2015). Laminar mixing in a SMX static mixer evaluated by positron emission particle tracking (PEPT) and magnetic resonance imaging (MRI). *Chemical Engineering Science*. **137**, 1014–1023.

Mihailova O., O'Sullivan, D., Bakalis, S. (2015). Characterisation of velocity fields in SMX static mixers using PEPT. *15th European Conference on Mixing proceedings*.

1.5.2 ORAL PRESENTATIONS (SPEAKER UNDERLINED)

Mihailova O., O'Sullivan, D., Bakalis, S. Application of PEPT in SMX static mixer characterisation. 15th European Conference on Mixing, St. Petersburg, Russia. 2015

Mihailova O., Bakalis, S. Characterisation of velocity in continuous processing equipment using PEPT. Mixing in Health and Personal Care Industries, UCL, London, UK. 2014

Mihailova O., O'Sullivan, D., Bakalis, S. Characterisation of flow and mixing in continuous processing equipment using PEPT. Mixing XXIV, North American Mixing Forum, Lake George, USA. 2014

1.5.3 POSTER PRESENTATIONS AT CONFERENCES (SPEAKER UNDERLINED)

Mihailova O., Lim, V., McCarthy, M.J., McCarthy, K.L., Bakalis, S. Application of PEPT and MRI techniques to characterise flow and mixing in SMX static mixers. IFT 2014 Annual Meeting, 2014

Mihailova O, O'Sullivan D., Ingram, A., Bakalis, S. Characterisation of velocity fields and mixing of complex fluids in SMX static mixers using PEPT. ECCE10, 2015

1.6 REFERENCES

Bakalis, S., Cox, P.W., Russell, A.B., Parker, D.J., Fryer, P.J. (2006) 'Development and use of positron emitting particle tracking (PEPT) for velocity measurements in viscous fluids in pilot scale equipment', *Chemical Engineering Science*, 61(6), 1864–1877.

Cardiel, J.J., Dohnalkova, A.C., Dubash, N., Zhao, Y., Cheung, P., Shen, A.Q. (2013) 'Microstructure and rheology of a flow-induced structured phase in wormlike micellar solutions.', *Proceedings of the National Academy of Sciences of the United States of America*, 110(18), 1653–1660.

Das, M.D., Hrymak, A.N., Baird, M.H.I. (2013) 'Laminar liquid–liquid dispersion in the SMX static mixer', *Chemical Engineering Science*, 101, 329–344.

Lai, K.-Y. (1996) *Liquid Detergents*, 2nd ed, CRC Press.

Legrand, J., Morançais, P., Carnelle, G. (2001) 'Liquid-Liquid Dispersion in an SMX-Sulzer Static Mixer', *Chemical Engineering Research and Design*, 79(8), 949–956.

Li, H.Z.Z., Fasol, C., Choplin, L. (1997) 'Pressure Drop of Newtonian and Non-Newtonian Fluids Across a Sulzer SMX Static Mixer', *Chemical Engineering Research and Design*, 75(8), 792–796.

P&G (2015) 'P&G Annual Report 2015', http://www.pginvestor.com/Cache/1001201800.PDF?O=P.

Paul, E.L., Atieno-Obeng, V.A., Kresta, S.M. (2004) *Handbook of Industrial Mixing*, John Wiley & Sons.

Rafiee, M., Bakalisa, S., Fryer, P.J., Ingram, A. (2011) 'Study of laminar mixing in kenics static mixer by using Positron Emission Particle Tracking (PEPT)', *Procedia Food Science*, 1, 678–684.

Rhein, L.D., Schlossman, M., O'Lenick, A., Somasundaran, P. (2006) *Surfactants in Personal Care Products and Decorative Cosmetics, Third Edition*, Surfactant Science, CRC Press.

Spitz, L. (2016) *Soap Manufacturing Technology*, Elsevier Science.

Tai, H.T. (2000) 'Formulating detergents and Personal Care Products', in *A Guide to Product Development*, AOCS Press, 16.

Watson, R., Showell, M. (2006) *Handbook of Detergents, Part D: Formulation*, CRC Press.

Yang, A., Martin, E.B., Montague, G.A., Fryer, P.J. (2008) 'Towards improved cleaning of FMCG plants: a model-based approach', in *18th European Symposium on Computer Aided Process Engineering*, Computer Aided Chemical Engineering, Elsevier, 1161–1166.

Yu, Y., Zhao, J., Bayly, A.E. (2008) 'Development of Surfactants and Builders in Detergent Formulations', *Chinese Journal of Chemical Engineering*, 16(4), 517–527.

CHAPTER 2. LITERATURE REVIEW

2.1 MIXING

A wide range of mixing solutions is available in industry, designed to achieve different mixing tasks, governed by the nature of the system being blended, e.g. liquid-liquid mixing, gas-liquid mixing, emulsification of immiscible liquids, solid dissolution or suspension, etc. The mixing process is further defined by the properties of the species, such as relative density, viscosity and other fluid properties, such as yield stress and shear thinning behaviour. Finally, the decision on the best mixer geometry is governed by the industrial process, where different approaches will be used for batch and continuous manufacturing (Paul et al., 2004). Furthermore, some products demand carefully selected energy dissipation rates to form the desired microstructure. The following sections will summarise some of the more popular mixer assemblies used in industry.

2.1.1 AGITATORS FOR BATCH MIXERS

Dip in agitators are some of the most frequently used solutions for bulk mixing. Such geometries are easy to manufacture, install and operate. Nevertheless, a wide range of agitator variants exist, including pitched and flat blade turbines, dispersion discs, hydrofoils, helical ribbons and Auger screws, illustrated in Figure 2.1. The type of agitator affects the flow patterns within the vessel, with some designs promoting axial mixing, while others favour radial mixing or induce local high shear rates (Torré et al., 2007).

In order to ensure high mixing efficiencies, it is often advised to use agitators with a high agitator diameter to vessel diameter ratio, with some geometries with the ratio of up to 0.95. This reduces stagnation near the vessel walls and ensures fluid motion even in complex fluids, such as those exhibiting shear thinning behaviour (Bao et al., 2015).

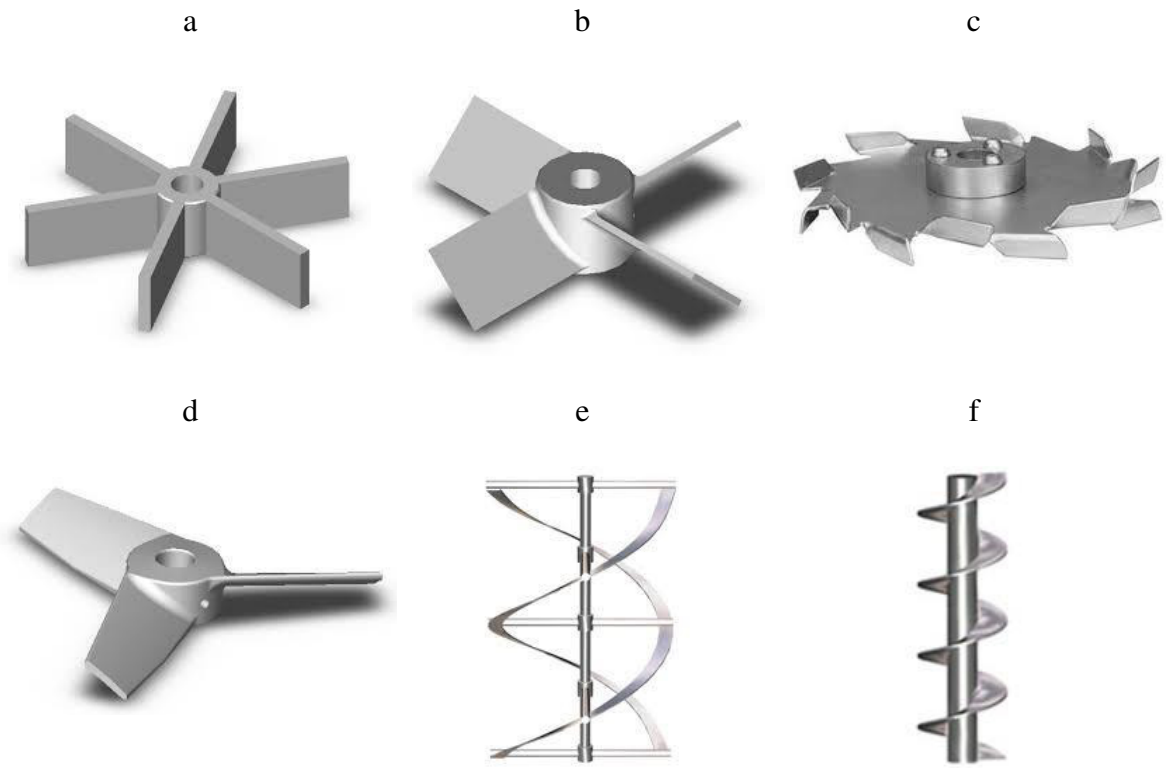

Figure 2.1. Different batch mixer designs. a. flat blade turbine. b. pitched blade turbine. c. dispersion disk. d. hydrofoil. e. helical anchor. f. Auger screw *(Post Mixing, 2015)*

2.1.2 IN-LINE DYNAMIC MIXERS

For continuous processes and batch processes containing a recirculation loop in-line mixers are often used. Dynamic in-line mixers deliver the energy necessary for the mixing process to take place by the use of moving parts, such as rotor-stator high shear mixers. In such mixers the rotor stator assembly is enclosed with the feed being injected into the centre of the assembly and then forced out towards the periphery of the device by centripetal forces induced by the rotor. As the fluid moves outwards it is forced through the perforations in the stator, applying a uniform and controlled amount of shear to the fluid, allowing control of parameters such as droplet size and rates of dissolution, when working with immiscible fluids or dissolving powders (Paul et al., 2004). Due to the enclosed nature of in-line mixers aeration of the product can be reduced and for the case of

recirculating batch processes the product can be passed through the device multiple times to achieve even better mixing and dissolution, or reach a narrower droplet size distribution (Kowalski et al., 2011). A typical in-line rotor-stator device is shown in Figure 2.2.

a b

Figure 2.2. a. Rotor of a typical 150/250 inline Silverson high shear mixer. b. Double emulsion stator screen of a typical inline Silverson high shear mixer (Kowalski et al., 2011).

2.1.3 IN-LINE STATIC MIXERS

In-line static mixers, unlike dynamic mixers, do not have any moving parts and the mixing process is induced by the mixer structure, which often is used to split and recombine the different feed streams. Static mixers are often used not only for blending, but also for heat transfer and continuous chemical reactions and can be found in both recirculating batch and continuous processes, with numerous designs available from a range of manufacturers, tailored to specific processing needs (Ghanem et al., 2014). Some of the more notable designs are shown in Figure 2.3 and include helices, e.g. Kenics (Chemineer, Inc.), corrugated plates, e.g. SMV (Sulzer, Inc.) and multilayer, e.g. SMX (Sulzer, Inc.).

Static mixers are usually designed to operate in a specific flow regime, with split and recombine (SAR) mixers, such as SMX, used for mixing of viscous fluids under laminar flow conditions, without back mixing. This type of mixer acts to divide and rotate the

streams of different fluids and then to fold them back onto themselves, in a fashion similar to kneading dough (Rauline and Blévec, 2000).

Static mixers have several key features which set them aside from the conventional stirred tank mixing used in the majority of batch processes. For example, in FMCG industries stirred tanks traditionally have substantial space requirements, to accommodate batches of up to 50 To, while a continuous process running through static mixers would require a significantly smaller footprint, of up to 20 mixer diameters in length, depending on the system (Singh et al., 2009). Furthermore, as no back mixing occurs in static mixers the product quality control can be brought down to a carful feed stream flowrate ratio control, ensuring consistent concentrations of each component available for axial mixing in the static mixer. Additionally, the lack of back mixing ensures that static mixers are significantly easier to clean than stirred tank mixers and also allows to easily change between product variants, e.g. dye, perfume or flavour, as the plug like flow through the mixer ensures that only a small amount of the product needs to be discarded during changeover (Han E H Meijer et al., 2012).

Systems with lower viscosity fluids, however, such as gas blending for water treatment, often require the blend to achieve turbulence for more efficient mass and heat transfer. In such cases static mixers, such as High-Efficiency Vortex (HEV) (Chemineer, Inc.) (Figure 2.3 (d)) can be inserted into an existing production line to achieve process intensification without the need for major modifications or capital expense (Ghanem et al., 2013).

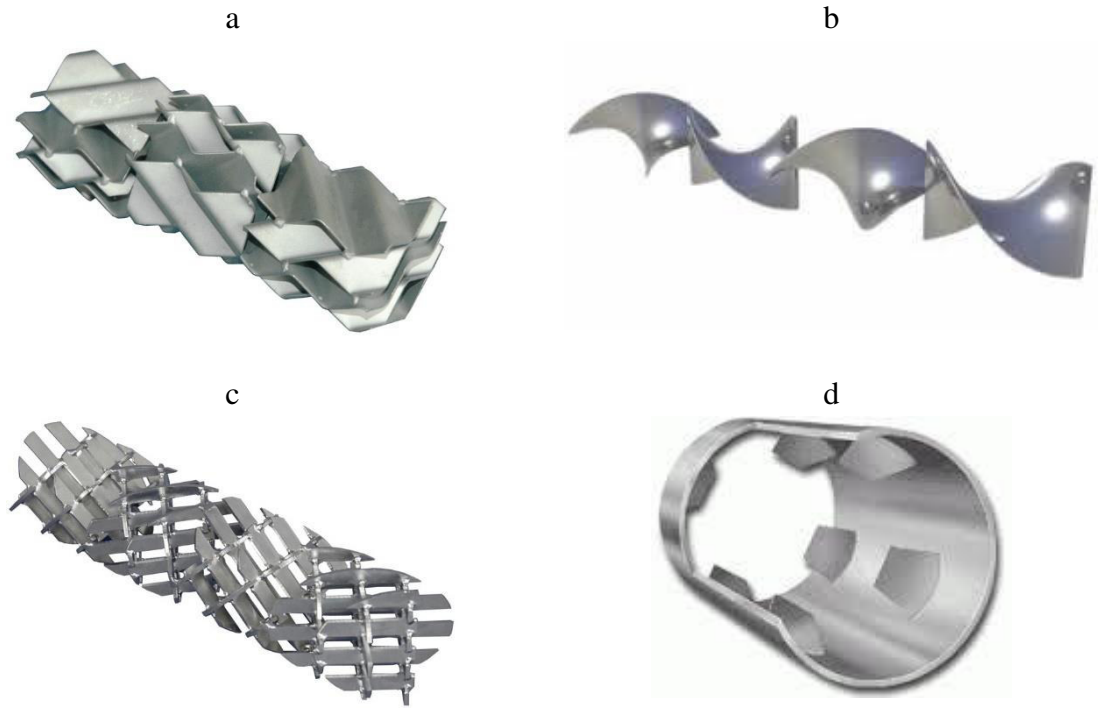

Figure 2.3. a. SMV corrugated plate static mixer. .b. Kenics helical static mixer. c. SMX multilayer static mixer. d. HEV high efficiency vortex static mixer (Post Mixing, 2015)

2.1.3.1 SMX STATIC MIXERS

SMX mixers are a type of split and recombine static mixer design developed by Sulzer. Since its introduction in the 1980s the SMX mixer has become an integral part of many continuous and batch processes across numerous industries. Small diameter mixers are used in specialist chemical industries and in the fast moving consumer goods sector, while larger mixers, often build adapted for the customer and reaching several metres in diameter, are used for gas scrubbing and heat exchange in oil and gas and polymer industries (Hirschberg et al., 2009).

The mixing dynamics within SMX mixers have been characterised using laminar and turbulent blending parameters, K_iL and K_iT, which are derived experimentally (Paul et al., 2004). Table 2.1 illustrates the blending parameters for some of the most widely used static mixer designs, with some designs only having either a K_iL or K_iT value, depending

on the flow regime for which the mixer was designed. These parameters are dependent on the mixer geometry and allow to determine the coefficient of variance, *CoV*, at the outlet of a set of mixer elements. The number of elements is described by the mixer length, *L*, divided by mixer diameter, *D*, as for a single element *L=D* typically. The expression describing the coefficient of variance is shown in Equation 2.1 (Morancais et al., 1999).

Table 2.1. Laminar and turbulent blending parameters for SMX, Kenics and SMV static mixers.

Mixer type	K_iL	K_iT
SMX	0.63	--
Kenics	0.87	0.5
SMV	--	0.21-0.46

$$CoV = K_i^{L/D} \qquad 2.1$$

$$CoV = \frac{\sigma}{\bar{X}} \qquad 2.2$$

$$CoV_0 = \left(\frac{1-f}{f}\right)^{0.5} \qquad 2.3$$

Coefficient of variance is a popular approach at describing the degree of segregation between the species which are being blended in a system. An alternative expression for *CoV* is the ratio between the standard deviation (σ) in the concentration and the average concentration of the species ($\bar{X}$), as shown in Equation 2.2. It is commonly accepted that when the coefficient of variance is reduced below 0.05 sufficient mixing has been achieved, however, further mixing could be required for some sensitive mixtures or reactions (Paul et al., 2004). The number of mixer elements required to achieve the desired mixing does not only depend on the mixer design, but also on the initial ratio of the two

species which are being blended. The initial coefficient of variance of the system at the beginning of the mixing process (CoV_0) can be calculated based on this ratio, as shown in Equation 2.3, where f is the fraction of the minor ingredient in the blend. Figure 2.4 shows the pattern of reduction CoV for a 50/50 mixture and a mixture with 10% minor, it can be seen that the system with a lower fraction of the minor ingredient has a higher CoV_0, and as the result requires more SMX mixer elements to achieve the desired level of homogeneity. For contrast the 50/50 mixture scenario in a Kenics mixer is also presented, where the 14 elements illustrated are not sufficient to achieve satisfactory homogeneity, in fact a length equivalent to 22 L/D is required for the CoV to fall below 0.05, over 3.7 times the length required to achieve this level of mixing with an SMX mixer (Godfrey, 2001).

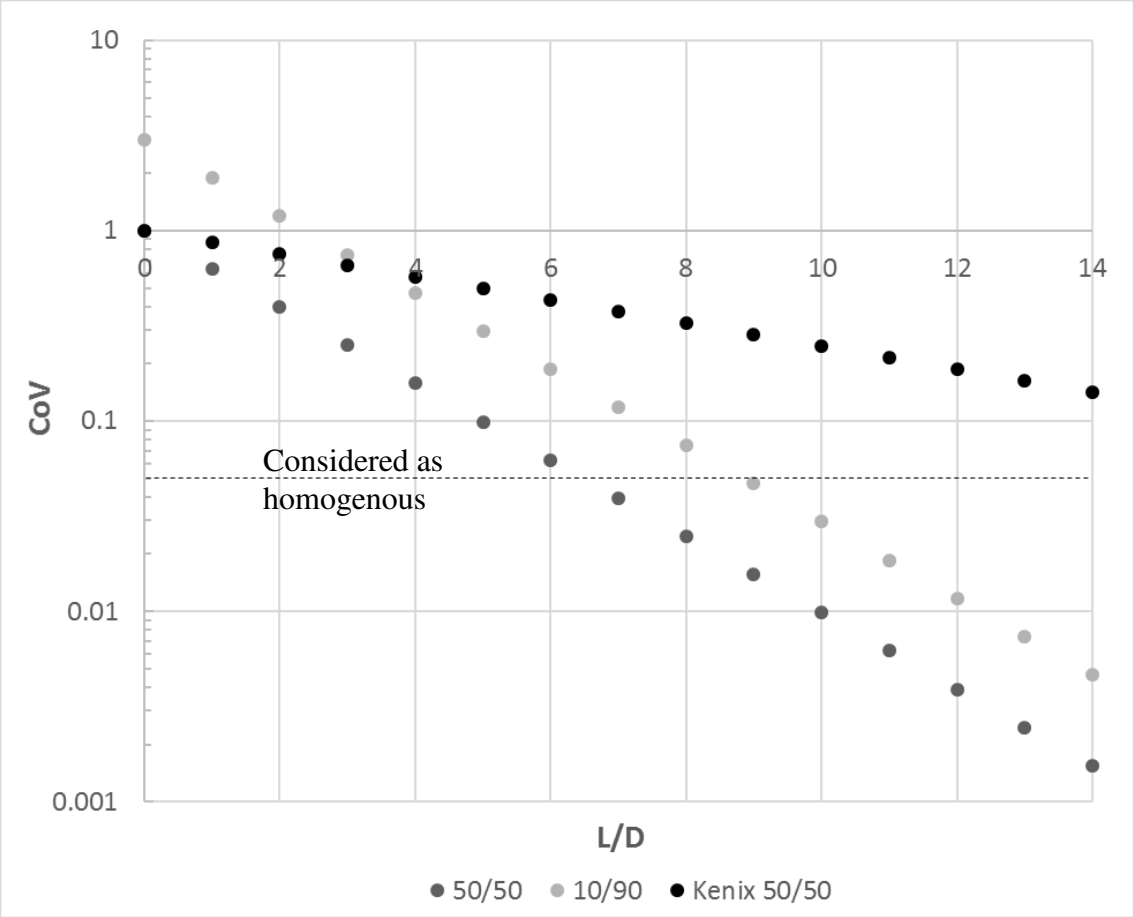

Figure 2.4. The change in the coefficient of variance across 14 SMX element for the 50/50 and 10/90 feed ratios.

This can also be seen from the values of K_{iL}, as the value of CoV is directly proportional to the value of K_{iL}, thus SMX mixers are more efficient at reducing the coefficient of variance than the Kenics mixers. In fact, SMX has the lowest K_{iL} of all the static mixers designed for laminar flow, however, this efficiency comes at an energy trade-off. To achieve mixing the consistency of the individual feeds into the mixer must be disrupted, which is an energy demanding process, and the efficiency of mixing is linked to the energy dissipation rate across the mixer. The energy used for mixing is static mixers comes from the pressure drop across the length of the mixer, which can be linked to the pressure drop in an empty pipe of equivalent length (ΔP_{pipe}) using a pressure drop parameter (K_L), as shown in Equation 2.4 (Shah and Kale, 1991). A similar expression can be applied for turbulent flows, where a constant K_T is used instead.

As can be seen from Table 2.2 for laminar flow SMX mixers have a significantly higher K_L than Kenics mixers, suggesting that for the same length of mixer SMX will result in 5.5 times the pressure drop. However, as was shown above, a significantly longer Kenix mixer is required to achieve the same degree of mixing. Therefore, based on theoretical blending efficiencies and pressure drops, the choice between the two mixer designs heavily relies on the balance between the pipe length available and the pressure drop which is acceptable in the system (Ghanem et al., 2014).

$$\Delta P_{smx} = K_L \Delta P_{pipe} \qquad 2.4$$

Table 2.2. Pressure drop parameters for SMX, Kenics and SMV static mixers in laminar and turbulent regimes.

Mixer type	K_L	K_T
SMX	37.5	500
Kenix	6.9	150
SMV	--	100-200

An alternative measure for the efficiency of mixing delivered by a static mixer is the intensity of segregation, which is similar to *CoV,* however, instead of comparing the standard deviation and the mean concentration, intensity of segregation focuses on the standard deviation evolution across the mixer, by comparing the standard deviations at different cross-sections (σ) to that at the mixer entrance (σ_o), as shown in Equation 2.5 (Kukukova et al. 2009).

$$I = \frac{\sigma^2}{{\sigma_o}^2} \qquad 2.5.$$

Shear rate is another factor of interest in static mixers, where it can be expected that due to the added obstruction to the flow and the added pressure drop the shear rates would increase when compared to those experienced by the fluid under similar conditions in an empty pipe. It becomes increasingly important when processing shear sensitive fluids or fluids exhibiting non-Newtonian behaviour. The expression for the estimation of the wall shear rate in static mixers is similar to that for empty pipes (Equation 2.6), however, due to the abovementioned complexity of the flow within the mixer effective shear rate can be estimated based on the fluid velocity, V (m/s) and pipe diameter, D (m) as shown in Equation 2.7. (Streiff et al., 1999).

$$\dot{\gamma} = 8\frac{V}{D} \qquad 2.6$$

$$\dot{\gamma} = 64\frac{V}{D} \qquad 2.7$$

Due to their efficiency and versatility SMX mixers are applied across processes in many industries, including oil and gas, water treatment and fast moving consumer goods. As the result the details of the dynamics of fluids and systems which are more complex than simple Newtonian flows are in demand. However, SMX mixers, as most static mixers, are traditionally constructed from stainless steel, and enclosed in stainless steel pipes, making it difficult to assess and characterise the mixing process as it happens. A number of techniques have been applied to address the mixing dynamics within static mixers, however, the mixer elements themselves are often treated as a black box, with the properties of the inlet and the outlet streams analysed to deliver an understanding of the mixing process.

One of the best known visualisation experiments which provided an insight into the SMX mixer was carried out by Promix Solutions, where two coloured resins were fed into the mixer side by side and allowed to set (Promix Solutions, 2016). The mixer was then cut up, perpendicular to the direction of the flow, exposing the local concentrations of the two resins and illustrating the mixing pattern, as shown in Figure 2.5. However, this approach does not provide any information on the system dynamics, such as local velocities, shear rates and residence times, for example.

a b c

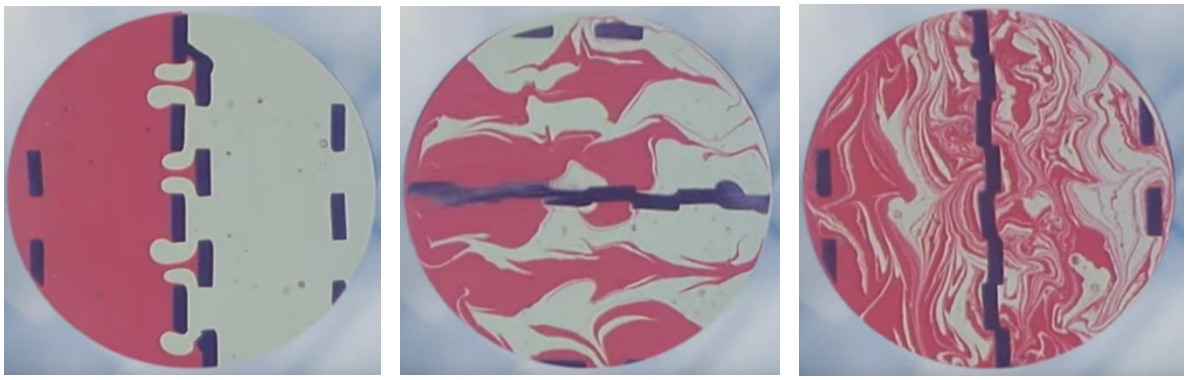

Figure 2.5. Two resin SMX mixing pattern experiment, where a. 1st element entrance, b. 2nd element entrance, c. 3rd element entrance (Promix Solutions, 2016).

To further the understanding of the dynamics within SMX mixers a wide range of techniques has been implemented. For example, Fradette and co-workers have worked on a number of systems, including liquid-liquid and gas-liquid blending in SMX mixers, with both Newtonian and non-Newtonian cross model fluids (Fradette et al., 2007, 2006). To assess the mixer performance these studies used image capture on the fluids exiting the mixer, which in conjunction with local pressure and temperature measurements before and after the mixer elements. This allowed to observe the effect of the number of mixer elements on the size of gas bubbles or oil droplets (depending on the experiment) within the continuous phase. By further comparing the performance of the SMX mixer to the Kenics mixer under the same flow conditions the team was able to determine the elongation is the dominant droplet breakup mechanism in SMX mixers, with the size reduction achieved in only a third of the length required when using Kenics.

An approach alternative to direct imaging of the emulsion droplets was applied to study the mixing dynamics in SMX mixers by Legrand and colleagues (Hammoudi et al., 2008; Hirech et al., 2003; Legrand et al., 2001). Here the outlet stream of the SMX mixer was fed to a tank where a polymerisation encapsulation process took place. This allows to

preserve the emulsion in a state similar to that at the mixer outlet for further analysis, where properties such as particle size distribution can be assessed offline. The approached allowed the authors to develop a model predicting the mean droplet size in water/oil and oil/water emulsions, based on the properties of the system, such as viscosities of both phases, size of the static mixer, dispersed phase fraction and interfacial tension between phases.

Liu and co-workers has attempted to take the insight into the droplet breakup dynamics a step further, as the mixer geometry allows to partially track the dynamics of a droplet in a single mixer element, if it is oriented with the large open spaces facing the camera (Liu et al., 2005). The observations on single droplet dynamics within the first element at various flowrates have provided sufficient information to develop a computation fluid dynamics (CFD) model of the breakup, where a range of forces acting on the droplet is considered, such as strain rate distribution in the mixer, break up mechanisms in different parts of the mixer and the effects of daughter droplet collisions. However, the model is limited by the 2D nature of the data acquired in the initial imaging process. The same research group also applied CFD to assess mixing of non-Newtonian fluids within SMX mixers across 4 elements, where they have found that shear thinning behaviour favours mixing, with the *CoV* reducing more rapidly for fluids with a lower Power law index.

Alongside the mixing and droplet breakup dynamics, the velocity field within SMX has been of continuous interest, as the velocity field ultimately dictates many properties of the mixer. However, traditional velocimetry techniques are difficult to apply to the case of static mixers for the same reason optical mixing assessment is challenging, as techniques like PIV and PTV require the system to be transparent. Nevertheless, some research has been carried out on SMX mixer velocity fields through the application of alternative

velocimetry techniques, such as pulsed ultrasonic velocimetry (Hammoudi et al., 2008). This technique relies on using the dispersed phase, in this case oil, as the tracer, where the continuous and the dispersed phase reflect the ultrasonic pulse differently, allowing to track the path of the dispersed phase. The work conducted using this technique focused on turbulent flow regimes, however the authors were able to illustrate the differences in the flow profiles between the empty pipe sections and the SMX mixer containing sections of the experimental set up, with velocity profiles reflecting the changes in the fluid direction enforced by the mixer structure.

Unfortunately, no existing experimental work focusing on laminar flow within the mixer exists to date. However, notable CFD investigations into the flow in SMX mixers have been attempted, with one study conducted by Zalc and co-workers, where local pressures at different mixer cross-sections, as well as normalised axial and radial velocities at a range of flow rates at the cross-section with the most variance are presented (Zalc et al., 2002). Here a clear difference between a sharp drop in axial velocity probability function at the maximum for low $Re \leq 10$ and a gradual drop for $Re = 100$ is shown, suggesting onset of the transitional regime and therefore deviation from laminar flow (Figure 2.6 (a)). This work also shows that the increase in *Re* has little to no effect of the axial velocity component, even when moving into transitional flow regimes (Figure 2.6 (b)). In addition, this work addresses the effect of *Re* on the mixing performance of the SMX mixer, and finds that in the range of flowrates considered, mixing is not dependant on the flow rate. While providing valuable insights into the flow and mixing dynamics in the mixer, this CFD work only focuses on Newtonian fluids, and along with other similar examples has not been experimentally validated.

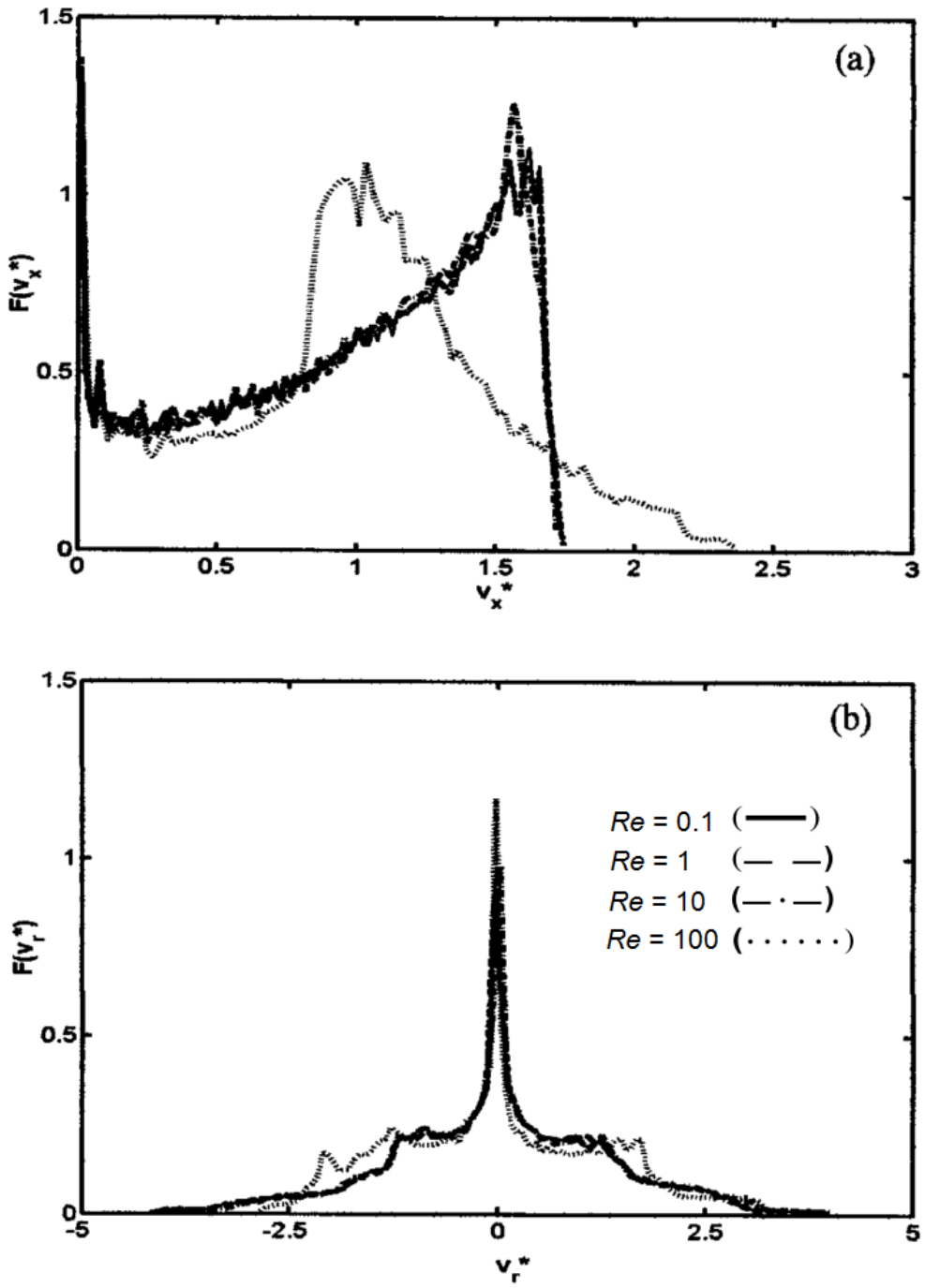

Figure 2.6. Probability distribution functions for axial (a) and radial (b) velocity profiles in an SMX mixer at different Re.(Zalc et al., 2002)

Another notable modelling study was carried out by Meijer and co-workers, where the performance of a number of static mixer designs based on standard SMX, Ross LPD and Kenics mixers was compared based on their efficiency at reducing the intensity of

segregation of a 50/50 mixer feed (Han E.H. Meijer et al., 2012). Here interface stretching was used as a metric of mixedness, as the static mixers selected for the study all apply the stretch and recombine mechanism to achieve mixing, the increase in the interface between the fluids which are being mixed infers a higher number of thinner strata and therefore better mixing. Figure 2.7 illustrates the pressure drop and length of mixer required to achieve the same levels of striation for different mixer designs.

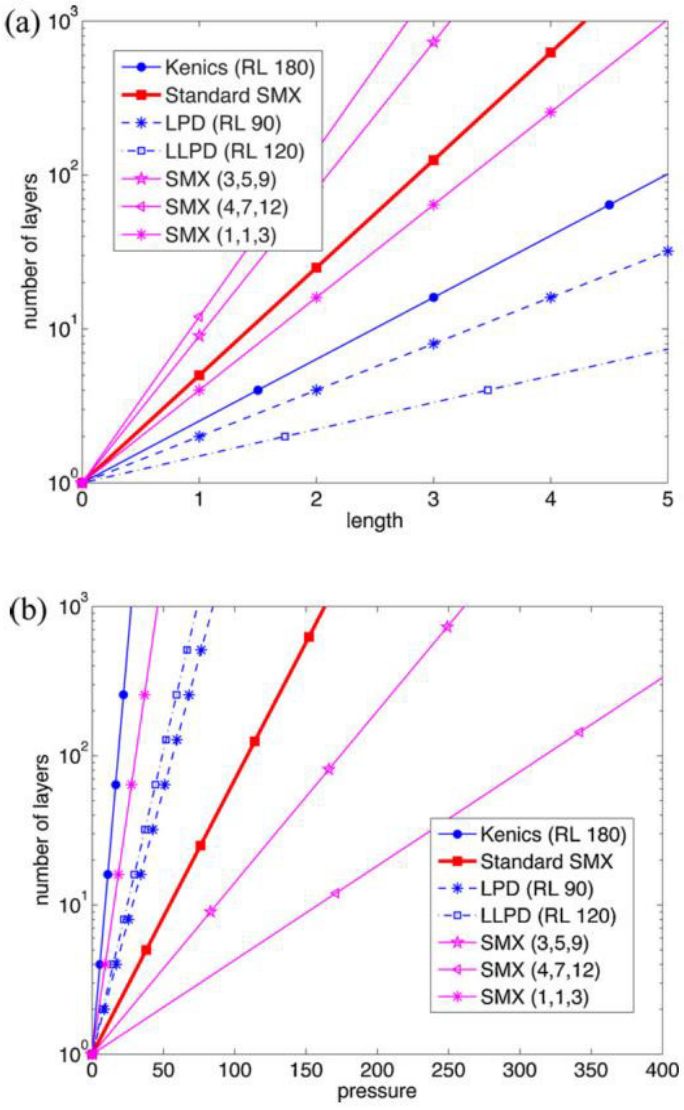

Figure 2.7. The change in the number of layers of the fluids being mixer across a range of static mixer designs, where (a) illustrates the effect of mixer length and (b) provides and estimation of the pressure drop required to achieve the desired level of striation (Han E.H. Meijer et al., 2012).

The work goes on to further compare the performance of mixers based on flux-weighed intensity of segregation, where it can be seen from Figure 2.8 that standard SMX mixers are one of the most efficient mixers per unit length, with some of the modified SMX designs achieving an even more efficient reduction in the intensity of segregation.

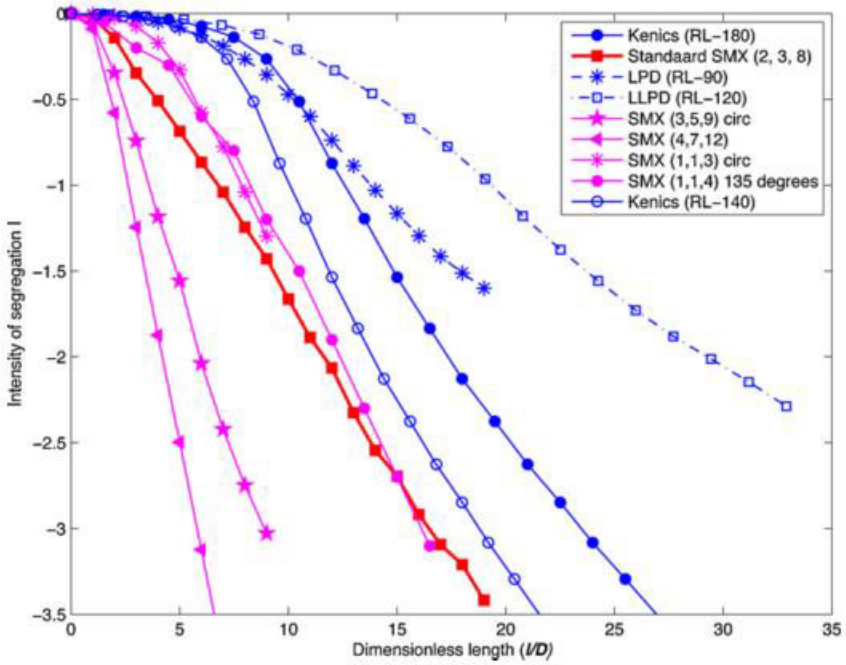

Figure 2.8. Reduction in intensity of segregation per unit length of mixer across a range of static mixer designs (Han E.H. Meijer et al., 2012).

The work to assess the dynamics within the SMX mixers is ongoing, with the inability to conduct experiments assessing the dynamics within the mixer directly, and not through proxy measurements, remaining the most notable challenge of this work.

2.2 VELOCIMETRY AND FLOW CHARACTERISATION TECHNIQUES

2.2.1 PARTICLE TRACER VELOCIMETRY

Particle Tracer Velocimetry (PTV) is a Eulerian velocimetry technique which relies on illuminating a plane of the system of interest with a laser sheet and seeding the flow with high contrast neutrally buoyant tracer particles. Images of the plane illuminated by the laser are taken during flow and can be analysed by either correlating several sequential images (nearest neighbour search) or by focusing on just two (image cross-correlation) to track individual particle motion (Fu et al., 2015).

The technique assumes that between frames the tracer particles have undergone only small displacements and that the path the tracer has taken was smooth. These assumptions define that between two frames the same tracers are in the field of view and that within the individual interrogation windows on the image, the velocity of all the tracers is the same, important conditions for both the neighbour search and cross-correlation techniques.

In addition to standard PTV 3D-PTV can be used for tracer particle tracking, as the name suggests, in 3D space. This technique relies on similar processing algorithms, but requires a second laser sheet, perpendicular to that used in traditional PTV, as well as a second camera (Moroni et al., 2003).

One of the main drawbacks of PTV, as well as other image capture techniques, is that fact that both the system construction material as well as the carried fluid studied must be transparent. This, however, is frequently not the case with real industrial systems, which means that modifications have to be made to the equipment and fluids replaced with mimics of acceptable rheological properties to enable the application of optical techniques.

2.2.2 PARTICLE IMAGE VELOCIMETRY

Particle Image Velocimetry (PIV) is a Lagrangian velocimetry technique which, similarly to PTV, relies on tracking of tracer particles illuminated by a laser sheet. However, for PIV the tracers are much smaller than in PTV and are seeded such a concentration that while individual tracers can be distinguished in the images, it is impossible to trace the path of every individual particle. Instead PIV is used to produce velocity vector fields, describing the flow.

One of the key features of PIV is the laser source, which has to be capable of producing high power light beams with short pulse durations, ensuring short exposure times for each frame. Typically Nd:YAG lasers are used for PIV, where the 532nm wavelength is isolated, which corresponds to green light which can be seen by the naked eye, which is an important safety precaution of the technique. To shape the light into a 2D laser plane a series of spherical and cylindrical lenses is used, which yield a 2D sheet, which at the focal point of the spherical lens is as thick as the wavelength of the light itself. This is the ideal distance for the location of the experimental point of interest, as it reduces the possibility of picking up events in areas outside of the intended 2D plane (Atkins, 2016).

To enable the capture of two sequential images that are separated only by a short time step and are suitable for cross-correlation analysis a high-speed camera is used which is synchronised with the laser light source. The par of shots is typically taken several hundred nanoseconds apart (Δt), and while this provides the opportunity for the capture of hundreds of pairs in the space of several seconds, the amount of data captured and the length of the capture process can be limited by the on-board camera storage capacity and the speed of data transfer to the computer controlling the data acquisition process. A synchroniser is

used to trigger the camera and the lasers at the desired times (Li, 2009). A typical PIV setup is shown in Figure 2.9.

The tracer particles can range in size anywhere between 1 to 100 micrometres in diameter and are selected on a basis of several criteria. The tracers must faithfully follow the flow of the fluid that is being seeded, responding quickly to any changes in the flow filed. This ability is inversely proportional to the difference in density between the fluid and the tracer, and is also inversely proportional to the square of the tracer diameter. This in turn means that if the densities are closely matched larger tracer particles can be used, while for tracers with significantly different densities, reduction of the tracer size is crucial. On the order hand, the tracers need to be large enough to scatter enough light to be detected, this is predominantly achieved through Mie scattering, which is directly proportional to the tracer particle diameter. Furthermore, the refractive index of the tracer must be significantly different from the carrier fluid which is being studied. With the key variables being closely and inversely linked to the size of the particles, a balance must be struck when selecting tracers, to satisfy both conditions. This is made possible by the wide range of tracer particles available, including glass, polystyrene and polyethylene beads, aluminium flakes and oil droplets of varying diameters (Atkins, 2016; Li and Hishida, 2009).

Once the frames are captured, they are split into many interrogation windows, forming a grid. A single velocity vector is calculated for each interrogation window, based on the velocity averages for the particles passing through for several hundred image pairs. The size of the windows depends on the expected average fluid velocity across the frame, ensuring that the window is large enough to contain some of the same tracers between the frames, however, at the same time not too big to average out any local phenomena that are of interest. The velocity vector is calculated by cross-correlating the images within the

same pain and is based on the displacement of the tracer between flames and the time delay Δt (Fu et al., 2015).

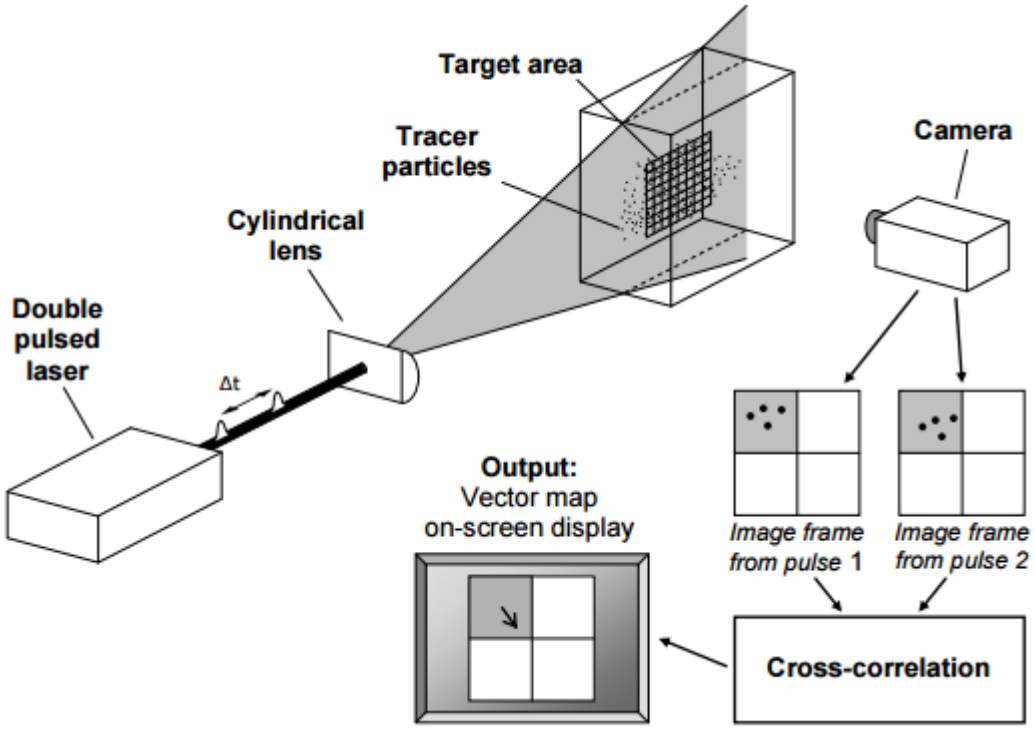

Figure 2.9. An example of a particle image velocimetry experimental and data acquisition set up (Li, 2009).

PIV has been successfully used to characterise flow in industrial equipment, such as mixing in tanks, fluidised beds, ducts and pipes, as well as air current flow around jet wings and cars in wind tunnels, ship propellers and many more (Cao et al., 2010; Chiti et al., 2011; Lehwald et al., 2008; Li, 2009; Versluis, 2013). However, as described above for the case of PTV, the systems which can be studied using PIV are limited by the opacity of the construction materials and fluids.

Another technique based on PIV is microfluidic PIV or micro-PIV, which while applying the same principles deals with significantly smaller scale equipment, such as microchannels of sub millimetre scale. To achieve this a microscope is attached to the high-speed camera and focused on the desired point within the channel. The ability

conduct PIV experiments on the micros scale allows to observe phenomena such as shear banding or surfactant liquid crystal dissolution (Matter et al., 2012; Wang and Wang, 2009).

2.2.3 COMPUTER-AIDED RADIOACTIVE PARTICLE TRACKING

Computer-Aided Radioactive Particle Tracking (CARPT) is one of the techniques which can help overcome the challenges faced by optical techniques described above. CARPT can be applied on a range of processing equipment, such as fluidised beds, bioreactors, bubble columns, etc.(Chen et al., 1999; Rammohan et al., 2001a; Wintenberg and Clonts, 2003).

The equipment can be left unmodified, with the flow within the equipment seeded with a radioactive tracer particle, while the CARPT detectors are located outside of the equipment. The tracer particle is selected to be neutrally buoyant and small, to faithfully track the changes in carried fluid flow, however, a balance in the particle size needs to be struck, to allow sufficient activity, and a typical tracer is several millimetres in diameter. The tracers are produced by making a hole in a spherical tracer particle, for example a polypropylene bead, the gamma ray emitting isotope, e.g. Scandium, is then placed inside and the hole is sealed, leaving an air gap between the isotope and the plug, allowing to make the tracer neutrally buoyant in many fluids, by changing the size of the air gap (Wintenberg and Clonts, 2003).

The tracer emits gamma rays which are picked up by an array of NaI detectors, where the location of the particle is estimated by determining the relative count rates on each detector, with less detection when the particle is further away for the detector, where the number of detectors in an array is determined by the volume of interest. The detectors require calibration by placing a tracer particle of known activity a known distance away

from the detector, allowing to develop a correlation between recorded activity and distance (Khopkar et al., 2005; Rammohan et al., 2001b). The capability to calculate the distance of the tracer particles from multiple detectors allows to determine the instantaneous position of the tracer, with a typical sampling frequency of 50Hz. The velocity and direction of motion of the tracer can be then estimated based on the position between two detections separated by a known time step. The volume of interest is divided into segments and the calculated velocity is assigned to the segment corresponding to the mean particle position between consecutive detections. Figure 2.10 shows an example of a CARPT set up for a bubble column and a schematic for a tracer particle cross-section (Degaleesan et al., 2002).

Several hours of data acquisition are required to obtain sufficient data for the estimation of local averages and the total duration depends on the size of the system, with some experiments running for up to 24h.

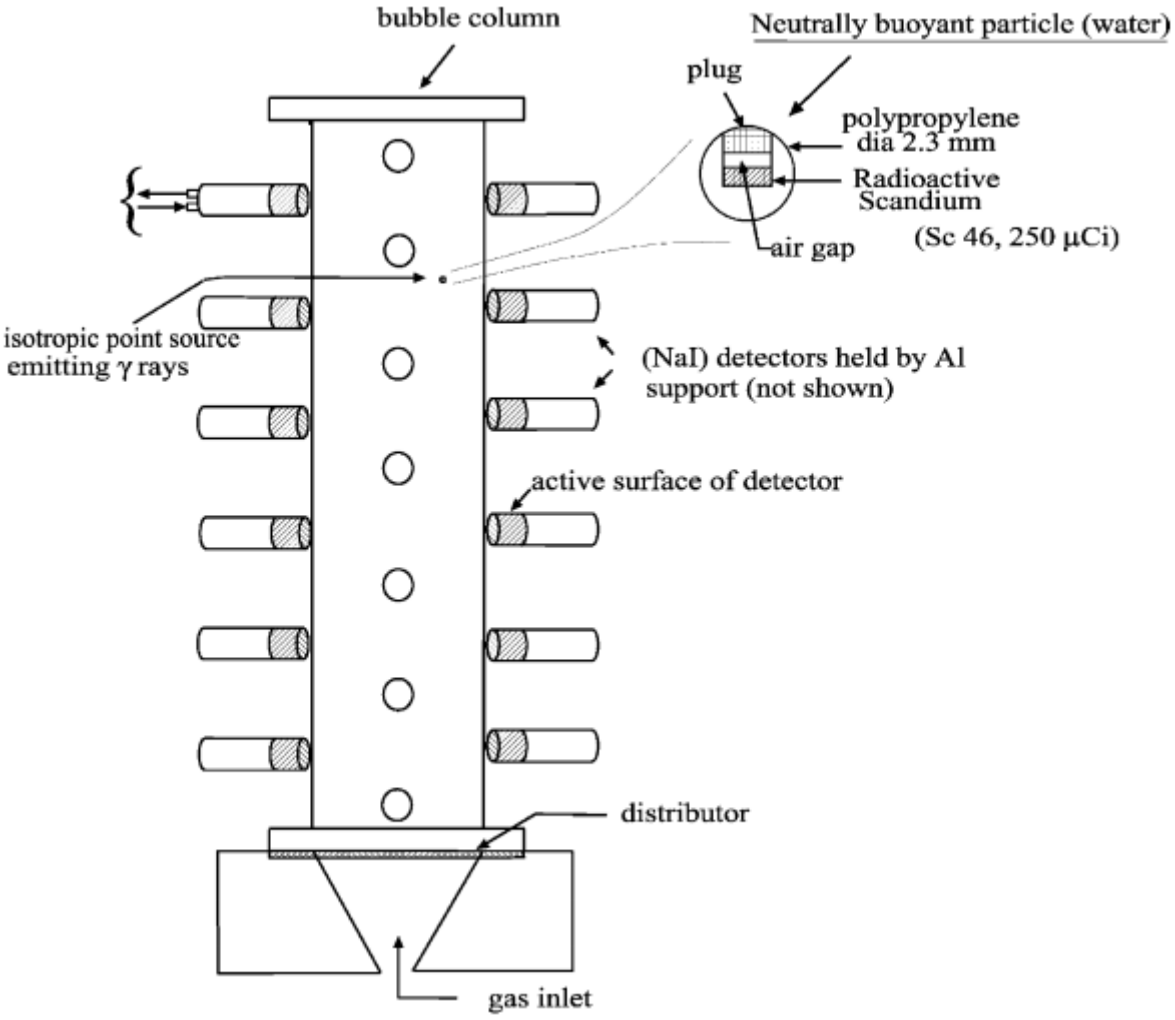

Figure 2.10. The assembly of CARPT array around a bubble column and the schematic of the tracer particle cross-section (Degaleesan et al., 2002).

CARPT has been successfully applied in the studies of a wide range of industrial processes, however, a relatively low resolution of the technique, which relies on the sensitivity and the number of detectors used and the relatively large tracer particle size prevents its applications for wider research (Wang, 2015).

2.2.4 X-RAY COMPUTED TOMOGRAPHY

X-ray computed tomography (XCT) is another technique which applies high energy radiation to visualised the properties of complex and opaque industrial systems. Like the

medical CT scan used for non-intrusive examination of the patient's internal organs XCT relies on the scanner to emit x-rays which are blocked to various degrees by the different structures within the object of interest. In a patient this could be the difference between different types of tissue, while in industrial applications the contrast is especially well visible in multiphase flows or as a means of identifying cracks and voids in structures, such as cast metal parts. The technique is often calibrated using objects with known size of voids or a known droplet size distribution for multiphase flows (Dudukovic, 2002).

The XCT technique relies on placing the object of interest between the x-ray source and the x-ray detector, which allows to image one time averaged 2D slice of the object. The x-ray source and detector are then rotated, providing the next 2D slice, which is repeated until sufficient number of 2D slices has been acquired to be stacked together forming a 3D representation of the object of interest. This process is illustrated in Figure 2.11 below, however alternative XCT setups also exist (Escudero and Heindel, 2014; Schafer et al., 2016).

XCT has been successfully applied for the characterisation of flows in porous media as well as oil recovery and air sparging through media such as wet sand, where a strong contrast between the gas and the other components of the system allows for high-resolution visualisation. The technique is also applied in studying foams, gas induction into stirred batch reactors, bubble columns and fluidised beds (Kinugasa et al., 2015).

While XCT offers a powerful visualisation tool, it is limited by the system constituent's ability to absorb X-rays, where some applications are not possible, such as single phase flows. In addition, due to the time-averaged nature of the technique it is impossible to assess local instabilities and chaotic flows within the system of interest (Bieberle and Barthel, 2016).

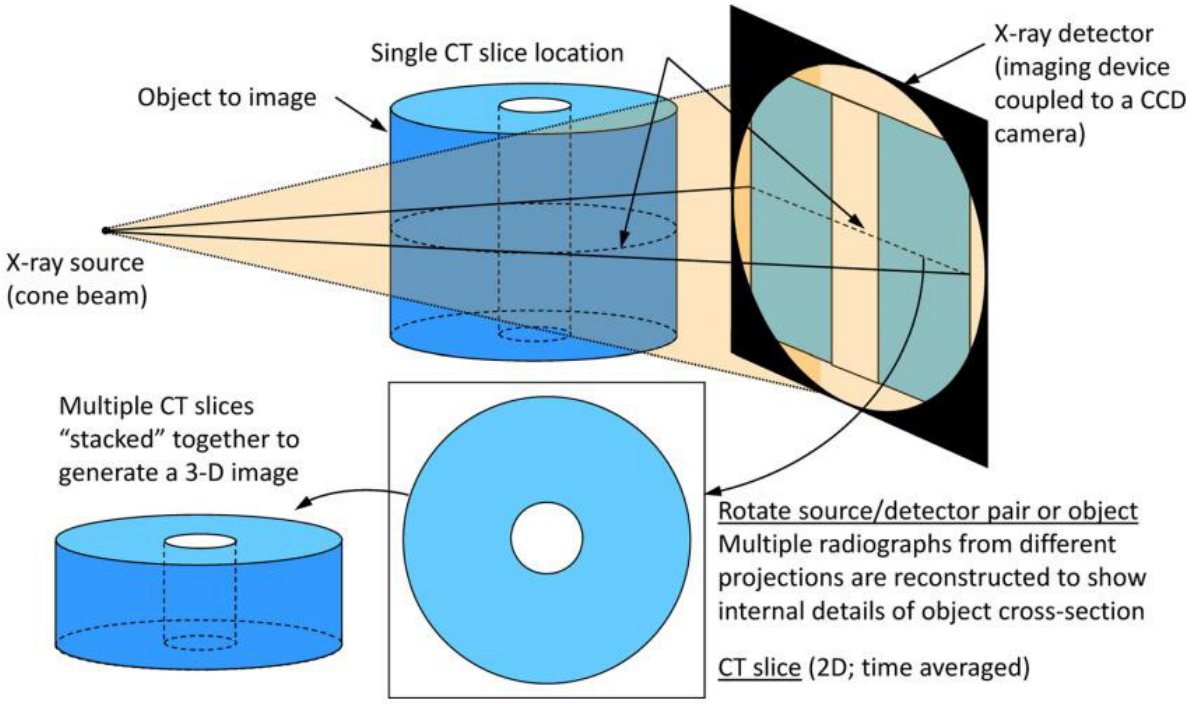

Figure 2.11. Schematic representation of x-ray computed tomography imaging (Schafer et al., 2016)

2.2.5 POSITRON EMISSION PARTICLE TRACKING

Positron emission particle tracking (PEPT) is another technique which utilises gamma ray emitting tracer particles to negate the need for transparent systems used in optical techniques, and is the predominant approach used to obtain data for this thesis. PEPT has been first developed at the University of Birmingham in the early 1990s and is based on a pre-existing medical technique known as positron emission tomography (PET) (Parker *et al.*, 1993).

The technique relies on tracing a single radioactive particle through the system of interest. The particle spatial location is estimated through triangulation of back to back γ-rays that are emitted during radioactive decay of a radioactive isotope, typically fluorine-18 (^{18}F), encapsulated in the particle, and picked up by an array of detectors, or cameras, on either side of the equipment (Stellema et al., 1998). For each location the triangulation algorithm uses up to 100 individual γ-ray pairs, with outliers and invalid pairings removed

through processing, to provide improved location accuracy (Parker et al., 1997a). Most isotopes used in PEPT tracer manufacture have a short half-life, with ^{18}F, having a half-life of under 110 minutes. This results in rapid positron emission and thus frequent γ-ray detection, allowing for triangulation frequency of up to 10 ms. Furthermore, due to the high energy nature of γ-rays, that can penetrate most materials, including steel, PEPT can be used on real, unmodified industrial systems (Boucher et al., 2015; Parker et al., 1993; Van de Velden et al., 2007). Obtaining the 3D tracer location data with respect to time allows the derivation of a number of system properties, such as bulk dynamics, local occupancies and concentrations, mixing efficiencies, local velocities and local shear rates (Bakalis et al., 2006).

A recent development in the technique has provided the possibility of tracking multiple tracers that are present in the PEPT camera field of view simultaneously, which was previously impossible due to the interference between the two tracers (Yang *et al.*, 2006). This advancement allows for new properties of the system to be studied, such as, for example, relative motion of particles of different size in a system with a large particle size distribution, or tracking different phases in multiphase flow simultaneous, *e.g.* in slurries, or studying the relative dynamics of objects in a system, *e.g.* dynamics of cloth in a washing machine.

Due to the unique features of PEPT as a characterisation technique, it has been applied on a variety of systems, both simplified and industrial, with the majority of the work focusing on characterising the behaviour of powders, liquids or slurries in various geometries. PEPT has been successfully used in a number of studies charactering a range of equipment, such as simple pipes (Fairhurst *et al.*, 2001), vertically stirred mills (Conway-Baker *et al.*, 2002), tumbling mills (Volkwyn *et al.*, 2011), stirred tanks (Chiti *et al.*, 2011), grinder mills (Barley *et al.*, 2004), static mixers (Rafiee et al., 2013) as well as

home appliances, such as washing machines (Mac Namara *et al.*, 2012) and dish washers (Pérez-Mohedano *et al.*, 2015).

2.2.5.1 POSITRON EMISSION PARTICLE TRACKING TECHNIQUE

This section addressed the PEPT methodology, the different types of cameras used, the conditions necessary for successful tracer detection and the different procedures of tracer preparation. Raw data processing and derivation of desired system properties is also assessed.

Detection

PEPT relies on the principle of instantaneous detection of back-to-back γ-ray pairs that get emitted when a positron released during the radioactive decay of the isotope contained in the tracer particle is annihilated with a free electron (Sadrmomtaz *et al.*, 2007). Each event detection represents a line of response (LOR) and after correction for attenuation and noise all LORs are expected to meet in one point, which defines the location of the source (tracer).

The detection takes place when the γ-ray strikes a scintillator crystal contained in the camera. Scintillation is the property of a material that results in luminescence when excited with high energy ionising radiation. The light is emitted as the molecules within the crystal return to their original energy state and this light is reabsorbed by a light sensor within the camera. The light sensor then transforms the light signal into an electric pulse, providing information about the high energy pulse that struck the crystal in the beginning of the process. Several modifications of PEPT cameras exist, where either single sodium iodide scintillator crystal detectors are positioned parallel to each other on either side of the field of view, or arrays of detectors with smaller Bismuth germinate ($Bi_4Ge_3O_{12}$) scintillator crystals are arranged around field of view (Leadbeater and Parker, 2011; Parker *et al.*,

2002). When a γ-ray strikes the detector crystals, an event is recorded, up to 5000 detections per second, depending on the activity of the tracer. The detections that coincide in time are recorded as one pair and used for the reconstruction of the γ-ray trajectory. The optimum tracer activity for successful and accurate detection is between 300 and 1000 μCi (Fan *et al.*, 2006).

In a standard PEPT assembly the separation of the two cameras arranged in parallel can reach up to 800 mm and the area of the detector array on each camera is 500 mm×500 mm, which allows for industrial size equipment to be fully inserted into the field of view of the camera (Parker *et al.*, 1997b). Figure 2.12 shows a photograph of the PEPT assembly at the University of Birmingham, which is a two sodium iodide crystal detector assembly. In the case of the radial arrangement of detectors, the field of view typically has a diameter of 82 cm, as in the case of the PEPT camera used in iThemba labs in Cape Town. The dimensions of the field of view for both types of camera are limited to these sizes, as the cameras were originally designed to accommodate the body of a patient undergoing a PET scan (Buffler *et al.*, 2010). Other modifications of the detector assembly exist and are used in more specific applications, such as the modular camera assembly discussed below.

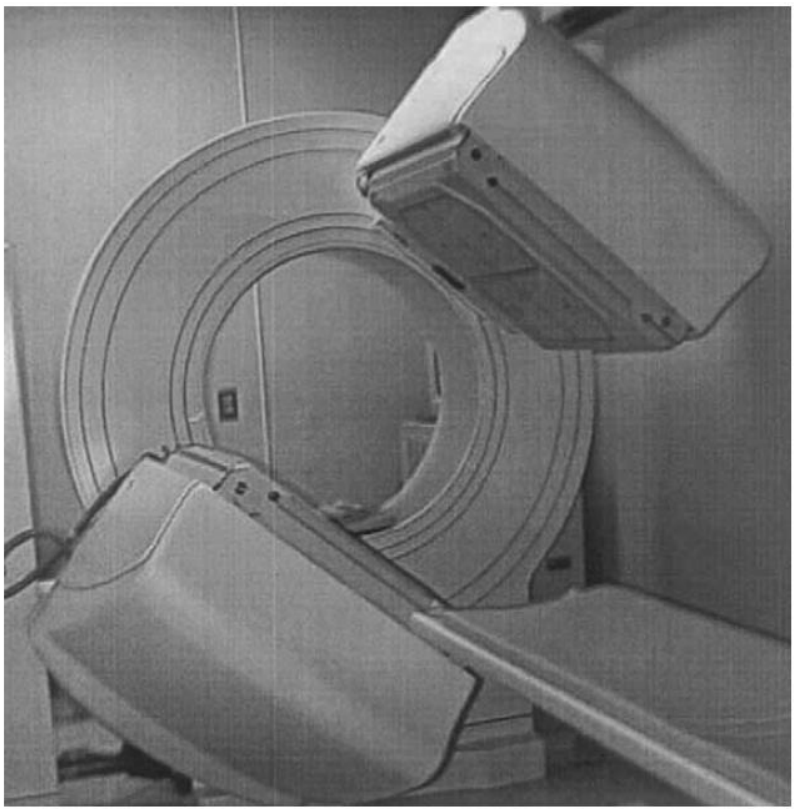

Figure 2.12. PEPT camera at the University of Birmingham. From (Parker et al., 2002)

Depending on the velocity at which the tracer moves through the field of view, the accuracy of location detection can vary, with lower velocities yielding higher accuracy, but a lower detection rate. For example, a slow moving tracer, e.g. 0.01 m/s, can be detected up to 50 times per second with the accuracy within ±0.5mm, while a tracer moving at 0.1 m/s can be detected over 250 times each second, but the location is accurate within as much as ±2.5 mm radius (Kuo *et al.*, 2003; Parker *et al.*, 1997a). The accuracy of detection relies on a number of other factors, such as the activity of the tracer, the separation of the cameras and the construction material of the system that is being studied. The radioactive isotopes chosen for PEPT decay predominantly through positron emission (β^+), however, before the positron is annihilated by a free electron it usually travels several millimetres, further affecting the accuracy of location estimation. During positron annihilation two γ-rays are emitted, typically with the energy of 511 keV, travelling back-to-back (Stellema *et*

al., 1998). Simultaneous detection of these γ-ray pairs is the key to the PEPT technique. More active tracers will undergo rapid decay, resulting in high numbers of γ-ray pair detections, however, it has been shown that over a certain emission rate the number of valid detections picked up by the camera does not change, however the number of incorrect pairings increases (Parker *et al.*, 2002), as shown in Figure 2.13. These arise due to the fact that when many γ-ray emission events happen within a very short period of time incorrect pairings can occur, as several sources of signal delay are present in the system, due to the rate of relaxation of the detector crystal from the excited state. Figure 2.14 shows an example of what a typical location reconstruction could look like, where the false pairings are shown in red. In addition to excessive tracer activity, incorrect pairings can result from background radiation, as well as due to the γ-ray deflection and attenuation when passing through other materials, such as the medium being studied or the equipment (Forrest *et al.*, 2003; Ingram *et al.*, 2005). Materials like metals tend to have high attenuation levels, therefore when conducting PEPT on industrial systems tracers with higher activity are preferred.

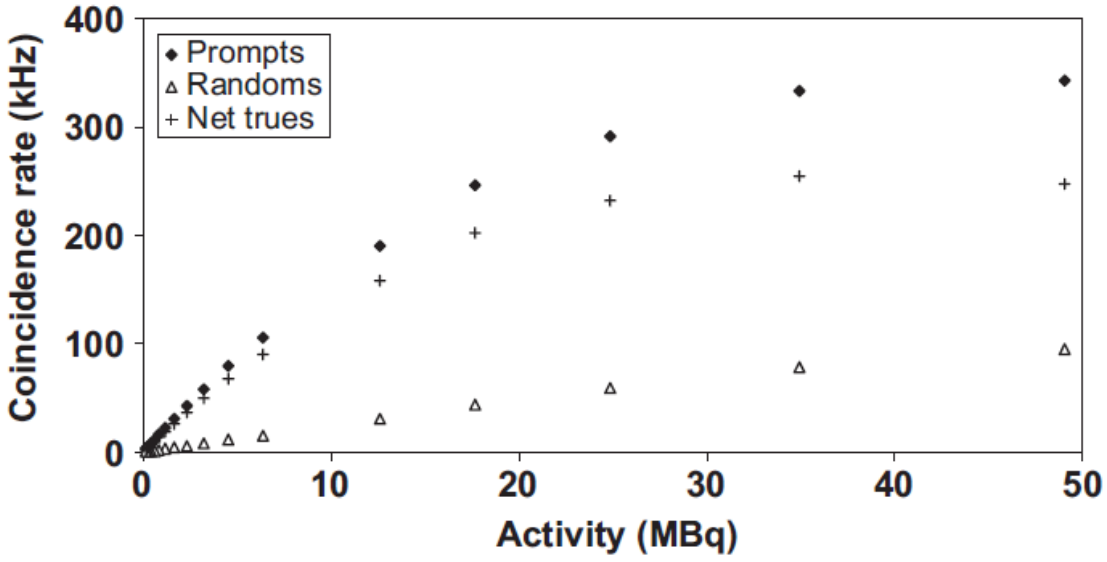

Figure 2.13. Overall (prompts), random (random) and true rate (net trues) of γ-ray detection represented by the coincidence rate as a factor of tracer activity. (Sadrmomtaz et al., 2007).

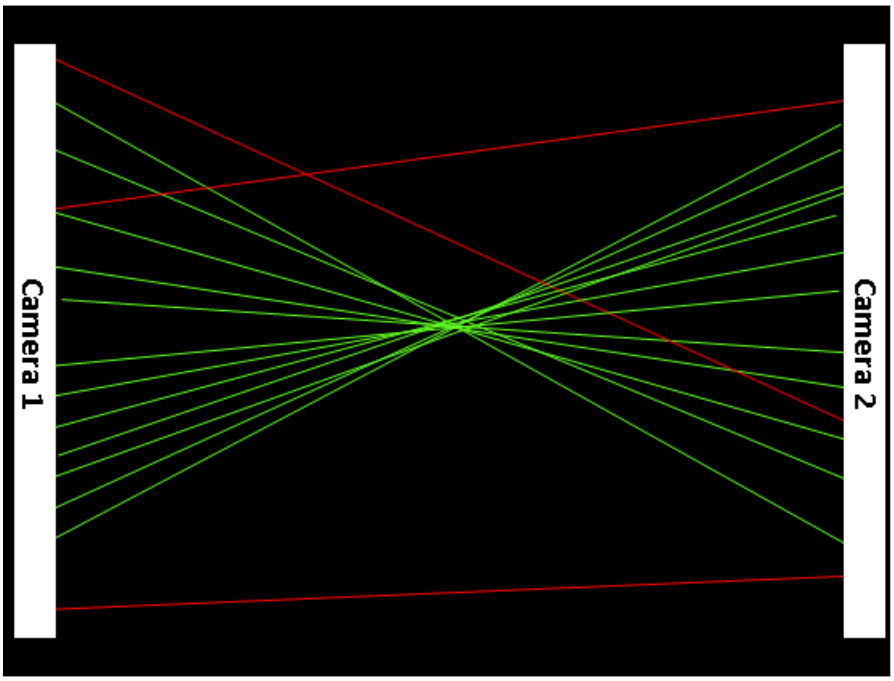

Figure 2.14. Example of valid back to back γ-ray detection (green) and invalid pairings (red)

In order to study more complex equipment that is impossible to fit into the traditional PEPT camera shown in Figure 1, the University of Birmingham has developed a modular PEPT camera, through acquiring several PET scanners with Bismuth germinate crystal array detectors and redistributing the detectors from these cameras on a modular frame (Leadbeater and Parker, 2011). Unlike the cameras used for traditional PEPT, where two parallel detector arrays are used, the modular camera is broken down into segments of 4 detector blocks per module, as shown in Figure 2.15, with up to 32 modules available to be connected for simultaneous detection. Figure 2.16 demonstrates a possible modular assembly which allows for high sensitivity due to the close positioning of the detector blocks. The figure further illustrates the field of view of each individual detector, where the light grey section corresponds to detector module 0. The uniform field of view results from the overlap of the fields of view of all 8 detectors modules and is shown in dark grey.

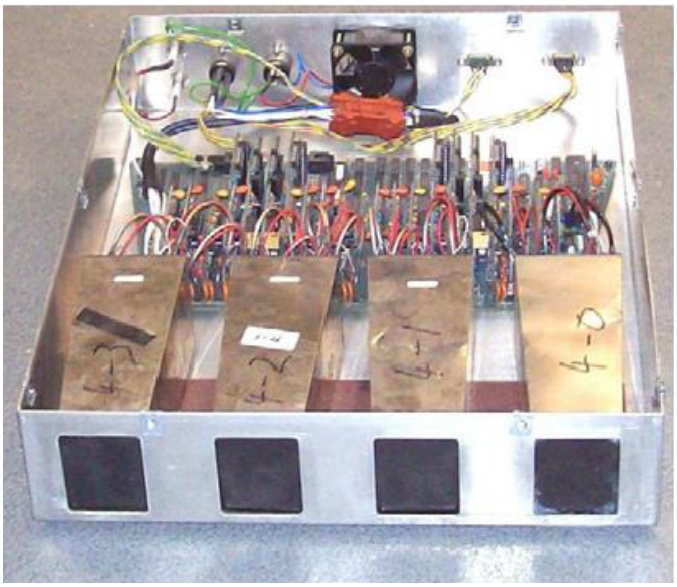

Figure 2.15. A detector block assembly of the modular camera. From (Leadbeater and Parker, 2011)

Ideally the volume of interest that is being characterised using PEPT should be located within the uniform field of view. In order for the modular assembly to be used, the detection and processing algorithms have to be adjusted for each geometry, specifying the dimensions of the system and distances between detector arrays. By arranging the detector modules around the equipment this approach allows to study much larger systems to be studied than traditional PEPT, alternatively the modular camera can be used for studying smaller systems in fine detail, as more γ-ray pairs can be detected due to the flexibility of the detector geometry, compared to traditional PEPT (Boucher *et al.*, 2014; Leadbeater *et al.*, 2012).

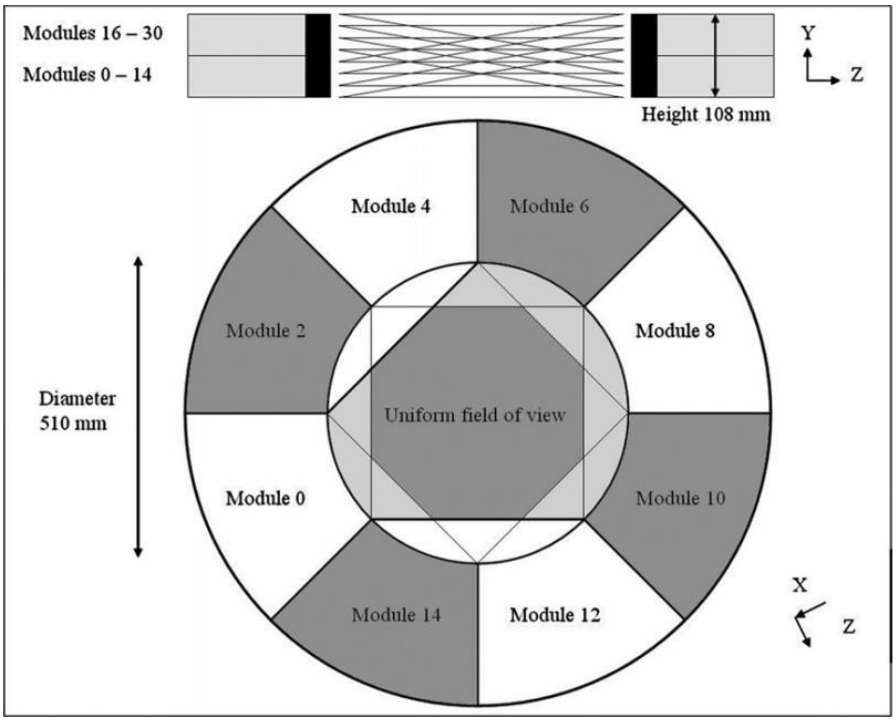

Figure 2.16. Example of a modular camera arrangement From (Parker et al., 2008)

Tracers

When the PEPT technique was first envisioned, the tracer particles relied on the decaying isotopes of relatively heavy elements, such as the metastable isotope of Technetium, $^{99}Tc^{m}$, which is one the standard isotopes used in nuclear medicine. However, elements such as $^{99}Tc^{m}$ have a half-life of up to 6 hours, meaning less positron emission over time for the same number of atoms compared to elements with a shorter half-life (Sadrmomtaz *et al.*, 2007). Furthermore, the energy of the γ-rays emitted by the $^{99}Tc^{m}$ is relatively low, approximately 140 keV, as the emissions do not occur due to positron annihilation, but instead as a result of gamma decay. The lower emission energy makes the $^{99}Tc^{m}$ γ-rays more susceptible to attenuation when passing through various media, such as the construction materials of the system of interest (Parker and McNeil, 1996). Equation 2.8 illustrates the correlation between the properties of the system, such as initial energy, attenuation coefficient and thickness of the medium, where *I* is the emerging intensity after

passing through a medium (keV), I_o is the initial intensity (keV), L_m is the thickness of the medium (cm) and μ_{ac} is the attenuation coefficient (cm^{-1}). The attenuation coefficient is correlated to the density and the atomic number of the medium as well as the energy of the gamma ray travelling through. Transmission, *T*, is a representation of the energy lost by the γ-ray as it travels through various media, as a function of the initial energy at emission (Nelson and Reilly, 1991).

$$I = I_o e^{-\mu_{ac} L_m} \quad 2.8$$

$$T = {}^{I}/_{I_o} \quad 2.9$$

Figure 2.17 demonstrates the transmission as the fraction of the initial energy, as estimated through Equation 2.9, where it can be clearly seen, that low energy γ-rays are very susceptible to attenuation, where approximately 0.45 cm of steel or 4.5 cm of water can reduce the energy of the γ-ray by 50%. This means that when using tracers such as $^{99}Tc^{m}$ the event rate during acquisition was low, even for systems with constructed of favourable materials. Therefore, alternative sources of tracer activity were explored, and were ultimately narrowed down to ^{18}F radioisotope of fluorine, with the half-life of just under 110 minutes, which allows acquiring accurate PEPT data even in fast moving systems and systems with high positron attrition. In addition, ^{18}F decays predominantly through positron emission (97% of the time), with only 3% of the time decaying through electron capture, making it a highly efficient tracer for PEPT (Parker *et al.*, 1997a; Stellema *et al.*, 1998). The energy levels produced during the annihilation of ^{18}F isotopes is 511 keV, much higher than that seen in $^{99}Tc^{m}$. It can be seen in Figure 2.17 that in order to achieve the loss of 50% of the energy at emission a 511 keV the γ-ray has to travel approximately 1 cm through steel and 7 cm through water, which makes it much more applicable in real systems.

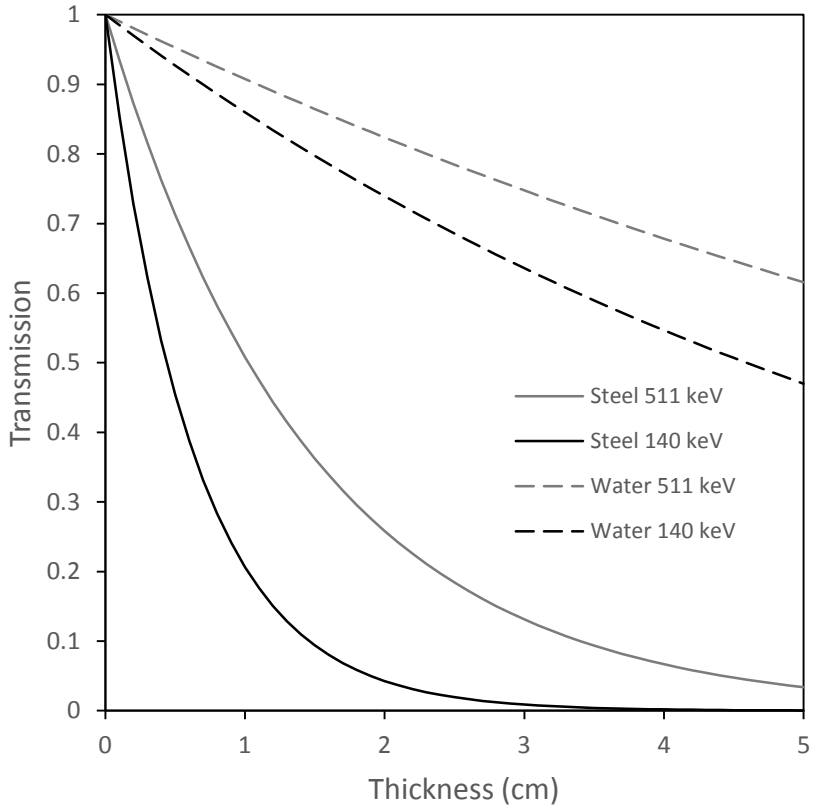

Figure 2.17. Fraction of γ-ray energy transmitted through a medium as a function of medium thickness and material and the initial energy of the γ-ray

Inclusion of ^{18}F isotopes in the tracer is carried out using one of two approaches. When the medium that is being traced is made up of relatively large particles, bigger than 1000 μm, and the material contains oxygen atoms, it is possible to activate the particles of the bulk material directly, by bombarding the tracer particle to be with a 35 MeV ^{3}He beam (Bbosa *et al.*, 2011). This converts some of the oxygen atoms in the particle into ^{18}F. However, due to only a small fraction of the oxygen being converted through direct activation, tracers exhibit low activity, and therefore need to be relatively large to achieve the activity threshold required for accurate detection (300 μCi) (Fan *et al.*, 2006).

When smaller tracers are required, *e.g.* in finer powders or liquids, the ion exchange approach is taken for tracer preparation. Initially the ^{18}F isotopes are obtained by using a cyclotron to bombard either pure or oxygen-18 enriched water, resulting in ^{18}F rich water

(Leadbeater *et al.*, 2012). Tracers made from ion exchange resin are then brought in contact with the ^{18}F rich water and through the exchange of counter ions, resin tracers as small as 200μm can be labelled with activity levels of up to 1000 μCi, allowing for accurate detection (Parker and Fan, 2008). However, due to the nature of the ion exchange resin the tracers made using this approach have the density of 1 g/cm^3 and are spherical, which limits their applications in studies involving solids, irregular particles and dense liquids. To expand the applications of PEPT to more systems alternative materials for use in ion exchange have been assessed, such as quartz, coal, polyurethane and others. These materials do not have a naturally high affinity for ion exchange and receive as little as 2 μCi of activity after the ion exchange process. In order to enhance the uptake of ^{18}F ions a surface modification approach using metallic ions, such as Cu^{2+} and Fe^{3+}, was developed. This enabled tracers made of various materials with poor ion exchange affinity to be labelled with activity levels of over 500 μCi, for 200 μm tracer diameter. Figure 2.18 shows an example of the effect of surface modification using Fe^{3+} ions on the number of molecules of ^{18}F absorbed by a quartz tracer (Fan *et al.*, 2006).

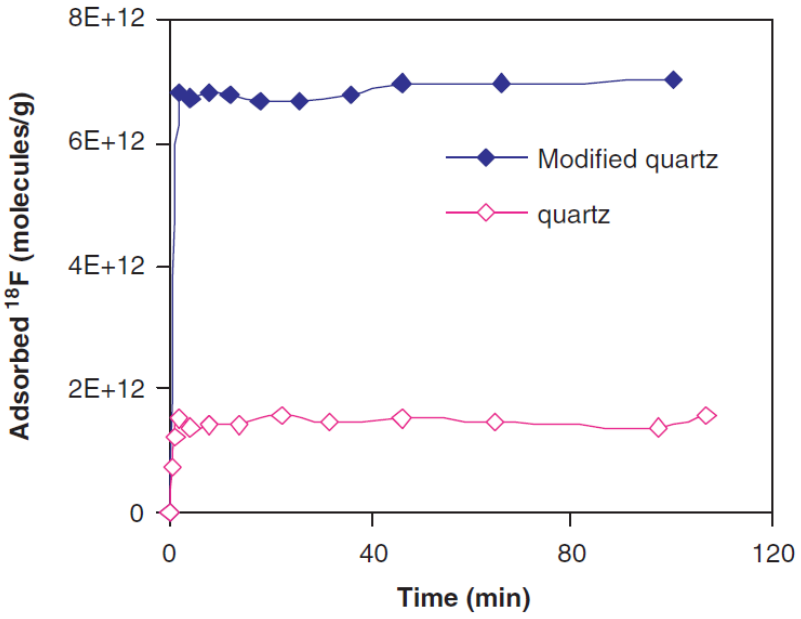

Figure 2.18.Effect of Fe^{3+} ions on adsorption of ^{18}F ions on quartz tracers(Fan et al., 2006)

The short half-life of the isotope, however, can prove to be an issue when using the modular PEPT camera in an industrial setting, away from the cyclotron, as the tracers lose a significant amount of activity during transport to the desired location. To mitigate the low tracer activity on arrival to location, tracers with a longer half-life can be used with the modular camera assembly (Parker *et al.*, 2008).

Another modification of the PEPT technique was introduced when the concept of multiple tracers being present in the field of view was introduced. Traditionally the processing algorithm is incapable of distinguishing between two strong sources of positron emission, resulting in noisy data. In this case during each location detection the algorithm focuses on the location of one of the emission sources, normally the stronger, more active tracer, where any detections from the other sources are discarded, thus dramatically reducing the number of valid detections available for triangulation of the location of the stronger tracer (Bickell *et al.*, 2012).

Multiple tracer tracking would be beneficial for a number of systems, especially where mixing or multiphase flow is concerned or dynamics of solids with large particle size distributions are being studied.

To accommodate for such demand the multiple positron emission particle tracking (MUPEPT) has been developed, where the algorithm can distinguish between two or more tracers present in the field of view simultaneously (Gundogdu and Tarcan, 2004; Yang *et al.*, 2007). To achieve this, the activity of the tracers in the system has to be significantly different from each other, with the strongest tracer having at least double the activity of the next strongest tracer. The data recorded from the system is then analysed using multiple passes algorithm, where the most active tracer is identified first, based on the location with the highest γ-ray coincidence rate. The data from the most active tracer is then ignored during the next pass and the tracer with the next highest activity level is identified and the

tracer location determined. The procedure can be repeated for as long as the tracers in the system are different enough and strong enough. This approach proves to be especially efficient when systems with particles with a wide particle size distribution or mixtures of two distinct particle sizes are studied, as the size difference provides an easy way to label the tracers with distinguishable activity levels.

2.2.5.2 DATA PROCESSING

Location of the tracer particle is estimated through a triangulation algorithm, which uses several γ-ray pairs per location, as mentioned above. The processed raw data results in a series of data points describing the location of the tracer particle in 3D space using a set of x, y and z coordinates. Each set of coordinates is assigned a time stamp as well as the relative error. The error describes the radius of the probability cloud around the coordinate in which the tracer was located. The uncertainty in the location arises due to invalid pairings, distance travelled by the positron before annihilation and due to attrition.

During processing the number of events used to resolve each tracer location (N_{slice}) is defined by the user and fed into the processing algorithm. N_{slice} is typically between 50 and 500 events, with lower values for fast moving tracers to reduce the effect of tracer motion on the accuracy of detection. Out of the range defined by N_{slice} a small subset of events is selected at random and the centroid for each line of response is determined. The location at which the distance between the centroids is minimised is selected as the first location guess. The events with the LORs furthest from the first guess are discarded and the centroid is recalculated using the remaining events defined by N_{slice} (Parker *et al.*, 1993). The procedure is repeated until only the predefined fraction of the initial set remaining (*f*). The final location of the tracer is then calculated using the minimum distance between the remaining events, with the standard deviation between event LOR centroids describing the

particle location probability cloud. The value of *f* typically lies between 0.05 and 0.40 and depends on the fraction of corrupt events due to scattering and attrition, which are determined by placing a stationary particle into the system of interest prior to the main experiment and recording the number of valid events. An example of the ratios between true and corrupt events can be seen in Figure 2.19 (Parker and McNeil, 1996). For a stationary particle the location precision depends on the camera rate of acquisition and is inversely proportional to $\sqrt{fN_{slice}}$ (Parker *et al.*, 2008; Volkwyn *et al.*, 2011). Figure 2.19 shows an example of how the error in detection, represented by the standard deviation of the particle location in 3D space is affected by variation of the processing parameters N_{slice} and *f*. Another variable used in PEPT data processing is the N_l, or the number of locations per slice, which allows extraction of more than one location out of the slice of data defined by N_{slice}.

As the radioactive isotope inside the tracer decays, the detection rate and accuracy could suffers, which is especially important for systems where the dynamics are being continuously traced over the course of several hours. In such cases, the raw data should be separated into intervals and different input parameters should be used when processing.

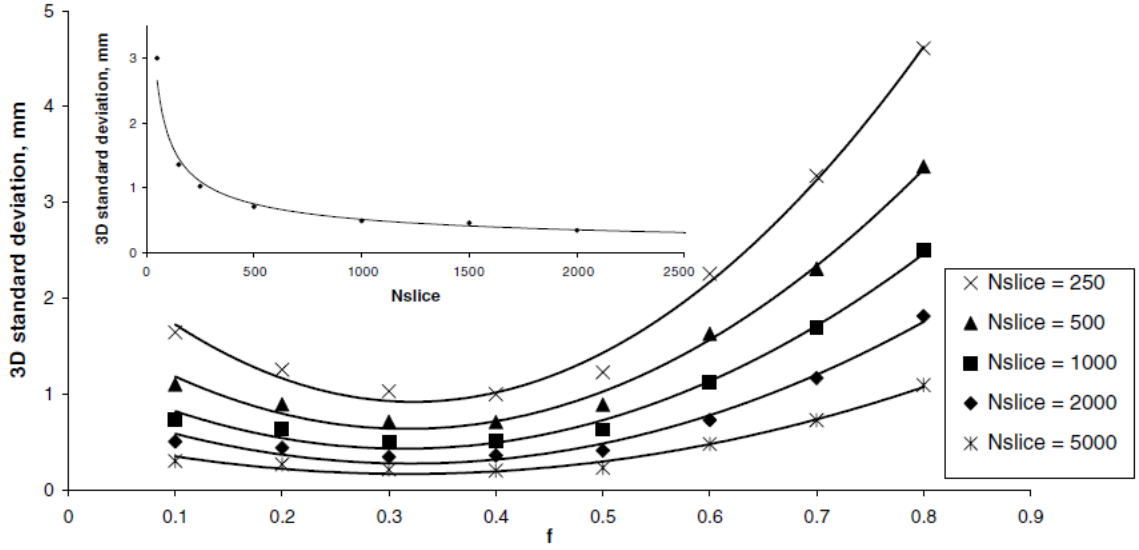

Figure 2.19. Effect of variation of f and N_{slice} on the 3D standard deviation in particle location From (Parker et al., 2008).

Further data processing of the particle location coordinates and the corresponding time stamp can be used to derive a number of properties of the system. PEPT is most frequently used to determine properties such as time based occupancy, residence time, as well as dynamic properties of the system, such as local velocity fields as well as shear fields. In addition, due to the discrete tracer detection provided by PEPT it is possible to track the behaviour of a representative element of the medium as opposed to the bulk tracking offered by some other characterisation techniques.

2.2.5.3 COMPLIMENTARY TECHNIQUES

The unique ability of PEPT to acquire data from systems that are traditionally impossible to study using more established techniques, such as optical techniques, Magnetic Resonance Imaging (MRI) or Computational Fluid Dynamics (CFD), puts PEPT in an exclusive position to be a complimentary/validation technique for other characterisation methods.

PEPT has been applied for validation, improvement and comparison of CFD or Discrete Element Method (DEM) models in systems where other established techniques, such as Particle Image Velocimetry (PIV), are not applicable. Such studies have been carried out on CFD/DEM models developed to describe particle motion in a liquid under agitation using a turbine (Boucher *et al.*, 2015). This is especially important in the cases of suspensions, where any technique that relies on visual observations of a transparent system becomes unsuitable after the concentration of the solids in the system reaches a certain level (Liu and Barigou, 2013). Furthermore, PEPT provides a unique perspective on the system, where observation of both bulk properties, as well as local dynamics of individual particles is desired.

PEPT has also been used in conjunction with optical techniques, such as in the case of tracking the motion of froths using both PEPT and high speed capture (Cole *et al.*, 2010a). The combination of the techniques allowed correlation of the velocities derived from PEPT particle motion and the images of the particles moving in a column, where random events, such as bubble coalescence, could be captured and used when interpreting the sudden changes in tracer velocity observed through PEPT.

Another system where PEPT was compared with other non-invasive techniques is a fluidised bed, where MRI and ultra-fast X-ray imaging were used to determine the size of the air jet as it travels through the bed (Pore *et al.*, 2015). In the study the jet shape obtained through imaging using MRI and X-ray techniques were contrasted against the fractional occupancy count derived from PEPT particle locations. Ultra-fast X-ray was shown to be the most accurate at imaging the jet at high velocities, but under predicted the size of the jet at low speeds, due to the minimum size of detection inherent of the technique. MRI on the other hand was better suited for slower moving jets, as at higher velocities attenuation was observed as the particles were passing out of the Imaging slice

during acquisition. Finally, PEPT was shown to produce reliable results across the velocity range, in addition to providing additional data about the system, such as tracer locations and movement patterns, which cannot be obtained using the other techniques applied. Figure 2.20 shows the correlation of jet dimensions to gas velocity as estimated using the three techniques.

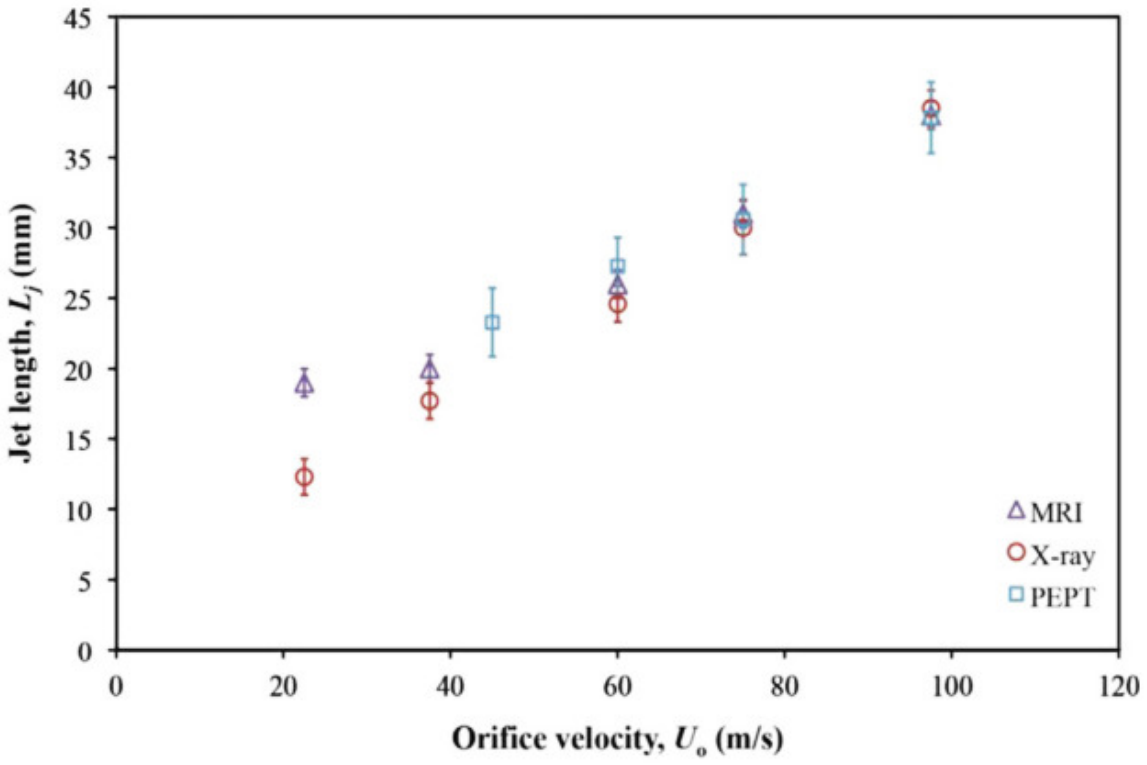

Figure 2.20. Jet length observed in fluidised beds measured using a characteristic parameter approach using 3 distinct techniques, through PEPT occupancy times and MRI and X-ray signal intensity. From (Pore et al., 2015)

2.2.5.4 PEPT APPLICATION FOR SOLID MEDIA TRACKING

Whether it is milling, extrusion, tumbling or flow of gasses through fluidised beds, or dynamics of slurries, relatively small solid particulates are widely used in many systems that pose interest to both academic and industrial research (Bbosa *et al.*, 2011; Fan *et al.*, 2008b; Yu *et al.*, 2015). Through traditional tracer preparation techniques as well as through surface chemistry modification with metal ions, as described above, many such

solid particulates can be either directly activated or mimicked using readily available materials, by matching properties such as size distribution and density. This allows a wide range of systems to be studied using PEPT without any additional modification to the established process, unlike other techniques, where either the construction materials or the medium that is being tracked need to be adapted to accommodate the technique used. Table 2.3 summarises the work that has been published on the topic of PEPT applications for characterisation of real systems.

This section reviews the research carried out using PEPT on systems where the bulk of the solid particles was tracked using a radioactive tracer.

Table 2.3. Summary of the recent publications using PEPT for the characterisation of various systems

Topic	**Authors**
Fluidised beds	(Hensler *et al.*, 2015) (Li *et al.*, 2014) (Laverman *et al.*, 2012) (Brems *et al.*, 2011) (Wong, 2006) (Stein *et al.*, 1998) (Snieders *et al.*, 1999) (Pore *et al.*, 2015) (Fan *et al.*, 2008b) (Van de Velden *et al.*, 2007) (Van de Velden et al., 2008a) (Schaafsma *et al.*, 2006) (Marston and Thoroddsen, 2015) (Garncarek *et al.*, 1997) (Mahmoudi *et al.*, 2012) (Mahmoudi *et al.*, 2011) (Hoomans *et al.*, 2001) (Depypere *et al.*, 2009) (Fan *et al.*, 2008a) (Stein *et al.*, 2000) (Stein *et al.*, 2002) (Chan *et al.*, 2010a) (Chan *et al.*, 2010b) (Chan *et al.*, 2009a) (Chan *et al.*, 2009b) (Chan *et al.*, 2009c)
Static mixers	(Rafiee *et al.*, 2013) (Rafiee *et al.*, 2011)
Granulators	(Lee *et al.*, 2012) (Saito *et al.*, 2011) (Laurent, 2005) (Ng et al., 2007a) (Forrest *et al.*, 2003)

	(Stewart *et al.*, 2001a) (Ng et al., 2007b)
Mills	(Volkwyn *et al.*, 2011) (Kallon *et al.*, 2011) (Bbosa *et al.*, 2011) (van der Westhuizen *et al.*, 2011) (Barley *et al.*, 2004) (Kallon *et al.*, 2011) (Yu *et al.*, 2015) (Govender *et al.*, 2013)
Hydrocyclones	(Radman *et al.*, 2014) (Chang *et al.*, 2011)
Mixers	(Pasha *et al.*, 2015) (Laurent and Cleary, 2012) (Kuo *et al.*, 2005) (Jones *et al.*, 2007) (Laurent, 2002) (Broadbent *et al.*, 1993) (Zhou *et al.*, 2004) (Marigo *et al.*, 2013) (Knight *et al.*, 2001) (Stewart *et al.*, 2001b) (Jones and Bridgwater, 1998) (Broadbent *et al.*, 1995) (Portillo *et al.*, 2010)
Stirred tanks	(Chiti *et al.*, 2011) (Pianko-Oprych *et al.*, 2009) (Fangary *et al.*, 2000) (Liu and Barigou, 2013) (Fangary *et al.*, 1999) (Fishwick *et al.*, 2005) (Fishwick *et al.*, 2003)
Rotating drums/cans	(Yang *et al.*, 2014) (Z. Yang et al., 2008) (Cox *et al.*, 2003) (Ingram *et al.*, 2005) (Yang *et al.*, 2003) (Lim *et al.*, 2003) (Ding *et al.*, 2002) (Parker *et al.*, 1997b)
Domestic appliances	(Pérez-Mohedano *et al.*, 2015) (Mac Namara *et al.*, 2012)
Foams/Froths	(Cole *et al.*, 2010a) (Cole *et al.*, 2010b) (Waters *et al.*, 2008)

Mills

PEPT has been applied in a number of studies investigating the dynamics of different types of mills, with the majority of work done on vertically stirred mills and tumbling mills.

In the case of vertically stirred mills PEPT was used to study how changing certain properties of the system affects the particle dynamics, where parameters such as impeller type (Figure 2.21), impeller speed, size of the solid beads used, filling ratio and density of the slurry were varied (Barley *et al.*, 2004). Three distinct areas were identified inside the milling vessel, above, below and around the impeller and the effects of varying the system properties on the dynamics in these regions was assessed using occupancy and tracer particle speed (Conway-Baker *et al.*, 2002). Furthermore, post milling the bulk of the slurry was analysed using a Malvern Mastersizer to assess the milling and correlate the dynamics of particle motion to the size reduction of the solid beads.

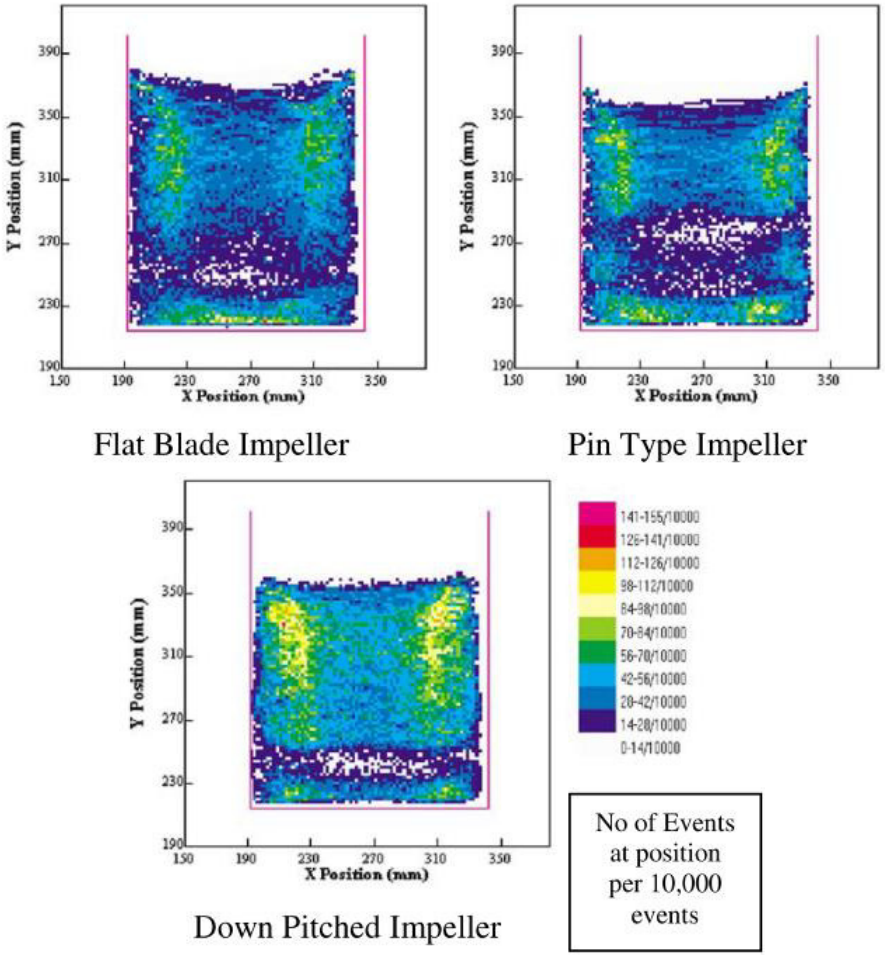

Figure 2.21. Occupancy plots in a vertically stirred mill for different impeller types at 520 rpm. From (Conway-Baker et al., 2002)

Fluidised beds

Different configurations of fluidised beds are found in industry, varying by the shape of the bed, the gas injection method and the type of particles used. Fluidised beds can be used for catalytic reactions and gas scrubbing (Scalo, 2013), coating (Depypere *et al.*, 2009), food processing (Smith, 2007), *etc.* The application of the fluidised bed dictates its type, for example stationary fluidised beds are defined by the low gas velocity and little to none motion of the solids, while circulating fluidised beds (CFB) operate at much higher gas velocities and are defined by the characteristic motion of the particles around the bed.

As can be seen in Table 2.3, fluidised beds are the system to which PEPT is applied most frequently, due to the lack of other reliable techniques for characterisation of such systems (Stein *et al.*, 2000). Understanding the particle and gas dynamics within fluidised beds is essential for design and scale up of equipment, as fluidised beds tend to be very sensitive to variations in processing conditions, where shifts between different operating regimes are possible if the system conditions are not correctly defined (Chan *et al.*, 2010b). PEPT has been used to gain insight into the dynamics of a range of fluidised bed configurations as well as utilised to validate existing models describing the bed dynamics. Using PEPT it was observed that in circulating fluidised beds the upward motion occurs in the centre, with the upward velocity of the particles *ca.*50% of the gas velocity, while downward motion takes place by the walls, for the case of Group B particles. Figure 2.22 illustrates an example of the velocity distribution in such a system (Fan *et al.*, 2008b). It was further established that lateral mixing in the above system only occurs on the top of the column, where the gas bubbles burst and near the distributor at the bottom, where the upward and downward motion cycles begin. Furthermore, the shear stress at the interface between the upward and downward moving particles was observed to lead to an increase in the granular temperature, promoting lateral mixing (Stein *et al.*, 2000). Other insights

into the dynamics of circulating fluidised beds included defining the different hydrodynamic regimes as the function of gas velocity and solid circulation flux, leading to an improvement in CFD design equations (Chan *et al.*, 2010b). Other PEPT application for fluidised beds included coating uniformity (Depypere *et al.*, 2009), bubble behaviour prediction (Li *et al.*, 2014; Schaafsma *et al.*, 2006), as well as other solids particle behaviour studies (Fan *et al.*, 2008a; Van de Velden *et al.*, 2008; Wong, 2006)

Experimental PEPT results revealed that the dynamics within fluidised beds are much more complex than predicted by existing models, therefore PEPT has been used to validate and improve granular dynamics simulations. A study has used 15000 simulated particles to model 45 s of fluidised bed operation. In order to compare these to a real system a fluidised bed was run in PEPT for an hour. Two different particle interaction models were used in the granular dynamics simulation, and it was found that when compared to PEPT the model using measured collision parameters performed significantly better, with results comparable to PEPT data, while the model with fully elastic smoot collision parameters described the system poorly (Hoomans *et al.*, 2001).

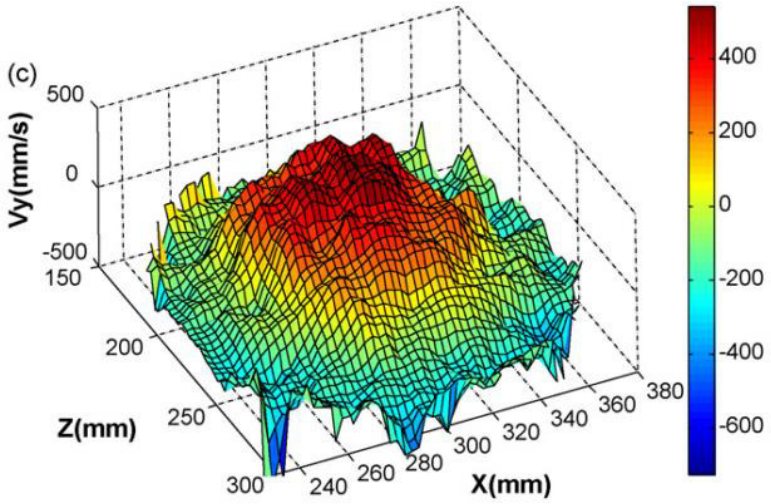

Figure 2.22. Example of a velocity map obtained through PEPT as seen at a cross-section at the top of a cylindrical circulating fluidised bed. From (Fan et al., 2008b)

Granulators

Granulators are used in industry to modify the size of the particles that are fed into the equipment or in order to prevent the segregation due to size or density differences within the particle mixture as it is fed into subsequent processes. Both wet and dry granulation processes are common, where wet granulation involves a binder fluid, which aids in forming the granules and is especially beneficial when very fine powders that do not flow well are used. Dry granulation is used on powders which could be sensitive to the addition of the binder and requires high pressure to achieve granulation (Boerefijn *et al.*, 2007; Litster and Ennis, 2013).

PEPT has been used to investigate the dynamics within both wet and dry granulator systems. It has been established that within a conical frustum-shaped vertical high shear mixer granulator the particles move in both vertical and horizontal directions under both wet and dry conditions, although after adding the liquid binder the circulation in the vertical direction decreases (Ng et al., 2007b). However, tangential motion of solids was found to be dominant under both conditions, with the maximum tangential velocity up to 12 times that of the axial and radial velocities. Furthermore, changing the speed of the impelled did not yield any observable change to the axial and radial velocities, while the ratio of tangential velocity to tip speed decreases with increasing tip speed (Ng et al., 2007a).

When applying PEPT to twin screw granulators it was concluded that in a wet granulator system when the speed and material throughput is increased the residence time decreases, as expected, however, the particle path trajectory remains comparable (Lee *et al.*, 2012). Furthermore, as different twin crew geometries were used, it was noted that the path trajectory still remained the same, implying that the different geometries used would result in a similar degree of axial mixing. However, to allow for particle location

acquisition lower speeds were used for this study, while studies using alternative techniques have determined an effect of feed rate and rpm of the screws on mixing (Kumar *et al.*, 2015).

Other solid tracking applications

PEPT has been used for a range of other applications tracking solid particle behaviour. Ploughshare mixers have been a focus of a number of papers, looking at factors such as fill levels and rotor frequency effect on the velocity distribution (Jones *et al.*, 2007), residence times (Jones and Bridgwater, 1998), flow patterns (Forrest *et al.*, 2003) and the validation of DEM model of the ploughshare mixer (Laurent and Cleary, 2012). Fill level and rotor frequency experiments have demonstrated that transaxial velocities are greater at higher rotor frequency and increase with fill level (Figure 2.23). It was also noted that the transaxial velocities are much greater than axial velocities.

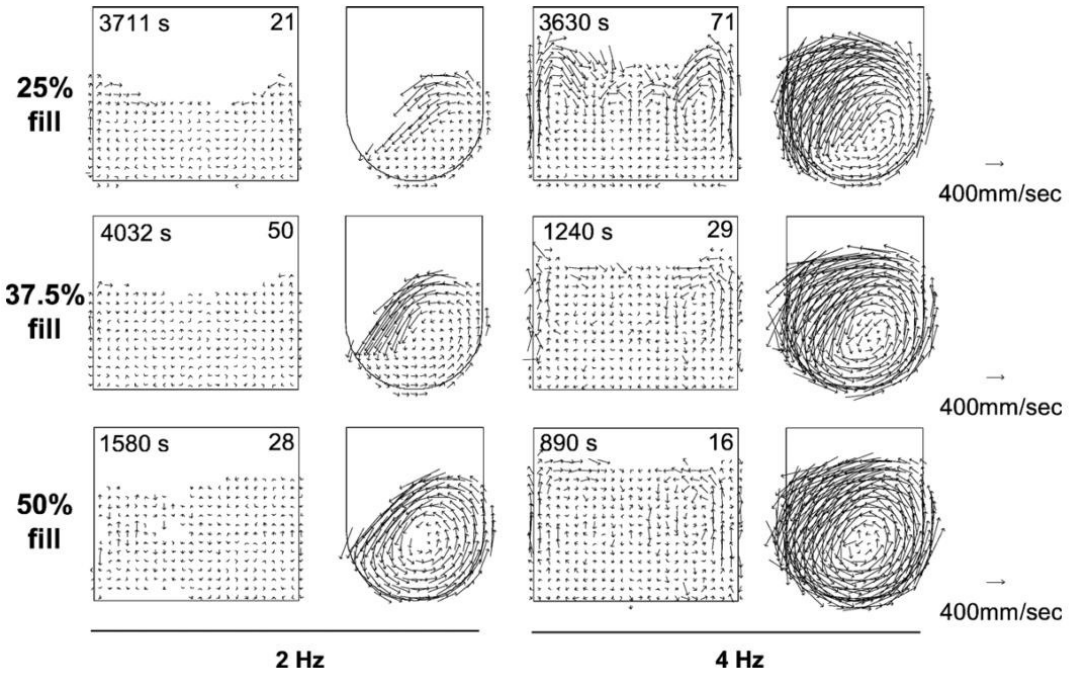

Figure 2.23. Side and end views of velocity at 2 Hz and 4 Hz for dry rice for fill levels from 25% to 50% v/v. Pixel size 10×10 mm. From (Jones et al., 2007)

Axial and radial dispersion assessment of particles in rotating drums has also been carried out using PEPT, where it was noted that the particle distribution is important in such systems, where mono- and poly-dispersed systems behaved differently, with axial and radial dispersion coefficients greater for poly-dispersed systems (Ingram *et al.*, 2005). Other studies have found agreement between the models using thin layer approximations to describe the dynamics within rotation drums and the results obtained from PEPT (Ding *et al.*, 2001).

2.2.5.5 PEPT APPLICATION FOR LIQUID TRACKING

Tracking the behaviour of the liquid continuous phase in industrial equipment can be beneficial when characterising a number of processes, ranging from simple geometries, such as pipes, to more complex equipment, such as static mixers or stirred tank reactors. The difficulty in characterising such systems using direct observation, such as optical techniques, or through modelling, traditionally lies not only in the complexities of the equipment, but also in the complexity of real, industrially relevant fluids, which often exhibit non-Newtonian behaviour. Applying PEPT to such systems allows tackling of both the geometry and the fluid complexity, by directly tracking the dynamics of the fluids.

When addressing a system which requires a liquid to be traced the approach to tracer selection is different than in a solid system. The tracer particles used need to be sufficiently small and possess density similar to that of the carrier fluid, to ensure neutral buoyancy, thus reducing the risk of particle separating from the fluid through either sedimentation or floatation. Smaller particle size also leads to reduced drag forces acting on the tracer, thus ensuring the tracer acts as a representation of a small volume of the carrier fluid, and not as a separate object. The ability of the tracer to act as a representation of a segment of the bulk fluid volume has been demonstrated by in previous work (Bakalis *et al.*, 2004), where the assessment of the particle trajectory when recirculated through a

simple geometry, such as circular pipes and rectangular channels, revealed that the reconstructed velocity profile based on particle locations derived from PEPT matched that predicted theoretically for a fully developed laminar flow. This has been demonstrated both for simple Newtonian fluids (Bakalis *et al.*, 2004), as well as for more complex non-Newtonian Power law fluids (Rafiee et al., 2013).

Stirred tanks

Stirred tanks have been studied using PEPT in conjunction with other techniques, both experimental and numerical. Different diameter baffled vessels containing fluids of varying viscosities and agitated by a Rushton turbine were studied by Chiti *et al.* (2011). The study compared the obtained results with those previously obtained using Laser Doppler Anemometry (LDA) on a similar system (Dyster *et al.*, 1993). While certain limitation were noted, such as reduction in detection density around the fast moving impeller, it was overall concluded that using PEPT to characterise a stirred tank under turbulent conditions results in accurate velocity detection across the entire volume of the system, as opposed to techniques such as LDA or particle image velocimetry (PIV), which only provide results across a 2D plane (Pianko-Oprych *et al.*, 2009).

Another study compared the performance of the different axial flow impellers, specifically Lightnin A320 and A410 (Fangary *et al.*, 2000). By comparing the velocity fields for Newtonian and non-Newtonian fluids, the authors found that while A320 has a higher agitation index and therefore produced higher velocities, A410 results displayed a better circulation index, suggesting higher efficiency and better circulation for a given power input.

Furthermore, PEPT has been used to verify CFD models of stirred tanks, for both liquids and solid-liquid suspensions. By assessing the “just suspended” state of a solid-

liquid system using PEPT it was possible to improve and finally validate a CFD model, accurately predicting the behaviour of the solids, even in hard to define areas of the system, such as the gap between the bottom of the tank and the impeller (Liu and Barigou, 2013). Further work successfully validated agitation regimes above the "just suspended" state, noticing a better distribution of finer particles, with homogeneity improving as the weight fraction of solids increases.

Static mixers

Static mixers are a type of inline equipment used to break up and redirect fluid streams, promoting mixing, often used as a part of continuous liquid processing lines. Conventional characterisation of such equipment often relies on assessing the outputs of immiscible fluid flow to determine the degree of mixing, for example oil and water (Das et al., 2013b) or gas and liquid (Fradette *et al.*, 2006), or though techniques such as MRI and ERT, which are limited by construction materials. Velocity profiles within static mixers have been predominantly studied using modelling (Fourcade *et al.*, 2001; Lisboa *et al.*, 2010), but have never been observed directly.

PEPT 3D spatial location and time data allows for the assessment of both the mixing dynamics as well as local velocities. This is achieved through the recirculation of a radioactive tracer through the system until enough particle passes have been obtained to cover the majority of the mixer volume, reaching up to 900 passes. Figure 2.24 illustrates an examples of the velocity maps as derived using PEPT data for different static mixer types (Rafiee et al., 2013).

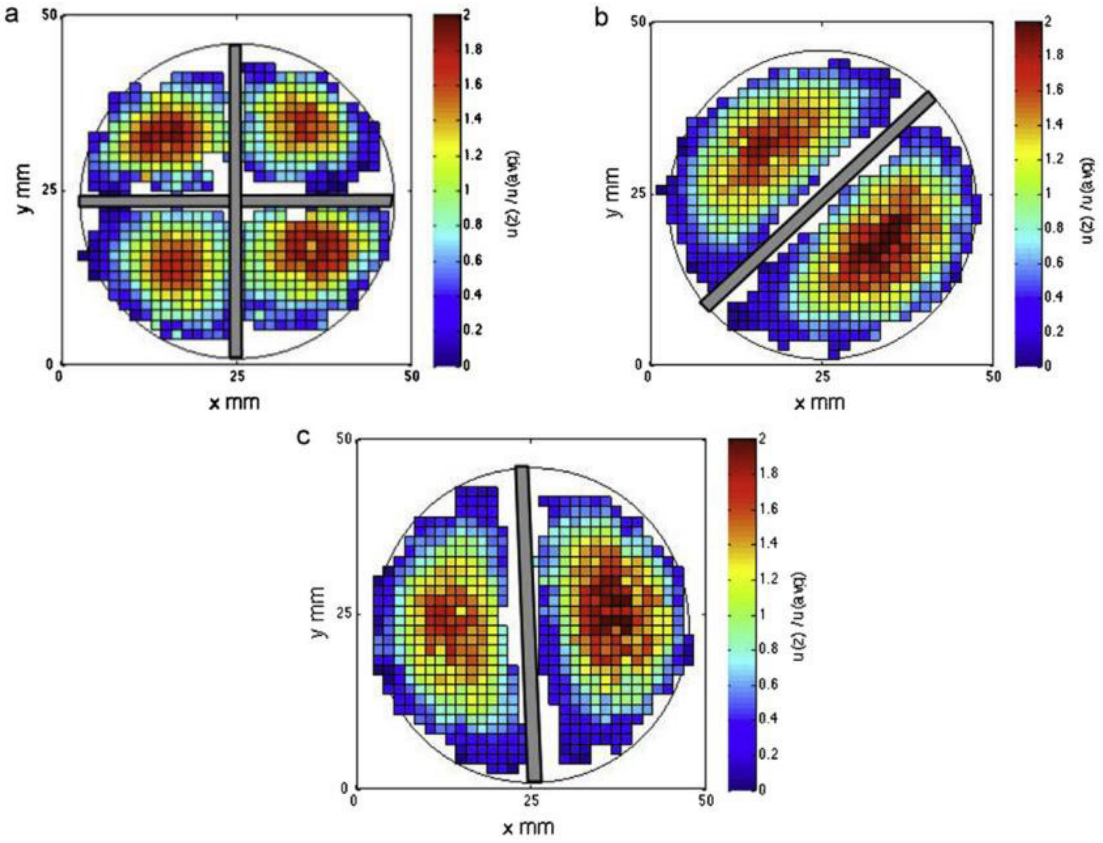

Figure 2.24. Eulerian axial velocity maps for glycerol flowing through a Sulzer mixer at various positions within the mixer. From (Rafiee et al., 2013)

Household appliances

The ability of γ-rays to penetrate significant thickness of metal, before attenuation renders the signal too weak has led to investigations of some unconventional systems, most notably washing machines (Mac Namara *et al.*, 2012) and dish washers (Pérez-Mohedano *et al.*, 2015).

The washing machine study most notably was capable of not only identifying the local velocity distributions and occupancies within the machine (Figure 2.25), but by further processing the velocity data the shear rate distributions were derived. These were noted to depend on the loading of the machine, *i.e.* the weight of the textile being washed. Shear rate is an essential factor during textile cleaning, as the removal of the soils relies on mechanical forces dislodging the particulates from the fabric.

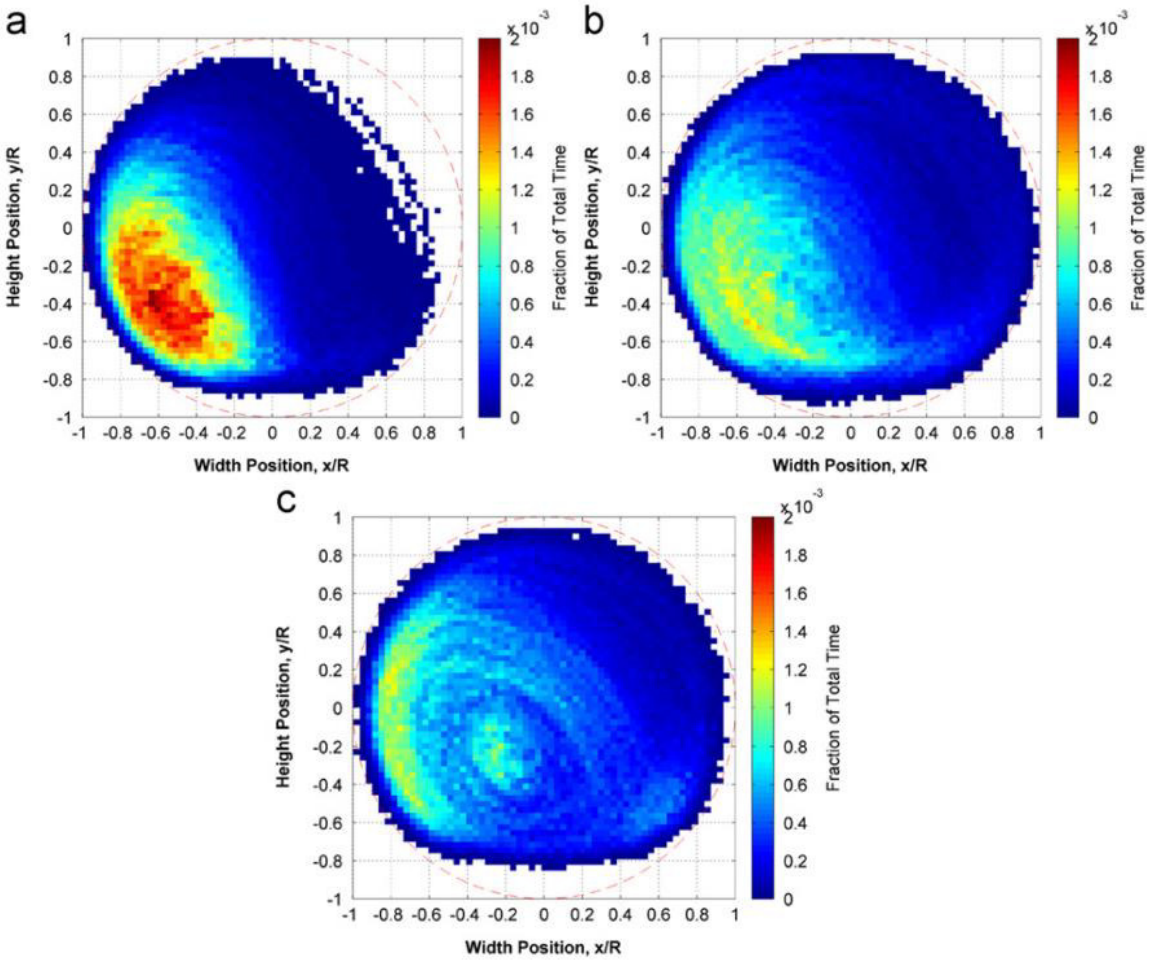

Figure 2.25. Occupancy results for different loadings in the washing machine (a) 1kg (b) 2kg (c) 3kg. From (Mac Namara et al., 2012)

2.3 CONCLUSIONS

The significance of static mixers across a range of industries is apparent from the versatility of their applications in both batch and continuous processes, however due to their complexity static mixers are often difficult to study. By looking at the existing academic literature it can be seen that SMX mixers in particular are of great interest and a source of great challenge to both the academic and the industrial communities, with the studies of internal mixer dynamics proving to be the most difficult.

The assessment of available techniques capable of overcoming the challenges presented by SMX mixers revealed that Positron Emission Particle Tracking is one of the more versatile techniques available for the job, with little to no modifications required to the static mixer equipment, while allowing to track flow in 3-dimentional space with respect to time.

Therefore, PEPT was selected as the main technique for the study of SMX mixer flow and mixing dynamics presented in this thesis.

2.4 REFERENCES

Atkins, M.D. (2016) 'Chapter 5 – Velocity Field Measurement Using Particle Image Velocimetry (PIV)', in *Thermo-Fluidic Measurement Techniques*, 125–166.

Bakalis, S., Cox, P.W., Russell, A.B., Parker, D.J., Fryer, P.J. (2006) 'Development and use of positron emitting particle tracking (PEPT) for velocity measurements in viscous fluids in pilot scale equipment', *Chemical Engineering Science*, 61(6), 1864–1877.

Bakalis, S., Fryer, P.J., Parker, D.J. (2004) 'Measuring velocity distributions of viscous fluids using positron emission particle tracking (PEPT)', *AIChE Journal*, 50(7), 1606–1613.

Bao, Y., Wang, B., Lin, M., Gao, Z., Yang, J. (2015) 'Influence of impeller diameter on overall gas dispersion properties in a sparged multi-impeller stirred tank', *Chinese Journal of Chemical Engineering*, 23(6), 890–896.

Barley, R.W., Conway-Baker, J., Pascoe, R.D., Kostuch, J., McLoughlin, B., Parker, D.J. (2004) 'Measurement of the motion of grinding media in a vertically stirred mill using positron emission particle tracking (PEPT) Part II', *Minerals Engineering*, 17(11–12), 1179–1187.

Bbosa, L.S., Govender, I., Mainza, A.N., Powell, M.S. (2011) 'Power draw estimations in experimental tumbling mills using PEPT', *Minerals Engineering*, 24(3–4), 319–324.

Bickell, M., Buffler, A., Govender, I., Parker, D.J. (2012) 'A new line density tracking algorithm for PEPT and its application to multiple tracers', *Nuclear Instruments and Methods in Physics Research Section A: Accelerators, Spectrometers, Detectors and Associated Equipment*, 682, 36–41.

Bieberle, M., Barthel, F. (2016) 'Combined phase distribution and particle velocity measurement in spout fluidized beds by ultrafast X-ray computed tomography', *Chemical Engineering Journal*, 285, 218–227.

Boerefijn, R., Dontula, P.-R., Kohlus, R. (2007) *Granulation*, Handbook of Powder Technology, Handbook of Powder Technology, Elsevier.

Boucher, D., Deng, Z., Leadbeater, T., Langlois, R., Renaud, M., Waters, K.E. (2014) 'PEPT studies of heavy particle flow within a spiral concentrator', *Minerals Engineering*, 62, 120–128.

Boucher, D., Gharib, N., Deng, Z., Leadbeater, T., Langlois, R., Waters, K.E. (2015) 'PEPT Validation of a CFD-DEM Model of a Fine Quartz Particle (60μm) Behaviour in Stirred Water', *Procedia Engineering*, 102, 1305–1315.

Brems, A., Chan, C.W., Seville, J.P.K., Parker, D., Baeyens, J. (2011) 'Modelling the transport disengagement height in fluidized beds', *Advanced Powder Technology*, 22(2), 155–161.

Broadbent, C.J., Bridgwater, J., Parker, D.J. (1995) 'The effect of fill level on powder mixer performance using a positron camera', *The Chemical Engineering Journal and The Biochemical Engineering Journal*, 56(3), 119–125.

Broadbent, C.J., Bridgwater, J., Parker, D.J., Keningley, S.T., Knight, P. (1993) 'A phenomenological study of a batch mixer using a positron camera', *Powder Technology*, 76(3), 317–329.

Buffler, A., Govender, I., Cilliers, J.J., Parker, D.J., Franzidis, J.-P., Mainza, A., Newman, R.T., Powell, M., van der Westhuizen, A. (2010) 'PEPT Cape Town: a new positron emission particle tracking facility at iThemba LABS', in *Proceedings of International Topical Meeting on Nuclear Research Applications and Utilization of Accelerators*, 4–8 May 2009, Vienna (IAEA, Vienna, 2010).

Cao, G., Sivukari, M., Kurnitski, J., Ruponen, M., Seppänen, O. (2010) 'Particle Image Velocimetry (PIV) application in the measurement of indoor air distribution by an active chilled beam', *Building and Environment*, 45, 1932–1940.

Chan, C.W., Brems, A., Mahmoudi, S., Baeyens, J., Seville, J., Parker, D., Leadbeater, T., Gargiuli, J. (2010) 'PEPT study of particle motion for different riser exit geometries', *Particuology*, 8(6), 623–630.

Chan, C.W., Seville, J., Fan, X., Baeyens, J. (2009a) 'Solid particle motion in a standpipe as observed by Positron Emission Particle Tracking', *Powder Technology*, 194(1–2), 58–66.

Chan, C.W., Seville, J., Fan, X., Baeyens, J. (2009b) 'Particle motion in L-valve as observed by positron emission particle tracking', *Powder Technology*, 193(2), 137–149.

Chan, C.W., Seville, J., Yang, Z., Baeyens, J. (2009) 'Particle motion in the CFB riser with special emphasis on PEPT-imaging of the bottom section', *Powder Technology*, 196(3), 318–325.

Chan, C.W., Seville, J.P.K., Parker, D.J., Baeyens, J. (2010) 'Particle velocities and their residence time distribution in the riser of a CFB', *Powder Technology*, 203(2), 187–197.

Chang, Y.F., Ilea, C.G., Aasen, L., Hoffmann, A.C. (2011) 'Particle flow in a hydrocyclone investigated by positron emission particle tracking', *Chemical Engineering Science*, 66(18), 4203–4211.

Chen, J., Kemoun, A., Al-Dahhan, M.H., Duduković, M.P., Lee, D.J., Fan, L.S. (1999) 'Comparative hydrodynamics study in a bubble column using computer-automated radioactive particle tracking (CARPT)/computed tomography (CT) and particle image velocimetry (PIV)', *Chemical Engineering Science*, 54(13–14), 2199–2207.

Chiti, F., Bakalis, S., Bujalski, W., Barigou, M., Eaglesham, A., Nienow, A.W. (2011) 'Using positron emission particle tracking (PEPT) to study the turbulent flow in a baffled vessel agitated by a Rushton turbine: Improving data treatment and validation', *Chemical Engineering Research and Design*, 89(10), 1947–1960.

Cole, K.E., Waters, K.E., Fan, X., Neethling, S.J., Cilliers, J.J. (2010) 'Combining Positron Emission Particle Tracking and image analysis to interpret particle motion in froths', *Minerals Engineering*, 23(11–13), 1036–1044.

Cole, K.E., Waters, K.E., Parker, D.J., Neethling, S.J., Cilliers, J.J., Parker, D.J., Neethling, S.J. (2010) 'PEPT combined with high speed digital imaging for particle tracking in dynamic foams', *Chemical Engineering Science*, 65(5), 1887–1890.

Conway-Baker, J., Barley, R.W., Williams, R.A., Jia, X., Kostuch, J., McLoughlin, B., Parker, D.J. (2002) 'Measurement of the motion of grinding media in a vertically stirred mill using positron emission particle tracking (PEPT)', *Minerals Engineering*, 15(1–2), 53–59.

Cox, P.W., Bakalis, S., Ismail, H., Forster, R., Parker, D.J., Fryer, P.J. (2003) 'Visualisation of three-dimensional flows in rotating cans using positron emission particle tracking (PEPT)', *Journal of Food Engineering*, 60(3), 229–240.

Das, M.D., Hrymak, A.N., Baird, M.H.I. (2013) 'Laminar liquid–liquid dispersion in the SMX static mixer', *Chemical Engineering Science*, 101, 329–344.

Degaleesan, S., Dudukovic, M.P., Pan, Y. (2002) 'Application of wavelet filtering to the radioactive particle tracking technique', *Flow Measurement and Instrumentation*, 13(1–2), 31–43.

Depypere, F., Pieters, J.G., Dewettinck, K. (2009) 'PEPT visualisation of particle motion in a tapered fluidised bed coater', *Journal of Food Engineering*, 93(3), 324–336.

Ding, Y.L., Forster, R., Seville, J.P.K., Parker, D.J. (2002) 'Segregation of granular flow in the transverse plane of a rolling mode rotating drum', *International Journal of Multiphase Flow*, 28(4), 635–663.

Ding, Y.L., Seville, J.P.K., Forster, R., Parker, D.J. (2001) 'Solids motion in rolling mode rotating drums operated at low to medium rotational speeds', *Chemical Engineering Science*, 56(5), 1769–1780.

Dudukovic, M.P. (2002) 'Opaque multiphase flows: Experiments and modeling', *Experimental Thermal and Fluid Science*, 26(6–7), 747–761.

Dyster, K.N., Koutsakos, E., Jaworski, Z., Nienow, A.W. (1993) 'An LDA study of the radial discharge velocities generated by a Rushton turbine: Newtonian fluids, Re ≥ 5', *Chemical engineering research and design*, 71(1), 11–23.

Escudero, D.R., Heindel, T.J. (2014) 'Acoustic fluidized bed hydrodynamics characterization using X-ray computed tomography', *Chemical Engineering Journal*, 243, 411–420.

Fairhurst, P.G., Barigou, M., Fryer, P.J., Pain, J.P., Parker, D.J. (2001) 'Using positron emission particle tracking (PEPT) to study nearly neutrally buoyant particles in high solid fraction pipe flow', *International Journal of Multiphase Flow*, 27(11), 1881–1901.

Fan, X., Parker, D.J., Smith, M.D. (2006) 'Enhancing 18F uptake in a single particle for positron emission particle tracking through modification of solid surface chemistry', *Nuclear Instruments and Methods in Physics Research Section A: Accelerators, Spectrometers, Detectors and Associated Equipment*, 558(2), 542–546.

Fan, X., Parker, D.J., Yang, Z., Seville, J.P.K., Baeyens, J. (2008) 'The effect of bed materials on the solid/bubble motion in a fluidised bed', *Chemical Engineering Science*, 63(4), 943–950.

Fan, X., Yang, Z., Parker, D.J., Armstrong, B. (2008) 'Prediction of bubble behaviour in fluidised beds based on solid motion and flow structure', *Chemical Engineering Journal*, 140(1–3), 358–369.

Fangary, Y., Seville, J.P.K., Barigou, M. (1999) 'Flow studies in stirred tanks by Positron Emission Particle Tracking (PEPT)', in *Fluid Mixing 6, 7-8 July, Bradford*, 23–34.

Fangary, Y.S., Barigou, M., Seville, J.P.K., Parker, D.J. (2000) 'Fluid trajectories in a stirred vessel of non-Newtonian liquid using positron emission particle tracking', *Chemical Engineering Science*, 55, 5969–5979.

Fishwick, R., Winterbottom, M., Parker, D., Fan, X., Stitt, H. (2005) 'The Use of Positron Emission Particle Tracking in the Study of Multiphase Stirred Tank Reactor Hydrodynamics', *The Canadian Journal of Chemical Engineering*, 83, 97–103.

Fishwick, R.P., Winterbottom, J.M., Stitt, E.H. (2003) 'Explaining mass transfer observations in multiphase stirred reactors: Particle-liquid slip velocity measurements using PEPT', in *Catalysis Today*, 195–202.

Forrest, S., Bridgwater, J., Mort, P.R., Litster, J., Parker, D.J. (2003) 'Flow patterns in granulating systems', *Powder Technology*, 130(1–3), 91–96.

Fourcade, E., Wadley, R., Hoefsloot, H.C.., Green, A., Iedema, P.D. (2001) 'CFD calculation of laminar striation thinning in static mixer reactors', *Chemical Engineering Science*, 56(23), 6729–6741.

Fradette, L., Li, H.-Z., Choplin, L., Tanguy, P. (2006) 'Gas/liquid dispersions with a SMX static mixer in the laminar regime', *Chemical Engineering Science*, 61(11), 3506–3518.

Fradette, L., Tanguy, P., Li, H.-Z., Choplin, L. (2007) 'Liquid/Liquid Viscous Dispersions with a SMX Static Mixer', *Chemical Engineering Research and Design*, 85(3), 395–405.

Fu, S., Biwolé, P., Mathis, C. (2015) 'A Comparative Study of Particle Image Velocimetry (PIV) and Particle Tracking Velocimetry (PTV) for Airflow Measurement', *International Journal of Mechanical, Aerospace, Industrial, Mechatronic and Manufacturing Engineering*, 9(1), 40–45.

Garncarek, Z., Przybylski, L., Botterill, J.S.M., Broadbent, C.J. (1997) 'A quantitative assessment of the effect of distributor type on particle circulation', *Powder Technology*, 91(3), 209–216.

Ghanem, A., Habchi, C., Lemenand, T., Della Valle, D., Peerhossaini, H. (2013) 'Energy efficiency in process industry – High-efficiency vortex (HEV) multifunctional heat exchanger', *Renewable Energy*, 56, 96–104.

Ghanem, A., Lemenand, T., Della Valle, D., Peerhossaini, H. (2014) 'Static mixers: Mechanisms, applications, and characterization methods – A review', *Chemical Engineering Research and Design*, 92(2), 205–228.

Godfrey, J.C. (2001) 'Static mixers', *Metal Finishing*, 99(11), 83–84.

Govender, I., Cleary, P.W., Mainza, A.N. (2013) 'Comparisons of PEPT derived charge features in wet milling environments with a friction-adjusted DEM model', *Chemical Engineering Science*, 97, 162–175.

Gundogdu, O., Tarcan, E. (2004) 'Location-allocation algorithm for multiple particle tracking using Birmingham MWPC positron camera', *Nuclear Instruments and Methods in Physics Research, Section A: Accelerators, Spectrometers, Detectors and Associated Equipment*, 523(1–2), 223–233.

Hammoudi, M., Legrand, J., Si-Ahmed, E.K., Salem, A. (2008) 'Flow analysis by pulsed ultrasonic velocimetry technique in Sulzer SMX static mixer', *Chemical Engineering Journal*, 139(3), 562–574.

Hensler, T., Tupy, M., Strer, T., Pöschel, T., Wirth, K.-E. (2015) 'Positron emission particle tracking in fluidized beds with secondary gas injection', *Powder Technology*, 279, 113–122.

Hirech, K., Arhaliass, A., Legrand, J. (2003) 'Experimental Investigation of Flow Regimes in an SMX Sulzer Static Mixer', *Industrial & Engineering Chemistry Research*, 42(7), 1478–1484.

Hirschberg, S., Koubek, R., Schöck, J. (2009) 'An improvement of the Sulzer SMXTM static mixer significantly reducing the pressure drop', *Chemical Engineering Research and Design*, 87(4), 524–532.

Hoomans, B.P.B., Kuipers, J. a M., Mohd Salleh, M. a., Stein, M., Seville, J.P.K. (2001) 'Experimental validation of granular dynamics simulations of gas-fluidised beds with homogenous in-flow conditions using Positron Emission Particle Tracking', *Powder Technology*, 116, 166–177.

Ilankoon, I.M.S.K., Cole, K.E., Neethling, S.J. (2013) 'Measuring hydrodynamic dispersion coefficients in unsaturated packed beds: Comparison of PEPT with conventional tracer tests', *Chemical Engineering Science*, 89, 152–157.

Ingram, A., Seville, J.P.K., Parker, D.J., Fan, X., Forster, R.G. (2005) 'Axial and radial dispersion in rolling mode rotating drums', *Powder Technology*, 158(1–3), 76–91.

Jones, J.R., Bridgwater, J. (1998) 'A case study of particle mixing in a ploughshare mixer using Positron Emission Particle Tracking', *International Journal of Mineral Processing*, 53, 29–38.

Jones, J.R., Parker, D.J., Bridgwater, J. (2007) 'Axial mixing in a ploughshare mixer', *Powder Technology*, 178(2), 73–86.

Kallon, D.V.V., Govender, I., Mainza, A.N. (2011) 'Circulation rate modelling of mill charge using position emission particle tracking', *Minerals Engineering*, 24(3–4), 282–289.

Khopkar, A.R., Rammohan, A.R., Ranade, V. V., Dudukovic, M.P. (2005) 'Gas-liquid flow generated by a Rushton turbine in stirred vessel: CARPT/CT measurements and CFD simulations', *Chemical Engineering Science*, 60(8–9 SPEC. ISS.), 2215–2229.

Kinugasa, T., Kuwagi, K., Leadbeater, T.W., Gargiuli, J., Parker, D.J., Seville, J.P.K., Yoshida, K., Amano, H. (2015) 'Three-dimensional dynamic imaging of sand particles under wheel via gamma-ray camera system', *Journal of Terramechanics*, 62, 5–17.

Knight, P.C., Seville, J.P.K., Wellm, A. B., Instone, T. (2001) 'Prediction of impeller torque in high shear powder mixers', *Chemical Engineering Science*, 56, 4457–4471.

Kowalski, A.J., Cooke, M., Hall, S. (2011) 'Expression for turbulent power draw of an in-line Silverson high shear mixer', *Chemical Engineering Science*, 66(3), 241–249.

Kumar, A., Alakarjula, M., Vanhoorne, V., Toiviainen, M., De Leersnyder, F., Vercruysse, J., Juuti, M., Ketolainen, J., Vervaet, C., Remon, J.P., Gernaey, K. V., De Beer, T., Nopens, I. (2015) 'Linking granulation performance with residence time and granulation liquid distributions in twin-screw granulation: An experimental investigation', *European Journal of Pharmaceutical Sciences*, 1–13.

Kuo, H.P., Knight, P.C., Parker, D.J., Burbidge, A.S., Adams, M.J., Seville, J.P.K. (2003) 'Non-equilibrium particle motion in the vicinity of a single blade', *Powder Technology*, 132(1), 1–9.

Kuo, H.P.P., T, P.C.K., Parker, D.J.J., Seville, J.P.K.P.K., Knight, P.C. (2005) 'Solids circulation and axial dispersion of cohesionless particles in a V-mixer', *Powder Technology*, 152(1–3), 133–140.

Laurent, B. (2002) 'Convection and segregation in a horizontal mixer', *Powder Technology*, 123(1), 9–18.

Laurent, B.F.C. (2005) 'Structure of powder flow in a planetary mixer during wet-mass granulation', *Chemical Engineering Science*, 60(14), 3805–3816.

Laurent, B.F.C., Cleary, P.W. (2012) 'Comparative study by PEPT and DEM for flow and mixing in a ploughshare mixer', *Powder Technology*, 228, 171–186.

Laverman, J. A., Fan, X., Ingram, A., Annaland, V.S.M., Parker, D.J., Seville, J.P.K., Kuipers, J. a M. (2012) 'Experimental study on the influence of bed material on the scaling of solids circulation patterns in 3D bubbling gas-solid fluidized beds of glass and polyethylene using positron emission particle tracking', *Powder Technology*, 224, 297–305.

Leadbeater, T.W., Parker, D.J. (2011) 'A modular positron camera for the study of industrial processes', *Nuclear Instruments and Methods in Physics Research, Section A: Accelerators, Spectrometers, Detectors and Associated Equipment*, 652(1), 646–649.

Leadbeater, T.W., Parker, D.J., Gargiuli, J. (2012) 'Positron imaging systems for studying particulate, granular and multiphase flows', *Particuology*, 10(2), 146–153.

Lee, K.T., Ingram, A., Rowson, N. a. (2012) 'Twin screw wet granulation: The study of a continuous twin screw granulator using Positron Emission Particle Tracking (PEPT) technique', *European Journal of Pharmaceutics and Biopharmaceutics*, 81(3), 666–673.

Legrand, J., Morançais, P., Carnelle, G. (2001) 'Liquid-Liquid Dispersion in an SMX-Sulzer Static Mixer', *Chemical Engineering Research and Design*, 79(8), 949–956.

Lehwald, A., Leschka, S., Zähringer, K., Thévenin, D. (2008) 'Fluid dynamics and mixing behavior of a static mixer using simultaneously Particle Image Velocimetry and Planar Laser-Induced Fluorescence measurements. Experimental set-up and measurement methods', in *14th Int Symp on Applications of Laser Techniques to Fluid Mechanics*, 7–10.

Li, F.-C., Hishida, K. (2009) 'Particle Image Velocimetry Techniques and its Applications in Multiphase Systems', in *Characterization of Flow, Particles and Interfaces*, 87–147.

Li, J. (2009) *Advances in Chemical Engineering 37: Characterization of Flow, Particles and Interfaces*, Advances in chemical engineering.

Li, Y., Fan, H., Fan, X. (2014) 'Identify of flow patterns in bubbling fluidization', *Chemical Engineering Science*, 117, 455–464.

Lim, S.Y., Davidson, J.F., Forster, R.N., Parker, D.J., Scott, D.M., Seville, J.P.K. (2003) 'Avalanching of granular material in a horizontal slowly rotating cylinder: PEPT studies', *Powder Technology*, 138, 25–30.

Lisboa, P.F., Fernandes, J., Simões, P.C., Mota, J.P.B., Saatdjian, E. (2010) 'Computational-fluid-dynamics study of a Kenics static mixer as a heat exchanger for supercritical carbon dioxide', *The Journal of Supercritical Fluids*, 55(1), 107–115.

Litster, J., Ennis, B. (2013) *The Science and Engineering of Granulation Processes*, Springer Science & Business Media.

Liu, L., Barigou, M. (2013) 'Numerical modelling of velocity field and phase distribution in dense monodisperse solid-liquid suspensions under different regimes of agitation: CFD and PEPT experiments', *Chemical Engineering Science*, 101, 837–850.

Liu, S., Hrymak, A.N., Wood, P.E. (2005) 'Drop Breakup in an SMX Static Mixer in Laminar Flow', *The Canadian Journal of Chemical Engineering*, 83(October), 793–807.

Mahmoudi, S., Baeyens, J., Seville, J. (2011) 'The solids flow in the CFB-riser quantified by single radioactive particle tracking', *Powder Technology*, 211(1), 135–143.

Mahmoudi, S., Chan, C.W., Brems, A., Seville, J., Baeyens, J. (2012) 'Solids flow diagram of a CFB riser using Geldart B-type powders', *Particuology*, 10(1), 51–61.

Marigo, M., Davies, M., Leadbeater, T., Cairns, D.L., Ingram, A., Stitt, E.H. (2013) 'Application of positron emission particle tracking (PEPT) to validate a discrete element method (DEM) model of granular flow and mixing in the Turbula mixer', *International Journal of Pharmaceutics*, 446(1–2), 46–58.

Marston, J.O., Thoroddsen, S.T. (2015) 'Investigation of granular impact using positron emission particle tracking', *Powder Technology*, 274, 284–288.

Matter, S., Haward, S.J., Ober, T.J., Oliveira, S.N., Alves, A., Mckinley, G.H. (2012) 'Extensional rheology and elastic instabilities of a wormlike micellar solution in a microfluidic cross-slot device', *Soft Matter*, (8), 536–555.

Meijer, H.E.H., Singh, M.K., Anderson, P.D. (2012a) 'On the performance of static mixers: A quantitative comparison', *Progress in Polymer Science*, 37(10), 1333–1349.

Meijer, H.E.H., Singh, M.K., Anderson, P.D. (2012b) 'On the performance of static mixers: A quantitative comparison', *Progress in Polymer Science*, 37(10), 1333–1349.

Mihailova, O., Lim, V., McCarthy, M.J., McCarthy, K.L., Bakalis, S. (2015) 'Laminar mixing in a SMX static mixer evaluated by positron emission particle tracking (PEPT) and magnetic resonance imaging (MRI)', *Chemical Engineering Science*, 137, 1014–1023.

Morancais, P., Hirech, K., Carnelle, G., Legrand, J. (1999) 'Friction factor in static mixer and determination of geometric parameters of SMX Sulzer mixers', *Chemical Engineering Communications*, 171(1), 77–93.

Moroni, M., Cushman, J.H., Cenedese, A. (2003) 'A 3D-PTV two-projection study of pre-asymptotic dispersion in porous media which are heterogeneous on the bench scale', *International Journal of Engineering Science*, 41(3–5), 337–370.

Mac Namara, C., Gabriele, A., Amador, C., Bakalis, S. (2012) 'Dynamics of textile motion in a front-loading domestic washing machine', *Chemical Engineering Science*, 75, 14–27.

Nelson, G., Reilly, D. (1991) 'Gamma-ray interactions with matter', in *Passive Non-destructive Analysis of Nuclear Materials*, 27–42.

Ng, B.H., Kwan, C.C., Ding, Y.L., Ghadiri, M., Fan, X.F. (2007a) 'Solids motion in a conical frustum-shaped high shear mixer granulator', *Chemical Engineering Science*, 62(3), 756–765.

Ng, B.H., Kwan, C.C., Ding, Y.L., Ghadiri, M., Fan, X.F. (2007b) 'Solids motion of calcium carbonate particles in a high shear mixer granulator: A comparison between dry and wet conditions', *Powder Technology*, 177, 1–11.

Parker, D.J., Allen, D. a., Benton, D.M., Fowles, P., McNeil, P. a., Tan, M., Beynon, T.D. (1997) 'Developments in particle tracking using the Birmingham Positron Camera', *Nuclear Instruments and Methods in Physics Research, Section A: Accelerators, Spectrometers, Detectors and Associated Equipment*, 392(1–3), 421–426.

Parker, D.J., Broadbent, C.J., Fowles, P., Hawkesworth, M.R., McNeil, P. (1993) 'Positron emission particle tracking - a technique for studying flow within engineering equipment', *Nuclear Instruments and Methods in Physics Research Section A: Accelerators, Spectrometers, Detectors and Associated Equipment*, 326(3), 592–607.

Parker, D.J., Dijkstra, A.E., Martin, T.W., Seville, J.P.K. (1997) 'Positron emission particle tracking studies of spherical particle motion in rotating drums', *Chemical Engineering Science*, 52(13), 2011–2022.

Parker, D.J., Fan, X. (2008) 'Positron emission particle tracking-Application and labelling techniques', *Particuology*, 6, 16–23.

Parker, D.J., Forster, R.N., Fowles, P., Takhar, P.S. (2002) 'Positron emission particle tracking using the new Birmingham positron camera', *Nuclear Instruments and Methods in Physics Research, Section A: Accelerators, Spectrometers, Detectors and Associated Equipment*, 477, 540–545.

Parker, D.J., Leadbeater, T.W., Fan, X., Hausard, M.N., Ingram, A., Yang, Z. (2008) 'Positron imaging techniques for process engineering: recent developments at Birmingham', *Measurement Science and Technology*, 19(9), 1–10.

Parker, D.J., McNeil, P.A. (1996) 'Positron emission tomography for process applications', *Measurement Science and Technology*, 7(3), 287–296.

Pasha, M., Hassanpour, A., Ahmadian, H., Tan, H.S., Bayly, A., Ghadiri, M. (2015) 'A comparative analysis of particle tracking in a mixer by discrete element method and positron emission particle tracking', *Powder Technology*, 270, 569–574.

Paul, E.L., Atieno-Obeng, V.A., Kresta, S.M. (2004) *Handbook of Industrial Mixing*, John Wiley & Sons.

Pérez-Mohedano, R., Letzelter, N., Amador, C., VanderRoest, C.T., Bakalis, S. (2015) 'Positron Emission Particle Tracking (PEPT) for the analysis of water motion in a domestic dishwasher', *Chemical Engineering Journal*, 259, 724–736.

Pianko-Oprych, P., Nienow, A.W., Barigou, M. (2009) 'Positron emission particle tracking (PEPT) compared to particle image velocimetry (PIV) for studying the flow generated by a pitched-blade turbine in single phase and multi-phase systems', *Chemical Engineering Science*, 64(23), 4955–4968.

Pore, M., Ong, G.H., Boyce, C.M., Materazzi, M., Gargiuli, J., Leadbeater, T., Sederman, J., Dennis, J.S., Holland, D.J., Ingram, A., Lettieri, P., Parker, D.J. (2015) 'A

comparison of magnetic resonance, X-ray and positron emission particle tracking measurements of a single jet of gas entering a bed of particles', *Chemical Engineering Science*, 122, 210–218.

Portillo, P.M., Vanarase, A.U., Ingram, A., Seville, J.K., Ierapetritou, M.G., Muzzio, F.J. (2010) 'Investigation of the effect of impeller rotation rate, powder flow rate, and cohesion on powder flow behavior in a continuous blender using PEPT', *Chemical Engineering Science*, 65(21), 5658–5668.

Post Mixing (2015) Optimization and Solutions [online], available: http://www.postmixing.com.

Promix Solutions (2016) Static Mixer Working Principle [online], available: http://www.promix-solutions.com/sulzer-mixer-plastic-processing.html.

Radman, J.R., Langlois, R., Leadbeater, T., Finch, J., Rowson, N., Waters, K. (2014) 'Particle flow visualization in quartz slurry inside a hydrocyclone using the positron emission particle tracking technique', *Minerals Engineering*, 62, 142–145.

Rafiee, M., Bakalis, S., Fryer, P.J., Ingram, A. (2011) 'Study of laminar mixing in kenics static mixer by using Positron Emission Particle Tracking (PEPT)', *Procedia Food Science*, 1, 678–684.

Rafiee, M., Simmons, M.J.H., Ingram, A., Stitt, E.H. (2013) 'Development of positron emission particle tracking for studying laminar mixing in Kenics static mixer', *Chemical Engineering Research and Design*, 91(11), 2106–2113.

Rammohan, A.R., Kemoun, A., Al-Dahhan, M.H., Dudukovic, M.P. (2001a) 'Characterization of Single Phase Flows in Stirred Tanks via Computer Automated Radioactive Particle Tracking (CARPT)', *Chemical Engineering Research and Design*, 79(8), 831–844.

Rammohan, A.R., Kemoun, A., Al-Dahhan, M.H., Dudukovic, M.P. (2001b) 'A lagrangian description of flows in stirred tanks via computer-automated radioactive particle tracking (CARPT)', *Chemical Engineering Science*, 56(8), 2629–2639.

Rauline, D., Blévec, J. Le (2000) 'A comparative assessment of the performance of the Kenics and SMX static mixers', ... *Research and Design*, 78(April).

Sadrmomtaz, A., Byars, L.G.G., Parker, D.J. (2007) 'Modification of a medical PET scanner for PEPT studies', *Nuclear Instruments and Methods in Physics Research A*, 573(1–2), 91–94.

Saito, Y., Fan, X., Ingram, A., Seville, J.P.K. (2011) 'A new approach to high-shear mixer granulation using positron emission particle tracking', *Chemical Engineering Science*, 66(4), 563–569.

Scalo, F. (2013) *Fluidized Bed Technologies for Near-Zero Emission Combustion and Gasification*, Fluidized Bed Technologies for Near-Zero Emission Combustion and Gasification, Elsevier.

Schaafsma, S.H., Marx, T., Hoffmann, C. (2006) 'Investigation of the particle flow pattern and segregation in tapered fluidized bed granulators', *Chemical Engineering Science*, 61(14), 4467–4475.

Schafer, T., Meitzner, C., Lange, R., Hampel, U. (2016) 'A study of two-phase flow in monoliths using ultrafast single-slice X-ray computed tomography', *International Journal of Multiphase Flow*, 86, 56–66.

Shah, N., Kale, D. (1991) 'Pressure drop for laminar flow of non-Newtonian fluids in static mixers', *Chemical engineering science*, 46(8), 2159–2161.

Singh, M.K., Anderson, P.D., Meijer, H.E.H. (2009) 'Understanding and Optimizing the SMX Static Mixer.', *Macromolecular rapid communications*, 30(4–5), 362–76.

Smith, P.G. (2007) 'Applications of Fluidization to Food Processing', in *Applications of Fluidization to Food Processing*, 1–244.

Snieders, F.F., Hoffmann, C., Cheesman, D., Yates, J.G., Stein, M., Seville, J.P.K. (1999) 'The dynamics of large particles in a four-compartment interconnected fluidized bed', *Powder Technology*, 101(3), 229–239.

Stein, M., Ding, Y., Seville, J.P., Parker, D. (2000) 'Solids motion in bubbling gas fluidised beds', *Chemical Engineering Science*, 55(22), 5291–5300.

Stein, M., Ding, Y.L., Seville, J.P.K. (2002) 'Experimental verification of the scaling relationships for bubbling gas-fluidised beds using the PEPT technique', *Chemical Engineering Science*, 57, 3649–3658.

Stein, M., Seville, J.P.K., Parker, D.J. (1998) 'Attrition of porous glass particles in a fluidised bed', *Powder Technology*, 100(2–3), 242–250.

Stellema, C.S., Vlek, J., Mudde, R.F., de Goeij, J.J.M., van den Bleek, C.M. (1998) 'Development of an improved positron emission particle tracking system', *Nuclear Instruments and Methods in Physics Research Section A: Accelerators, Spectrometers, Detectors and Associated Equipment*, 404(2–3), 334–348.

Stewart, R.L., Bridgwater, J., Parker, D.J. (2001) 'Granular flow over a flat-bladed stirrer', *Chemical Engineering Science*, 56(14), 4257–4271.

Stewart, R.L., Bridgwater, J., Zhou, Y.C., Yu, B. (2001) 'Simulated and measured flow of granules in a bladed mixer- A detailed comparison', *Chemical Engineering Science*, 56(19), 5457–5471.

Streiff, F.A., Jaffer, S., Schneider, G. (1999) 'Design and application of motionless mixer technology', in *ISMIP3, Osaka*, 107–114.

Torré, J.-P., Fletcher, D.F., Lasuye, T., Xuereb, C. (2007) 'Single and multiphase CFD approaches for modelling partially baffled stirred vessels: Comparison of

experimental data with numerical predictions', *Chemical Engineering Science*, 62(22), 6246–6262.

Van de Velden, M., Baeyens, J., Seville, J.P.K., Fan, X. (2008a) 'The solids flow in the riser of a Circulating Fluidised Bed (CFB) viewed by Positron Emission Particle Tracking (PEPT)', *Powder Technology*, 183(2), 290–296.

Van de Velden, M., Baeyens, J., Seville, J.P.K., Fan, X. (2008b) 'The solids flow in the riser of a Circulating Fluidised Bed (CFB) viewed by Positron Emission Particle Tracking (PEPT)', *Powder Technology*, 183, 290–296.

Van de Velden, M., Baeyens, J., Smolders, K. (2007) 'Solids mixing in the riser of a circulating fluidized bed', *Chemical Engineering Science*, 62(8), 2139–2153.

Versluis, M. (2013) 'High-speed imaging in fluids', *Experiments in Fluids*, 54(2).

Volkwyn, T.S., Buffler, A., Govender, I., Franzidis, J.-P., Morrison, A.J., Odo, A., van der Meulen, N.P., Vermeulen, C. (2011) 'Studies of the effect of tracer activity on time-averaged positron emission particle tracking measurements on tumbling mills at PEPT Cape Town', *Minerals Engineering*, 24(3–4), 261–266.

Wang, H., Wang, Y. (2009) 'Measurement of water flow rate in microchannels based on the microfluidic particle image velocimetry', *Measurement*, 42(1), 119–126.

Wang, M. (2015) *Industrial Tomography, Systems and Applications*, Elsevier.

Waters, K.E., Rowson, N. a., Fan, X., Parker, D.J., Cilliers, J.J. (2008) 'Positron emission particle tracking as a method to map the movement of particles in the pulp and froth phases', *Minerals Engineering*, 21, 877–882.

Van der Westhuizen, A.P., Govender, I., Mainza, A.N., Rubenstein, J. (2011) 'Tracking the motion of media particles inside an IsaMill™ using PEPT', *Minerals Engineering*, 24(3–4), 195–204.

Wintenberg, A.L., Clonts, L.G. (2003) 'Energy discrimination and counting electronics for Computer-Aided Radioactive Particle Tracking', *2003 IEEE Nuclear Science Symposium. Conference Record (IEEE Cat. No.03CH37515)*, 2, 1228–1232.

Wong, Y.S. (2006) 'Particle motion in relatively thin fluidised bed models', *Chemical Engineering Science*, 61(18), 6234–6238.

Yang, R.Y., Zou, R.P., Yu, A.B. (2003) 'Micro-dynamic analysis of particle flow in a horizontal rotating drum', *Powder Technology*, 130(1), 138–146.

Yang, Z., Fan, H., Parker, D.J., Fryer, P.J., Bakalis, S., Fan, X. (2014) 'Study on solids translational and rotational motions in rotating cans', *LWT - Food Science and Technology*, 57(1), 383–392.

Yang, Z., Fan, X., Bakalis, S., Parker, D.J., Fryer, P.J. (2008) 'Impact of Solids Fraction and Fluid Viscosity on Solids Flow in Rotating Cans', *Food Research International*, 41(6), 658–666.

Yang, Z., Fryer, P.J., Bakalis, S., Fan, X., Parker, D.J., Seville, J.P.K. (2007) 'An improved algorithm for tracking multiple, freely moving particles in a Positron Emission Particle Tracking system', *Nuclear Instruments and Methods in Physics Research, Section A: Accelerators, Spectrometers, Detectors and Associated Equipment*, 577, 585–594.

Yang, Z., Parker, D.J., Fryer, P.J., Bakalis, S., Fan, X. (2006) 'Multiple-particle tracking-an improvement for positron particle tracking', *Nuclear Instruments and Methods in Physics Research, Section A: Accelerators, Spectrometers, Detectors and Associated Equipment*, 564, 332–338.

Yu, S., Wu, C.-Y., Adams, M.J., Reynolds, G., Gururajan, B., Gargiuli, J., Leadbeater, T., Roberts, R., Parker, D.J. (2015) 'The use of positron emission particle tracking (PEPT) to study milling of roll-compacted microcystalline cellulose ribbons', *Powder Technology*, 285, 74–79.

Zalc, J.M., Szalai, E.S., Muzzio, F.J., Jaffer, S. (2002) 'Characterization of flow and mixing in an SMX static mixer', *AIChE Journal*, 48(3), 427–436.

Zhou, Y.C., Yu, A.B., Stewart, R.L., Bridgwater, J. (2004) 'Microdynamic analysis of the particle flow in a cylindrical bladed mixer', *Chemical Engineering Science*, 59(6), 1343–1364.

CHAPTER 3. LAMINAR MIXING IN SMX STATIC MIXERS EVALUATED BY POSITRON EMISSION PARTICLE TRACKING (PEPT) AND MAGNETIC RESONANCE IMAGING (MRI)

The work presented in this chapter was conducted in collaboration with Prof. Kathryn McCarthy and Prof. Michael McCarthy of UC Davis, California, USA. The MRI data was acquired by the team at UC Davis, while the PEPT data acquisition and the analysis of the results for both MRI and PEPT were carried out by the author of this thesis.

Data and discussions contained within this chapter have been published within:

Mihailova, O., Lim, V., McCarthy, M.J., McCarthy, K.L., Bakalis, S., 2015. Laminar mixing in a SMX static mixer evaluated by positron emission particle tracking (PEPT) and magnetic resonance imaging (MRI). Chemical Engineering Science. **137**, 1014–1023.

3.1 ABSTRACT

Static mixers are implemented across many industries and are used for mixing, heating and reacting processes. This chapter reports the combined use of Positron Emission Particle Tracking (PEPT) and Magnetic Resonance Imaging (MRI) to assess mixing in the industrially important SMX static mixer geometry. The focus of this study was distributive mixing for a Newtonian fluid, glycerol, flowing in the laminar regime in the standard SMX static mixer.

By implementing PEPT and MRI techniques, the work elucidated mixing indices that incorporate both local velocities and concentration fields within the structure of the mixer element at 0.5 mm intervals over a length of nine DN25 SMX elements. The experimental results are placed in context with previously published computational studies for this geometry.

MRI data was originally acquired by the team at UC Davis for the publication of the a separate SMX mixer study (Lim *et al.* 2015). The author of this thesis reprocessed this data to derive an approach for the comparison of the PEPT and MRI techniques and for the derivation of complimentary PEPT and MRI data processing.

3.2 INTRODUCTION

The shift towards continuous processing is ever increasing, as it allows for more streamlined and cost effective manufacturing. Continuous processing reduces energy consumption and waste production when compared to an equivalent amount of product manufactured by batch methods. As many of these processes rely on mixing and heat transfer, static mixers are increasingly incorporated into processing systems (Etchells and Meyer 2003; Ghanem *et al.* 2014). The insert-type configuration of the static mixer redistributes fluid flow in directions transverse to the main flow due to a series of motionless elements. This type of distributive mixing is by convection rather than diffusion. The focus of this study was distributive mixing for a Newtonian fluid flowing in the laminar regime for a specific type of static mixer, the standard SMX static mixer (Sulzer Chemtech, Winterthur, Switzerland).

The SMX mixer has been the subject of a number of experimental and computational studies, well summarised by Thakur and co-workers (2003), Singh and co-workers (2009), and Meijer and co-workers (2012). Significant strides have been made using computational fluid dynamics (CFD) and the mapping method to assess performance of the SMX mixer (Rauline and Blévec 2000; Zalc *et al.* 2002; Liu *et al.* 2006; Singh *et al.* 2009). In general, but not without exception, computational results have been challenging to validate or to compare with experimental mixing performance due to the geometrically complex nature of the mixing system. In a proof of concept portfolio paper, Leschka and co-workers illustrated simultaneous measurements using Planar Laser-induced Fluorescence (PLIF) and Particle Image Velocimetry (PIV) for flow behind the SMX static mixer (Leschka *et al.* 2007). However, this technique was never successfully applied for qualitative characterisation of the dynamics within the SMX mixers.

This chapter introduces two different experimental techniques that are combined to evaluate the qualitative and quantitative measure of mixedness through the SMX mixer: Positron Emission Particle Tracking (PEPT) and Magnetic Resonance Imaging (MRI). Previously, Positron Emission Tomography (PET) and MRI have been combined to utilise their complementary abilities to enhance medical diagnostics (Zaidi and Guerra 2011; Herzog 2012). Small scale PET/MRI systems have recently become available for use in preclinical research (Aspect Imaging 2015). PEPT, a technique developed in the University of Birmingham and based on PET, allows non-invasive spatial tracking of a neutrally buoyant radioactive labelled tracer particle (Parker *et al.* 1993; Eesa and Barigou 2008). This technique has been successfully used to characterise a number of industrial processes, such as tumbling mills (Volkwyn *et al.* 2011) and stirred vessels (Chiti *et al.* 2011), as well as a number of domestic appliances, washing machines (Mac Namara *et al.* 2012) and dish washers (Pérez-Mohedano *et al.* 2015), as well as characterisation of Kenics static mixers (Rafiee *et al.* 2013). The technique relies on tracking a single neutrally buoyant particle through the system. As the particle emits back to back γ-rays, the location of the tracer can be accurately triangulated by the PEPT algorithm at short time intervals, in the order of microseconds, which consequently allows calculation of the 3D velocity of the tracer. The technique depends on recirculating the tracer until the particle passes sufficiently cover the volume of the system (Parker *et al.* 1993).

Nuclear Magnetic Resonance (NMR) and Magnetic Resonance Imaging (MRI) are spectroscopic techniques that are based on the interaction between nuclear magnetic moments and applied external magnetic fields. These techniques are used to measure composition, structure, molecular mobility, molecular diffusion and bulk material motion. Discussion of the techniques and applications are given in McCarthy and McCarthy (2013, 2014). MRI studies of mixing processes have been reported in the literature for both batch

and continuous systems. Representative studies from the University of California, Davis lab include: McCarthy and McCarthy 2000; Lee *et al.* 2001; McCarthy *et al.* 2002; Choi and McCarthy 2004. Relevant to this SMX static mixer work, Tozzi and co-workers reported the use of MRI to characterise mixing at low Reynolds number in a split and recombine (SAR) static mixer (Tozzi *et al.* 2012, 2013).

These studies are performed by introducing components with different magnetic relaxation properties. For flow studies that involve the mixing of multiple fluid streams, the use of a small amount of NMR contrast agent, such as manganese chloride or gadolinium chloride, is common since it does not significantly alter flow properties of the fluid (McCarthy *et al.* 2002). Changes in NMR signal intensity (SI) are attributed to the mixing of the fluid streams. With calibration techniques, the 2D MR images are converted to concentration maps.

By implementing PEPT and MRI techniques, the current work reports an assessment of both local velocities and concentration fields within the structure of the mixer element. Conventional statistical methods are presented to illustrate mixing as a function of axial position within the SMX mixer. Lastly, the experimental results from both techniques are combined in a flux-weighted intensity of segregation as a measure of homogeneity.

3.3 MATERIALS AND METHODS

3.3.1 MATERIALS

3.3.1.1 TEST FLUID

Glycerol, a model Newtonian fluid, was utilised as the test fluid for MRI and PEPT trials. In the case of PEPT experiments unmodified glycerol was used, with a single neutrally buoyant tracer particle. Glycerol was acquired from Reagent (Cheshire, UK). The glycerol rheology was characterised using a rotational rheometer (AR 1000, TA

Instruments, UK), with a 40 mm stainless steel cone and plate geometry, yielding a viscosity of 1.262 ± 0.005 Pa·s.

For MRI experiments, glycerol (Essential Wholesale and Lab, Portland, OR) was doped with the NMR contrast agent, gadolinium chloride ($GdCl_3$) (Sigma Aldrich, St. Louis, MO). Two levels of doping were used to provide Signal Intensity (SI) contrast between two fluid streams: 4×10^{-4} M and 20×10^{-4} M $GdCl_3$ in glycerol. These levels of doping minimise change in physical properties of the test fluid while sufficiently altering the NMR signal intensity values. For simplicity, the higher level of doping at $20x10^{-4}$ M $GdCl_3$ in glycerol will be further referred to as "doped". The rheology of these solutions were characterised using a rotational rheometer (Bohlin CVO, Malvern Instruments, UK) yielding viscosities of 0.95 ± 0.004 Pa·s and 0.92 ± 0.008 Pa·s, respectively.

Rheological differences between the glycerol used for PEPT and for MRI trials can be attributed to the different suppliers and the addition of the contrast agent. However, all the grades of glycerol used retain the Newtonian fluid properties, therefore, any differences in viscosity are not expected to have a significant effect on the mixing results, as long as the flow conditions remain laminar.

3.3.1.2 SMX MIXER

Static mixers are effective pipeline mixing devices in the laminar flow regime. Etchells and Meyer (2004) provide an excellent discussion of design and application of various types of inline mixing. The SMX mixer, initially developed jointly by Koch and Sulzer, is an ideal choice for mixing/blending of miscible fluids of similar or dissimilar viscosities. The DN25 SMX (1") elements were used in both MRI and PEPT trials. The SMX element has a diameter of 25.4 mm and a length of 25.4 mm, for a length to diameter ratio (L/D) of 1. Each element is comprised of six planes of 3.18 mm x 1.9 mm bars spaced 3.18 mm apart. Three planes of bars are spaced 9 mm apart with the remaining

three planes placed orthogonally. The axial direction is offset 45° from both sets of planes. Each consecutive element is oriented at 90° to the preceding one, alternating the direction of fluid flow through the mixer, achieving the desired stretch and fold mixing mechanic characteristic of the SMX mixers (Zalc *et al.* 2002). This geometry is typically described as the "standard" SMX (2, 3, 8) design with 2 units over the height of the channel, 3 parallel bars along the length of one element and 8 cross bars over the width of the channel (Figure 3.1).

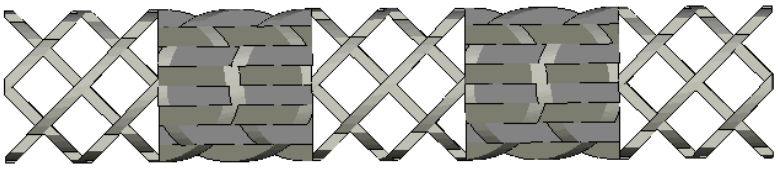

Figure 3.1. CAD diagram of five consecutive elements of a standard SMX mixer

Although industrial mixing applications typically use metals as the material of construction, metal cannot be used in the MR magnet since it distorts or shields signal from the hydrogen nuclei in the fluid.

For the MRI study, individual plastic elements of ABS-like (thermoplastic acrylonitrile-butadiene-styrene) material were purchased from Sulzer Chemtech USA Inc. (Tulsa, OK). Nine SMX elements were secured in a Schedule 40 transparent plastic tube as described above. A flat flow splitter that spanned the diameter of the tube was inserted into the tube upstream of the first SMX element to isolate the two test fluids in two semi-elliptic channels.

Though the PEPT technique does not have the same constraint, the plastic elements cause less scattering, as the γ-rays pass more readily through plastic than metal (Mansfield and O'Sullivan 2010). Therefore, the elements for both the MRI and PEPT studies were constructed from plastic.

For the PEPT trials, two 5-element SMX mixers were 3D-printed by TEAM Design, Prototyping, and Fabrication Laboratory (University of California, Davis) based on CAD drawings of the ABS-like SMX element. The material of construction was Objet VeroClear (a transparent acrylic compound; Stratasys, Eden Prairie, MN).

3.3.2 METHODS

3.3.2.1 MRI TECHNIQUE

Figure 3.2a gives a schematic representation of the experimental set up for the MRI trials. The nine-element SMX mixer assembly was centered in the imaging section of a 1T permanent magnet. MR imaging was performed using an Aspect Imaging spectrometer with a 0.3 T/m peak gradient strength (Shoham, Israel). The radio frequency coil was a solenoid with four turns, encasing a cylindrical volume of 60 mm in diameter and 60 mm in length.

a b

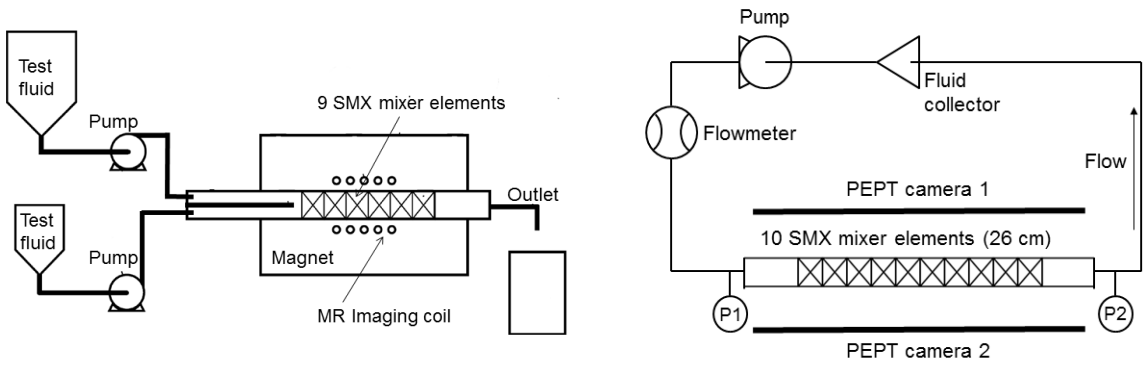

Figure 3.2. Schematic representation of the experimental set up for (a) MRI trials, (b) PEPT trials

Two positive displacement pumps (FH100X Peristaltic Pump, Thermo Scientific, Fisher Scientific, Houston, TX) pumped the test solutions from two reservoirs at a constant volumetric flow rate of 9.7 L/h each to achieve a 50:50 ratio of the two fluids. The combined flow rate was 19.4 L/h into the SMX mixer for a Reynolds number of 0.4 in the

empty pipe. Both glycerol-based test fluids were pumped through the mixer until steady flow was achieved. The pumps were then simultaneously stopped and MR images were obtained using a multi-slice gradient recall echo sequence in the sagittal orientation on the stationary fluid. The MRI parameters were repetition time (TR) of 5.7 ms, echo time (TE) of 1.9 ms, slice thickness of 0.5 mm, and 128 slices, yielding an image resolution of 0.313 mm. Once a set of images was acquired normal to the flow direction at a given axial location, the SMX mixer was moved to image a downstream axial position. The pumping and imaging procedure was repeated at the new axial position. The flow system was single pass and the fluids were not recirculated. Calibration vials with 6 different levels of dopant were prepared and MR imaged to a obtain calibration curve that quantified the signal intensity at different mixtures of the two test fluids (4 replicates). The relationship between the signal intensity and level of $GdCl_3$ was linear with a coefficient of determination of 0.94.

3.3.2.2 MRI DATA PROCESSING

The MR images were standardised to provide a means of image to image comparison. Experimental noise was addressed first. For each image signal from void regions (regions of air or plastic) were zeroed so their values did not contribute to the sum of signal intensities of the image. Signal intensities (SI) arising from fluid in contact with the plastic of the SMX element or tube wall were also zeroed to eliminate the effect of partial volume averaging, for example if half of the imaging pixel is occupied by the mixer, while the other half is occupied by fluid with high signal intensity, when averaged, the pixel will only display half of the intensity of the fluid Therefore, to avoid false readings the signal intensity in pixels which are found on wall borders are assigned SI of zero.

The remaining signal intensity values were nonzero values solely due to the signal from fluid. Signal intensities were then converted to percentage of doped test fluid with the

linear regression equation of the calibration curve, yielding values from 0 to 100. Each image was then divided by its average value to yield images that had exactly an average of 50 % doped fluid. All images in each set were then divided by the maximum signal intensity of the set and multiplied by 100 to yield a range of values between 0 and 100. The last procedure was performed to acknowledge that unmixed fluid had a distribution of signal intensities. Dividing by the maximum signal intensity was dividing by the value that was essentially three standard deviations above the mean of the high SI test fluid, as the SI range followed a normal distribution, where three standard deviations corresponds to 99.7% of the data. The images were cropped to 83 x 83 pixels to accommodate comparison to PEPT data. MATLAB 2013a (The MathWorks, Inc., Natick, MA) was used to perform image and data analysis.

3.3.2.3 POSITRON EMISSION PARTICLE TRACKING TECHNIQUE

As the PEPT technique relies on tracking a single neutrally buoyant tracer particle at any given time, a closed loop system was used, which allowed recirculation of the fluid seeded with the tracer (Eesa and Barigou, 2008). A schematic representation of the experimental set up for the PEPT trials is shown in Figure 3.2b. A plastic pipe DN25 (26 mm) was used with 10 plastic SMX mixer elements located in the middle of the pipe. The mixer section of the system was positioned centrally in the field of view of the PEPT apparatus, allowing empty pipe regions to be present in the field of view. For all experiments, the flow rate was controlled at 300 L/h for a Reynolds number of 5.5 in the empty pipe. While this Re number is different to that used in the MRI studies, it was assumed that due to the laminar nature of the flow in both experiments and the Newtonian nature of the fluid, the effects of Re were not significant, this assumption is supported by CFD findings on varied Re numbers in SMX mixers (REF). Pressure and temperature in

the pipeline were monitored and logged using a pair of pressure/temperature transducers located either side of the PEPT field of view.

Fluid was circulated using a flexible impeller pump, minimising the stress exerted on the tracer particle, prolonging its stability and reducing contamination of the bulk fluid with radioactive material. By minimizing the total volume of the system to 3 L it was possible to achieve a particle pass through the field of view approximately every 90 s. The experiment had to be reset every 3 hours due to degradation of particle activity and bulk contamination, until a minimum of 800 particle passes were recorded achieving sufficient coverage at all radial positions across both the empty pipe and the static mixer regions.

3.3.2.4 PEPT DATA PROCESSING

Processing the raw data collected by the PEPT cameras yields sets of x-y-z coordinates with respect to time. These data points were rotated in a way that aligns the internal structure of the mixer with the Cartesian coordinate planes. The resulting sets of coordinates were separated into individual particle passes, based on the time delay between consecutive detections, as the time between detections in the same pass is on the order of milliseconds, while the time it takes for the particle to recirculate into the field of view after a pass was over a minute. A number of typical particle passes with respect to time and spatial direction are illustrated in Figure 3.3. Where it can be seen that the particle travels extensively across both the x and the y planes, perpendicular to the flow, but follows a steady pattern in the direction of flow. No back mixing was observed in the system and the velocity component in the z direction was always positive. Table 3.1 summarises a typical particle pass, where it can be seen that on average detection occurred every 8 ms, resulting in approximately 315 particle locations per pass.

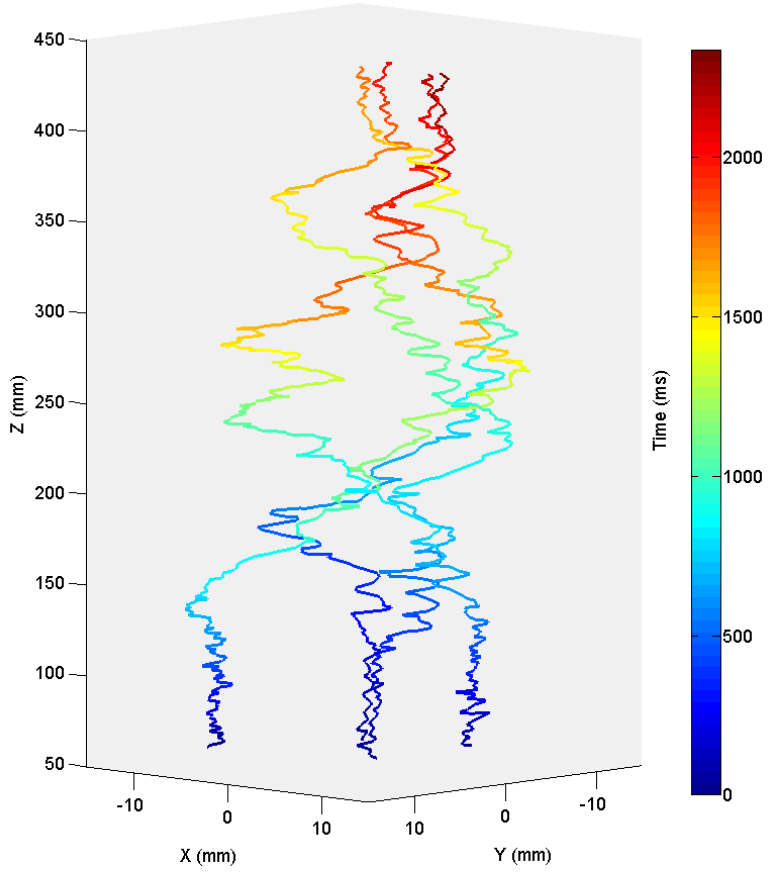

Figure 3.3. Four typical particle passes, where the position of the particle along the x-, y-, and z-axes is illustrated against time from the moment the particle enters the field of view

Particle spatial location data with respect to time allowed estimates of local velocities. PEPT was previously shown to characterise velocity distributions within simple and complex geometries (Bakalis *et al.* 2004; Mac Namara *et al.* 2012). By the same approach, the x-, y-, z-velocity components were estimated for the current system. A second order polynomial was fit to a set of 7 points along each of the axis as a function of time, describing the path of the particle in time:

$$i = at^2 + bt + c \qquad 3.1$$

where i represents the x, y or z direction component, t is time and a, b and c are constants.

Table 3.1. Average particle pass statistics, showing number of detections used for location triangulation, residence time, locations detected per particle pass, time between detections and divergence from laminar flow in the empty pipe region.

Parameter	**Value**
Number of γ-ray pairs used for location triangulation (–)	125 ± 12
Residence time (s)	2.52 ± 0.66
Locations per particle pass (–)	315 ± 70
Time between detections (ms)	8 ± 2
Divergence from flow in the laminar region of the pipe (mm)	0.55 ± 0.20

The resulting polynomial was differentiated, yielding the rate of change of displacement with respect to time in a given direction, *i.e.* velocity component, U_i:

$$U_i = \frac{di}{dt} = 2at + b \qquad 3.2$$

where the constants are as in Equation 3.1. The individual velocity components (U_x, U_y and U_z) were then combined to give the overall velocity of the fluid, U:

$$U = \sqrt{U_x^2 + U_y^2 + U_z^2} \qquad 3.3$$

The velocity profile of Newtonian fluid flowing under laminar conditions in a simple geometry, such as an empty pipe, can be estimated theoretically (Chhabra and Richardson, 2008). Agreement between theoretical profiles and the local velocities obtained through PEPT data analysis indicates that when more complex geometries or fluids are considered, the velocities tracked using PEPT are valid (Bakalis *et al.* 2004; Marigo *et al.* 2013). Figure 3.4 illustrates how the theoretical velocity profile for a Newtonian fluid flowing in a

1" circular pipe at 300 L/h compares to the PEPT data acquired under the same flow conditions. It must be noted that the data quality declines towards the centre of the pipe. This is due to the volumetric effect across the pipe cross-section, where when radial distances are taken at consistent increments the area corresponding to those closer to the centre is significantly smaller than those further away. This in turn means that the tracer particle is less likely to be found at a position between two radial increments closer to the pipe centre. It can also be seen that the data quality also is reduced closer to the pipe wall. This arises due to a different phenomenon, where the tracer particle is rarely found by the wall boundary layer, as this typically means the particle getting "trapped" in the boundary layer and the experiment having to be reset. Therefore, very few particle passes are available for this part of the system, providing a poor data pool for the estimation of average local velocities.

In order to assess mixing, individual passes were labelled differently depending on the location of the particle as it was entering the first SMX element, with traces entering on one side of the pipe midpoint assigned the equivalent of the high contrast intensity, and the low contrast intensity assigned to the tracers entering on the other side. This procedure allowed effective separation of the flow into two streams, with a 50:50 volumetric ratio of the two fluids, in a manner similar to the MRI trials described previously (*cf.* Section 3.2.2.1).

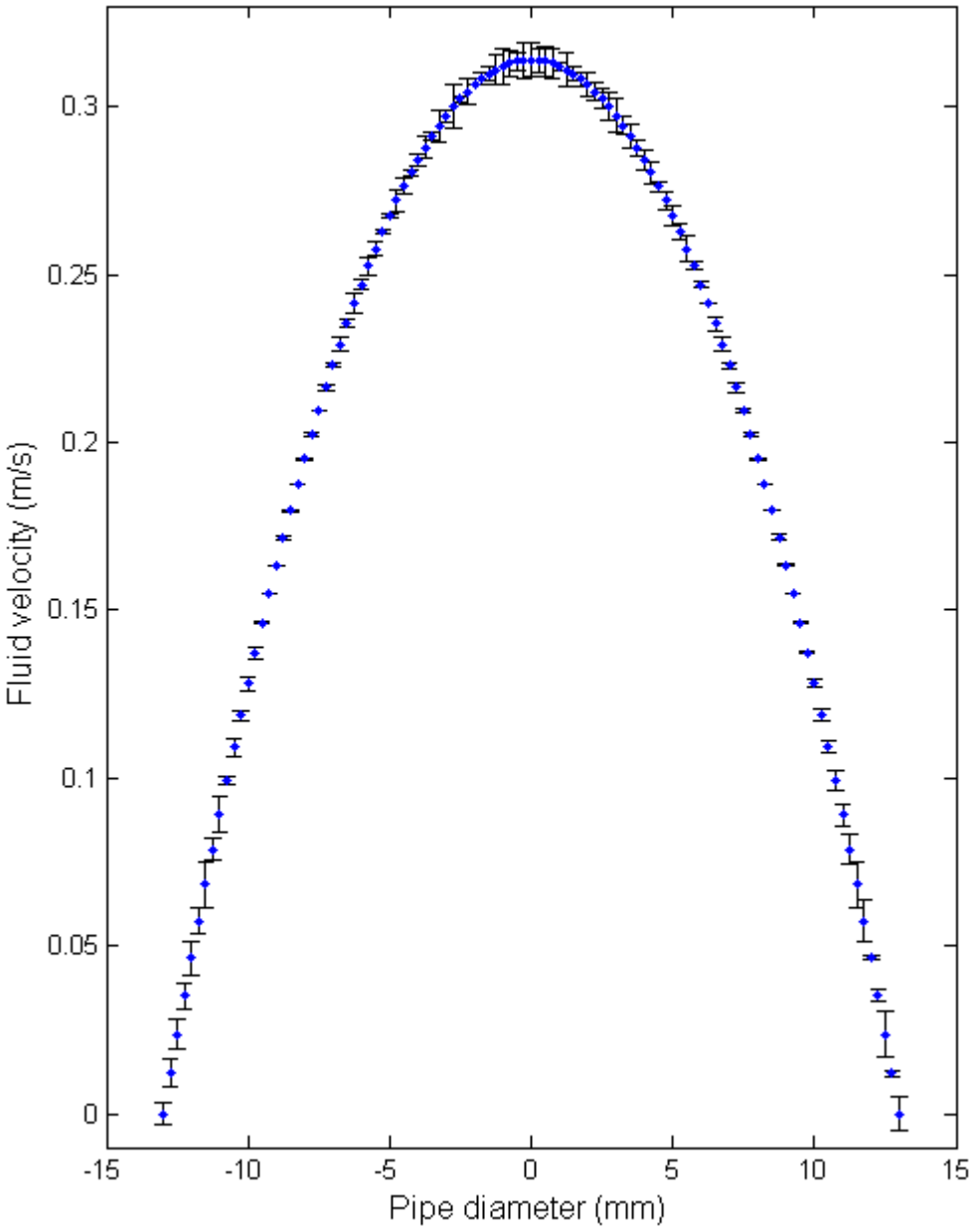

Figure 3.4. The theoretical velocity profile of a Newtonian fluid in a 1" circular pipe @ 300 L/h (blue dots), with the average PEPT data deviation from the theoretical prediction illustrated in the form of error bars, based on the glycerol at 300 L/h experimental data

Furthermore, to increase the detection density across one element the 10 element mixer was "cut up" into individual elements based on the dimensions of system. These 10 individual elements were then rotated accordingly and superimposed, condensing all experimental data into one element. This resulted in the number of passes through the

element to rise to over 6,000, allowing for a more detailed characterisation of both the mixing patterns and velocity fields within the element. To carry out this operation it was assumed that no entrance or exit effect are present in the first and last element respectively. To validate this assumption 1 mm slice of data along the z axis was taken from the entry and the exit of each element. The entrance slice for the first element and the exit slice for the last element were then compared to the corresponding positions in elements within the mixer structure using a t-test. The results of the test have shown that within 95% confidence interval the velocity data at the entry and exit of the entire mixer assembly belongs to the same continuous distribution as the entry and exit velocities for mixer elements within the assembly.

In addition, PEPT data were viewed as slices in the same fashion as MRI data allowing for side by side comparison. The SMX element resulting from superimposing all experimental data was divided into 0.5 mm slices and within each slice an 83 x 83 element grid with a 0.313 x 0.313 mm resolution was applied. Each grid segment contained the information for the given area of the cross-section, including spatial location, time of detection and the concentration value for each particle pass based on its entry location to the collated element. MATLAB 2013a (The MathWorks, Inc., Natick, MA) was used to perform image and data analysis.

3.4 RESULTS AND DISCUSSION

3.4.1 MRI RESULTS

Figure 3.5 illustrates representative MR images for the first SMX element. The images are arranged from left to right, top to bottom at the designated axial positions. The colour map for each image is the same with high signal intensity fluid (red) flowing from the upper semi- elliptic channel into the SMX mixer and the low signal intensity fluid (blue) flowing from the lower semi-elliptic channel into the SMX mixer at $z = 0$. The dark blue regions within the cross-section are due to the SMX geometry where plastic does not contribute to NMR signal and the signal intensity has been zeroed. Background regions, as well, are zero signal intensity values and given as dark blue. Each image is an additional 1/8 of a L/D downstream. As fluid moves downstream the mixer blades distort the initial region of doped fluid into spade-like structures that extend the cross-section of the mixer. Striations in the fluids become more pronounced as the fluid progresses through the element. Qualitatively these images are strikingly similar to the computed mixing patterns given in Zalc *et al.* (2002; Fig. 9) in their study of laminar flow and mixing of a Newtonian fluid in a SMX mixer assessed by computational techniques.

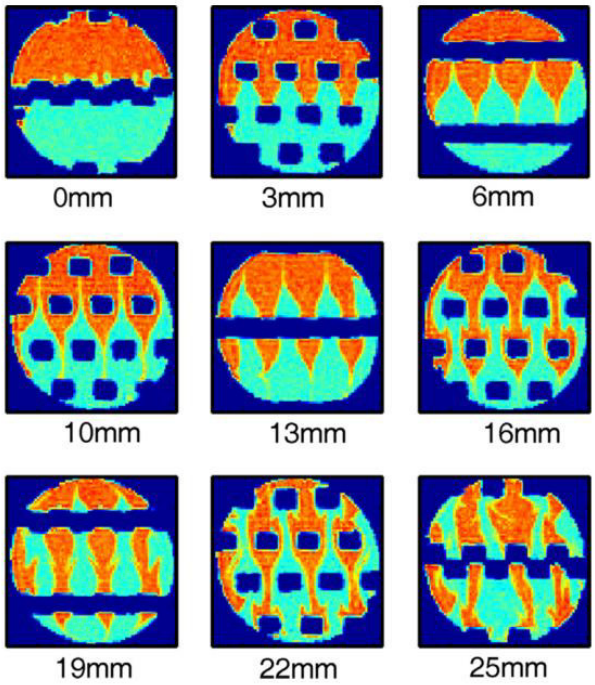

Figure 3.5. MR images of the 2 glycerol streams at 50:50 volume ratio in the first SMX element.

First and second order statistics quantify the extent of mixing. In particular, the intensity of segregation and coefficient of variation incorporate the variance s^2 (-) and its square root, the standard deviation (s) as spread characteristics. The intensity of segregation, I (-), is defined as:

$$I = \frac{s^2}{s_0^2} \tag{3.4}$$

where s_0^2 is the initial variance (-). The coefficient of variation (CV), is defined as:

$$CV = \frac{s}{\bar{X}} \tag{3.5}$$

where the mean concentration, $\bar{X}$ (-), is the mean signal intensity of the standardised MR image. Due to the standardisation procedure (*cf.* Section 3.2.2.2), the mean concentration for each image was the same value at 59.4.

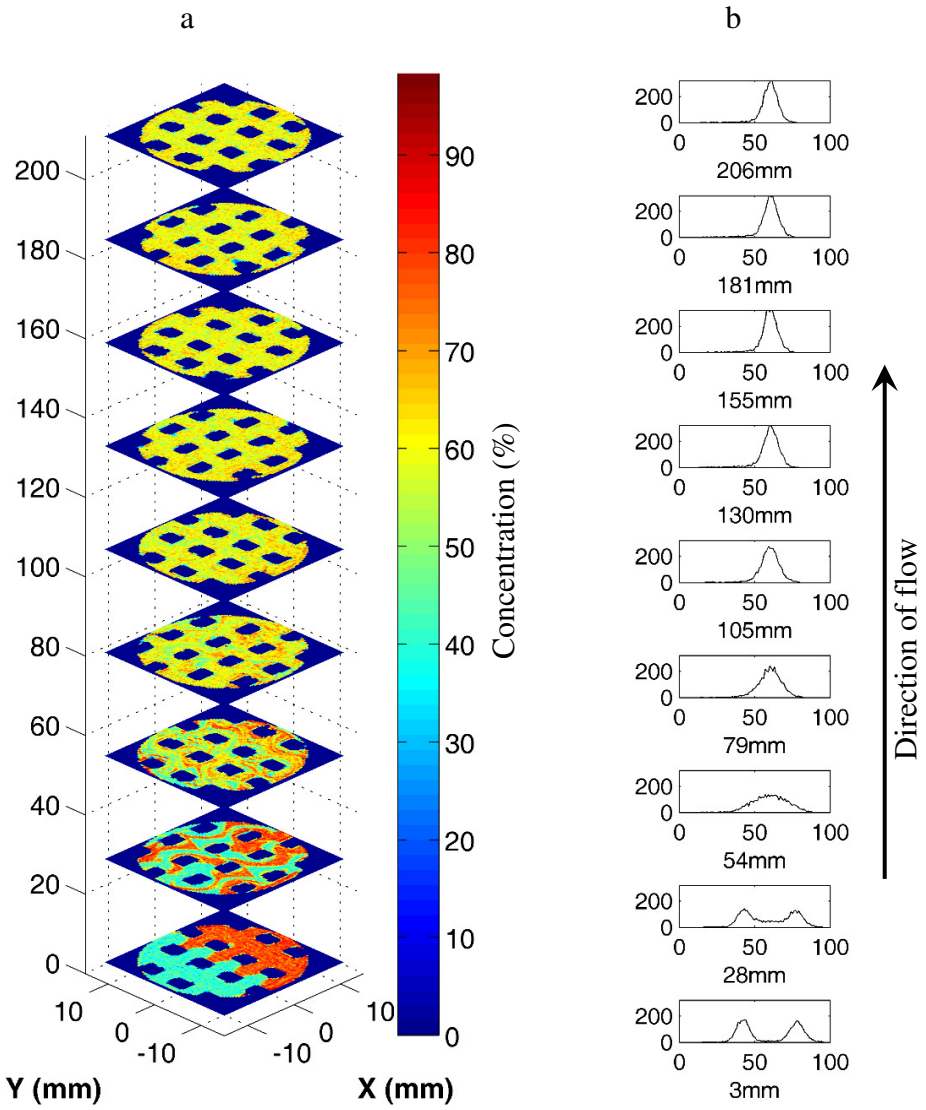

Figure 3.6. Mixing of the 2 glycerol streams at 3mm into consecutive SMX elements (a) MR image and (b) corresponding histograms.

Figure 3.6a illustrates MR images of the mixing of the two glycerol streams at a position 3 mm into each of the 9 consecutive SMX elements. For the two glycerol solutions, the striations in the fluid are visually distinct through the fourth SMX element (at a distance of 79 mm). By the fifth element the two fluids have mixed to visual resolution. Figure 3.6b gives histograms for each position in Figure 3.6a. Initially the SI peaks are centered at values of 42 and 77, reflecting the two initial contrasting agent concentrations. The bimodal distribution becomes unimodal, centered at 61, and the

standard deviation subsequently decreases from 10 to 4, suggesting that the two fluids are mixed.

Quantitatively, the entire set of 520 MR images are described by *I*, *CV* and length scale (*L/D*), as a function of position (Figure 3.7). The values of these statistics were calculated for images upstream of the SMX mixer in the semi-elliptic flow channels and are plotted as values at negative *L/D* prior to the SMX mixer. Intensity of segregation values in Figure 3.7a drop linearly over the first three SMX elements and level off at approximately 0.08, whereas the intensity in the empty pipe downstream of the static mixer was 0.04. In other words, the last few points in Figure 3.7a illustrate the resolution of the image. Figure 3.7b illustrates the coefficient of variation on a semi logarithmic plot. The calculated maximum *CV* for the MR images at *L/D* = 0 was 0.30, (Equation 3.5). As fluid travelled through the SMX elements, the *CV* dropped from 0.30 to approximately 0.10. Further downstream, the *CV* of fluid in the empty pipe was 0.06, again yielding an indication of the resolution of the technique. For context, Figure 3.7b incorporates data taken from Etchells and Meyer (2004; Fig. 7.5) to illustrate homogeneity in the SMX mixer when an additive is introduced at the middle of the pipe at a level of 50%. It is important to note that the coefficient of variation for an unmixed sample given by statistical theory and based on unmixed volume fraction is 1 at *L/D*=0. In contrast, experimentally coefficient of variation is considerably lower as initial SI data take values other than completely unmixed (for instance, at solely 0 or 1).

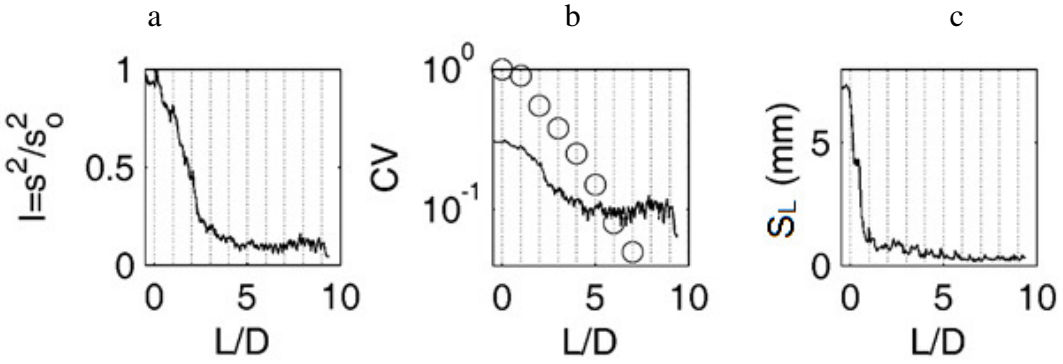

Figure 3.7. Mixing statistics based on MR images as a function of L/D for (a) intensity of segregation, (b) coefficient of variation with data (o) from Etchells and Meyer (2004), and (c) length scale.

The scale of segregation, or the length scale, is a second order statistic and was calculated for each image. This statistic is based on the coefficient of correlation:

$$R(r) = \frac{\sum_{i=1}^{N}(X_A - \bar{X})(X_B - \bar{X})}{N_{S^2}} \qquad 3.6$$

where X_A (-) and X_B (-) are concentrations separated by radius r (mm), $\bar{X}$ is the mean concentration (-), and N is the number of and pairs separated by distance r. Values of R are calculated for all values of r. These values are integrated for the length scale:

$$S_L = \int_0^{\xi} R(r)dr \qquad 3.7$$

where ξ is at $R(r = \xi) = 0$ (Tadmor and Gogos 2006). Length scale (S_L) values as a function of L/D are plotted in Figure 3.7c.

The lower the length scale, the better the two fluids have mixed in the cross section. Similar to the intensity of segregation, rapid and dramatic change occurs over the first three SMX elements and then a more gradual decrease in length scale values. The intent of this research was to assess both local velocities and concentration fields within the structure of the SMX mixer element. PEPT results are now described and then the two experimental techniques compared directly.

3.4.2 PEPT RESULTS

PEPT data can be used to estimate a number of properties of a system, such as velocities, concentrations, flow patterns and local shear fields(Bakalis *et al.* 2004; Mac Namara *et al.* 2012). For the purposes of this research the focus was on concentration and velocity fields.

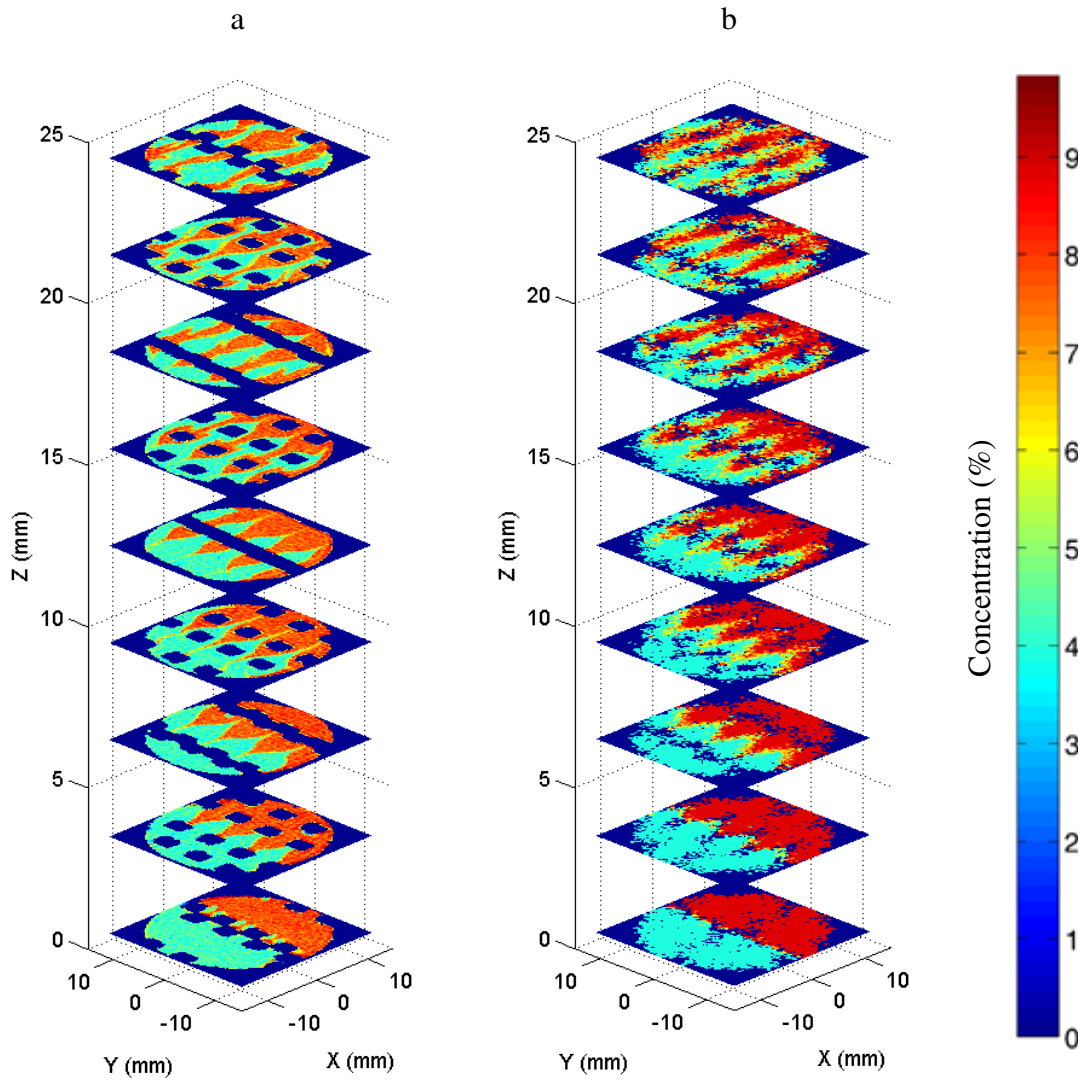

Figure 3.8. Mixing patterns for the 2 glycerol streams at 50:50 volume ratio illustrated by (a) MR images and (b) PEPT particle pass tracking.

As mentioned previously, due to the nature of the technique and the tracer particle, the mixer inlet was labelled as necessary by identifying individual particle passes. In order to

match the experimental setup used for MRI, the feed was divided into two equal streams based in the axial position of the tracer particle at the inlet of the first mixer element. Consequently, depending on the position of the tracer the particle pass was assigned an initial concentration value of either 40 or 80 in the first cross section, depending on the location. In the consequent slices (that is, cross sections), the concentration was calculated by dividing the x-y plane into 83×83 element grid and taking the average concentration of all the passes present in each segment of the grid. The concentration changes and the degree of mixing were then assessed in a manner similar to that applied for the MRI data processing. Figure 3.8 illustrates the MRI concentration images (Figure 3.8a) and PEPT concentration images (Figure 3.8b) through the first SMX element; qualitative agreement with the MRI results provided confidence in the PEPT tracking algorithm and the approach to trace individual particle passes.

The power of PEPT was to acquire local velocities of the fluid as it travels through the mixer. Local velocity fields offer an improved understanding of the mixing mechanisms and can be used to determine other properties of the system, such as local shear rate distribution, which play an important role when processing shear sensitive fluids.

The velocity field within the SMX mixer was dictated by the geometry of the mixer. Due to the orientation of the blades, laminar mixing occurs only along the axes perpendicular to the flow. This flow pattern for the velocity along the x-axis is shown in Figure 3.9a. Velocity values ranged between -0.3 and 0.3 m/s, with the maximum velocity at the center of each gap. The symmetric probability functions that arise in this plane are consistent with those reported in the radial and azimuthal direction by Zalc *et al.* (2002).

It can be seen that even in regions of the mixer with no physical barrier, *e.g.* slices at 6 mm (*L/D*=0.25) and 12 mm (*L/D*=0.5), clear bands of fluid with opposite direction are present (Figure 3.9a). This suggests that the fluid experiences significant shear forces as

the streams with opposing direction flow past one another. In contrast, the direction of axial flow was always positive, with the maximum of 0.4 m/s reached in the middle of each gap between the mixer blades and the minimum of 0.05 m/s reached at the walls (Figure 3.9b). Even though the velocity was expected to reach zero at the tube wall to satisfy the no slip condition, the particle was not observed to enter this boundary layer region.

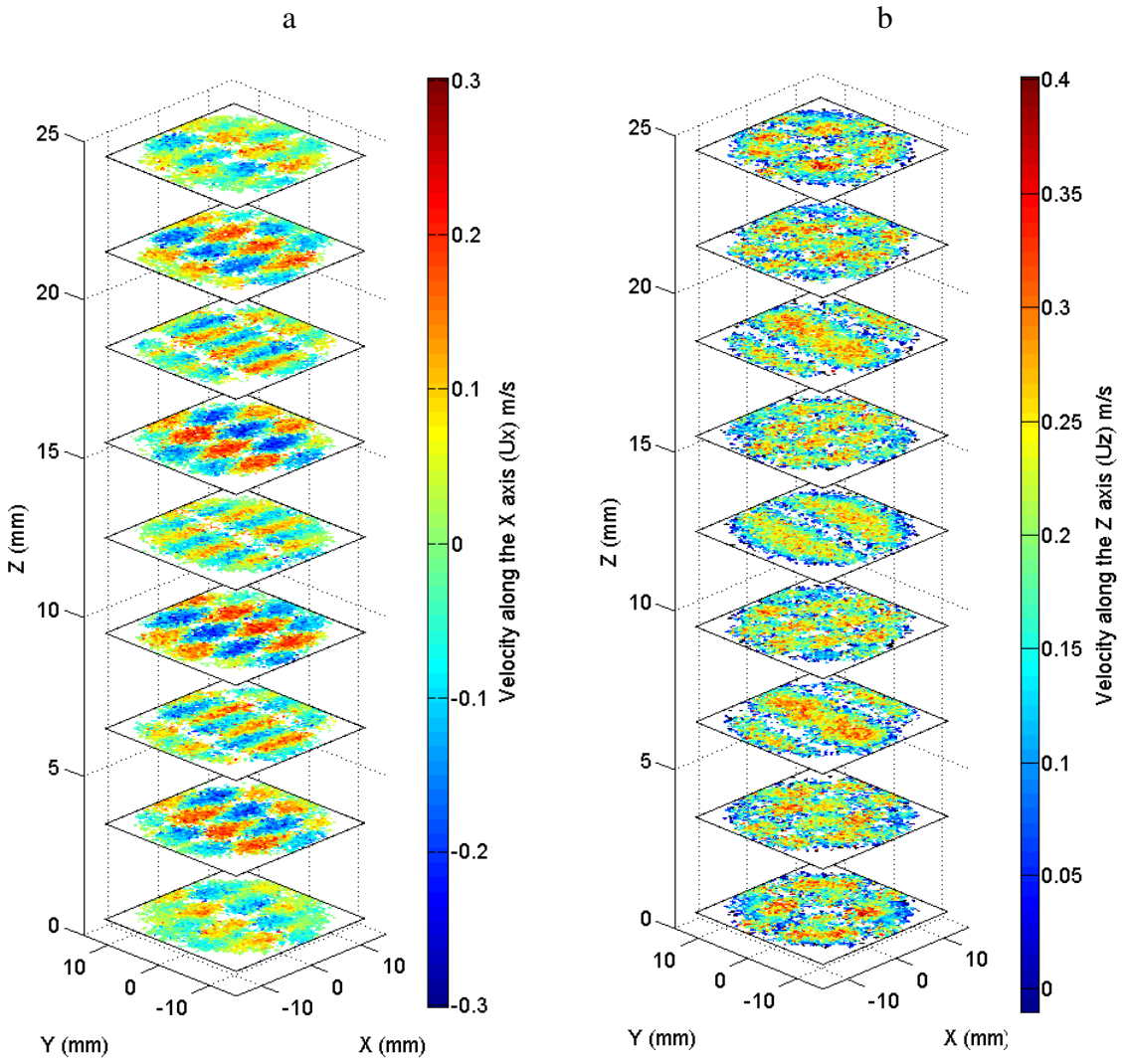

Figure 3.9. Velocity distribution calculated from PEPT data (a) along the x-axis (Ux), perpendicular to the flow and (b) along the z-axis (Uz), parallel to the flow, at 3 mm increments within an SMX element for glycerol at 300L/D

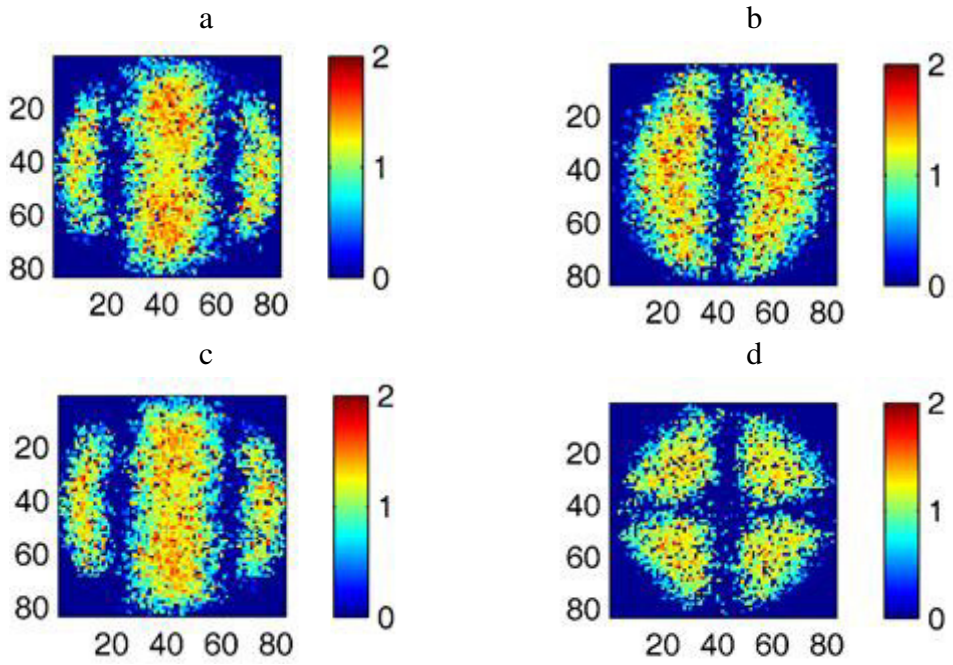

Figure 3.10. PEPT axial velocity images at 0.25 L/D, 0.5 L/D, 0.75 L/D and 1 L/D, dimensionless with the average velocity.

Axial PEPT velocities maps at 4 planes were selected: 0.25 *L/D*, 0.50 *L/D*, 0.75 *L/D*, and 1.0 *L/D*. Figure 3.10 illustrates these maps as dimensionless velocities normalised with the average velocity at the specified axial location, at the volumetric flow rate of 300 L/h. The average velocity was calculated for each plane and was found to be consistent at all cross-sections, which allowed to normalise the velocity maps. Furthermore, the consistency in the average velocities across multiple planes illustrates that when applying the PEPT measurement technique mass was conserved between cross-sections, which is an important validation for techniques applying discrete particle tracking, as opposed to volume total volume tracking. With the exception of 1.0 *L/D*, the average velocity in the planes was roughly 0.2 m/s, about 20 % greater than the average velocity in the empty pipe, 0.16 m/s, due to approximately 20 % of the pipe cross-section being occupied by the mixer. At 1 *L/D*, the average velocity was 0.4 m/s since the effective cross sectional area was reduced further as fluid left one element and entered the next element. Histograms

were constructed to view the velocity data in these planes in a quantitative way (Figure 3.11a). The histograms are essentially centered at the dimensionless velocity of 1 and normally distributed. For comparison, the analytical velocity maps were calculated for the semi-elliptic channel and the empty pipe. The semi-elliptic channel geometry was relevant for the flow upstream of the SMX mixer for the MRI trials. The 150 mm entrance length was sufficient to ensure fully developed flow for the glycerol streams, based on Equation 3.8, where the hydrodynamic entry length required to achieve a fully developed laminar flow under the flow conditions of the experiment was found to be 0.0125 m or 12.5 mm. The analytical solution for this geometry was presented by Alassar and Abushoshah (2012) to describe flow through the semi-elliptic channel formed by the flat flow splitter. Hagen-Poiseuille flow in an empty pipe was relevant for the flow downstream of the SMX mixer. Qualitatively the histograms for these geometries differ than those for the SMX mixer (Figure 3.11b). The histogram for flow in the semi-elliptic channel is relatively flat over the dimensionless velocities from 0 to 2 as compared to the empty pipe histogram that peaks at a dimensionless velocity of 2.

$$L_{h,laminar} = 0.05ReD \qquad 3.8$$

Similar in concept to the histogram, probability distributions functions were given by Zalc and co-workers (2002; Fig. 8) for glycerol fluid properties in the SMX mixer at $Re <$ 10. In contrast to Figure 3.11a, those distributions drop sharply at a dimensionless velocity of 1.7. The computational study also yielded a much larger fraction of dimensionless velocities in the range from 0 to 0.5. As stated above, though fluid velocity was expected to be zero at solid surfaces to satisfy the no slip condition, the PEPT particle was not observed to enter this boundary layer region, presumably due to its size. Therefore, in the experimental study with PEPT, the lower velocities in a histogram should be expected to be under-represented due to the technique.

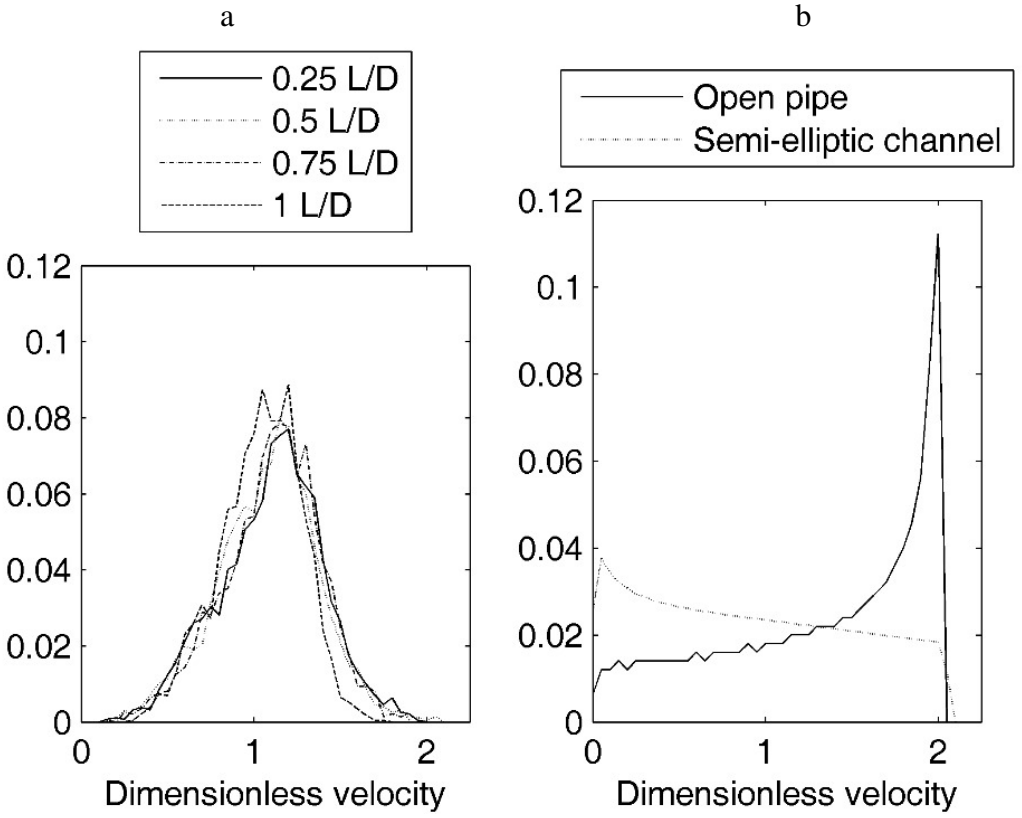

Figure 3.11. Histograms for (a) PEPT data at the positions given in Fig. 9, and (b) analytical velocity maps for upstream and downstream geometries flow.

3.4.3 PEPT & MRI RESULTS

In 2002, Galaktionov and co-workers introduced flux-weighted intensity of segregation to assess mixing in a Kenics mixer (Galaktionov *et al.* 2002). This group later applied the concept to SMX mixers with a recent article being Meijer *et al.* (2012). The flux-weighted intensity of segregation incorporated both flow and concentration at cross sections of the mixer obtained through computational methods. As with the intensity of segregation given in Equation 3.4, the flux-weighted intensity of segregation is the ratio of local variance to initial variance. The variance is now flux-weighted variance and is given by:

$$s_F^2 = \frac{1}{F}\sum_{i_n=1}^{N}\left(X_{i_n} - \bar{X}\right)^2 f_{i_n} \qquad 3.9$$

where f_i (m s^{-1}) is the volumetric flux (that is, axial velocity) through pixel i_n and F is the total flux through the mixer (m s^{-1}). Equation 3.9 is incorporated into the flux-weighted intensity of segregation:

$$I_F = \frac{s_F^2}{s_{Fo}^2} \qquad 3.10$$

For the same reason that the experimental coefficient of variation was used in this study (Figure 3.7b), the initial variance in the denominator of Equation 3.10 was also calculated from experimental concentration (*i.e.* standardised signal intensity) data rather than statistical theory.

Due to the data analysis procedures for MRI and PEPT, images at the same axial location were 83 x 83 pixels and superimposable. Individual PEPT pixel velocities in an image corresponded to f_i in Equation 3.9. Standardised MR signal intensity values corresponded to X_i in Equation 3.9. For each of the 9 SMX elements in the MR study, pixel-by-pixel operations were performed using the corresponding PEPT image (Figure 3.10) at 0.25 *L/D*, 0.5 *L/D*, 0.75 *L/D* and 1 *L/D* to yield the flux-weighted intensity of segregation at that position. Both the non flux-weighted (Figure 3.7a) and flux-weighted intensity of segregation are given in Figure 3.12 on the more conventional semi-logarithmic axes. For this MR study with the two viscosity matched glycerol test solutions delivered to the SMX mixer at a 50:50 ratio, the non flux-weighted and the flux-weighted intensity of segregation values are quite similar, with the exception that the flux-weighted values are subject to less fluctuation at *L/D* values greater than 4. Over the second, third and fourth elements, the values of the two statistics show a characteristic linear decrease on the semi-logarithmic scale. It must be noted, that the flowrates of glycerol are not

consistent between the MR and PEPT experiments. However, when comparing the changes in the intensity of segregation across the mixer obtained using PEPT at different flowrates, no evidence of fluid velocity effect was observed, suggesting that this inconsistency would not affect the ability to combine the results across the two techniques. The comparison between different feed and flow conditions on the intensity of segregation will be discussed in detail in Chapter 5.

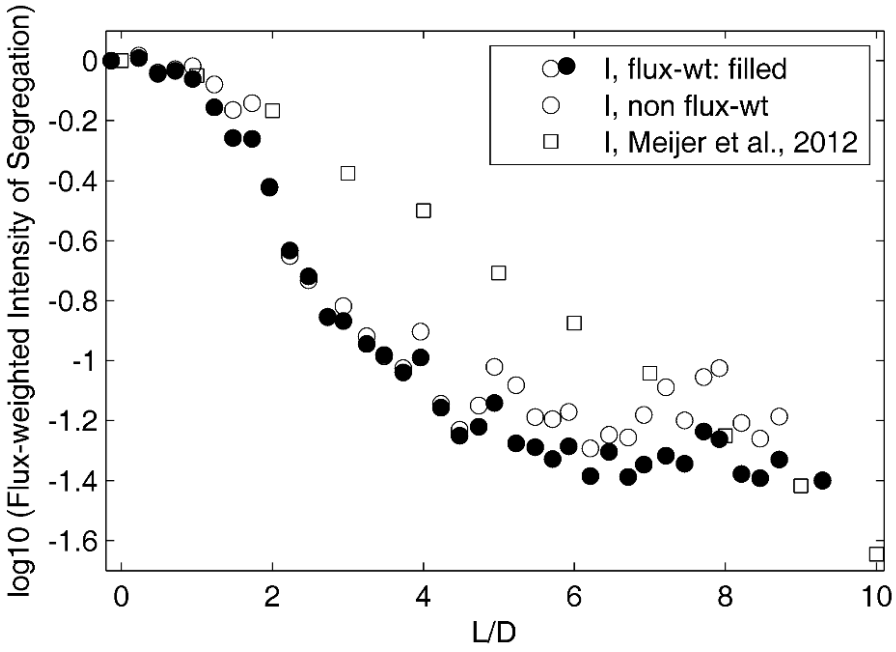

Figure 3.12. Intensity of segregation as a function of L/D, (●) MR concentration data from Fig. 5a, (○) combining PEPT velocity data and MR concentration data, and (□) published flux-weighted intensity of segregation for the same geometry, Standard SMX (2, 3, 8).

As stated in Section 3.2, Meijer and co-workers (2012) incorporated flux-weighted intensity of segregation as part of the quantitative comparison of different types of static mixers. The intent of that study was to provide assessment on the performance of industrially relevant static mixers; the comparison of performance within the study is more relevant than comparison to this work. Nonetheless, values of flux-weighted intensity of segregation for a standard SMX (2, 3, 8) taken from their Fig. 11 (Meijer *et al.* 2012) are

plotted on Figure 3.12. From the figure, it can be clearly seen that the experimental results obtained using the PEPT and MRI methods show much more efficient mixing performance than that found using a computational approach by Meijer *et al*. In order to carry out such computational work some assumptions need to be made about the system under investigation, such as fluid dynamics models. For systems, such as those describing flow through pipes and static mixers CFD models traditionally apply assumptions and models that describe the fluid dynamics through sets of differential equations, solved at every node within the model mesh. The SMX models were created using Navier-Stokes equations, which are widely used for fluid dynamics simulations and have been experimentally validated to be sufficiently accurate for both laminar and turbulent systems. However, the classical set of Navier-Stokes of equations, as the one used by Meijer *et al*., does not account for certain instabilities in the flow, such as vortex shedding off the back of obstacles in the flow field, while modified equations have been proposed to include such phenomena (Hirech *et al.* 2003; Ghanem *et al.* 2013). This lack of ability to predict certain local phenomena that are likely to occur in a system as complex as an SMX mixer could be the underlying reason for the disagreement between the CFD and the experimental results shown in Figure 3.12. Local instability, such as vortex shedding off the joints between the mixer elements or the individual blades, would contribute to local mixing, even under laminar flow conditions, reducing the intensity of segregation more efficiently than what can be expected of a model system which assumes mixing only due to the redirection and folding of the fluid by the mixer geometry. However, such phenomena cannot be directly observed due to the resolution of the techniques used.

Furthermore, the resolution of the experimental technique prevents the differentiation of the changes in the intensity of segregation beyond the 4^{th} mixer element, as at this stage the size of the individual striations becomes finer than the grid into which the cross-section

of the mixer is broken down for analysis. Nevertheless, the first four elements in which mixing can be tracked provide strong evidence to the presence of additional mixing mechanisms, alongside the stretch and fold mechanic of the SMX.

3.4.4 PEPT AND MRI COMPARISON

These two experimental techniques have been utilised to characterise mixing and the data are in excellent agreement for equivalent experimental setups. The strength of the PEPT technique is the ability to measure particle velocities which are used to calculate both velocity and concentration as a function of position in the mixer. Metal structures may also be used in the PEPT apparatus. In contrast the strength of MRI is the ability to measure fluid concentration as a function of position. Only extremely limited uses of metal in the object to be imaged are possible inside the MRI system and hence non-metallic structures are required for the mixing and piping network. To achieve the most accurate concentration measurements the fluid flow inside the MRI should be stopped during acquisition. Methods exist to flow compensate the data acquisition however the concentration results will likely have some degradation in accuracy. MRI may also be used to measure fluid velocity and molecular diffusion (Callaghan 2011). In mixing of suspensions the potential exists to measure particle behaviour using PEPT and fluid behaviour using MRI permitting an almost complete characterisation of the material and mixing process.

3.5 CONCLUSIONS

PEPT and MRI are powerful experimental techniques that can be employed, either separately or together, to study a variety of flow systems. By proper experimental design, the limitation of each technique was addressed. For MRI, material of construction was non-metal; for PEPT, the recirculation loop was designed to maximise the activity of the γ-ray emitting particle.

MRI signal intensity data were successfully related to local component concentrations within the SMX static mixer. The resulting concentration images were discussed in terms of conventional mixing statistics. PEPT captured the real-time spatial location of the tracer particle which was interpreted in terms of both local concentration and velocity vectors. The PEPT technique offers the advantage of future analysis of velocity gradients and shear rate distribution within the mixer. The discussion of laminar mixing in the SMX was enhanced by the incorporation of PEPT velocity information and MRI concentration information in the flux-weighted intensity of segregation. Comparisons of the results of this study were made to computational studies performed with CFD and the mapping method. CFD concentration maps and MR images are qualitatively and quantitatively similar with respect to the development of "spade-like" structures and the spatially-periodic chaotic flow. The mapping method provided an excellent means to combine local velocity and concentration information in a single statistic, the flux-weighted intensity of segregation. The experimental data from PEPT and MRI suggest that mixing is more effective in the initial stages of the SMX mixing elements than predicted from CFD and that shorter length static mixing sections could achieve desired results.

The ability to combine these two techniques, MRI and PEPT, opens a range of possibilities for future complementary studies. For example, the techniques can be

combined to evaluate slurries in complex processing geometries, where MRI is used to track the liquid component of the slurry while the PEPT tracer particle represents the suspended solids, resulting in a full characterisation of the system. Additional MRI based measurements could be added to characterise colloidal structures and material domain sizes further extending the description of the state of a system. With the recent introduction of a commercially available combined PET/MRI spectrometer and the continued research efforts to integrate the two technologies the cost associated with the equipment should be significantly reduced in the future. Lower cost of this type of combined spectrometer will enable the transition into more applications in process analysis and process control.

3.6 REFERENCES

Alassar, R.S., Abushoshah, M. (2012) 'Hagen–Poiseuille flow in semi-elliptic micro-channels', *J. Fluids Eng.*, 134(12), 124502 (4 pp.).

Aspect Imaging (2015) M2TM High-Performance Compact MRI System Including Novel Magnet and Gradients Are Used to Power Mediso's NanoScanTM Integrated Whole-Body Pre-Clinical PET-MR and SPECT-MR Systems for In-Line Multimodality Pre-Clinical Imaging. [online], available: http://www.aspectimaging.com/pre-clinical/product/mediso-nanoscan [accessed 4 Jul 2015].

Bakalis, S., Fryer, P.J., Parker, D.J. (2004) 'Measuring velocity distributions of viscous fluids using positron emission particle tracking (PEPT)', *AIChE Journal*, 50(7), 1606–1613.

Callaghan, P.T. (2011) *Translational Dynamics and Magnetic Resonance: Principles of Pulsed Gradient Spin Echo NMR*.

Chiti, F., Bakalis, S., Bujalski, W., Barigou, M., Eaglesham, A., Nienow, A.W. (2011) 'Using positron emission particle tracking (PEPT) to study the turbulent flow in a baffled vessel agitated by a Rushton turbine: Improving data treatment and validation', *Chemical Engineering Research and Design*, 89(10), 1947–1960.

Choi, Y., McCarthy, M. (2004) 'MRI for process analysis: Co-rotating twin screw extruder', *Journal of Process Analytical Chemistry*, 89(10), 72–85.

Eesa, M., Barigou, M. (2008) 'Horizontal laminar flow of coarse nearly-neutrally buoyant particles in non-Newtonian conveying fluids: CFD and PEPT experiments compared', *International Journal of Multiphase Flow*, 34(11), 997–1007.

Etchells, A.W., Meyer, C.F. (2003) 'Mixing in Pipelines', in *Handbook of Industrial Mixing*, John Wiley & Sons, Inc., 391–477.

Galaktionov, O.S., Anderson, P.D., Peters, G.W.M., Meijer, H.E.H. (2002) 'Morphology development in kenics static mixers (application of the extended mapping method)', *Canadian Journal of Chemical Engineering*, 80(4), 604–613.

Ghanem, A., Habchi, C., Lemenand, T., Della Valle, D., Peerhossaini, H. (2013) 'Energy efficiency in process industry – High-efficiency vortex (HEV) multifunctional heat exchanger', *Renewable Energy*, 56, 96–104.

Ghanem, A., Lemenand, T., Della Valle, D., Peerhossaini, H. (2014) 'Static mixers: Mechanisms, applications, and characterization methods – A review', *Chemical Engineering Research and Design*, 92(2), 205–228.

Herzog, H. (2012) 'PET/MRI: Challenges, solutions and perspectives', *Zeitschrift fur Medizinische Physik*, 22(4), 281–298.

Hirech, K., Arhaliass, A., Legrand, J. (2003) 'Experimental Investigation of Flow Regimes in an SMX Sulzer Static Mixer', *Industrial & Engineering Chemistry Research*, 42(7), 1478–1484.

Lee, Y., McCarthy, M.J., McCarthy, K.L. (2001) 'Extent of mixing in a two-component batch system measured using MRI', *Journal of Food Engineering*, 50(3), 167–174.

Leschka, S., Thévenin, D., Zähringer, K., Lehwald, A. (2007) 'Fluid dynamics and mixing behavior of a SMX-type static mixer', *Journal of Visualization*, 10(4), 342–342.

Lim, V., Hobby, A.M., McCarthy, M.J., McCarthy, K.L. (2015) 'Laminar mixing of miscible fluids in a SMX mixer evaluated by magnetic resonance imaging (MRI)', *Chemical Engineering Science*, 137, 1024–1033.

Liu, S., Hrymak, A., Wood, P. (2006) 'Laminar mixing of shear thinning fluids in a SMX static mixer', *Chemical Engineering Science*, 61, 1753–1759.

Mansfield, M., O'Sullivan, C. (2010) *Understanding Physics, 2nd Edition*, Wiley.

Marigo, M., Davies, M., Leadbeater, T., Cairns, D.L., Ingram, A., Stitt, E.H. (2013) 'Application of positron emission particle tracking (PEPT) to validate a discrete element method (DEM) model of granular flow and mixing in the Turbula mixer', *International Journal of Pharmaceutics*, 446(1–2), 46–58.

McCarthy, K.L., Lee, Y., Green, J., McCarthy, M.J. (2002) 'Magnetic resonance imaging as a sensor system for multiphase mixing', *Appl. Magn. Reson.*, 22, 213–222.

McCarthy, K.L., McCarthy, M.J. (2000) 'MRI for process analysis: Kenics static mixer', *J. Process. Anal. Chem*, 5(3, 4), 94–104.

McCarthy, M.J., McCarthy, K.L. (2013) 'Ch. 25 Advanced Sensors, Quality Attributes and Modeling in Food Process Control', in *Yanniotis, S., Taoukis, P., Stoforos, N. G., Karathanos, V.T. (Eds.), Food Engineering Series*, Springer: New York, 2–6.

McCarthy, M.J., McCarthy, K.L. (2014) 'Magnetic resonance imaging and nuclear magnetic resonance spectroscopy.', in *O'Donnell, C., Fagan, C.C., Cullen, P.J. (Eds.),* Springer: New York.

Meijer, H.E.H., Singh, M.K., Anderson, P.D. (2012) 'On the performance of static mixers: A quantitative comparison', *Progress in Polymer Science*, 37(10), 1333–1349.

Mac Namara, C., Gabriele, A., Amador, C., Bakalis, S. (2012) 'Dynamics of textile motion in a front-loading domestic washing machine', *Chemical Engineering Science*, 75, 14–27.

Parker, D.J., Broadbent, C.J., Fowles, P., Hawkesworth, M.R., McNeil, P. (1993) 'Positron emission particle tracking - a technique for studying flow within engineering equipment', *Nuclear Instruments and Methods in Physics Research Section A: Accelerators, Spectrometers, Detectors and Associated Equipment*, 326(3), 592–607.

Pérez-Mohedano, R., Letzelter, N., Amador, C., VanderRoest, C.T., Bakalis, S. (2015) 'Positron Emission Particle Tracking (PEPT) for the analysis of water motion in a domestic dishwasher', *Chemical Engineering Journal*, 259, 724–736.

Rafiee, M., Simmons, M.J.H., Ingram, A., Stitt, E.H. (2013) 'Development of positron emission particle tracking for studying laminar mixing in Kenics static mixer', *Chemical Engineering Research and Design*, 91(11), 2106–2113.

Rauline, D., Blévec, J. Le (2000) 'A comparative assessment of the performance of the Kenics and SMX static mixers', *Chemical Engineering Research and Design*, 78(April).

Singh, M.K., Anderson, P.D., Meijer, H.E.H. (2009) 'Understanding and Optimizing the SMX Static Mixer.', *Macromolecular rapid communications*, 30(4–5), 362–76.

Tadmor, Z., Gogos, C.G. (2006) *Principles of Polymer Processing (2nd Ed.)*.

Tozzi, E.J., Bacca, L.A., Hartt, W.H., McCarthy, M.J., McCarthy, K.L. (2013) 'Study of multi-lamination of a non-Newtonian fluid in a split and recombine static mixer using magnetic resonance imaging', *Chemical Engineering Science*, 93, 140–149.

Tozzi, E.J., McCarthy, K.L., Bacca, L.A., Hartt, W.H., McCarthy, M.J. (2012) 'Quantifying mixing using magnetic resonance imaging', *J. Vis. Exp.*, (59), e3493.

Volkwyn, T.S., Buffler, A., Govender, I., Franzidis, J.-P., Morrison, A.J., Odo, A., van der Meulen, N.P., Vermeulen, C. (2011) 'Studies of the effect of tracer activity on time-averaged positron emission particle tracking measurements on tumbling mills at PEPT Cape Town', *Minerals Engineering*, 24(3–4), 261–266.

Zaidi, H., Guerra, A. Del (2011) 'An outlook on future design of hybrid PET/MRI systems', *Medical Physics*, 38(10), 5667.

Zalc, J.M., Szalai, E.S., Muzzio, F.J., Jaffer, S. (2002) 'Characterization of flow and mixing in an SMX static mixer', *AIChE Journal*, 48(3), 427–436.

CHAPTER 4. VELOCITY FIELD CHARACTERISATION IN SMX MIXERS FOR NEWTONIAN AND NON-NEWTONIAN FLUIDS USING PEPT

Data and discussions contained within this chapter have been published within:

Mihailova, O., O'Sullivan, D., Ingram, A., Bakalis, S., 2016. Velocity Field Characterisation of Newtonian and Non-Newtonian Fluids in SMX Mixers Using PEPT. *Chemical Engineering. Research & Design,* **108**, 126–138.

Mihailova O., O'Sullivan, D., Bakalis, S. (2015). Characterisation of velocity fields in SMX static mixers using PEPT. 15th European Conference on Mixing proceedings.

4.1 ABSTRACT

The ability to predict fluid behaviour, such as velocity distribution or degree of mixing, is a critical step in designing industrial mixing processes. However, the majority of processing technologies are difficult to study using traditional approaches, due to the opacity/impermeability of the construction materials, as well as employed fluids, and geometric complexities of such systems.

The current work applies Positron Emission Particle Tracking (PEPT), which allows characterisation of complex systems. PEPT relies on triangulation of γ-rays emitted by a radioactive tracer particle, allowing the study of geometrically complex systems regardless of the system properties. This study compares the velocity distributions a Newtonian fluid, glycerol, and a non-Newtonian fluid, guar gum solution (0.7% w/w), flowing through 10 elements of a DN25 SMX mixer at 300 L/h.

Axial velocity remained positive throughout and no back-mixing was exhibited. The velocity components appeared to be independent of rheology, with the overall flow across 10 mixer elements resembling plug flow. Radial velocities were unimodally distributed around zero in the direction where no mixing was induced, while in the direction in which radial mixing is induced the velocity distributions were either uni- or bimodal, depending on the geometry of the cross-section.

4.2 INTRODUCTION

Continuous processing presents several benefits over the traditional batch or semi-batch approaches which are predominantly used in fast moving consumer goods (FMCG) industries. Continuous processing allows reductions in waste and energy, as well as consumption of material, which leads to more streamlined processes and optimised processing times (Nienow *et al.*, 1997). Many continuous processing steps involve mixing and blending of streams with different rheological properties, with the properties of the combined streams often differing to that of the inlet streams. Such processing steps are often achieved by the application of static mixers, therefore understanding and characterising the processes occurring within static mixers is crucial for efficient process development (Han E.H. Meijer et al., 2012; Mihailova et al., 2015)

The current work addresses the demand for an enhanced understanding of flow patterns within industrially utilised SMX static mixers (Figure 4.2). SMX mixers, originally developed by Sulzer, are used in a variety of applications, including mixing miscible components (*e.g.* blending), combining immiscible streams (*e.g.* emulsification, encapsulation, *etc.*), as well as for processes that include a reaction step between the inlet streams (*e.g.* purification) (Das, 2011; Fradette *et al.*, 2007). Furthermore, SMX mixers can be applied to multiphase processes, dispersing gases or solids through a liquid phase (Fradette *et al.*, 2006; Laporte *et al.*, 2015). SMX mixers are designed for laminar flow applications and rely on breaking and recombining the bulk of the inlet streams into smaller streams, using a series of channels (Paul *et al.*, 2004). For the case of miscible fluids, such as those addressed in this study, the individual channels guide the streams to come in contact with each other, creating striations within the bulk. The alternating

geometry of the mixers induces the development of such striations across the entire cross-section of the mixer, ultimately leading to fully a mixed flow (Mihailova *et al.*, 2015).

The majority of evaluation of such systems to date has been conducted using indirect approaches, due to the complexity and impermeability of the construction materials, such as stainless steel, and the opacity of materials flowing through the system, for example shampoo (Fradette *et al.*, 2007; Visser and Rozendal, 1999). As a result the majority of characterisation relies upon the analysis of the mixer output stream, through particle image velocimetry (PIV) (Leschka *et al.*, 2007), pulsed ultrasonic velocimetry (Hammoudi *et al.*, 2008), as well as, blending of immiscible materials to assess the level of dispersion at the outlet (Das et al., 2013b; Fradette et al., 2006; Hammoudi et al., 2012). Moreover, the flow and mixing patterns within SMX mixers have been explored using computational fluid dynamics (CFD), where numerical simulations were used to predict the velocity fields within the boundaries of the mixer based on a series of assumptions about the underlying forces and the resulting properties of the flow (Visser and Rozendal, 1999; Zalc *et al.*, 2002). The definition of the velocity fields further allows seeding tracer particles into the system, assessing the mixing patterns and the degree of mixing at the output (Liu *et al.*, 2006).

Positron Emission Particle Tracking (PEPT) offers a novel direct approach for tracking flow within systems, for instance static mixers, which are not readily applicable for study using applied methods. PEPT has been demonstrated as an effective technique for the characterisation of flow within Kenics static mixers (Rafiee *et al.*, 2011). With neutrally buoyant 200 μm radioactive tracer particles, that are sufficiently small to behave as a representative volume of the fluid, with the Stokes number below 2×10^{-5}, it is possible to trace the flow through the system of interest irrespective of the materials used in construction or the fluids flowing through the system.

The current chapter focuses on characterising local velocity distributions within a 25 mm SMX static mixer assembly, containing 10 mixer elements. Local velocity estimations can be achieved by analysing the rate of displacement of individual particle passes as they travel through the mixer. This work focuses on comparing local velocity fields of two fluids with distinct rheological properties, Newtonian glycerol and non-Newtonian shear-thinning guar gum solution (0.7% w/w), moving through the mixer assembly at 300 L/h. Understanding the effects of rheology on the flow of fluids through the mixer provides valuable insight into the dynamics of the mixer and allows superior process design, optimising manufacturing processes which utilise SMX mixers.

4.3 MATERIALS AND METHODS

4.3.1 MATERIALS

4.3.1.1 FLUIDS

Pure glycerol (Reagent, UK) and 0.7% w/w guar gum solution (Impexar, UK) were used for the current work. These fluids were chosen as the majority of fluids used in continuous liquid mixing processes exhibit either Newtonian (glycerol) or shear thinning (guar gum) behaviour under the conditions of the flow (Singh et al., 2009) (Figure 4.1). The behaviour of guar gum under shear was best described by the Carreau–Yasuda model (Equation 4.1), that estimates the effective viscosity of the solution (μ_{eff}; Pa.s) at a given shear rate ($\dot{\gamma}$; s^{-1}) based on the initial viscosity of the solution (at zero shear) (μ_0; Pa.s), the viscosity at infinite shear rate (μ_{inf}; Pa.s), relaxation time (λ; s), the power index (n_y; -) and transition constant (a; -) (Yasuda et al., 1981).

$$\mu_{eff}(\dot{\gamma}) = \mu_{inf} + \left(\mu_0 - \mu_{inf}\right)(1 + (\lambda\dot{\gamma})^a)^{\frac{n_y-1}{a}} \quad 4.1$$

Where μ_{inf} = 0.01 Pa.s, μ_0 = 5.27 Pa.s, λ = 0.76 s, n_y = 0.23 (-) and a = 0.80 (-). However, based on the Streiff-Jaffer correlation (Equation 4.2) it is possible to determine the expected average shear rate in a static mixer based on the average velocity (V; ms^{-1}) and the diameter of the mixer (D; m) (Streiff et al., 1999).

$$\dot{\gamma}_{SMX} = \frac{64V}{D} \quad 4.2$$

Under the conditions of the flow, the expected average shear rate is ca. 380 s^{-1}. As can be seen in Figure 4.1, for this range of shear rates it is possible to assume that the fluid behaves as a simple Power law fluid (Equation 4.3), correlating effective viscosity with the shear rate via power index (n_p; -) and flow consistency index (m; Pa.s) where the constants are as follows n_p = 0.32 and m = 4.50 Pa.s.

$$\mu_{eff}(\dot{\gamma}) = m\dot{\gamma}^{n_p-1} \quad 4.3$$

For all models the effective viscosity is representative of the bulk viscosity, at higher shear rates. As a Newtonian fluid glycerol maintains a constant viscosity of 1.13 Pa.s across the entire range of shear rates at constant temperature. For guar gum solution the shear rate at the wall was chosen for the estimation for the apparent viscosity, as it has been previously applied for similar calculations in SMX mixers (Li et al., 1997).

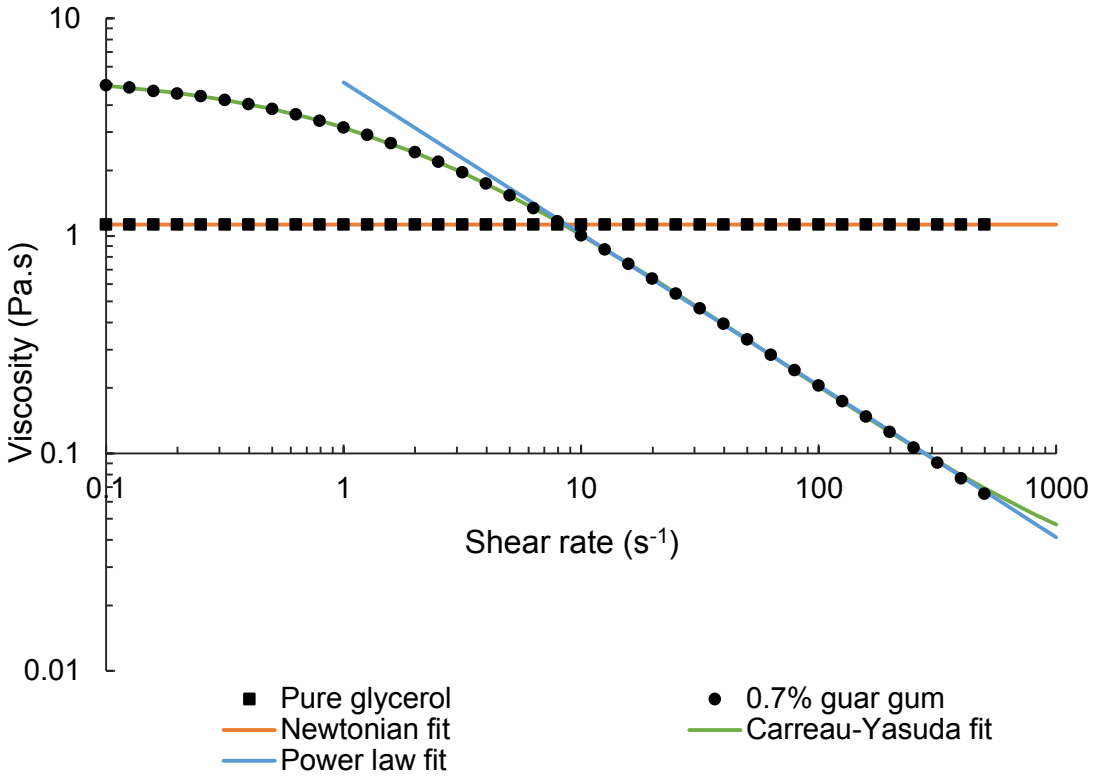

Figure 4.1. Effect of shear rate on the viscosity of glycerol and 0.7% w/w guar gum solution, at 22.5°C. Solid markers represent experimental data obtained using rotational rheometry. Colour lines represent fluid model fits, Newtonian for glycerol (orange), and Carreau-Yasuda (green) and power law (blue) for guar gum solution.

4.3.1.2 SMX MIXERS

For the purposes of this work SMX mixers with diameter of 25 mm, or DN25, were used. The SMX static mixers elements have a characteristic structure with 6 planes of blades, where each alternating plane is at 90° to the preceding (Figure 4.2a), creating a crisscross lattice which redirects the fluids in a stretch and fold manner inducing mixing across the pipe cross-section in the direction parallel to the orientation of the blades. Each consecutive mixer element is mounted at 90° to the preceding, which in turn induces mixing across the pipe cross-section, but perpendicular to that in the prior element. SMX assemblies normally contain an even number of elements, to allow for the same number of

elements in each orientation, to ensure balanced mixing in every direction. For this work, the two cross-sectional planes at 6.5 mm and 9.5 mm will be considered, along with the mixer as a whole. Despite the different distribution of the mixer geometry across the cross-section (Figure 4.2b), the area that is unobstructed and available for the flow of the fluid remains constant. These two cross-sections illustrate how the geometry of the mixer changes along the mixer length, presenting the two extreme cases, a cross-section divided into larger section by solid walls (6.5 mm) and a cross-section with smaller compartments segregated, but not isolated, by the mixer blades (9.5 mm).

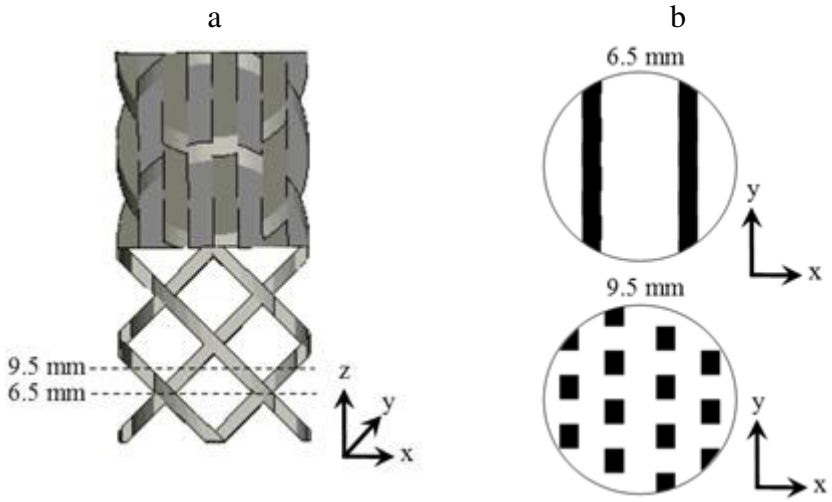

Figure 4.2. (a) Schematic representation of two SMX mixer elements and (b) cross-sections at 6.5 and 9.5 mm into the first mixer element.

To reduce the effect of the metal lattice on the path of the γ-rays that are emitted by the PEPT tracer particles and are used in location mapping the SMX mixers used in the current work were 3D printed in VeroClear plastic (Stratasys Ltd, USA), with the mixer blades 2 mm thick, as opposed to the stainless steel (SS) alternative typically used in industry, with the blade thickness of 1 mm. The blades were made thicker to enhance the structural integrity of the assembly. However, this reduces the voidage of the system, which in turn results in increased pressure drop across the mixer. Through comparing pressure drop data in both SS and plastic mixers of equivalent diameters at a range of

flowrates it was established that pressure drop across the 3D printed mixer is *ca.* 20 % greater than that in a SS mixer, for both fluids. This observed difference in pressure drop agrees with the expected pressure drop difference estimated using the Darcy-Weisbach equation, when accounting for the reduction of the cross-sectional area available for flow.

4.3.2 METHODS

4.3.2.1 POSITRON EMISSION PARTICLE TRACKING

Positron Emission Particle Tracking (PEPT) has been first developed at the University of Birmingham in the early 1990s and is based on a pre-existing medical technique known as Positron Emission Tomography (PET) (Parker *et al.*, 1993). PEPT has been successfully used in a number of studies characterising a wide range of industrial equipment, such as vertically stirred mills (Conway-Baker *et al.*, 2002), tumbling mills (Volkwyn *et al.*, 2011), stirred tanks (Chiti *et al.*, 2011), as well as home appliances, such as washing machines (Mac Namara *et al.*, 2012).

The technique relies on tracing a single radioactive particle through the system of interest. The particle spatial location is estimated through triangulation of back to back γ-rays that are emitted during radioactive decay of the fluorine-18 isotope, encapsulated in the particle, and picked up by an array of detectors, or cameras, either side of the equipment. For each location the triangulation algorithm uses up to 100 individual γ-ray pairs, with outliers and invalid pairings removed, to provide improved location accuracy. With fluorine-18 having a half-life < 110 minutes γ-ray emission is rapid enough to estimate the averaged particle location once every ten milliseconds and due to the application of γ-rays, that can penetrate most materials, allows using the technique on real, unmodified industrial systems. However, a balance between the rate of displacement and the rate of location acquisition needs to be struck, to ensure reliable results. The 3D tracer

location data with respect to time allows the derivation of a number of system properties, such as occupancies, concentrations, mixing efficiencies, local velocities and local shear rates (Bakalis *et al.*, 2006).

For the current work neutrally buoyant *ca.* 200 µm diameter tracer particles were used. A single particle was present in the flow at any given time and allowed to recirculate until the activity was lost and a new particle could be introduced. In excess of 800 individual particle passes were recorded for each set of experimental conditions, to give a high probability of detection across the entire system, sufficient to reconstruct the flow regime in the volume of the mixer element using PEPT particle locations.

4.3.2.2 EXPERIMENTAL RIG

Figure 4.3 below illustrates a schematic representation of the experimental rig used for the PEPT trials studying SMX mixers. 10 SMX elements were encased in a 26 mm diameter Perspex pipe and placed between the PEPT detectors, with approximately 15 cm of empty pipe on either side of the mixer within the field of view, to assess the velocity distribution within simple geometries, for technique validation (Abulencia and Theodore, 2009). The flow rate was controlled using a variable speed pump (Xylem, UK) and monitored using an inline flow meter (Krohne, USA), the fluid carrying the tracer particle was continuously recirculated around the system. Two pressure transducers (Keller AG, Switzerland) were located either side of the field of view. The temperature was not controlled, but was monitored, and throughout all trials remained within the 22.5 ± 0.5^{o}C. Laboratory scale rheological tests on a rotational rheometer (TA Instruments, USA) using a 60 mm aluminium cone and plate geometry have shown that such temperature variations do not affect the rheological properties of the fluids significantly, with a much higher 5 ^{o}C temperature deviation leading to up to 3 % change in viscosity of the fluid.

The volume of the system outside of the field of view was minimised, to reduce the time it takes for the particle to return to the field of view, as well as the volume of the carrier fluid required for the experiments. The radioactive components within the tracer particle were observed to leach into the carrier fluid, leading to an increase in background radiation, reducing the contrast between the tracer and the background, requiring the system to be periodically emptied and refilled with uncontaminated fluid.

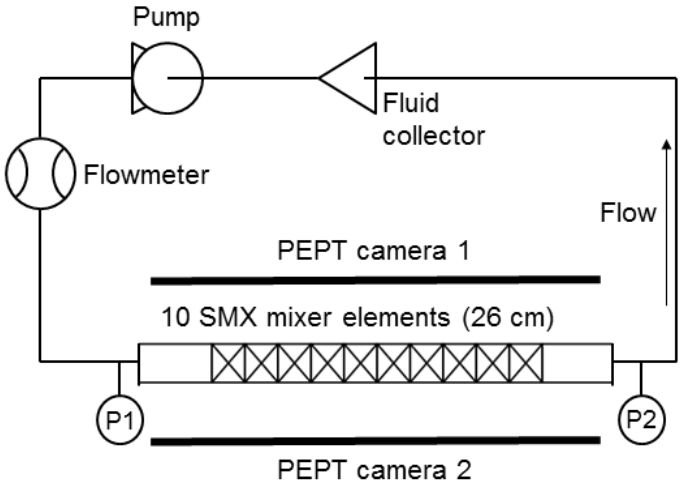

Figure 4.3. Schematic representation of the experimental set up, showing the camera field of view and the recirculation system used.

The flowrate of both fluids was maintained at 300 L/h throughout all experimental resets. This flowrate was chosen as it reflects typical industrial flowrates for such mixer diameters while maintaining the Reynolds number for both fluids under 20, ensuring laminar flow. Traditional estimations of Reynolds number for simple empty pipes would not be applicable for determining the flow regime inside the SMX mixer, as the diameter of the individual channels within the mixer governs the magnitude of Re, as opposed to the pipe diameter. To resolve this issue a number of studies have applied the pore Reynolds number, Re_p,(Equation 4.4), where the mixer is treated as a porous medium with known porosity and tortuosity (Hammoudi *et al.*, 2008; Hirech *et al.*, 2003). This allows to differentiate the flow in individual pores, or in the case of the SMX mixer channels.

Morancais et al define the values for the mixer tortuosity based on the mixer length and individual pore diameter (Morancais et al. 1999). For the mixer with the diameter of 25 mm the tortuosity was found to be 1.48. Based on these values of tortuosity and the porosity value which was found previously in Section and the apparent viscosity of the fluid based on the average shear rate derived from Equation 4.2 the Re_p < 15 for glycerol and Re_p < 11 for guar gum at 300 L/h, confirming that flow within the mixer at these flowrates is expected to be laminar

$$Re_p = \frac{\rho V \tau d_p}{\varepsilon \mu_{eff}} \quad 4.4$$

Where V is the average velocity in the empty pipe (m s^{-1}), ρ is the density (kg m^{-3}), τ is the tortuosity (-), μ_{eff} is the viscosity (Pa.s), ε is the porosity (-) and d_p is the pore diameter (m), where τ=1.48 (Hammoudi et al., 2012)

This permitted the particle to quickly travel through the system outside the field of view, while maintaining high detection count of up to 450 locations per pass through the field of view.

4.3.2.3 DATA PROCESSING

Raw binary PEPT data was processed using in-house algorithms in order to obtain the tracer location in 3D space with respect to time, which allows the visualisation of the entire volume of the system using tracer locations. The data was then separated into individual particle passes based on time between subsequent detections, where positions belonging to the same pass will have a time difference in the order of milliseconds, while different particle passes will differ by approximately one minute, as that is the time required for the tracer to travel though the system outside of the field of view. Up to 800 particle passes were extracted per set of experimental conditions.

By fitting a polynomial expression to a series of sequential points describing the particle trajectory over time and taking a derivative of this expression with respect to time it is possible to determine the local velocity both along individual axes, as well as overall (Mihailova *et al.*, 2015). In order to estimate the local velocity components U_x, U_y and U_z that represent the component in the corresponding direction, a polynomial expression was fitted to a set of 7 sequential particle locations, with the central point of the range being the fitting point of interest, as shown in Figure 4.4. The resulting expression took on a form shown in Equation 4.5, where the location of the particle along one of the axis (i, mm) at a given time is determined by the particle trajectory with respect to the corresponding axis (x, y or z) and time (t; ms), where the number of constants a and n used depend on the degree of the polynomial fit. After the velocities at the mid-point of the set of sequential data points is determined the algorithm shifts by one point along the time dimension, selecting a new set of 7 points. This process allows to determine the velocity values along the entire particle pass, with some points left out at the beginning and end of the particle pass, as there is no way the first and last 3 points can be placed in the middle of the 7-point data sub-set. However, as the particle passes span significantly outside the SMX mixer into the empty pipe region, the loss of these points does not affect the quality of the dataset.

By differentiating the particle location expression (Equation 4.5), it is possible to obtain the rate of change of location with respect to time, U_i (m s^{-1}), *i.e.* velocity (Equation 4.6).

$$i = a_1 t^n + a_2 t^{n-1} + \ldots + a_{n-1} t + a_n \qquad i = \text{x, y, z} \qquad 4.5$$

$$U_i = \frac{di}{dt} = n a_1 t^{n-1} + (n-1) a_2 t^{n-2} + \ldots + a_{n-1} \qquad i = \text{x, y, z} \qquad 4.6$$

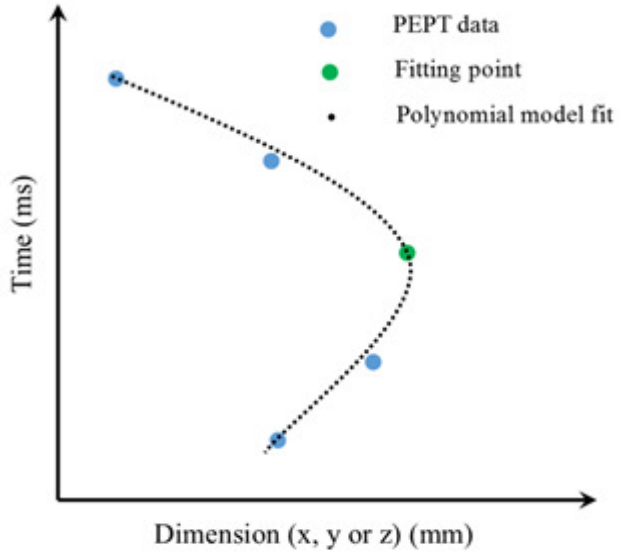

Figure 4.4. Schematic representation of polynomial curve fitting for local velocity estimation

When processing the experimental data n vas assigned a value of either 2 or 3depending on whether a quadratic or a cubic function best described the pass taken by the particle between the points to which the polynomial fit was applied. Under the laminar flow conditions maintained in the experiments, the main variations to the particle trajectory were expected to originate from the changes in geometry. Based on the predicted particle velocity and the dimensions of the mixer, the particle is not expected to change trajectory more than twice in the section of each fit, therefore a cubic expression is expected to be the highest order polynomial which can be applied to the data without accounting any variations due to the noise in the signal as real data. However, for sections with less variation in the particle trajectory, a quadratic fit often describes the particle path better than the cubic fit. The decision on which polynomial describes the experimental data best was made for each set of points based on the R^2 value for both fits. Based on the average random error in both the distance and the time measurements, the error of the function derivative can reach ± 0.01 m s^{-1}, *i.e.* up to 5% of the average values calculated using this approach.

To enhance the resolution of the data and due to the symmetry of the mixer elements it was possible to separate the data in the mixer section into 10 discrete segments, representing one mixer element each, as shown in Figure 4.5. Every second element had to be rotated 90 degrees on the x-y plane, to achieve alignment. The velocity fields in first and last elements were compared to those in the remaining elements, and it was concluded that entry/exit effects were not causing discrepancies in the velocity distributions. The 10 elements were then superimposed to significantly increase the number of detections per element volume, up to 8000 particle passes, resulting in a detailed representation of a single SMX element (Figure 4.5).

The detailed SMX element was then separated into slices perpendicular to the z-axis (*i.e.* direction of the flow) allowing to visualise and assess the velocity distribution filed within the different zones of the mixer element.

Velocity distributions across the SMX mixer were assessed by comparing them to standard unimodal and bimodal distributions, where a unimodal distribution exhibits a single mode, *i.e.* only single highest value is observed, and conversely a bimodal distribution, is a superposition of two unimodal distributions, exhibiting two distinct maxima.

The Kolmogorov-Smirnov two-sample test with a 95% confidence interval was used to assess the significance of the results. Data with $P < 0.05$ was considered statistically significant.

All of the above computational processing was conducted for both fluids using in-house developed scripts in MATLAB R2013a (MathWorks, USA).

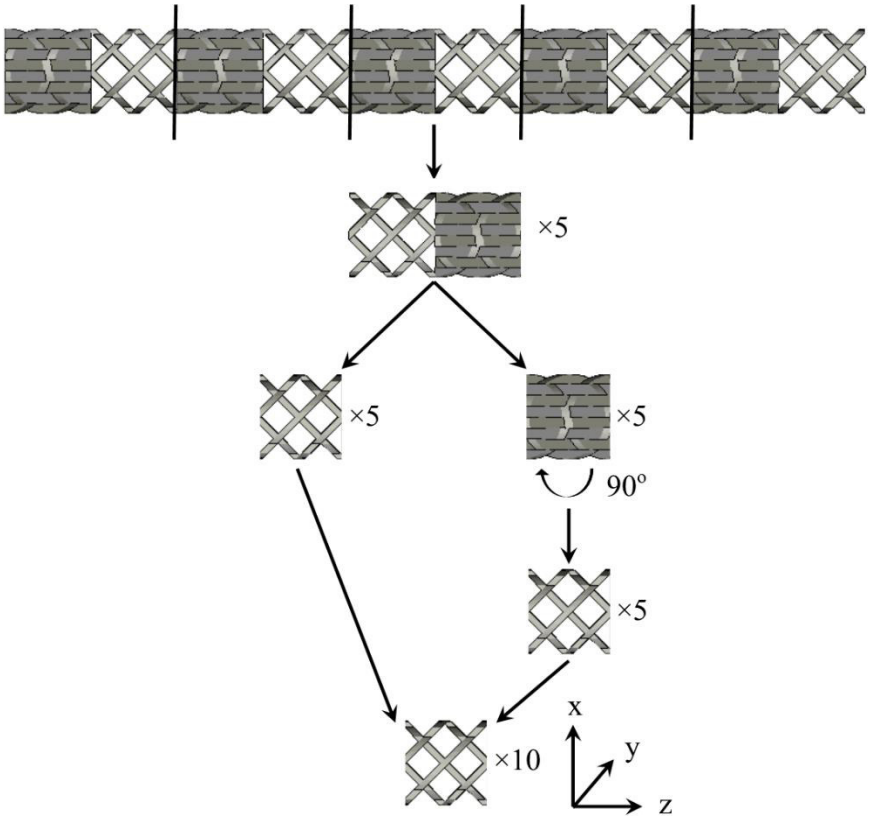

Figure 4.5. Schematic representation for the separation of the 10 element mixer assembly into individual elements.

4.4 RESULTS AND DISCUSSION

Based on the dramatically different geometry of the mixer cross-sections (*cf.* Figure 4.2b) and the intricate lattice of the mixer blades, it can be expected the velocity distribution within the mixer element relies on the geometry, which is designed to redirect and alter fluid streams to induce mixing. However, it has to be noted that depending on the specific location within the mixer element the intensity of the velocity field varies, as the walls, or blades, of the mixer geometry come together and move apart, blending the streams. In addition to the differences in the geometry of the cross-section, it is also important to consider the orientation of the mixer element, which defines the direction in which mixing is induced.

After collapsing the data from 10 mixer elements into one, the orientation of the resulting element is such, that radial velocity component U_x becomes the velocity in the direction of induced radial mixing, with the flow parallel to the mixer blade alignment, while U_y becomes the velocity perpendicular to the direction in which mixing is induced. Figure 4.2b illustrates the geometry of the cross-sections in resulting mixer element. It can be expected that the magnitude of the velocity field in the direction of induced mixing will be higher than that in the direction in which mixing is not actively induced. However, when a number of elements are considered, due to the nature of the SMX mixer geometry, where each consecutive element is oriented at 90^o to the preceding element, the direction in which mixing is brought about by the arrangement of the mixer blades changes. This means that radial velocities U_x and U_y alternate at being the velocities in the direction of induced mixing and direction in which mixing is not induces in each element.

Similar velocity patterns were observed both in the Newtonian and non-Newtonian fluids. Before analysing the velocity fields at different locations within the mixer, it is important to consider how the velocity fields in the empty pipe region of the system compare to the theoretical distributions that are expected based on fluid rheology. The solid lines in Figure 4.6a demonstrate the expected theoretical velocity profiles in the circular pipe, for the two fluids of interest, flowing at 300 L/h, symmetrical around the centre of the pipe (Abulencia and Theodore, 2009). The error bars show the average deviation of the PEPT data from the model, where the error is much greater around the centre of the pipe, due to low particle pass probability, as the result of the decreasing cross-sectional area with increasing distance from the pipe wall. The error is also high close to the wall, as particles rarely pass through this region, due to a boundary layer formed near the wall. Any particles entering the wall boundary layer became immobilised, remaining at the boundary, this often required the flowrate to be increased to dislodge the

particle, or in extreme cases, required a full clean and reset of the system, leading to invalid passes being recorded in both situations. However, in the areas with high particle pass detection probability, the model and the experimental data are in agreement, where the experimental data points fit the corresponding models with coefficients of determination (R^2) of 0.951 and 0.946 for glycerol and guar gum solution, respectively.

While it is impossible to fit the velocity distribution within the mixer to the same models as the velocity distribution in the empty pipe, these data sets can be compared on the basis of how frequently the tracer particle exhibits a velocity within a certain range. Such distributions are shown for both glycerol and guar gum within the mixer in Figure 4.6b. No negative velocities were observed for either fluid, suggesting that no back mixing occurs when lateral mixing is induced. The differences in the distribution ranges of U_z were similar to the distributions observed in the empty pipe, with the velocity frequency distribution peaking at a higher value, but overall achieving lower velocities than glycerol. However, these differences were not as pronounced, suggesting that within the channels of an SMX mixer the rheological properties of the fluids maintain an effect on the axial velocity as in the empty pipe, but the internal dynamics of the mixer reduces the overall impact of rheology.

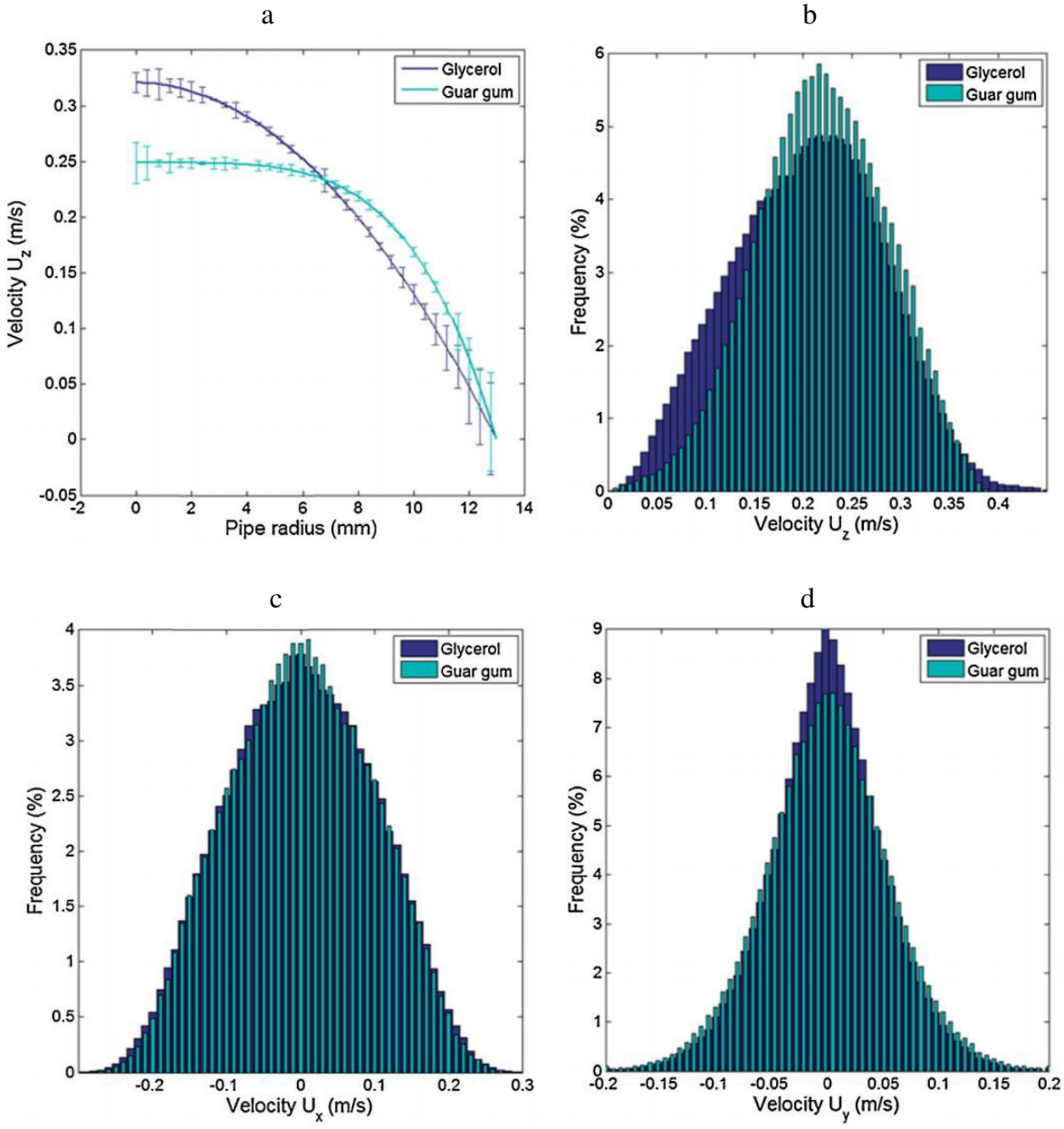

Figure 4.6. (a) Comparison of the empty pipe velocity profiles of glycerol and guar gum, as described by the model based on the fluid rheology. Experimental data fits illustrated by error bars. (b) Glycerol and guar gum solution velocity distribution in the direction of the flow, (U_z) inside of the mixer (c) Glycerol and guar gum solution velocity distribution in the direction of mixing, (U_x) inside of the mixer (d) Glycerol and guar gum solution velocity distribution in the direction perpendicular to the direction of mixing, (U_y) inside of the mixer. All at 300 L/h.

On average axial velocities of the two fluids were 30 % greater inside the mixer than in the empty pipe region. This can be explained by the fact that inside the mixer the cross-

sectional area available for flow is reduced, due to the introduction of the mixer structure. Based on the CAD files from which the mixer elements were printed, it is possible to calculate that the mixer occupies *ca.* 30 % of the empty pipe volume, suggesting $\varepsilon \approx 0.7$, this value is consistent across all cross-sections along the mixer length. Similar values have been previously quoted in literature, where $\varepsilon \approx 0.67$ for a DN25 SMX mixer, indicating that 33 % of the pipe volume is occupied by the mixer (Theron and Sauze, 2011). As the flowrate stays the same, it can be estimated that for the expected reduction in area available for flow, the increase in the average axial velocity inside the mixer is *ca.* 30 % of that of the average axial velocity in the empty pipe. When comparing the glycerol velocity distributions inside and outside the mixer the increase is *ca.* 31 %, with the average value of axial velocity (U_z) outside the mixer of *ca.* 0.16 m/s and the average U_z inside the mixer of *ca.* 0.21 m/s, for glycerol.

For the case of the guar gum solution the average velocity inside the mixer increases by *ca.* 30 %, with the average U_z inside and outside of the mixer of *ca.* 0.22 m/s and *ca.* 0.17 m/s respectively. Similar patterns were previously described by using pulsed ultrasonic velocimetry for velocity field reconstruction, where the overall shape of the profile resembled that of an empty pipe, but exhibited higher values (Hammoudi *et al.*, 2008). Furthermore, in order to validate the porosity of the mixer, it is possible to calculate the total flowrate across any mixer cross-section using velocity maps as the ones shown in Figure 4.7a and c, where the size of each cell on the grid is 0.5 mm × 0.5 mm. For the case of glycerol, the average flowrate based on local velocity values was 287 ± 5 L/h, while for guar gum solution the average flowrate was 292 ± 7 L/h, which compares well to the nominal flowrate across the system determined by the flowmeter.

Within the empty pipe region any velocity components perpendicular to axial flow are equal to zero, however, within the mixer the velocity components across the x-y plane,

perpendicular to the flow, become imperative to inducing the mixing. For the case of the radial velocity component in the x-direction (U_x), the direction in which radial mixing is induced in the current orientation of the mixer element, both glycerol and guar gum solution displayed a normal unimodal distribution around zero between -0.3 and 0.3 m/s, shown in Figure 4.6c. The velocity distribution in the y-direction (U_y), where little mixing occurs, for both fluids, is between -0.2 and 0.2 m/s, normal around zero (Figure 4.6d). It has to be noted, that U_x is the velocity in the direction of mixing due to the geometry, as in this orientation of the mixer element the mixer blades are parallel to the x-axis. The fluid follows the channels formed by the mixer blades, and due to the laminar nature of the flow, motion along the y-axis is not expected. Therefore, the magnitude of U_y is lower than U_x and an increase in U_y is predominantly observed at interfaces of counter-flowing fluid elements.

It has been observed that all the distributions presented in the study display lower than expected frequency counts at lower values of the U_z. This is attributed to the fact that the probability of the tracer particle entering the slow flowing regions close to the assembly walls is significantly lower than the probability of finding the particle in faster moving regions, leading to reduced event counts at lower velocities. Furthermore, when the particle does enter the boundary layers, similar limitations apply as in the empty pipe, where the tracer gets permanently embedded in the stagnant fluid regions close to the wall.

When local velocity fields are considered at cross-sections perpendicular to the flow the unimodal pattern is not consistently observed. Depending on the geometry of the cross-section (Figure 4.2b) both unimodal and bimodal distributions can be displayed.

It was observed, that for case of the axial velocity component, U_z, the distribution at individual cross-sections matches that demonstrated when the entire mixer is considered. Unimodal distribution patterns were displayed for both fluids, irrespective of the position

of the cross-sectional plane (Figure 4.7). Comparison of U_z values at 6.5 mm (Figure 4.7 b) and 9.5 mm (Figure 4.7d) cross-sections demonstrate that velocity distributions for each fluid at these cross-sections are consistent, with the averages comparable within the space of experimental error.

As before (Figure 4.6b), for glycerol the observed range was between 0.00 and 0.43 m/s, with the mean at 0.21 m/s, while for guar gum solution the range was between 0.00 and 0.38 m/s with the mean at 0.22 m/s, at both cross-sections and the same as when the mixer is considered as a whole. Using the Kolmogorov-Smirnoff t-test analysis it is possible to conclude that the velocity distributions for both fluids belong to the same continuous distribution ($P > 0.05$), nevertheless, a weak effect of fluid rheology is noticeable, with glycerol consistently exhibiting higher maximum velocities, while more tracers seeded in guar gum solution are found with velocities closer to the maximum observed for the fluid. Figure 4.7a and c show velocity maps, highlighting the effects of the geometry on the local velocity fields. The similarities in the distributions at different radial cross-sections are due to constant cross-sectional area available for flow, irrespective of the location of the cross-section (Figure 4.2b) and a constant flowrate across each x-y-plane.

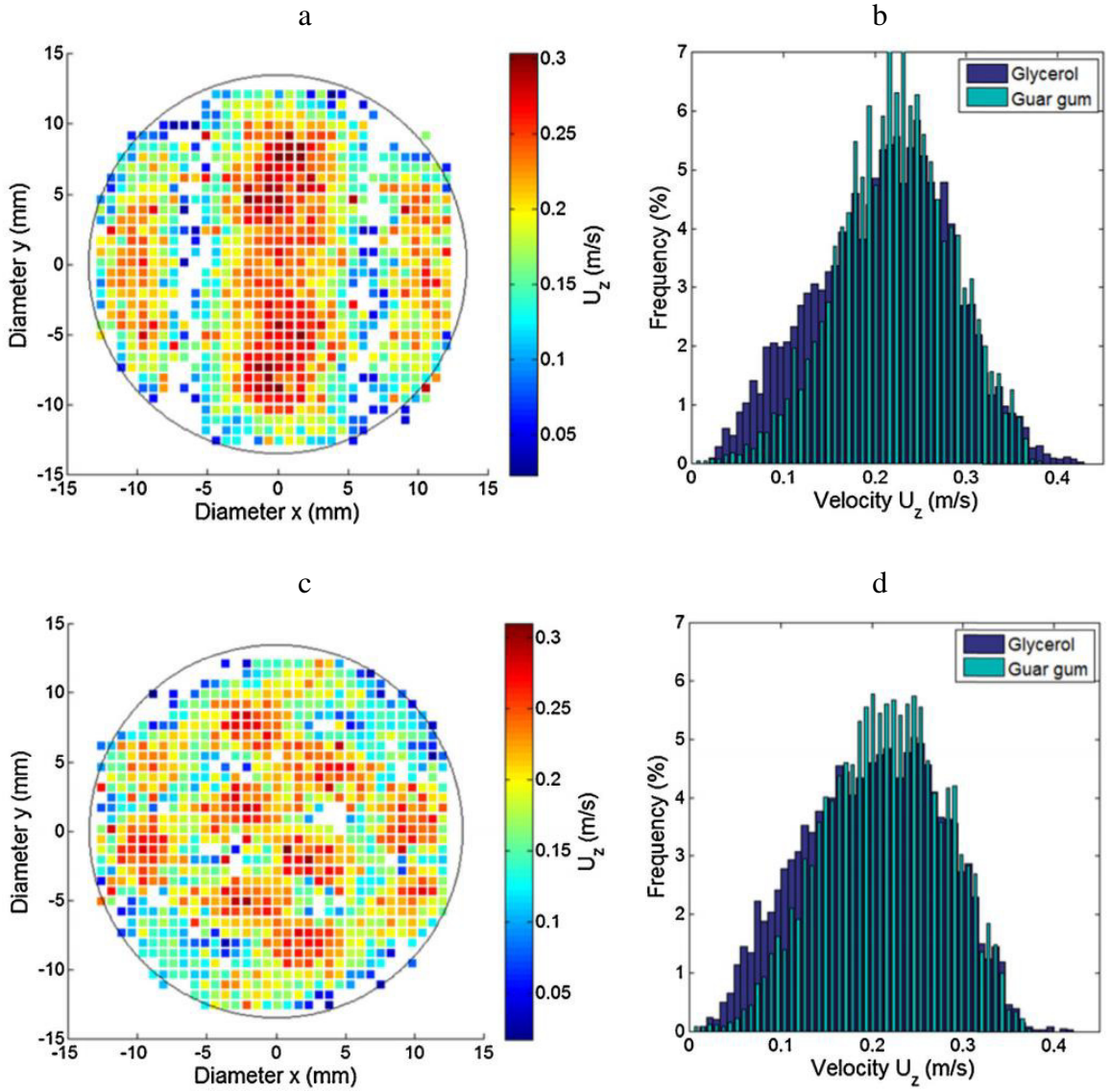

Figure 4.7. (a) U_z velocity map across the mixer cross-section at 6.5 mm for glycerol at 300 L/h and (b) the corresponding distributions for glycerol and guar gum solution. (c) U_z velocity map across the mixer cross-section at 9.5 mm for glycerol at 300 L/h and (d) the corresponding distributions for glycerol and guar gum solution.

Figure 4.8a represents the map of U_x distribution for glycerol flowing at 300 L/h across a cross-section at 6.5 mm into the SMX element, while Figure 4.8b illustrates the frequency of detection for different ranges of U_x at that cross-section, for both fluids. It can be seen that both distributions are unimodal around 0, while the differences in the fluid rheology do not appear to have an effect on the distribution. Conversely, Figure 4.8c

shows the distribution of U_x at the x-y plane 9.5 mm into the mixer element. When considering the frequency of detection plot, Figure 4.8d, it is clear that the distribution is bimodal, with the two maxima at -0.1 and 0.1 m/s. The difference in velocity patterns between the two cross-sections is attributed to the changing geometry of the cross-section at different points along the z-axis.

At 6.5 mm the blades of the mixer converge and the cross-section is divided into three parts, with a larger section in the middle and two smaller sections on the sides, where fluid flowing in opposite directions comes in close contact, resulting in areas where the opposing velocities cancel each other, reducing U_x, leading to a dominant peak at ~0 m/s.

Furthermore, at 9.5 mm the cross-section is divided into 14 similarly sized sections, which can be clearly seen in Figure 4.8 as areas of opposing velocity magnitudes. This segmentation of the geometry in turn leads to a more defined division of the fluid into streams flowing in opposite directions, thus resulting in the bimodal distribution observed at 9.5 mm cross-section, as the contrasting streams do not come in contact. Such patterns of cross-section geometry are observed throughout the mixer, leading to varying velocity distribution patterns.

Unlike the velocity component in the axial direction of flow, U_z, the velocity component in the x-direction does not appear to be influenced by the rheological properties of the fluid, and the distributions for guar gum display the same patterns to those shown for glycerol, spanning the same range of values with the same mean (Figure 4.8b and d).

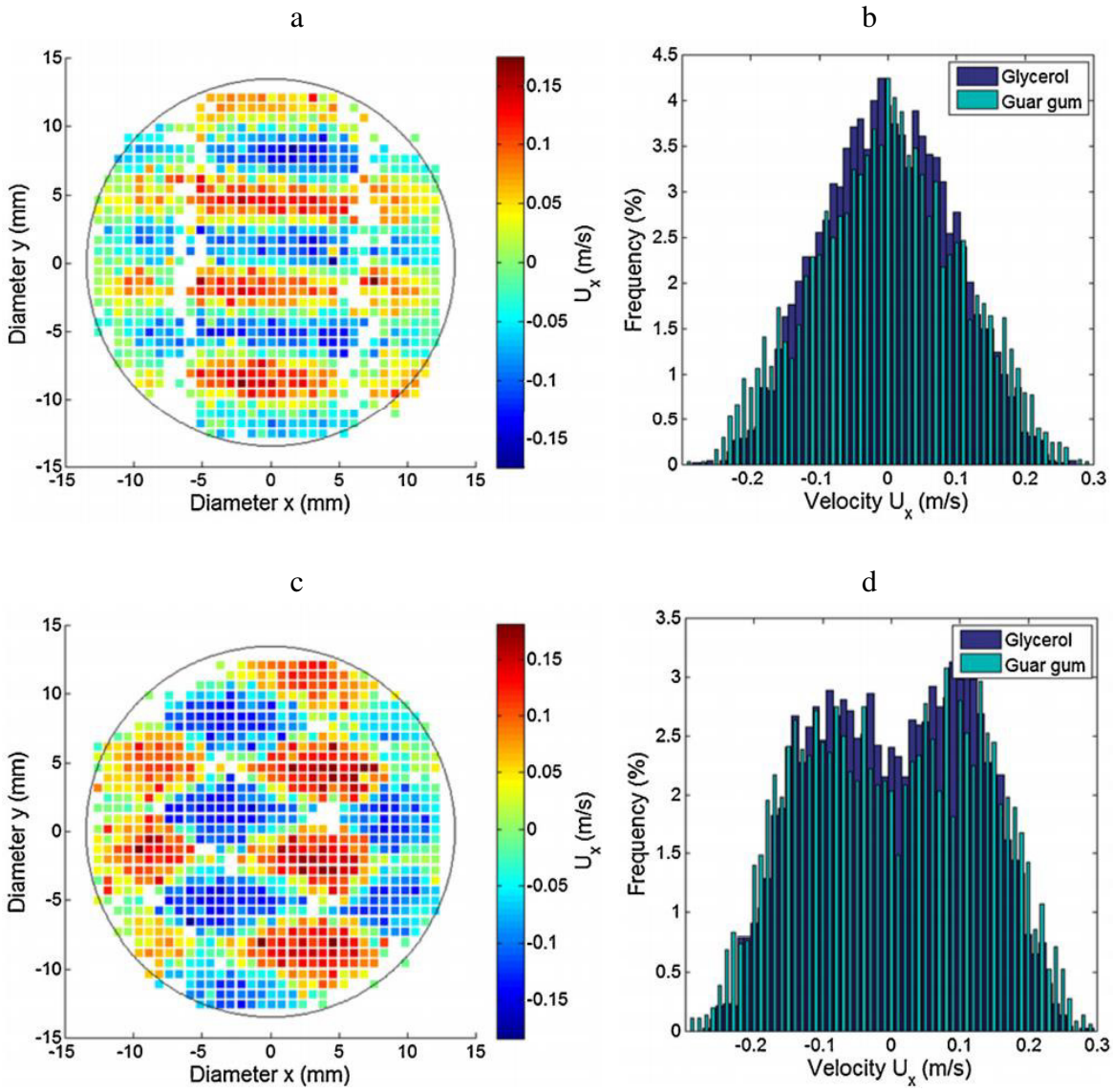

Figure 4.8. (a) U_x velocity field across the mixer cross-section at 6.5 mm for glycerol at 300 L/h and (b) the corresponding distributions for glycerol and guar gum solution. (c) U_x velocity field across the mixer cross-section at 9.5 mm for glycerol at 300 L/h and (d) the corresponding distributions for glycerol and guar gum solution.

When the velocity field in the y-direction is examined (U_y), the distribution remains unimodal, irrespective of the point of the cross-section, however, the range of velocities observed varies. For glycerol flowing at 300 L/h it can be seen that at the x-y-plane at 6.5 mm depth (Figure 4.9b) the range is wider, between -0.2 and 0.2 m/s, while the x-y-plane at 9.5 mm depth, shown in Figure 4.9d, has a narrower range, between -0.15 and 0.15 m/s.

The difference in the velocity range can be explained by referring back to the U_x distribution shown in Figure 4.8. Due to a higher fraction of the fluid moving at higher velocity in the x-direction at the depth of 9.5 mm and assuming that energy dissipated at each cross-section is the same at a constant flowrate (Hammoudi *et al.*, 2012), the energy remaining for flow induction in the y-direction is lower, hence the narrower range of velocities observed, as U_z distribution is maintained consistent at each cross-section.

For all glycerol and guar gum solution velocity distribution pairs shown in Figure 4.8 and Figure 4.9 it was demonstrated that the differences between the distributions are statistically insignificant ($P > 0.05$).

By considering the residence time distributions and the total distances travelled by the tracer particles it is possible to gain further insight into the dynamics within SMX mixers. Figure 4.10a illustrates the time to breakthrough for the empty pipe of the length equivalent to 10 SMX elements. It can be clearly seen that rheology has a dramatic effect on the residence time distribution, where the shear thinning guar gum solution exhibits a more plug flow behaviour when compared to Newtonian glycerol, with 95% of the tracers clearing the length of the pipe in under 2100 ms, while for glycerol it takes over 3500 ms for 95% of the tracers to travel the same distance. Here, due to the laminar nature of the flow the distance travelled by the tracers is constant and equal to the length of the pipe. However, when considering the residence time distribution within the mixer itself it becomes apparent that the differences between the two fluids are less pronounced, with both exhibiting plug flow like behaviour, which is a defining future of SMX static mixers as convection is induced in directions normal to the flow (Hirschberg *et al.*, 2009) (Figure 4.10b). For both fluids the first tracers start emerging from the tenth mixer element at approximately 900 ms after entering at the first element, where 95% of the particles following guar gum reach the end of the last element after 1500 ms, while for the particles

in glycerol it takes 1700 ms for 95% of the tracers to exit. The minor differences observed between the two fluids breakthrough times across the 10 mixer elements can be attributed to a weak effect of the fluid rheology on the U_z component of the velocity profile, as was illustrated in Figure 4.6b. Nevertheless, for both fluids the presence of the mixer elements reduces the residence time variability and significantly shortens the breakthrough time.

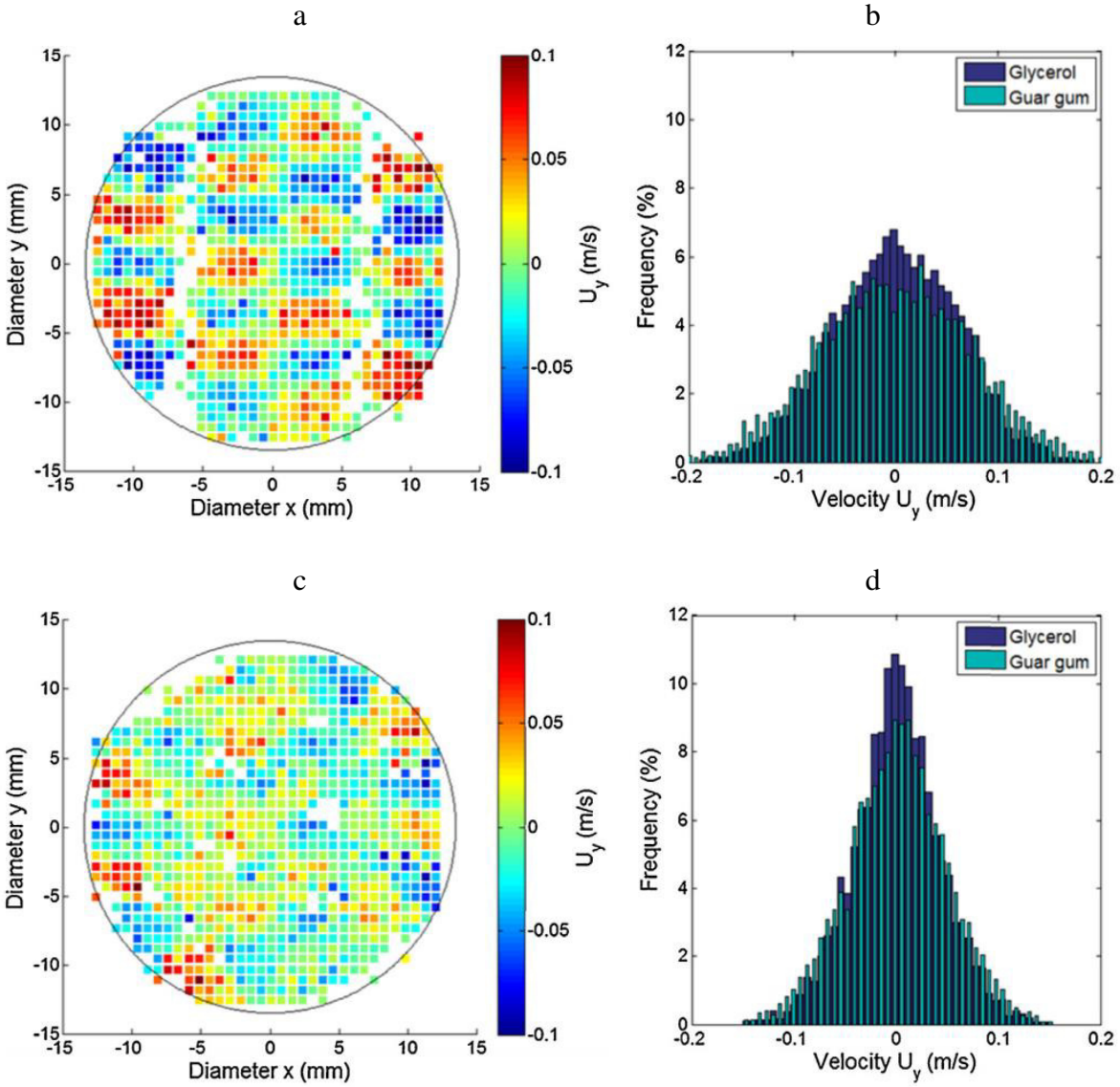

Figure 4.9. (a) U_y velocity field across the mixer cross-section at 6.5 mm for glycerol at 300 L/h and (b) the corresponding distributions for glycerol and guar gum solution. (c) U_y velocity field across the mixer cross-section at 9.5 mm for glycerol at 300 L/h and (d) the corresponding distributions for glycerol and guar gum solution.

Due to the axial movement of the tracer particles the total distance travelled by the tracers is almost double the distance travelled in an empty pipe of the same length and diameter, specifically, the length of 10 SMX mixer elements is 260 mm while the particles in both glycerol and guar gum solutions travel approximately 560 mm on average (Figure 4.10c).

Based on these values it is possible to establish that the average total velocity, U, at which the particle travels through the mixer is equal to *ca.* 0.22 m/s for glycerol and *ca.* 0.23 m/s for guar gum solution, where these velocities are comparable to the predicted interstitial velocity, *i.e.* $Q/(A\varepsilon)$.

The similarities between the local and the averaged phenomena observed for two fluids with distinct rheological properties within the SMX mixer suggests that the dynamics within the mixer are dominated by the mixer structure and are not significantly affected by the fluid rheology. This can be explained by the ongoing redirection, splitting and recombination of the flow, where the fluid does not travel sufficient distances to achieve fully developed flow after encountering an obstruction. For the dimensions of the system used in the current study the entry length within the mixer range between 1.8 mm, for more open cross-sections, for example at 6.5 mm SMX depth, to 0.7 mm for cross-sections with multiple narrow channels, like those at 9.5 mm SMX depth (Equation 4.7) (Shah and Bhatti, 1987). However, changes in the SMX geometry are perpetual and rapid along the length of the mixer, as is demonstrated by the dramatic changes in geometry between 6.5 and 9.5 mm cross-sections. Therefore, it can be concluded that both fluids would exhibit plug flow like behaviour, inherent of underdeveloped laminar flow, blurring the lines between Newtonian and shear-thinning fluid dynamics, with local velocity profiles indistinguishable at a constant flowrate.

$$L_e = 0.05ReD_c \qquad 4.7$$

These observations raise interesting questions about the mixing dynamics within SMX mixers and whether non-Newtonian rheology of the fluids being mixed affects the efficiency of mixing. It can be theorised, that under the flow conditions described, two fluids with matching apparent viscosities would mix at a comparable rate, regardless of the nature of the fluids. Here the assumption of the apparent viscosity derived from the wall shear rate could be applicable, as was shown in previous findings, where apparent viscosity derived from the wall shear rate has been successfully used to develop a universal model for pressure drop across SMX mixers for both Newtonian and non-Newtonian fluids (Li *et al*., 1997). Confirming such dynamics would allow designing processes with high mixing efficiency based on the rheological properties of the fluids.

The assessment of mixing within systems as the one described above is a crucial part of the future work on SMX mixer characterisation.

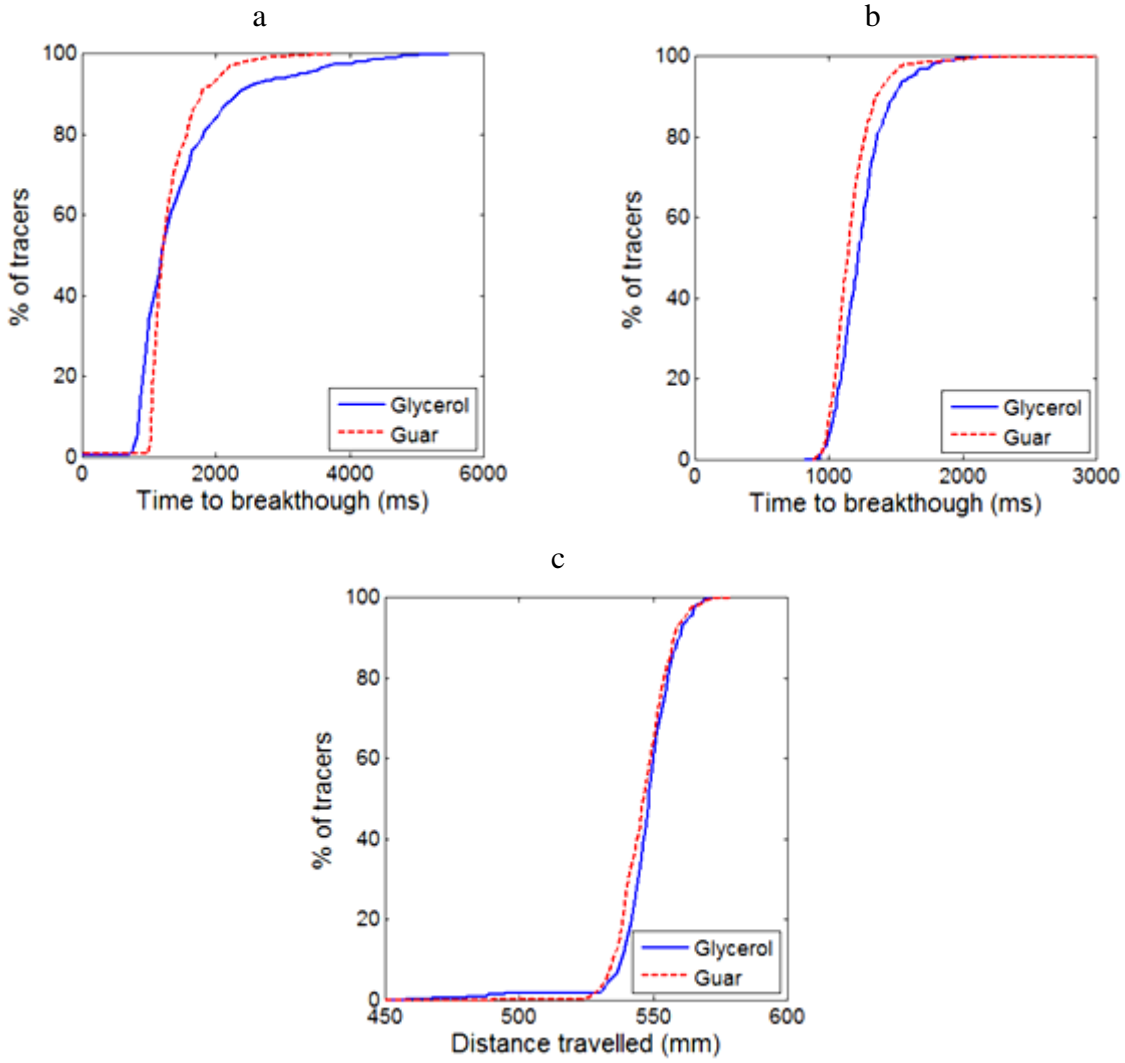

Figure 4.10. (a) Residence time distributions for glycerol and guar gum solution with respect to the total number of tracer particles passing through a length of empty pipe equivalent in length to 10 SMX mixer elements. (b) Residence time distributions for glycerol and guar gum solution with respect to the total number of tracer particles passing through 10 SMX mixer elements. (c) Distributions of the total distance travelled by the tracers for glycerol and guar gum solution with respect to the total number of tracer particles passing through 10 SMX mixer elements.

4.5 CONCLUSIONS

The velocity distribution within SMX static mixers was assessed using PEPT and it was observed that variations in the velocity field were dependent upon location within the mixer element, predominantly differing in the direction in which mixing is induced owing to the mixer geometry.

It was shown that the velocity distribution in the direction of the flow, U_z, for the empty pipe region, was with the theoretical velocity profile expected based on the flow conditions and the rheological properties of the fluids.

U_z distribution patterns within the mixer display similar variation between the two fluids, however the variation was not as pronounced, to such a degree that the velocities from different fluid could be attributed to the same continuous distribution, within 95% certainty. Moreover, when considering U_z distribution at specific mixer x-y-cross-sections, velocity patterns and magnitudes remain consistent, due to a constant flowrate and cross-sectional area.

Bimodal distribution patterns were exhibited by U_x, velocity in the direction of actively induced radial mixing, at locations with a high number of well-defined compartments, for example the x-y-plane 9.5 mm into the mixer element. This in turn results in a significant decrease in the magnitudes of U_y, the velocity perpendicular to the direction of induced radial mixing, when compared to cross-sections with a smaller number of larger compartments, for example the x-y-plane 6.5 mm into the mixer element.

For the U_z velocity component a mild effect of the fluid rheology was found, however, the mixer geometry brings the axial velocity profiles for both fluids closer to that of plug flow, when compared to flow within an empty pipe. This is further supported by analysing the total residence time and total distance travelled by the tracer particles in the entire 10

element assembly, where both fluids exhibited strong plug flow behaviour, uncharacteristic of fully developed laminar flow, especially for the case of Newtonian glycerol. For velocity components U_x and U_y it was found that when the two fluids are considered the patterns are not significantly ($P > 0.05$) affected by the rheological properties of the fluids used in the study. These observations lead to the conclusion that the structure of the mixer itself has a dramatic effect on the flow, not permitting the flow to develop fully, by constantly changing the geometry of the x-y cross-section, leading to underdeveloped flow inside the mixer, comparable to plug flow. It can therefore be concluded that for fluids flowing at the same flowrate the velocity distribution would not be significantly influenced by rheology.

4.6 REFERENCES

Abulencia, J.P., Theodore, L. (2009) *Fluid Flow for the Practicing Chemical Engineer*, Wiley-Blackwell.

Bakalis, S., Cox, P.W., Russell, A.B., Parker, D.J., Fryer, P.J. (2006) 'Development and use of positron emitting particle tracking (PEPT) for velocity measurements in viscous fluids in pilot scale equipment', *Chemical Engineering Science*, 61(6), 1864–1877.

Chiti, F., Bakalis, S., Bujalski, W., Barigou, M., Eaglesham, A., Nienow, A.W. (2011) 'Using positron emission particle tracking (PEPT) to study the turbulent flow in a baffled vessel agitated by a Rushton turbine: Improving data treatment and validation', *Chemical Engineering Research and Design*, 89(10), 1947–1960.

Conway-Baker, J., Barley, R.W., Williams, R.A., Jia, X., Kostuch, J., McLoughlin, B., Parker, D.J. (2002) 'Measurement of the motion of grinding media in a vertically stirred mill using positron emission particle tracking (PEPT)', *Minerals Engineering*, 15(1–2), 53–59.

Das, M. (2011) 'Study of Liquid-Liquid Dispersion of High Viscosity Fluids in SMX Static Mixer in the Laminar Regime', *Open Access Dissertations and Theses*, Paper 6228.

Das, M.D., Hrymak, A.N., Baird, M.H.I. (2013) 'Laminar liquid–liquid dispersion in the SMX static mixer', *Chemical Engineering Science*, 101, 329–344.

Fradette, L., Li, H.-Z., Choplin, L., Tanguy, P. (2006) 'Gas/liquid dispersions with a SMX static mixer in the laminar regime', *Chemical Engineering Science*, 61(11), 3506–3518.

Fradette, L., Tanguy, P., Li, H.-Z., Choplin, L. (2007) 'Liquid/Liquid Viscous Dispersions with a SMX Static Mixer', *Chemical Engineering Research and Design*, 85(3), 395–405.

Hammoudi, M., Legrand, J., Si-Ahmed, E.K., Salem, A. (2008) 'Flow analysis by pulsed ultrasonic velocimetry technique in Sulzer SMX static mixer', *Chemical Engineering Journal*, 139(3), 562–574.

Hammoudi, M., Si-Ahmed, E.K., Legrand, J. (2012) 'Dispersed two-phase flow analysis by pulsed ultrasonic velocimetry in SMX static mixer', *Chemical Engineering Journal*, 191, 463–474.

Hirech, K., Arhaliass, A., Legrand, J. (2003) 'Experimental Investigation of Flow Regimes in an SMX Sulzer Static Mixer', *Industrial & Engineering Chemistry Research*, 42(7), 1478–1484.

Hirschberg, S., Koubek, R., Schöck, J. (2009) 'An improvement of the Sulzer SMXTM static mixer significantly reducing the pressure drop', *Chemical Engineering Research and Design*, 87(4), 524–532.

Laporte, M., Della Valle, D., Loisel, C., Marze, S., Riaublanc, A., Montillet, A. (2015) 'Rheological properties of food foams produced by SMX static mixers', *Food Hydrocolloids*, 43, 51–57.

Leschka, S., Thévenin, D., Zähringer, K., Lehwald, A. (2007) 'Fluid dynamics and mixing behavior of a SMX-type static mixer', *Journal of Visualization*, 10(4), 342–342.

Li, H.Z.Z., Fasol, C., Choplin, L. (1997) 'Pressure Drop of Newtonian and Non-Newtonian Fluids Across a Sulzer SMX Static Mixer', *Chemical Engineering Research and Design*, 75(8), 792–796.

Liu, S., Hrymak, A., Wood, P. (2006) 'Laminar mixing of shear thinning fluids in a SMX static mixer', *Chemical Engineering Science*, 61, 1753–1759.

Meijer, H.E.H., Singh, M.K., Anderson, P.D. (2012) 'On the performance of static mixers: A quantitative comparison', *Progress in Polymer Science*, 37(10), 1333–1349.

Mihailova, O., Lim, V., McCarthy, M.J., McCarthy, K.L., Bakalis, S. (2015) 'Laminar mixing in a SMX static mixer evaluated by positron emission particle tracking (PEPT) and magnetic resonance imaging (MRI)', *Chemical Engineering Science*, 137, 1014–1023.

Mac Namara, C., Gabriele, A., Amador, C., Bakalis, S. (2012) 'Dynamics of textile motion in a front-loading domestic washing machine', *Chemical Engineering Science*, 75, 14–27.

Nienow, A., Edwards, M., Harnby, N. (1997) *Mixing in the Process Industries*, Butterworth-Heinemann.

Parker, D.J., Broadbent, C.J., Fowles, P., Hawkesworth, M.R., McNeil, P. (1993) 'Positron emission particle tracking - a technique for studying flow within engineering equipment', *Nuclear Instruments and Methods in Physics Research Section A: Accelerators, Spectrometers, Detectors and Associated Equipment*, 326(3), 592–607.

Paul, E.L., Atieno-Obeng, V.A., Kresta, S.M. (2004) *Handbook of Industrial Mixing*, John Wiley & Sons.

Rafiee, M., Bakalis, S., Fryer, P.J., Ingram, A. (2011) 'Study of laminar mixing in kenics static mixer by using Positron Emission Particle Tracking (PEPT)', *Procedia Food Science*, 1, 678–684.

Shah, R.K., Bhatti, M.S. (1987) 'Laminar Convection Heat Transfer in Ducts', in *Handbook of Single-Phase Convective Heat Transfer*.

Singh, M.K., Anderson, P.D., Meijer, H.E.H. (2009) 'Understanding and Optimizing the SMX Static Mixer.', *Macromolecular rapid communications*, 30(4–5), 362–76.

Streiff, F.A., Jaffer, S., Schneider, G. (1999) 'Design and application of motionless mixer technology', in *ISMIP3, Osaka*, 107–114.

Theron, F., Sauze, N. Le (2011) 'Comparison between three static mixers for emulsification in turbulent flow', *International Journal of Multiphase Flow*, 37(5), 488–500.

Visser, J., Rozendal, P. (1999) 'Three-dimensional numerical simulation of flow and heat transfer in the Sulzer SMX static mixer', *Chemical Engineering Science*, 54, 2491–2500.

Volkwyn, T.S., Buffler, A., Govender, I., Franzidis, J.-P., Morrison, A.J., Odo, A., van der Meulen, N.P., Vermeulen, C. (2011) 'Studies of the effect of tracer activity on time-averaged positron emission particle tracking measurements on tumbling mills at PEPT Cape Town', *Minerals Engineering*, 24(3–4), 261–266.

Yasuda, K., Armstrong, R.C., Cohen, R.E. (1981) 'Shear flow properties of concentrated solutions of linear and star branched polystyrenes', *Rheologica Acta*, 20(2), 163–178.

Zalc, J.M., Szalai, E.S., Muzzio, F.J., Jaffer, S. (2002) 'Characterization of flow and mixing in an SMX static mixer', *AIChE Journal*, 48(3), 427–436.

CHAPTER 5. CHARACTERISATION OF MIXING, VELOCITY AND CHANGEOVER IN SMX STATIC MIXERS

Parts of this chapter have been submitted for review to The Journal of Visualization and The Chemical Engineering Journal

5.1 ABSTRACT

Changeover, flow and mixing of fluids with complex rheological properties, e.g. non-Newtonian fluids, are key performance indicators of in-line static mixers; however, it is difficult to characterise these phenomena using traditional measurement techniques. The work presented in this chapter demonstrates the results for velocity field estimation, mixing and changeover characterisation using Positron Emission Particle Tracking (PEPT), for various fluids, both Newtonian and non-Newtonian shear thinning, at a range of flowrates. Using PEPT tracer path analysis it was found that when mixing is considered, the feed orientation is a crucial factor for the quality and efficacy of fluid mixing, with concentric feed orientation delivering superior and consistent results, for all fluids, independent of rheology, compared to side-by-side feeds. High speed image capture was used to illustrate the differences between changeover in systems containing and SMX mixer and those without mixers. PEPT tracer path data was also used to develop an expression that allows prediction of the time required to achieve the desired level of changeover for a given number of SMX mixer elements, based on the rheological properties of the fluids and volumetric flowrate. Furthermore, the changeover pattern illustrated that the flow regime within the SMX mixer strongly resembles plug flow, suggesting that when a changeover takes place on production scale, the changeover in the SMX mixer will be considerably more efficient than in empty pipe sections of the line, such as recirculation loops or packing lines.

5.2 INTRODUCTION

The shift towards continuous processing is ever increasing, as it allows for more streamlined and cost effective manufacturing. Continuous processing reduces energy consumption and waste production when compared to an equivalent amount of product manufactured by batch methods. As many of these processes rely on mixing and heat transfer, static mixers are increasingly incorporated into processing systems (Etchells and Meyer, 2003; Ghanem *et al.*, 2014). Inline static mixers redistribute fluid flow in directions transverse to the main flow due to a series of motionless inserts, or elements. This type of distributive mixing is by convection rather than diffusion. The focus of this study was mixing efficiency, changeover patterns and velocity fields of Newtonian and non-Newtonian fluids flowing in the laminar regime in a standard SMX static mixer (Sulzer, Switzerland).

SMX mixers have been the subject of a number of experimental and computational studies, well summarised by Meijer *et al.*, (2012); Singh *et al.*, (2009) and Thakur *et al.*, (2003). Advancements in understanding of in-mixer dynamics have been achieved using computational fluid dynamics (CFD) and mapping methods (Liu *et al.*, 2006; Rauline and Blévec, 2000; Singh *et al.*, 2009; Zalc *et al.*, 2002). In general, but not without exception, computational results have been challenging to validate or to compare with experimental mixing performance due to the geometrically complex nature of the mixing system. In a proof of concept portfolio paper, Leschka and co-workers illustrated simultaneous measurements of concentration and velocity profiles using Planar Laser-induced Fluorescence (PLIF) and Particle Image Velocimetry (PIV) for flow behind the SMX static mixer (Leschka *et al.*, 2007). However, this technique was never successfully applied for quantitative characterisation of the dynamics within the SMX mixers until now.

Transparent 3D printed SMX elements were used to assess the fluid changeover within the mixer elements using high speed image capture. The transparent fluid contained within the mixer at the start of the experiments was displaced using a fluid containing nigrosine dye, and the process was captured at 1000 fps. Through image analysis it was possible to estimate the degree of changeover within the system as the fluid displacement took place.

In addition, this chapter describes the use of PEPT to assess fluid mixing and changeover within SMX static mixers. PEPT has been successfully used to characterise Kenics static mixers (Rafiee *et al.*, 2013), a number of industrial processes, such as tumbling mills (Volkwyn *et al.*, 2011) and stirred vessels (Chiti *et al.*, 2011), as well as a number of domestic appliances, washing machines (Mac Namara *et al.*, 2012) and dish washers (Pérez-Mohedano *et al.*, 2015), with the main focus on local occupancies and velocity fields.

By processing PEPT particle pass data within the SMX mixer it was possible to assess the mixing performance as a function of various feed configurations, fluid properties, as well as flowrates. Flux-weighted intensity of segregation was used as a measure of homogeneity, combining local concentration data with local velocity fields calculated in Chapter 4.

A different approach to the analysis of the same PEPT data set allowed assessment of the degree of product changeover within the mixer, based on the relative fluid ratios at cross-sections along the mixer length. The analysis resulted in the development of an expression which allows estimation of the time required to carry out the changeover in a mixer of a known length to a desired degree, as a function of fluid and flow properties.

5.3 MATERIALS AND METHODS

5.3.1 MATERIALS

Three fluids were used in this study, pure glycerol (Reagent, UK), 0.7% w/w guar gum powder (Impexar, UK) in water solution and 1% w/w CMC powder (M_W ~700,000) (Sigma-Aldrich, USA) in water solution. These fluids were chosen as they exhibit different degrees of deviation from the Newtonian fluid model, where glycerol is a fully Newtonian fluid with a constant viscosity at any shear rate, and guar gum and CMC solutions are both non-Newtonian shear thinning fluids with different rheological properties that can be best described using the Carreau-Yasuda model (see Equation 5.1), with the model coefficients presented in Table 5.1.

Under the experimental conditions the fluid flow through the system was either 200 or 300 L/h, where these flowrates were chosen as they represent typical continuous processing conditions for a DN25 mixer size, i.e. mixer with 25 mm diameter, as advised by P&G. According to the Streiff-Jaffer correlation the average shear rate range under the conditions of the flow is either 250 or 380 s^{-1} for the two flowrates (Equation 5.2) (Streiff et al., 1999).

$$\mu_{eff}(\dot{\gamma}) = \mu_{inf} + \left(\mu_0 - \mu_{inf}\right)(1 + (\lambda\dot{\gamma})^a)^{\frac{n_y - 1}{a}} \quad 5.1$$

$$\dot{\gamma}_{SMX} = \frac{64V}{D} \quad 5.2$$

$$\mu_{eff}(\dot{\gamma}) = m\dot{\gamma}^{n-1} \quad 5.3$$

This allows approximation of the Carreau-Yasuda model fluids to a simpler Power law model, shown in Equation 5.3, within the range of shear rates fluids experience during flow, as shown in Figure 5.1. These Power law parameters are summarised in Table 5.2

and can further be correlated with the differences in the fluid behaviour during mixing and changeover.

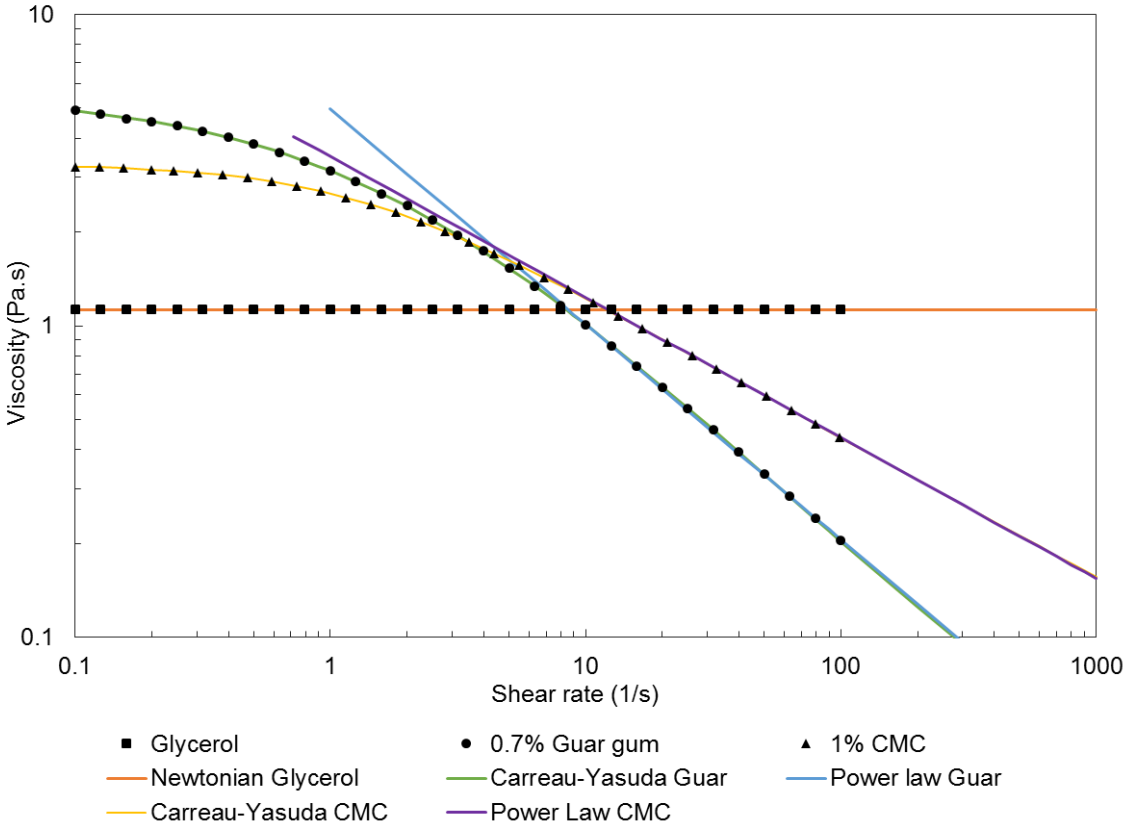

Figure 5.1. Rheograms of the fluids used in the current study and the model fits used to describe the fluids behaviours.

Table 5.1. Carreau-Yasuda coefficients for 1% CMC solution and 0.7% Guar gum solution

Fluid	μ_{inf}	μ_0	λ	n_y	a
1% CMC solution	0.069	5.749	0.352	0.003	0.661
0.7% Guar gum solution	0.002	4.553	0.181	0.037	0.485

Table 5.2. Power law coefficients for glycerol and CMC and guar gum solutions used.

Fluid	Flow index, n	Consistency coefficient, m
Glycerol	1	1.2
1% CMC solution	0.55	2.9
0.7% Guar gum solution	0.30	3.5

5.3.2 EXPERIMENTAL SET UP

The same experimental rig described previously in Mihailova *et al.*, (2016) was used to obtain PEPT mixing and changeover data (Figure 5.2). A 10 element DN25 (25mm diameter) SMX mixer was placed between the PEPT detectors, with a variable speed pump (Xylem, UK) and an inline mass flow meter (Krohne, USA) placed outside the detector field of view for flow control. The fluid containing the radioactive tracer particle was recirculated around this loop, until sufficient data was collected.

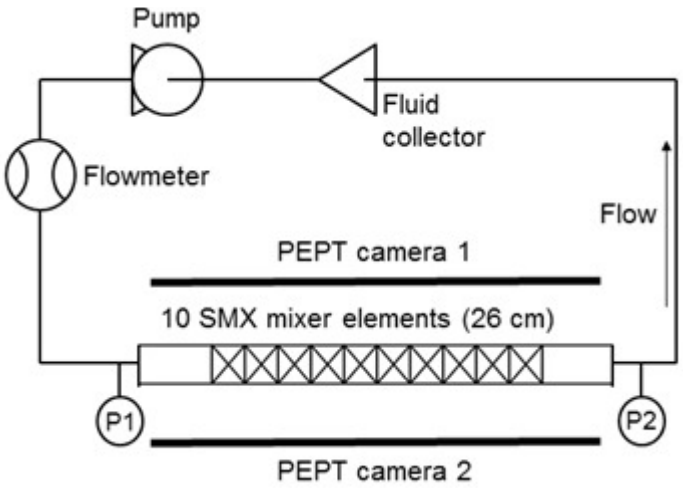

Figure 5.2. The experimental set up for PEPT data acquisition, with 10 SMX elements in the field of view of the camera.

The SMX mixer elements were 3D printed in transparent VeroClear plastic (Stratasys Ltd, USA), which allowed applying a number of techniques to the set up. The dynamics in the mixer were additionally assessed using high speed capture with a Photron FASTCAM XLR-1024 camera as well as Particle Image Velocimetry (PIV) (Please see Appendix for details on the PIV proof of concept work).

High speed capture at 1000 fps was predominantly used for changeover characterisation, where the system was initially filled with a transparent fluid which is displaced by a fluid stained with nigrosine dye. Due to the nature of the fluids, only glycerol and CMC solutions could be used as the initial fluid, as guar gum solution is opaque at the concentration used in this work, and therefore would not allow changeover tracking. For the dyed fluid, on the other hand, any of the three fluids could be used. The experimental rig used was the same as the one for the PEPT data acquisition, except a three-way valve was added before the pipe containing the mixer. The valve was closed and the pipe was filled with the initial transparent fluid over the top and allowed to de-aerate. The pump was connected to a reservoir containing the second fluid stained with nigrosine dye. The stained fluid was brought up to the desired flowrate by recirculation, bypassing the field of view using a three-way valve setup, as shown in Figure 5.3. The camera was set to record as the valve was switched to feed the dyed fluid into the field of view. The camera was left to record for 30 s after the valve was switched, where the recording time was limited by the camera on-board memory. Two setups were used in the field of view, an empty 1” acrylic pipe and an identical pipe containing 10 transparent 3D printed SMX elements, with only the top (last) element visible in the camera field of view.

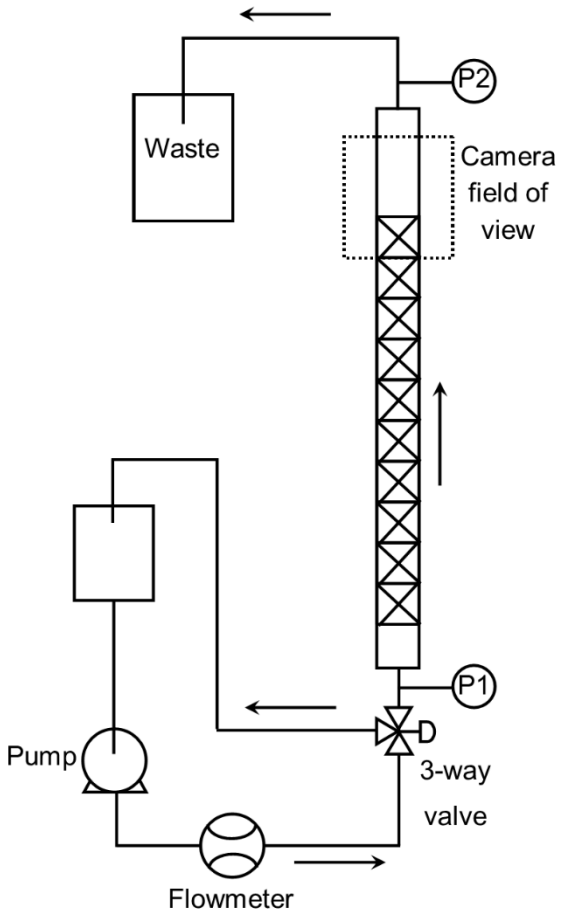

Figure 5.3. The experimental set up for high speed camera and PIV image capture, showing the set up option with the SMX mixer present.

5.3.3 DATA PROCESSING

In order to assess the mixing and changeover properties of the system a single detailed element reconstructed from individual elements described previously is insufficient (Mihailova et al., 2016), as a length of several elements needs to be assessed. However, the data contained in the 10 element full length mixer raw data is not detailed enough to develop concentration maps. In order to perform the analysis of the desired mixer properties a compromise between the number of elements and the level of available detail needed to be struck. Based on previous research it is has been found that a length of five elements provides sufficient insight into the mixing dynamics (Paul et al., 2004).

In order to construct a data set describing five SMX mixer elements an approach similar to the one used to construct the single element for velocity field assessment was used (Mihailova et al., 2016). The raw data set was divided into five element sections, e.g. elements 1-5, 2-6, 3-7 etc. These sections were then rotated along the x-y plane to ensure a matching mixer geometry pattern on all sections. The z coordinate of the first x-y plane of each element was set to zero, to ensure all particle passes originate on the same plane. The five element assemblies were then superimposed, resulting in a data set with approximately 2,500 valid particle passes per given set of conditions. This data manipulation process is illustrated in Figure 5.4.

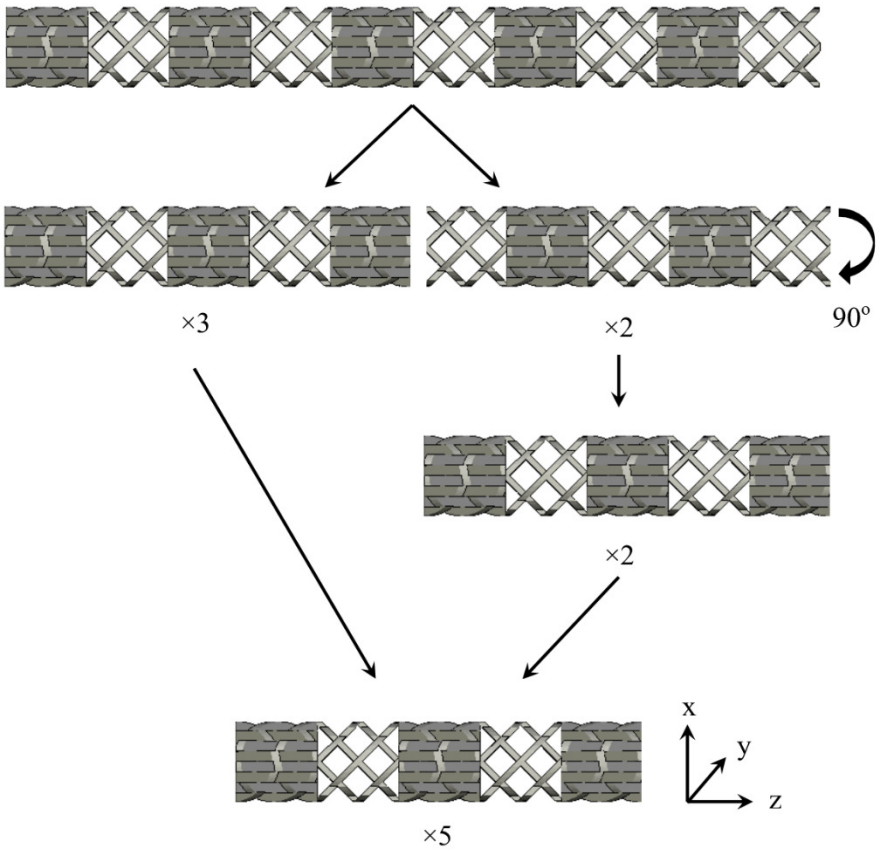

Figure 5.4. Schematic representation for the separation of the 10 element mixer assembly into a superimposed five element assembly.

The raw data was then processed separately for the assessment of mixing and the analysis of the fluid changeover patterns.

5.3.3.1 FLUID MIXING

In order to characterise the degree of mixing, an approach similar to the one previously described in the literature was used (Mihailova et al., 2015). Individual particle passes were assigned one of two distinct concentration values depending on the entry location of the tracer at the first x-y plane, at z = 0, where one of the fluids has a concentration of 0 and the second fluid has a concentration of 100, depending on the location at entrance. This approach allows the flexibility of using the same data set to assess different mixer feed configurations, where the ratios of the two species being mixed can be varied, as well as the pattern of the feed, allowing concentric or side by side species break down at entry. Figure 5.5 illustrates the investigated mixer feed configurations achieved using the particle pass labelling technique, for a 50/50 split between the feed fluids, where the key variance between the different feeds is the orientation with respect to the first mixer element.

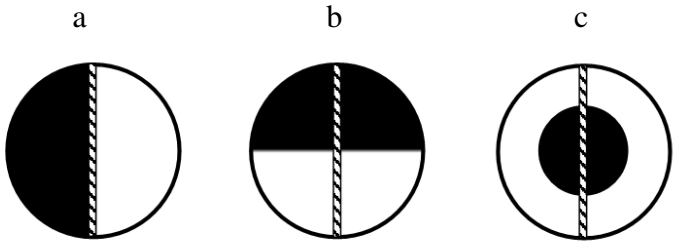

Figure 5.5. Flow orientations for a 50/50 feed. a. the fluids are fed parallel to the first mixer element geometry b. fluid feed is perpendicular to the first mixer element geometry c. the fluids are fed in a concentric manner

Once the individual particle passes are assigned a concentration value it is possible to assess mixing at each x-y plane across the mixer. Taken at 1 mm intervals along the z axis

the x-y planes were broken down into a 1x1 mm grid, where to estimate the concentration within each grid element an average of the concentration values of all the particle passes contained within the boundaries of a grid element is taken. This grid size allows for five particle passes, on average, in each grid element. Reducing the grid size would result in a grid too fine to accommodate the 200 μm tracer particle and the corresponding location uncertainty, which could reach several particle radii in size. Increasing the grid size, on the other hand, would make the size of each grid element too big to effectively assess mixing, as average concentrations would be taken over large areas, smoothing out any local discrepancies.

Figure 5.6 illustrates the concentration fields for glycerol at 300 L/h across the first element inlet, half way through the first element and end of the first element for the three feed orientations, obtained through the method described above.

The highest feed ratio difference assessed was 75% to 25% split, as for higher ratios insufficient particle passes were assigned the values for the fluid with the lower feed fraction, resulting in inconsistent concentration detection between adjacent x-y planes.

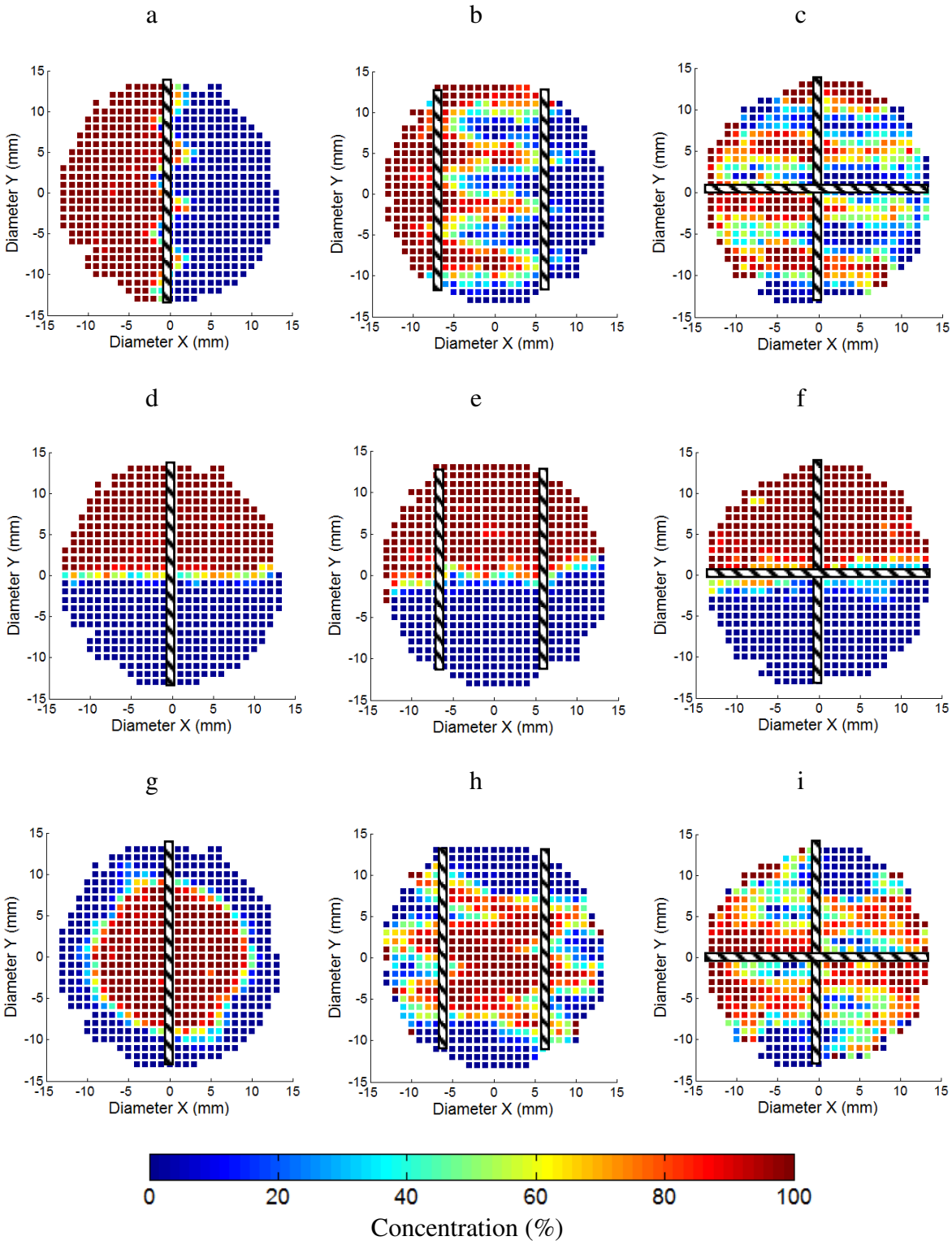

Figure 5.6. Concentration maps for a 50/50 feed of glycerol flowing at 300 L/h, at x-y planes at the 1st element entrance (a, d, g), 13 mm (50%) into the first element (b, e, h) and 26 mm (100%) into the first element, as it transitions into the second element (c, f, i), The feed orientations are parallel to the mixer geometry (a, b, c), perpendicular to the mixer geometry (d, e, f) and concentric (g, h, i).

Once the local concentration maps across all x-y planes are generated, it is possible to assess how mixing develops along the mixer. The flux weighted intensity of segregation has previously been demonstrated as an effective measure of the mixedness of the system (Mihailova *et al.*, 2015). Combining the local concentrations with local average velocities, derived as shown in Mihailova et al. (2016), it is possible to calculate the flux weighted intensity of segregation using Equation 5.4. Flux weighted intensity of segregation takes both the local concentrations and local residence times into consideration, when comparing different mixing conditions, where s_F^2 is the flux weighted variance of flow, s_{Fo}^2 is the flux weighted variance of flow at the entrance cross-section and I_F is the flux weighted intensity of segregation (-).

The flux weighted variance of flow is calculated as shown in Equation 5.5, where the flux across the cross-section is directly proportional to the fluid velocity, F is the total flux across the cross-section (m^{-2} s^{-1}), f_i is the flux across a grid element (m^{-2} s^{-1}), $\bar{X}$ is the average concentration across the cross-section (-), X_i is the concentration in a grid element (-) and N is the number of grid elements (-).

$$I_F = \frac{s_F^2}{s_{Fo}^2} \tag{5.4}$$

$$s_F^2 = \frac{1}{F}\sum_{i=1}^{N}(X_i - \bar{X})^2 f_i \tag{5.5}$$

5.3.3.2 FLUID CHANGEOVER

The changeover was initially assessed using high speed image capture, where the mixer assembly was filled with a transparent fluid at the start, which was then replaced by a fluid stained with nigrosine, flowing at the desired flowrate. The high speed capture allows to assess the differences in the changeover dynamics between empty pipes and pipes containing SMX mixer elements. The captured images were thresholded at the value equal to the image background using ImgaeJ software. This allowed an estimation of the volume of the pipe occupied by the dyed fluid, as after thresholding any part of the pipe containing the fluid was assigned the colour value of 1 (black), while all parts that were same as or lighter than the background were assigned the value of 0 (white).

However, this approach does not address the changeover within the mixer and does not provide the desired level of detail in terms of boundary layers between the two fluids.

In order to understand the dynamics within the mixer itself, as opposed to the SMX assembly exit point the five element PEPT data set previously applied for mixing assessment was used. For the changeover characterisation, in addition to zeroing the z position of each particle pass at entry when combining the elements, the time was zeroed as well, where each particle pass starts at t_0. This allows pinpointing of the position of each tracer particle within the mixer at any given time, as it travels through the mixer element assembly. The changeover was assessed at the exit of each one of the five elements available. For each exit location the particles were labelled according to their relative position at a given time, i.e. if at time t the particle z-location is less than the exit coordinate it belongs to the original fluid. On the other hand, if the tracers z-location is greater than the exit coordinate, it belongs to the second fluid. Hence an assessment of the number of particles that have crossed the element exit threshold at any given time during

the process can be made, providing an insight into the ratio between the fluid initially in the system, and the fluid being used to replace it, during changeover.

5.4 RESULTS

5.4.1 FLUID MIXING

The concentration variation across the x-y planes of the mixer are of major interest, as it has been shown that the axial flow through the mixer resembles plug flow with no back mixing (Mihailova et al., 2016), suggesting that rheological properties will have little to no effect on mixing.

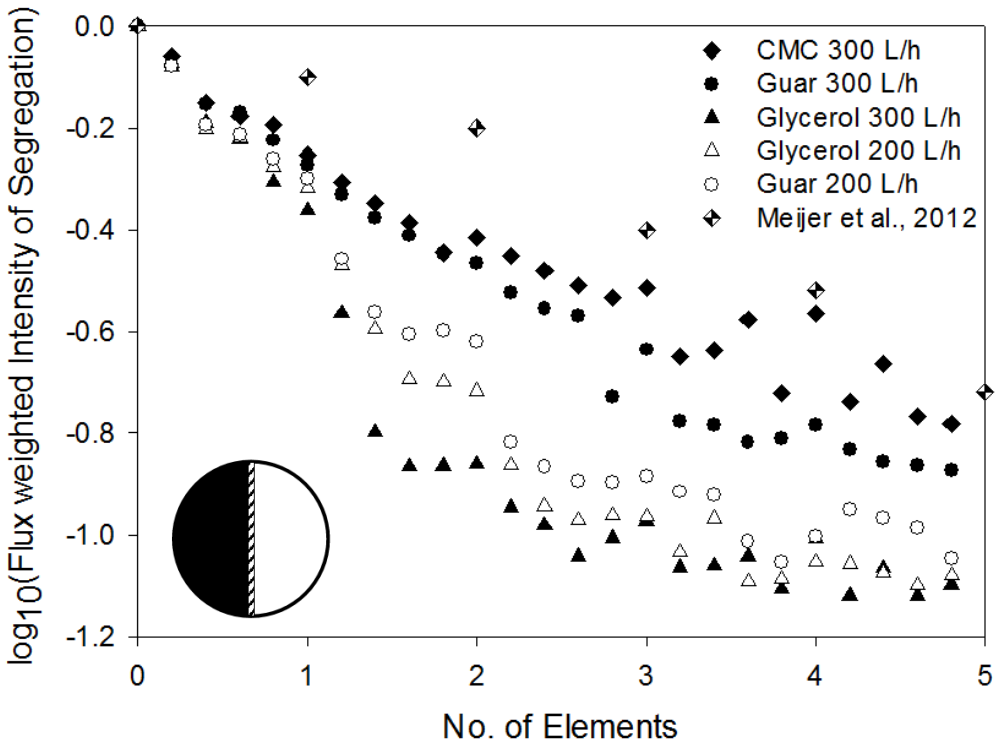

Figure 5.7. The flux weighted intensity of segregation development across the five elements of the SMX mixer when a 50/50 mixture of the two fluids were fed parallel to the mixer alignment, as shown in the bottom left corner. Additional data extracted from computational work on fluid mixing in SMX mixers (Han E.H. Meijer et al., 2012).

Figure 5.7 illustrates I_f for the case of the fluid being fed parallel to the mixer structure, i.e. the orientation of the first bar of the first mixer element. This is the feed orientation that was previously assessed using computational techniques by Meijer and coworkers (2012), the results of which are also presented in the Figure. The concentration dynamics across the first mixer element for this orientation for glycerol flowing at 300 L/h are illustrated in Figure 5.6 (a, b, c).

From the intensity of segregation plot (Figure 5.7) it can be seen that initially I_f varies consistently for all the fluids, however, after the first element discrepancies begin to appear, with glycerol displaying the highest efficiency of mixing at both flowrates, when compared to the non-Newtonian fluids. The experimental results obtained for all fluids are noticeably different from the computational results obtained for Newtonian fluids by Meijer *et al.* (2012). It has to be noted that as mentioned previously in Chapter 3 the idealised nature of computational work does not take into consideration deviations from theoretical flow profiles, such as vortices, based on predicted velocity fields and therefore can underpredict mixing when compared to experimental results. However, it has been previously illustrated that the velocity distribution within SMX mixers can display substantial variation from the predicted dynamics, for instance through the introduction of significant amount of flow in the direction perpendicular to the one in which the geometry actively encourages mixing (Mihailova *et al.*, 2016). The effect of this can be clearly seen in the changes of $\log_{10}(I_F)$ across the first element for the perpendicular feed orientation (Figure 5.8), where despite the lack of active mixing induced by the mixer geometry itself, the intensity of segregation nevertheless decreases.

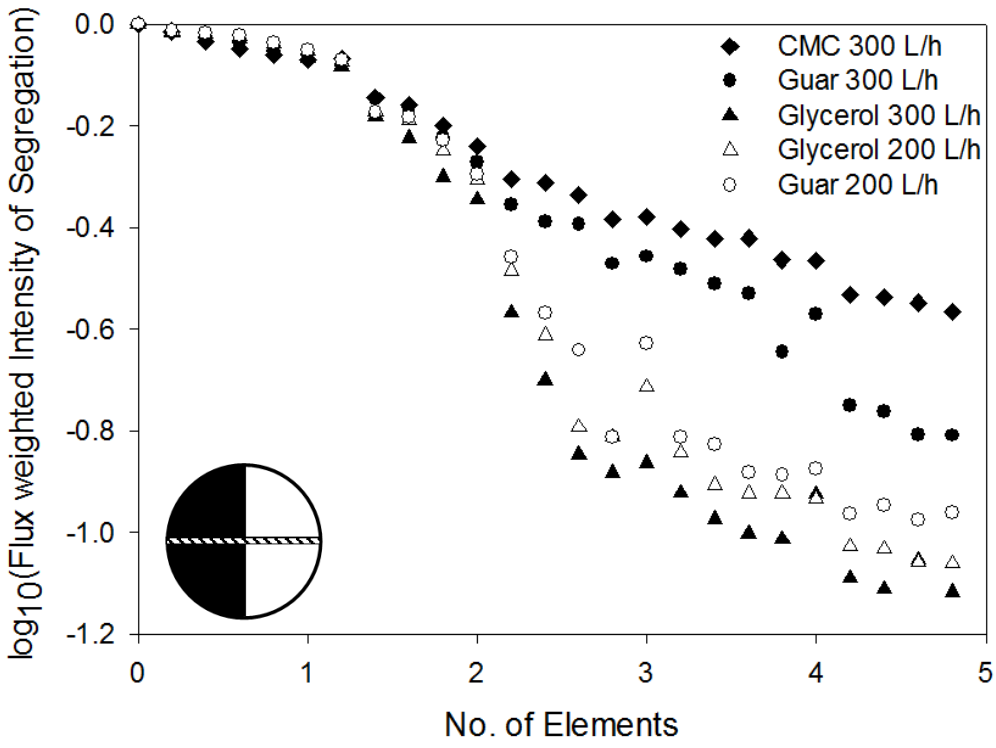

Figure 5.8. The flux weighted intensity of segregation development across the five elements of the SMX mixer when a 50/50 mixture of the two fluids were fed perpendicular to the mixer alignment, as shown in the bottom left corner.

Figure 5.8 provides further details for the case of the two fluids being fed perpendicular to the mixer orientation, where the concentration maps for the first element can be seen in Figure 5.6 (d, e, f) After the first element, where little mixing occurs due to the geometry orientation, once the geometry begins to favour mixing, a pattern similar to the one observed in the parallel feed scenario can be seen again, with glycerol at 300 L/h achieving the greatest reduction in the intensity of segregation, while CMC at 300 L/h demonstrates the worst mixing of all the cases considered.

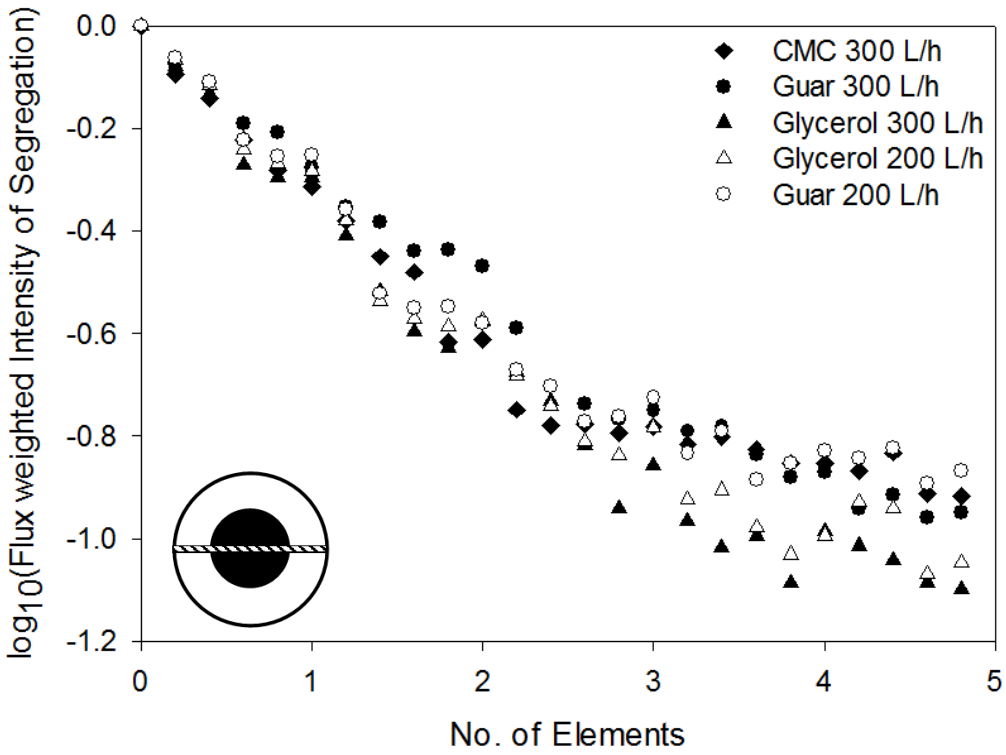

Figure 5.9. The flux weighted intensity of segregation development across the five elements of the SMX mixer when a 50/50 mixture of the two fluids were fed concentrically, as shown in the bottom left corner.

Finally, the case of the concentric mixer feed is considered, where the concentration patterns across the first element can be seen in Figure 5.6 (g, h, i). Figure 5.9 shows that this feed pattern results in the most efficient intensity of segregation reduction, i.e. better mixing, than the side by side feed orientations described previously. In addition, the quality of mixing does not appear to be affected by the fluid rheology or flowrate, as was seen in the side by side orientation presented above, with values of log10(I_F) reaching -1.0 for all fluids after five elements and a t-test showing that the intensity of segregation for all fluids in a concentric feed belongs to the same data set, with P = 0.012. It has to be noted that based on computational studies this level of I_F is expected after over 10 mixer elements (Han E.H. Meijer et al., 2012). Assessing a different feed ratio of 25% to 75%

between the two fluids in a concentric orientation has further demonstrated the consistency between the different fluids and flowrates (Figure 5.10).

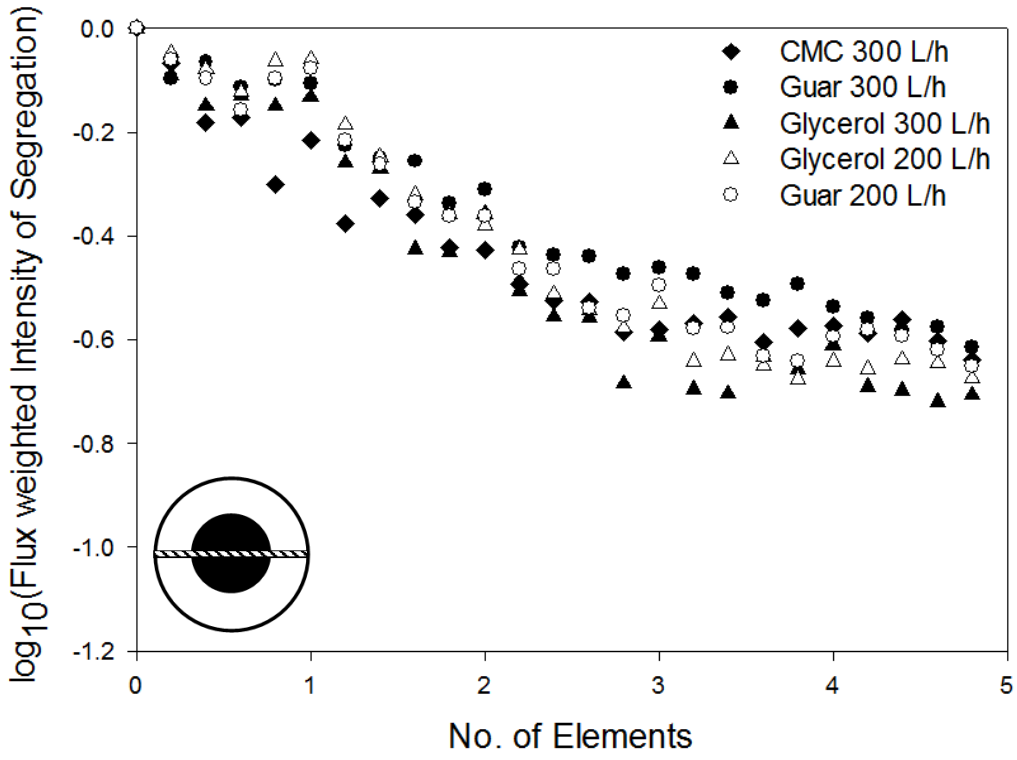

Figure 5.10. The flux weighted intensity of segregation development across the five elements of the SMX mixer when a 25/75 mixture of the two fluids were fed concentrically, as shown in the bottom left corner.

The improved mixing can be attributed to the different feed orientation, which is independent on the relative feed and mixer geometry alignment, ensuring efficient mixing begins as soon as the fluid enters the mixer. The consistency of mixing across the fluids with different rheological properties and at different volumetric flowrates when using the concentric feed further emphasises that for the all cases assessed this feed orientation would be preferred.

In addition to assessing the behaviour of different fluids when introduces into the mixer under the same feed conditions, it is also of interest to consider the behaviour of the same fluid under different feed conditions. Figure 5.11 illustrates the behaviour of glycerol

under all flow and feed conditions assessed. It can be clearly seen that for glycerol the feed orientation parallel to the mixer geometry being the most efficient at reducing the intensity of segregation and hence providing better mixing. However, the concentric feed does provide comparable results, and would prove more reliable all around solution when mixing fluids with different rheological properties or densities. The flowrate does not appear to affect this behaviour, with very similar patterns for the same feed orientation at both 200 and 300 L/h. For the case of guar gum solution, the overall final value of the intensity of segregation reached after 5 elements is higher than that of for glycerol, but the overall pattern remains the same as shown in Figure 5.11.

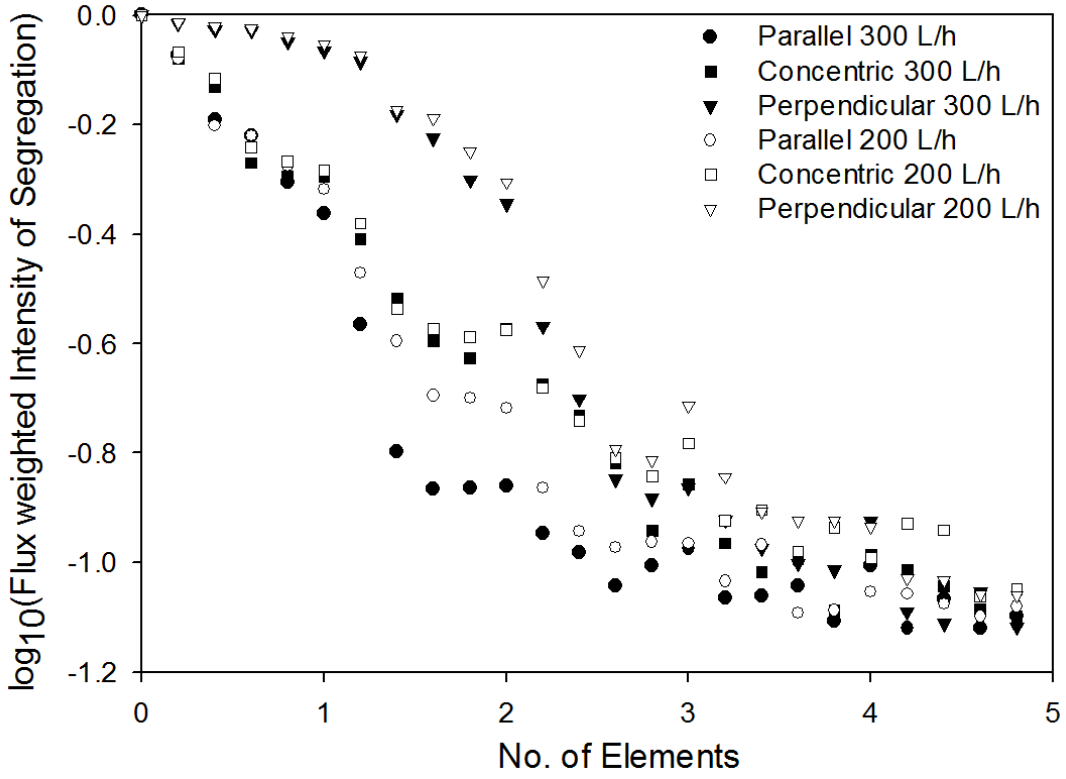

Figure 5.11. The flux weighted intensity of segregation development across the five elements of the SMX for glycerol under different segregation conditions. Here the different feed orientations are described by their direction when entering the first mixer element.

Another point of interest is the importance of the first element of the mixer in the feed orientation which does not favour mixing in that element. To assess that the results for the cases with the feed perpendicular to the mixer were "shifted" by assigning the second element entrance the same parameters as those normally assigned to the first element entrance, which can be seen for the case of glycerol in Figure 5.12. It is clearly shown that once the first element in the unfavourable orientation is ignored the intensity of segregation reduction patterns are similar for the two feed orientations for both flowrates. This further emphasizes the importance of the correct feed orientation for efficient mixing.

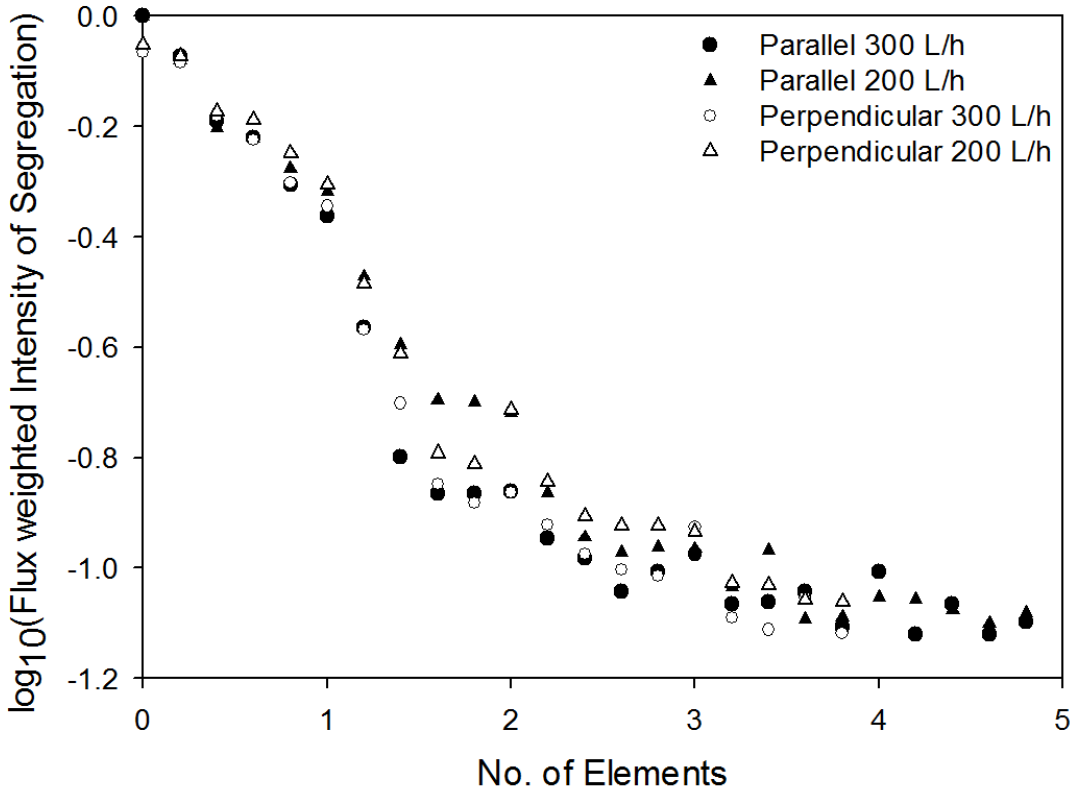

Figure 5.12. The flux weighted intensity of segregation development across the five elements of the SMX for glycerol at 200 and 300 L/h, where the first element in the perpendicular feed orientation is ignored and the mixing after entering element 2 is directly compared to that of the parallel feed in element 1.

Figure *5.13* illustrates the same scenario for guar gum solution, and while the effect of removing the first element in the poor feed orientation remains the same, this figure

emphasises the effect of flowrate on non-Newtonian fluid mixing efficiency. From the case of glycerol it was shown above that for a fluid with constant viscosity flowrate effects are insignificant, however for a shear thinning fluid it is clear that increasing the flowrate and hence reducing the fluid viscosity reflects negatively on the mixing efficiency. It was previously suggested that the deviation from the mixing patterns between different fluids could manifest due to local deviations from laminar flow, however, such effects are known to become more pronounced with the increase in Reynolds number. For a shear thinning fluid, such as guar gum solution, the Reynolds number would increase significantly with the increase in flowrate, due to both an increase in velocity and drop in viscosity, however, the improvement in mixing that was observed appears to contradict this expected behaviour. In contrast, fluids with higher viscosity, such as glycerol or guar gum solution at low flowrate, demonstrate superior mixing to lower viscosity fluids. This phenomenon cannot be explained by the differences found in the velocity fields described in Chapter 4, however, due to the size of the grid in the velocity maps, it is possible that some local effects would get smoothed out. Previously, a hypothesis regarding vortex shedding has been discussed, but effects such as vortex formation are once again known to be positively correlated with Reynolds number. Some other form of local instability could be present, however, PEPT data does not provide high enough resolution to address such phenomena, and further work using alternative visualisation techniques is required to explain this phenomenon.

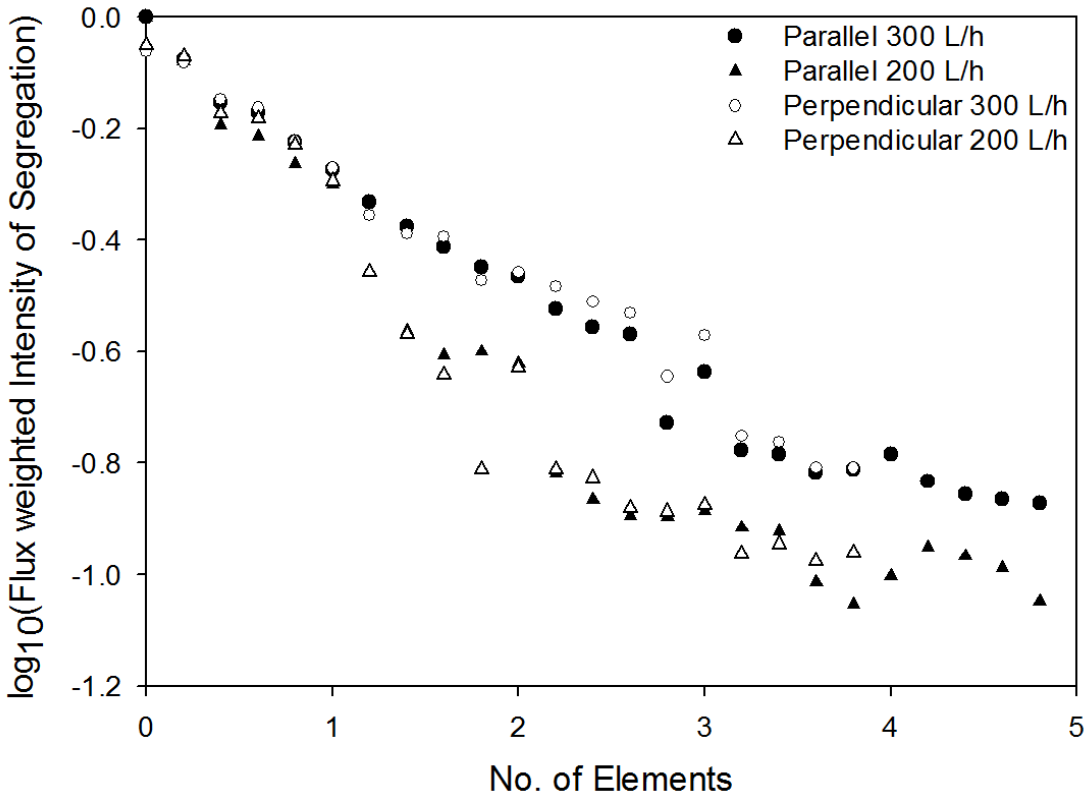

Figure 5.13. *The flux weighted intensity of segregation development across the five elements of the SMX for guar gum solution at 200 and 300 L/h, where the first element in the perpendicular feed orientation is ignored and the mixing after entering element 2 is directly compared to that of the parallel feed in element 1.*

5.4.2 FLUID CHANGEOVER CHARACTERISATION USING HIGH SPEED IMAGE CAPTURE AND PEPT

The high speed capture approach was found to provide an insight into the fluid changeover post SMX mixer. Figure 5.14 demonstrates the cases of glycerol being replaced with guar gum solution, at the beginning of the changeover, after 0.2 seconds and after 9 seconds have elapsed, where Figure 5.14 a, c and e illustrate the empty pipe, while b, d and f illustrate the SMX containing pipe. The differences in the fluid behaviour can be seen from the moment guar gum solution enters the frame, where the empty pipe demonstrates the fluid entering in the middle, typical of fully developed parabolic flow

(Figure 5.14a), while in the pipe containing the SMX mixer the dyed fluid enters the field of view simultaneously across the entire pipe radius (Figure 5.14b).

After 9 seconds the bulk of the fluid has been displaced and it can be seen that for the case of the empty pipe a significant fraction of the volume is still occupied by the transparent fluid (Figure 5.14e). However, the changeover in the pipe containing the SMX mixer demonstrates a much higher fraction of the volume occupied by the dyed fluid (Figure 5.14f). The high speed captured images were analysed using ImageJ image processing software, to compare the changeover dynamics.

Figure 5.15 demonstrates the difference in the cross-sectional area of the pipe occupied by the original fluid as the changeover takes place, where the changeover time starts as soon as the second fluid enters the frame for the empty pipe configuration and as soon as the second fluid leaves the SMX mixer for the mixer configuration. The area occupied is calculated by processing the images to find the radius of the pipe occupied by the dyed fluid at the length of pipe corresponding to the cross-section of interest, either the frame entrance or the mixer exit, depending on the configuration. As the feed is concentric, it is possible to estimate the area occupied based on radius, as shown in Equation 5.6, which in this case is directly correlated to the concentration of the fluids in the pipe.

$$A = \pi(R^2 - r^2) \qquad 5.6$$

Where A is the area of the cross-section of interest occupied by the original fluid (m^2), R is the total pipe radius (m) and r is the radius occupied by the dyed fluid (m).

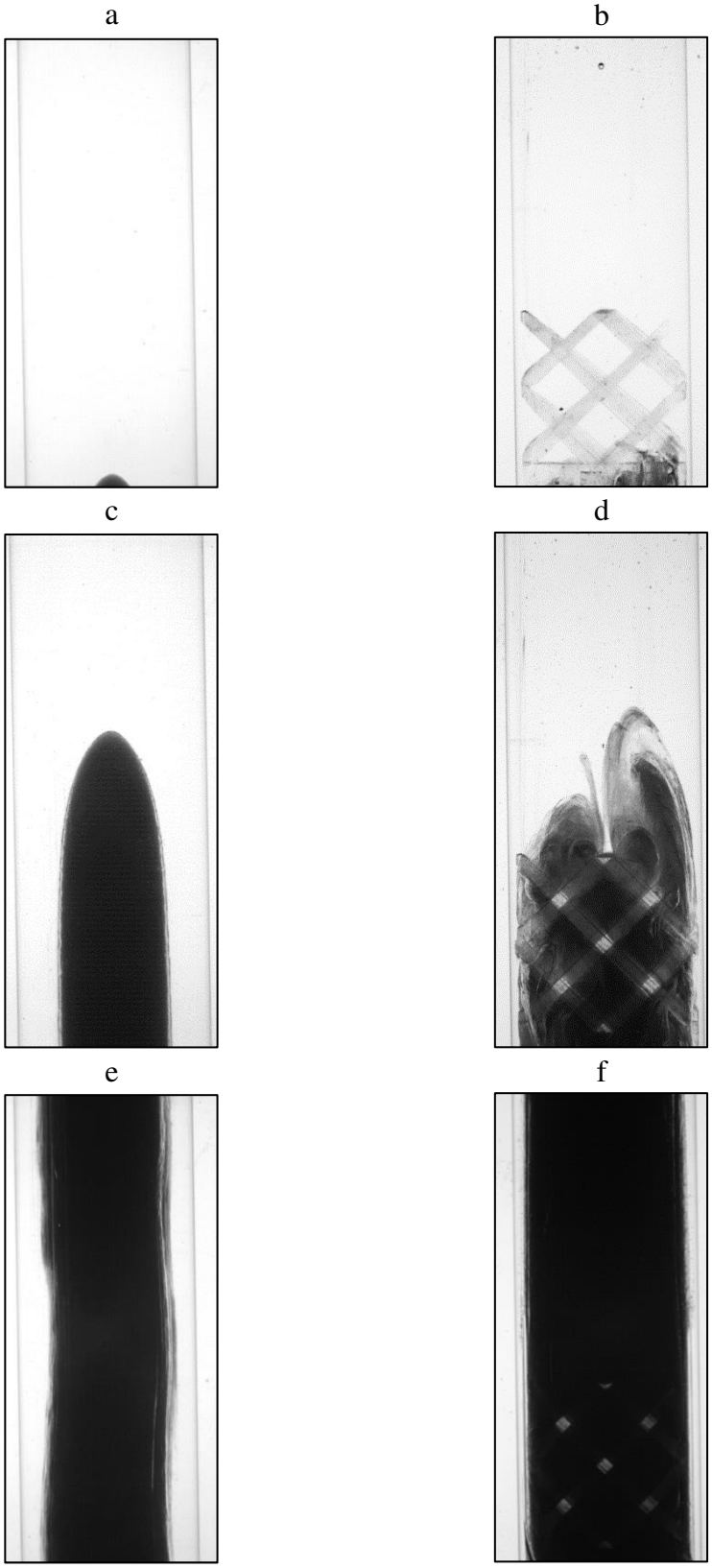

Figure 5.14. Changeover process between glycerol (clear) and 0.7% guar gum solution (black) in an empty pipe (a, c, d) and an SMX mixer (b, d, f), as guar gum solution enters the field of view (a, b), after 0.2s (c, d) and 9s after the initial entry (e, f).

It can be clearly seen from Figure 5.15, where glycerol is being changed over with dyed guar solution that the amount of time taken to remove the majority of the original fluid is much shorter for a cross-section preceded by an SMX mixer. This is due to the nature of flow within the mixer, which was previously shown to resemble plug flow, therefore it is to be expected that the changeover time immediately outside the mixer will be significantly shorter than in an empty pipe with fluid exhibiting parabolic flow.

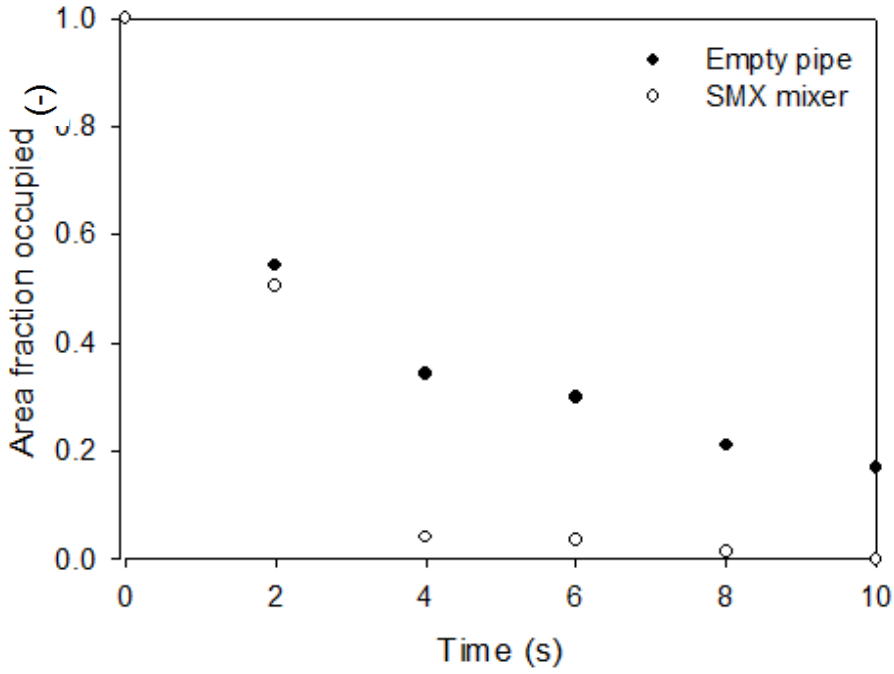

Figure 5.15. The comparison of the pipe cross-section occupied by the original fluid over time, as the changeover progresses, for glycerol changeover with guar solution at 300L/h

However, the high speed approach only allows assessment of the changeover outside the mixer, as the image within the mixer gets distorted by the presence of the mixer elements. Despite the transparent construction material, the differences between the fluid and the plastic mixer refractive indices cannot be completely eliminated. Furthermore, as not all fluids can be used as the initial fluid, due to their opacity, certain scenarios are impossible to assess using visual techniques.

To address this complication PEPT data was used for the assessment of changeover within the mixer. While the technique only allows assessment of changeover between fluids with the same rheological properties, it is still of major interest, as different products in continuous manufacturing are often variations of the same formulations, with small changes which do not significantly affect rheology, such as variations on colour, fragrance, flavour or minor actives.

The solid lines in Figure 5.16 illustrate the concentration changes over time as observed using the approach described previously at the exits of each of the five elements in the assembly.

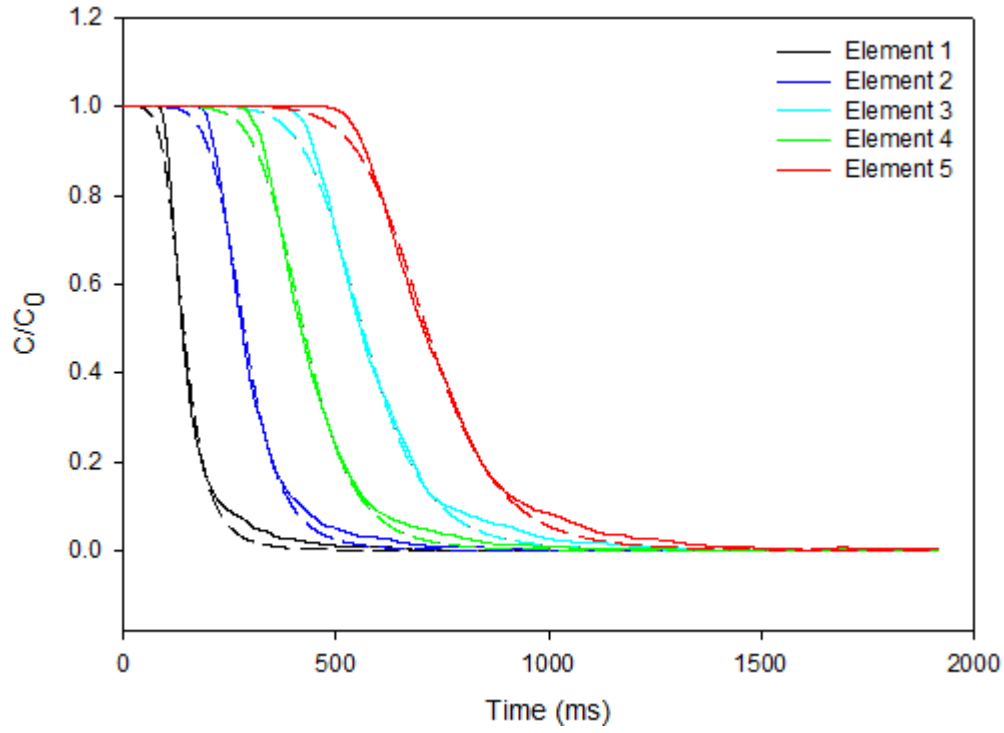

Figure 5.16. The concentration profiles across five element exits for 1% CMC solution flowing at 300 L/h, where the solid lines represent the experimental data and the dashed lines represent the model fit (Equation 5.7).

The correlation between the time elapsed and the concentration of the initial fluid is represented by Equation 5.7, where C is the concentration of the initial fluid at time t (-),

C_0 is the initial concentration (-), t is the time elapsed from the beginning of the changeover (ms), i.e. the second fluid entering the first element of the assembly, t_{50} is point in time where half of the original fluid is removed from a cross-section (ms), and k is a dimensionless consistency coefficient (-), related to the steepness of the curve, an indication of the "plugnes" of the changeover front, with higher k values indicating more plug-like flow. Therefore, a more efficient changeover process is achieved when t_{50} is minimised and k is maximised. Through non-linear regression the expression yields fits to the experimental data with $R^2 > 0.98$.

$$\frac{C}{C_0} = 1 - \frac{1}{1 + \left(\frac{t}{t_{50}}\right)^{-k}} \tag{5.7}$$

The dashed lines in Figure 5.16 illustrate the experimental concentration data and the fit described by Equation 5.7 for the 1% CMC solution flowing through the mixer at 300 L/h as seen at the exits of the 5 elements in the mixer assembly.

The expressions for k and t_{50} can further be deconstructed based on the individual values at different mixer locations as well as the variation of the constants for different fluids and flow conditions. Table 5.3 and Table 5.4 illustrate the variability of the consistency coefficient k and 50% changeover time t_{50}.

Table 5.3. Values of the consistency coefficient k for various fluids and flow rates

No. elements	$k_{\text{Glycerol 300}}$ (-)	$k_{\text{CMC 300}}$ (-)	$k_{\text{Guar 300}}$ (-)	$k_{\text{Glycerol 200}}$ (-)
1	4.1	5.3	6.0	4.0
2	5.1	6.2	6.9	5.8
3	6.0	7.3	7.9	6.6
4	6.8	8.3	9.1	7.9
5	7.5	9.3	10.2	9.3

Table 5.4. Values of t_{50} for various fluids and flow rates

No. elements	t_{50}Glycerol 300 (ms)	t_{50}CMC 300 (ms)	t_{50}Guar 300 (ms)	t_{50}Glycerol 200 (ms)
1	148	143	137	221
2	293	283	272	432
3	445	427	411	657
4	596	572	546	876
5	742	722	684	1090

It can be seen that both k and t_{50} are dependent on the number of elements, N (-), the flowrate, Q (L/h) and the rheology of the fluid, i.e. power law constant, n (-). This is further emphasised in Figure 5.17, where it can be seen that the values of k for different fluids form parallel lines. The fluids with higher n values having a lower k value, while the same fluid flowing at a lower flow rate also has a higher value of k. Increasing the number of elements increases k for all fluids at all flowrates. The value of k is inherently liked to the rate at which the fluid is completely displaced within the mixer. It can also be seen that for fluids which displayed better mixing in the analysis presented in Section 5.4.1., the value of k is lower, suggesting longer changeover times, for example glycerol at 300 L/h has a k value of 4.1, while guar gum solution at the same flowrate has the value of 6, when changeover in one element is considered. This reiterates the conclusion made previously, that more non-laminar behaviour is observed in fluids such as glycerol within the SMX mixer, leading to both better mixing and longer residence/changeover times.

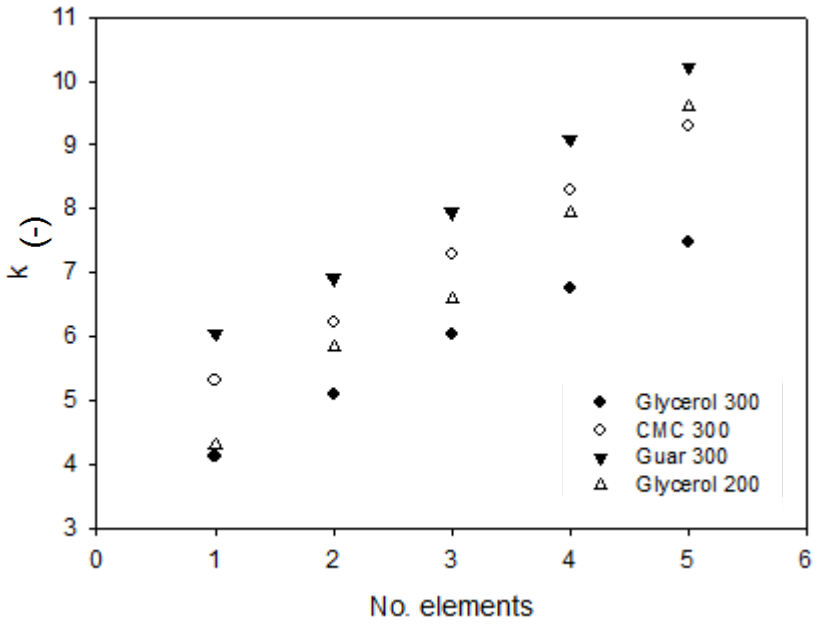

Figure 5.17. Consistency coefficient, k, as a function of the number of mixer elements

Figure 5.18 illustrates the trends for t_{50}, where the values of t_{50} increases with increasing N, as expected, as the fluid takes longer to travel a given distance, and therefore achieve 50% changeover further down the mixer. It can also be seen that reducing the flowrate increases the value of t_{50}, which is also expected, as due to lower velocity the changeover fluid will take longer to travel the mixer length when compared to a higher flowrate fluid. Finally, the power law constant, n, does not appear to affect the value of t_{50}, this is due to the fact that for all fluids the flow within the SMX mixer resembles plug flow, as described previously, therefore breakthrough and consequently 50 % changeover would occur at approximately the same time for all fluids (Mihailova et al., 2016). However, using a Student's t-test it was shown that the results for t_{50} at different values of n belong to distinct distributions, with $P < 0.05$.

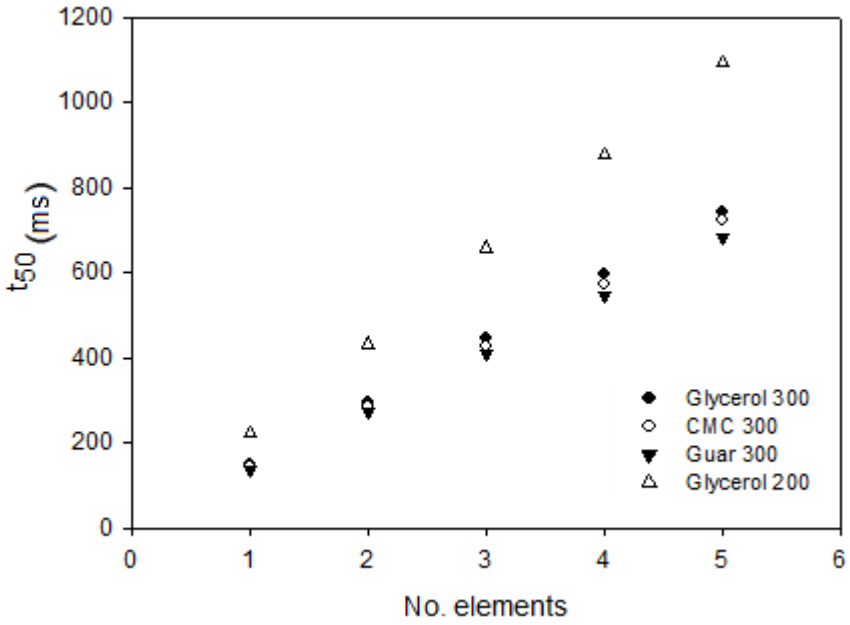

Figure 5.18. 50% changeover time, t_{50}, as a function of the number of mixer elements

In order to correlate the values for t_{50} and k with the number of elements (N) and the flow rate (Q) a linear regression was performed on the data illustrated in Figure 5.17 and Figure 5.18, with respect to the number of elements, resulting in the following expressions:

$$t_{50} = c\frac{N}{Q} \tag{5.8}$$

$$k = a\frac{N}{Q} + b \tag{5.9}$$

Where the values of constants a, b and c are still dependent on the power law coefficient n, as shown in Table 5.5 and Figure 5.19.

Table 5.5. The values of constants a, b and c with respect to the power law coefficient n

Flow index n	a	b	c
1.00	0.84	3.38	149
0.55	0.98	4.38	142
0.30	1.06	4.93	138

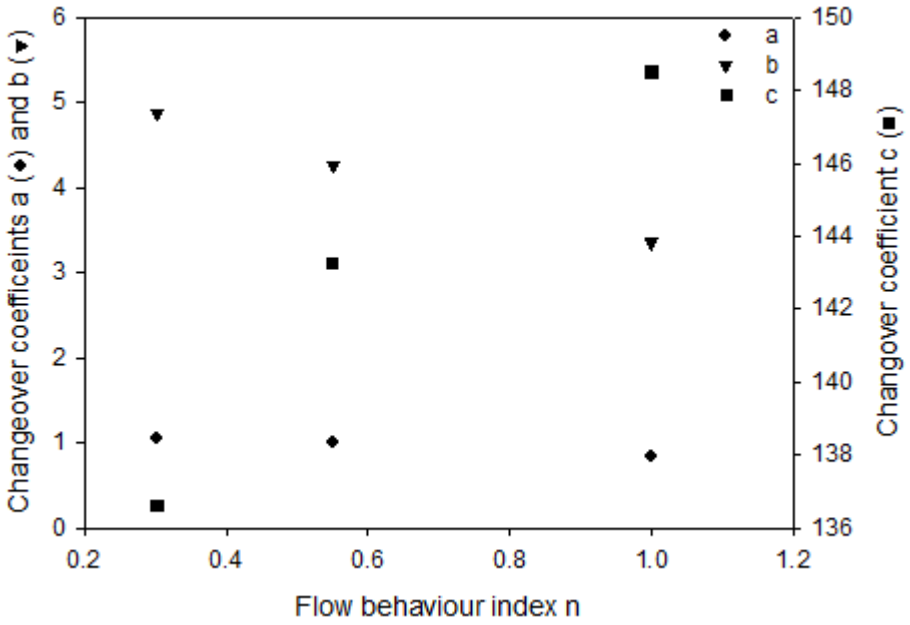

Figure 5.19. Changeover coefficients a, b and c as a function of the power law flow behaviour index n.

In order to accommodate for the variations in the fluid rheology further linear regression on the data shown in Figure 5.19 was carried out, with respect to the power law coefficient, providing the Universal constants shown in Table 5.6, which are can be applied to estimate the values of t_{50} and k as in Equations 5.10 and 5.11 respectively.

$$t_{50} = (c_1 n + c_2)\frac{N}{Q} \tag{5.10}$$

$$k = (a_1 n + a_2)\frac{N}{Q} + b_1 n + b_2 \tag{5.11}$$

$$t = \left(\frac{1}{1 - \frac{C}{C_0}} - 1\right)^{\frac{1}{-k}} t_{50} \tag{5.12}$$

By rearranging Equation 5.7 it is possible to obtain an expression which allows calculation of the time required to achieve a desired level of changeover, using the derived constants, as shown in Equation 5.12. This expression universally predicts the changeover

time across a given number of elements for fluids with Newtonian and non-Newtonian (Power law) behaviour, for the fluids flowing at flowrates that maintain laminar a flow regime.

Table 5.6. Universal changeover constants

Constant	
a_1	-90.8
a_2	344
b_1	-2.22
b_2	5.60
c_1	4920
c_2	39800

The main limitation of the resulting model arises from the fact that the mixer elements of the same diameter were used for all fluids and flowrates in the current experimental work. It is therefore impossible to comment on the effect of mixer diameter on the changeover coefficients. Further work across various mixer diameters is required to further develop this correlation.

The changeover time required in an SMX mixer was finally contrasted against the time required to clean a simple circular pipe of the same diameter, under laminar and plug flow conditions. For the purposes of the comparison the time required to remove 95 % of the original fluid is considered, where Equation 5.12 was solved for $C/C_0 = 0.05$. As can be seen in Figure 5.20 the changeover time over the length of five SMX elements is comparable between all fluids that were assessed, and is very similar to the time that would be required to clean an empty pipe under plug flow conditions. However, when the

same length of pipe without a mixer present is assessed, the time required to achieve 95 % changeover increases significantly, with glycerol taking almost 7 times longer to achieve the desired changeover in the empty pipe as in the SMX mixer. This leads to the conclusion, that when changing over fluids on production scale, the removal of the original fluid inside the mixer will require a fraction of the time required for the remaining pipe work. Furthermore, the similarity in the changeover time between the different fluids suggests that when it comes to SMX mixers the relative rheological properties of the two fluids being changed over is not as significant as it is in an empty pipe, where the changeover of fluids with different rheological properties can be problematic (Wiklund et al., 2010).

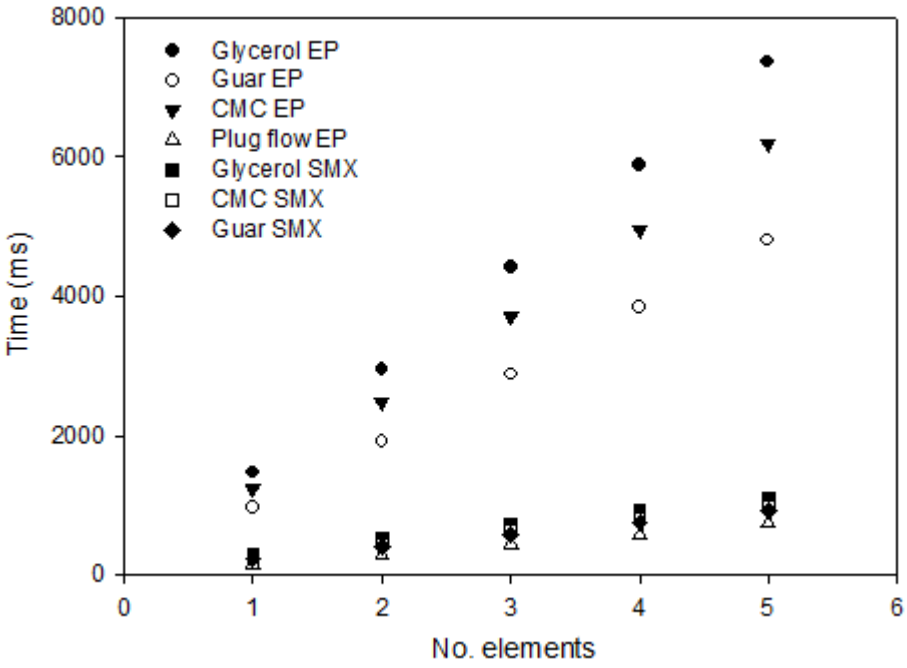

Figure 5.20. The comparison of the time required to remove 95% of the original fluid from a circular pipe (EP) and the SMX mixer of equivalent diameters, over the length equivalent to five SMX mixer elements for a fluid flowing at 300 L/h. Also contrasted with the time required for the 95% changeover under plug flow conditions.

5.5 CONCLUSIONS

Understanding mixing, changeover and other dynamics in static mixers is integral to the optimisation of their performance, helping the users to select the number of elements required to achieve the desired product properties as well as the requirements for the cleaning of the production lines between products, to ensure high quality outputs. Different techniques can be applied to achieve this goal, with a different balance of accuracy, acquisition speed and limitations. The case of DN25 SMX mixers was addressed using multiple techniques.

Mixing was evaluated by calculating the intensity of segregation on x-y cross-section along the length of five DN25 SMX elements. It was shown that the concentric feed for the mixing species yields the best mixing efficiency and provides the same level of mixing for fluids with different rheological properties, as well as remaining consistent across different flowrates. The side by side feed configuration favoured mixing between Newtonian fluids, where the non-Newtonian fluid mixing efficiency was observed to be negatively affected when increasing the fluid flowrate. It was also illustrated that when the mixer is incorrectly oriented with respect to the side-by-side feed, the first mixer element delivers no reduction in the intensity of segregation, and hence does not provide any mixing.

Finally, characterisation of changeover across five mixer elements was addressed using two approaches. The process of the displacement of a transparent fluid by a dyed fluid was captured within and outside of the mixer element using a high speed camera at 1000 fps. This approach provided an estimation of the rate of changeover and the differences between the changeover patterns between pipes containing SMX mixers and empty pipes, under same flow conditions. It was demonstrated that systems containing SMX mixers undergo a much more rapid changeover, due to the mixer inducing a pseudo

plug flow as the second fluid leaves the mixer. However, the technique does not allow to assess the 3D dynamics within the mixer elements, as the field of view is rapidly obstructed by the dyed fluid.

Therefore, PEPT data was once again used to study the changeover in more detail, where the individual particle pass location with respect to time was assessed to infer the fraction of the original fluid remaining at a given cross-section. An expression was derived based on data from various fluids and flowrates which allows prediction of the time required to achieve a desired level of changeover across a specified number of elements. As the study was carried out on a single SMX diameter, the expression does not take into consideration the effect of mixer diameter on the changeover time. Thus concluding that the changeover time is dependent on the fluid properties, as well as the total flowrate.

Comparing the theoretical changeover times for empty pipes with parabolic flow, plug flow and the results from the SMX mixer changeover further confirms that the flow within the mixer is close to plug flow. This suggests that during production line cleaning SMX mixers are one of the easiest parts of the process to clean or switch to a new product.

5.6 REFERENCES

Chiti, F., Bakalis, S., Bujalski, W., Barigou, M., Eaglesham, A., Nienow, A.W. (2011) 'Using positron emission particle tracking (PEPT) to study the turbulent flow in a baffled vessel agitated by a Rushton turbine: Improving data treatment and validation', *Chemical Engineering Research and Design*, 89(10), 1947–1960.

Etchells, A.W., Meyer, C.F. (2003) 'Mixing in Pipelines', in *Handbook of Industrial Mixing*, John Wiley & Sons, Inc., 391–477.

Ghanem, A., Lemenand, T., Della Valle, D., Peerhossaini, H. (2014) 'Static mixers: Mechanisms, applications, and characterization methods – A review', *Chemical Engineering Research and Design*, 92(2), 205–228.

Leschka, S., Thévenin, D., Zähringer, K., Lehwald, A. (2007) 'Fluid dynamics and mixing behavior of a SMX-type static mixer', *Journal of Visualization*, 10(4), 342–342.

Liu, S., Hrymak, A., Wood, P. (2006) 'Laminar mixing of shear thinning fluids in a SMX static mixer', *Chemical Engineering Science*, 61, 1753–1759.

Meijer, H.E.H., Singh, M.K., Anderson, P.D. (2012) 'On the performance of static mixers: A quantitative comparison', *Progress in Polymer Science*, 37(10), 1333–1349.

Mihailova, O., Lim, V., McCarthy, M.J., McCarthy, K.L., Bakalis, S. (2015) 'Laminar mixing in a SMX static mixer evaluated by positron emission particle tracking (PEPT) and magnetic resonance imaging (MRI)', *Chemical Engineering Science*, 137, 1014–1023.

Mihailova, O., O'Sullivan, D., Ingram, A., Bakalis, S. (2016) 'Velocity Field Characterisation of Newtonian and Non-Newtonian Fluids in SMX Mixers Using PEPT', *Chemical Engineering Research and Design*, 108, 126–138.

Mac Namara, C., Gabriele, A., Amador, C., Bakalis, S. (2012) 'Dynamics of textile motion in a front-loading domestic washing machine', *Chemical Engineering Science*, 75, 14–27.

Paul, E.L., Atieno-Obeng, V.A., Kresta, S.M. (2004) *Handbook of Industrial Mixing*, John Wiley & Sons.

Pérez-Mohedano, R., Letzelter, N., Amador, C., VanderRoest, C.T., Bakalis, S. (2015) 'Positron Emission Particle Tracking (PEPT) for the analysis of water motion in a domestic dishwasher', *Chemical Engineering Journal*, 259, 724–736.

Rafiee, M., Simmons, M.J.H., Ingram, A., Stitt, E.H. (2013) 'Development of positron emission particle tracking for studying laminar mixing in Kenics static mixer', *Chemical Engineering Research and Design*, 91(11), 2106–2113.

Rauline, D., Le Blévec, J.M., Bousquet, J., Tanguy, P. a (2000) 'A Comparative Assessment of the Performance of the Kenics and SMX Static Mixers', *Chemical Engineering Research and Design*, 78(3), 389–396.

Singh, M.K., Anderson, P.D., Meijer, H.E.H. (2009) 'Understanding and Optimizing the SMX Static Mixer.', *Macromolecular rapid communications*, 30(4–5), 362–76.

Streiff, F.A., Jaffer, S., Schneider, G. (1999) 'Design and application of motionless mixer technology', in *ISMIP3, Osaka*, 107–114.

Thakur, R., Vial, C., Nigam, K. (2003) 'Static mixers in the process industries—a review', *Chemical Engineering Research and Design*, 81(Part A), 787–826.

Volkwyn, T.S., Buffler, A., Govender, I., Franzidis, J.-P., Morrison, A.J., Odo, A., van der Meulen, N.P., Vermeulen, C. (2011) 'Studies of the effect of tracer activity on time-averaged positron emission particle tracking measurements on tumbling mills at PEPT Cape Town', *Minerals Engineering*, 24(3–4), 261–266.

Wiklund, J., Stading, M., Trägårdh, C. (2010) 'Monitoring liquid displacement of model and industrial fluids in pipes by in-line ultrasonic rheometry', *Journal of Food Engineering*, 99, 330–337.

Zalc, J.M., Szalai, E.S., Muzzio, F.J., Jaffer, S. (2002) 'Characterization of flow and mixing in an SMX static mixer', *AIChE Journal*, 48(3), 427–436.

CHAPTER 6. PRESSURE DROP IN SMX STATIC MIXERS. P&G CASE STUDY

The work presenting in this chapter was carried out at the P&G pilot plant in Brussels Innovation Center. All data collection and analysis was carried out by the author of this thesis.

6.1 ABSTRACT

A pilot plant study at P&G Brussels Innovation Centre was carried out in order to develop a better understanding of the pressure drop of complex structured fluids across SMX mixers. The study spanned a range of SMX sizes, DN15, DN25 and DN40 and was conducted on four fluids, three fluids exhibiting a Carreau-Yasuda model behaviour, and one Newtonian fluid (glycerol). It was found that under the assumption that all fluids behave as Newtonian fluids inside the mixer, it is possible to demonstrate that the viscosity – shear rate correlation inside the mixer closely resembles that described by models derived from offline oscillatory rheometry. The fluid models were then used in pressure drop predictions, which were compared with the experimental pressure drop results, showing that within the standard operating conditions for SMX mixers, the assumption of constant viscosity within the mixer and the application of dynamic viscosity models allows to accurately predict pressure drop. This finding illustrates that shear banding which leads to the deviation between oscillatory and rotational rheological measurements, does not occur inside the SMX mixer under standard operating conditions.

6.2 INTRODUCTION

SMX mixers are used in a range of industrial processes, and the pressure drop across the mixers is one of the key variables during process design. The pressure drop provides the energy required for the mixing and can be quite significant, even for thin fluids, such as water (Li et al., 1997). Not being able to predict pressure drop across the mixer assembly could result in exceeding pump capacities or damaging equipment due to pressure build up. Currently pressure drop predictive models only cover fluids with simple rheologies, mainly Newtonian or shear thinning with a Power law index (n) > 0.8, through approximation to Newtonian fluids (Liu et al., 2006). However, the complexity of the real fluids used in manufacturing processes requires the ability to predict pressure drop for structured fluids, such as shampoos, conditioners, laundry and dish detergents.

The aim of this study is to improve the understanding of pressure drop in SMX mixers for fluids exhibiting rheological properties best described by the Carreau-Yasuda fluid model and develop an approach that would allow the prediction of the pressure drop of such complex non-Newtonian fluids across SMX mixers (Mihailova et al., 2016).

Further interest in the behaviour of the fluids used is due to other non-Newtonian features, such as shear banding. Shear banding usually occurs due to formation of layers with unequal strain rates, but equal stress. For example, under standard non-shear banding conditions the strain rate between the wall and the centre of the pipe decreases at a constant rate, as the effects of the wall no-slip boundary condition diminish further away from the wall. When shear banding occurs two or more bands with different strain rate gradients are formed, which nevertheless average to match the total strain rate expected from a continuous shear-thinning fluid undergoing the deformation under the same conditions. And while within each band the fluid viscosity does follow the expected non-

Newtonian model or velocity profile based on the local strain rate, there is no consistency between bands making it impossible to predict the pressure drop for such systems (Cates and Fielding, 2006; Spenley et al., 1993). Fluids with wormlike micellar surfactant structures, such as shampoos, liquid dish and laundry detergents and body washes are susceptible to shear banding and are of particular interest to FMCG companies, such as P&G (Parker and Fieber, 2013; Yesilata, 2002). Shear banding is viewed as an intermediate step between fully developed flow and wall-slip, where the severity of the effect is linked to the concentration of the surfactant in the system and the phase behaviour of micellar solutions (Helgeson et al., 2009).

The ability to predict pressure drop in the mixer, combined with the mixing and changeover predictions described earlier (Chapter 5) would allow design of mixer assemblies with the best trade-off between operating costs and final product quality, as well as size auxiliary equipment, such as pumps.

The pressure drop across a range of SMX mixers of different lengths (10 or 18 elements) and diameters (15, 25 or 40 mm) was recorded using a pilot plant rig at P&G Brussels Innovation Centre, along with flowrate and temperature. The apparent viscosity of the fluid can be calculated based on the process variables and compared with the rheological models derived based on flow or oscillatory rheological measurements conducted offline. An agreement between a fluid model derived offline and measurements taken in-process allows a prediction of apparent viscosity at any process conditions, in turn allowing for the estimation of the pressure drop based on variables such as flowrate and system geometry, e.g. number of mixer elements and their diameter. As the result an approach was developed that minimises the difference between calculated (predicted) and observed pressure drop, allowing for better pressure drop prediction during process design.

6.3 MATERIALS AND METHODS

6.3.1 EXPERIMENTAL SET UP

The pressure drop across a range of SMX mixer configurations was captured using the pilot plant rig shown in Figure 6.1. The fluids of interest were stored in a 200 L tank and recirculated through the static mixer assemblies at different flow rates.

Three sizes of stainless steel SMX mixer were assessed, DN15, DN25 and DN40 (Sulzer, Switzerland), with either 10 or 18 elements per assembly, depending on availability. In addition to SMX mixer assemblies, empty pipe sections were also studied, for validation purposes.

The recirculation rate was varied across the permitted range, with the lowest flowrate determined by a detectable pressure drop across the mixer assembly and the maximum limited by the safety features of the rig, where the pressure of over 5 bar on the P1 sensor caused the pump to trip. Table 6.1 summarises the SMX assemblies used in the study and the flowrate ranges achieved in each one. The trade names of the fluids in the study cannot be disclosed, so they will be referred to as fluids A, B and C throughout.

The variables recorded during the experiments were the temperature and pressure before and after the mixer assembly, as well as the volumetric flowrate. All the data was logged automatically using the process control software as well as manually, directly from the sensors, for validation. The temperature was controlled using jacketed pipes and remained at $20\pm0.5^{o}C$ throughout the experiment.

Table 6.1. The sizes of SMX mixers used in the study and the flow rate ranges that could be achieved in each assembly, within the constraints of the equipment.

	Glycerol L/h	Fluid A L/h	Fluid B L/h	Fluid C L/h
DN25 10el	100-390	10-540	70-900	20-1030
DN25 18el	100-320	15-370	70-800	20-750
DN15 18el	50-130	12-255	50-520	10-290
DN40 10el	280-640	20-645	170-1000	15-990
DN40 18el	170-620	12-450	160-920	15-820

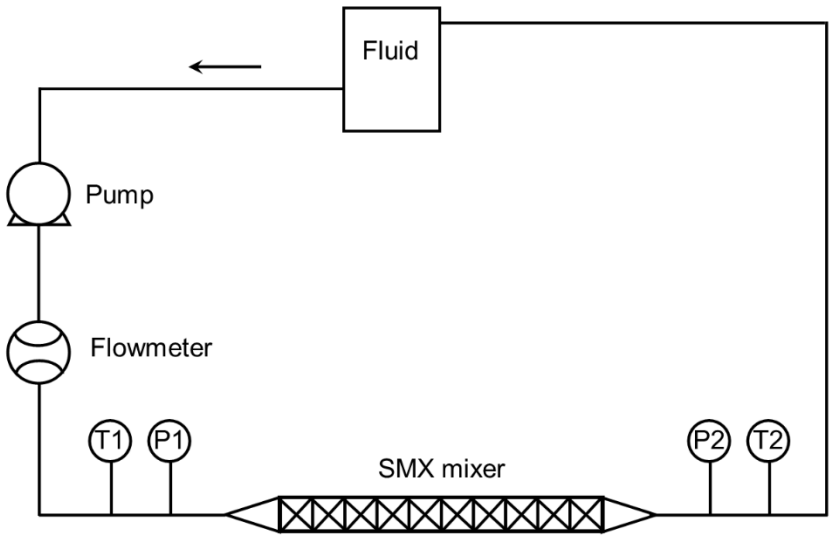

Figure 6.1. The pilot plant set up used for the pressure drop in SMX mixers study

6.3.2 FLUIDS AND RHEOLOGICAL MODELS

A range of industrially relevant non-Newtonian fluids were used in the study, all exhibiting Carreau-Yasuda fluid properties. Under low shear the fluids appear Newtonian, maintaining a constant viscosity until a critical shear rate is reached, when the fluid begins to shear thin. After undergoing significant thinning, the fluid reaches the second

Newtonian plateau, where further increasing the shear does not affect the viscosity any further. This fluid model is typical for structured fast moving consumer goods products, for example dish washing liquids and shampoos. The Carreau-Yasuda fluid model is shown in Equation 6.1, where μ_{eff} is the apparent viscosity (Pa.s), μ_0 is the viscosity at the initial Newtonian plateau at low shear rates (Pa.s), μ_{inf} is the viscosity at the second Newtonian plateau at high shear rates (Pa.s), $\dot{\gamma}$ is the shear rate (s^{-1}), λ is the relaxation time (s), a is the transition constant (-) and n is the power index (-).

$$\mu_{eff} = \mu_{inf} + \left(\mu_0 - \mu_{inf}\right)\left(1 + (\lambda\dot{\gamma})^a\right)^{\frac{n-1}{a}} \quad 6.1$$

$$|\mu_c| = \frac{|G^*|}{\omega} \quad 6.2$$

The non-Newtonian fluids in the study have been known to display shear-banding, due to the characteristic worm-like micellar surfactant assemblies present in such fluids. Shear banding is known to lead to apparent wall slip in pipes as well as slip in rotational (flow) rheometers, resulting in under-predictions for fluid viscosities at high shear rates. In order to negate any shear banding effects the current study uses dynamic (oscillatory) rheology along with traditional flow rheology, which is not subject to shear banding, as no continuous forces are applied on the sample. Furthermore, oscillatory measurements allow results to be obtained at shear rates higher than rotational measurements, of up to 600 s^{-1}, which was found lead to sample degradation under rotational conditions in the fluids used for this study (Mütze et al., 2014). The Cox-Merz correlation dictates that for complex fluids, such as polymer melts and surfactant structured fluids, the steady state shear viscosity can be directly correlated with the complex viscosity, μ_c (Pa.s), derived from angular frequency, ω (Hz), and the complex modulus G^* (Pa) (Equation 6.2) (Cox and Merz, 1958). All oscillatory measurements were carried out at strain = 10%, which was found to lie well within the linear viscoelastic region for all fluids tested. Table 6.2

summarises the rheological constants of the fluids used in the study obtained using both the flow and the dynamic rheometry.

Table 6.2.Carreau-Yasuda model coefficients for the fluids in the study, obtained using both flow and dynamic methods

Fluid	μ_0	μ_{inf}	λ	n	a
A flow	2.69	0.000	0.016	0.004	3.16
A dynamic	2.69	0.000	0.009	0.006	1.98
B flow	0.78	0.003	0.002	0.001	1.52
B dynamic	0.76	0.001	0.001	0.001	1.06
C flow	4.96	0.000	0.029	0.008	3.25
C dynamic	4.96	0.036	0.013	0.008	2.00

In addition to the complex fluids Newtonian glycerol was used in all mixer and pipe assemblies, allowing validation of the models proposed for the pressure drop estimation, as they were originally developed for Newtonian fluids.

6.3.3 PRESSURE DROP ESTIMATION

In order to isolate the pressure drop across the mixer assembly, pressure losses in various fittings had to be accounted for, as the pressure sensors were located a significant distance away from the SMX mixer elements, and due to differences in mixer diameters, expansion and contraction fittings had to be used throughout.

The pressure drop across the expansion and contraction fittings, ΔP_f (Pa), can be estimated using Equations 6.3-6.5, where the value of the resistance coefficient, K (-), is different depending on the type of fitting, K_r for the reductions in diameter and K_e for the

expansions (Menon, 2005). Pipe diameters D_1 and D_2 correspond to the larger and smaller pipe respectively (m), and Re_1 is based on the velocity in the larger pipe. Finally, velocity V_f (m s^{-1}) in Equation 6.3 corresponds to the velocity in the first pipe in the fitting, i.e. larger pipe for contraction and smaller pipe for the expansion.

$$\Delta P_f = \rho K \frac{{V_f}^2}{2} \tag{6.3}$$

$$K = K_r = \left(1.2 + \frac{160}{Re_1}\right)\left[\left(\frac{D_1}{D_2}\right)^4 - 1\right] \quad \text{For reducing diameter} \tag{6.4}$$

$$K = K_e = 2\left[1 - \left(\frac{D_2}{D_1}\right)^4\right] \quad \text{For increasing diameter} \tag{6.5}$$

The pressure drop across any sections of empty pipe was calculated using the Darcy-Weinbach equation (Equation 6.6) which is dependent on the Darcy friction coefficient (Equation 6.7), where the viscosity of the fluids, μ (Pa.s), can be estimated by applying the apparent shear rate in the pipe (Equation 6.8) to the correct fluid models.

$$\frac{\Delta P}{L} = f_D \frac{\rho}{2} \frac{{V_f}^2}{D} \tag{6.6}$$

$$f_D = \frac{64\mu}{V_f D \rho} \tag{6.7}$$

$$\dot{\gamma} = \frac{8V_f}{D} \tag{6.8}$$

6.4 RESULTS

The pressure drop was calculated using a range of variables that were recorded along with the actual pressure drop during the experimental trials. While most variables could be recorded directly, the viscosity of the fluid was calculated based on the constants in Table 6.2 obtained using offline rheology.

By substituting Equation 6.7 into Equation 6.6 and rearranging it is possible to calculate the viscosity of the fluid that would result in the pressure drop observed. This apparent viscosity, μ_a (Pa.s), is calculated under the assumption that the fluid is Newtonian and viscosity is constant throughout the mixer (Equation 6.9). Here V is the velocity inside the mixer containing pipe, based on the flowrate (m s^{-1}), L is the length of the mixer (m) and ΔP is the pressure drop across the mixer assembly only (Pa).

$$\mu_a = \frac{\Delta P}{L}\frac{D^2}{32V} \tag{6.9}$$

$$\dot{\gamma}_{SMX} = \frac{64V}{D} \tag{6.10}$$

The apparent shear rate inside an SMX mixer is described by the Streiff-Jaffer correlation, and is dependent on the fluid velocity and the mixer diameter (Equation 6.10) (Streiff et al., 1999). The correlation is derived from a similar expression for empty pipes (Equation 6.8), however, due to the presence of the mixer in the pipe, the apparent shear rate is higher.

In order to validate the method, the viscosity required for the observed pressure drop was first estimated for Newtonian glycerol. Figure 6.2a illustrates how the calculated values relate to the actual viscosity of glycerol at the temperature of the experiments, μ_a = 1.4 Pa.s. The data shown covers all mixer sizes in the study and spans the flowrate range discussed above. It can be seen that the calculated values relate closely to the actual fluid viscosity, with $R^2 > 0.98$.

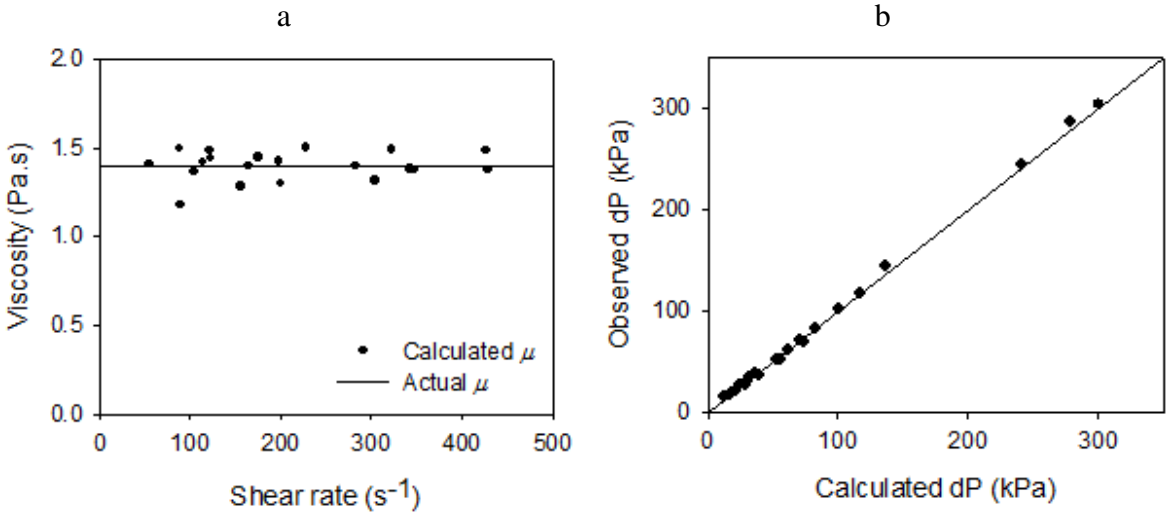

Figure 6.2. For glycerol flowing through SMX mixers of various lengths and diameters (a) The predicted viscosity based on the measured dP(from Equations 6.9 and 6.10). (b) The comparison between the observed dP and the dP calculated based on the system properties.

A different approach to the method validation was also taken, where the known parameters of the flow, such as flowrate, geometry and viscosity of the fluid were used to calculate the theoretical pressure drop across the mixer. Figure 6.2b demonstrates the correlation between the calculated pressure drop and that observed experimentally. Once again, the correlation is strong between observed and experimental results for glycerol, with the $R^2 > 0.97$.

The validation carried out with glycerol allows to proceed to the complex fluids described previously. Using the same approach, the apparent viscosities in the mixers were calculated for fluids A, B and C, which can then be compared to the rheological models derived based on the flow and dynamic rheometer measurements. Figure 6.3 illustrates the apparent viscosities derived from the observed pressure drop and apparent the shear rates derived using the Streff-Jaffer correlation for the different SMX mixer sizes across all three fluids. It can be seen that the fluid models obtained using flow viscosity describe the apparent viscosities poorly. However, the fluid models derived from dynamic rheometry

match the apparent viscosity closely, with R^2 values of 0.85, 0.94 and 0.91 for Fluid A, B and C respectively.

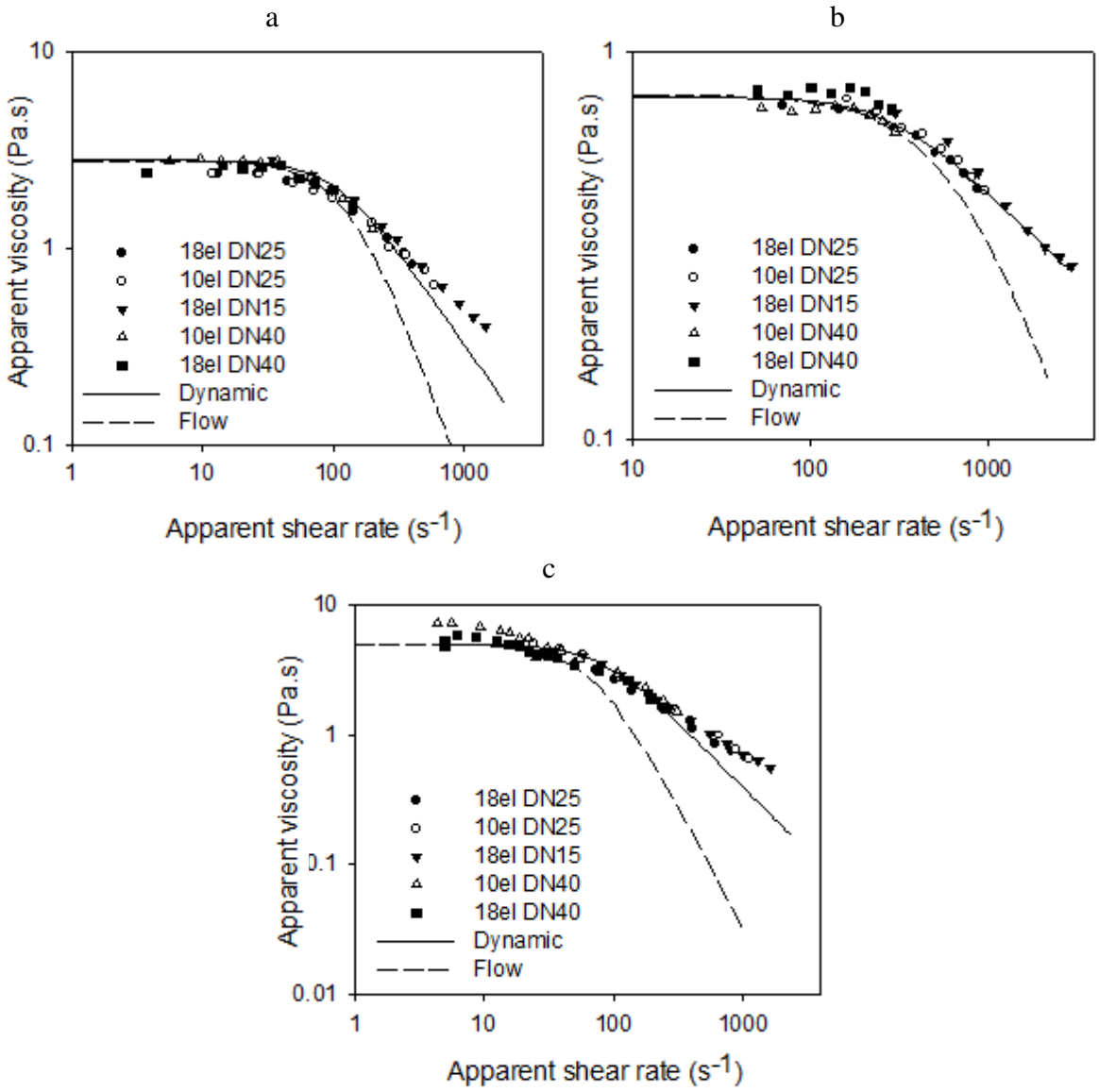

Figure 6.3. Apparent viscosity based on measured dP against apparent shear rate estimated from the Streff-Jaffer correlation (Equation 6.10), the compared to the rheological Carreau-Yasuda models for (a) fluid A, (b) fluid B and (c) fluid C.

The consistency between the flow curves obtained using oscillatory rheometry and those estimated from the pressure drop data can be due to the nature of the flow fields within the SMX mixer, where flow similar to plug flow has been observed (Mihailova et al., 2016, Chapter 5). Under plug flow conditions even shear thinning fluids appear to

maintain constant viscosity, as no overall velocity gradient is exerted on the fluid. Therefore, it is acceptable to assume that the fluid viscosity remains constant under plug flow conditions and is equal to the viscosity of the fluid at the apparent shear rate within the system. Based on the Equation 6.10 this assumption is valid within the studied region (Sankar and Hemalatha, 2007). However, deviations from the models set in at higher shear rates, and in mixers with smaller diameters, which could be caused by a number of factors, including shear banding at higher shear rates or development of parabolic velocity profiles at higher axial velocities. It can also be noted that for fluid B, which has the lowest initial viscosity, the match between theoretical and observed viscosities is the closest, while the fluids with higher initial viscosities have higher deviations from the model. The data collected during the study, however, is insufficient to draw conclusions on whether the correlation with the model viscosity is dependent on the initial viscosity, mixer geometry or if other fluid properties play a role.

The pressure drop across the SMX mixer assemblies was then calculated based on the dynamic fluid models and compared to the pressure drop recorded during the experimental trials. Figure 6.4 demonstrates how the pressure drops compare for the three fluids that were used in the study. The flow viscosity model proves inadequate in pressure drop prediction, which can be expected, based on the apparent viscosity trends seen in Figure 6.3. The application of the dynamic viscosity model, on the other hand, results in a satisfactory pressure drop prediction. For fluids A and C deviation still manifests at higher shear rates in mixers with smaller diameters, at standard operating conditions, where the average axial velocity across the mixer is maintained below 0.15 m/s, the pressure drop correlation demonstrate $R^2 > 0.92$. It is therefore acceptable to apply dynamic viscosity models to predict pressure drop across SMX mixers, under the assumption of Newtonian fluid behaviour within the mixer, as long as the process remains within the standard

operating constraints. These series of results suggest that shear banding does not occur in SMX static mixers, at least within standard operating conditions, allowing the oscillatory rheology models to be applied for pressure drop predictions.

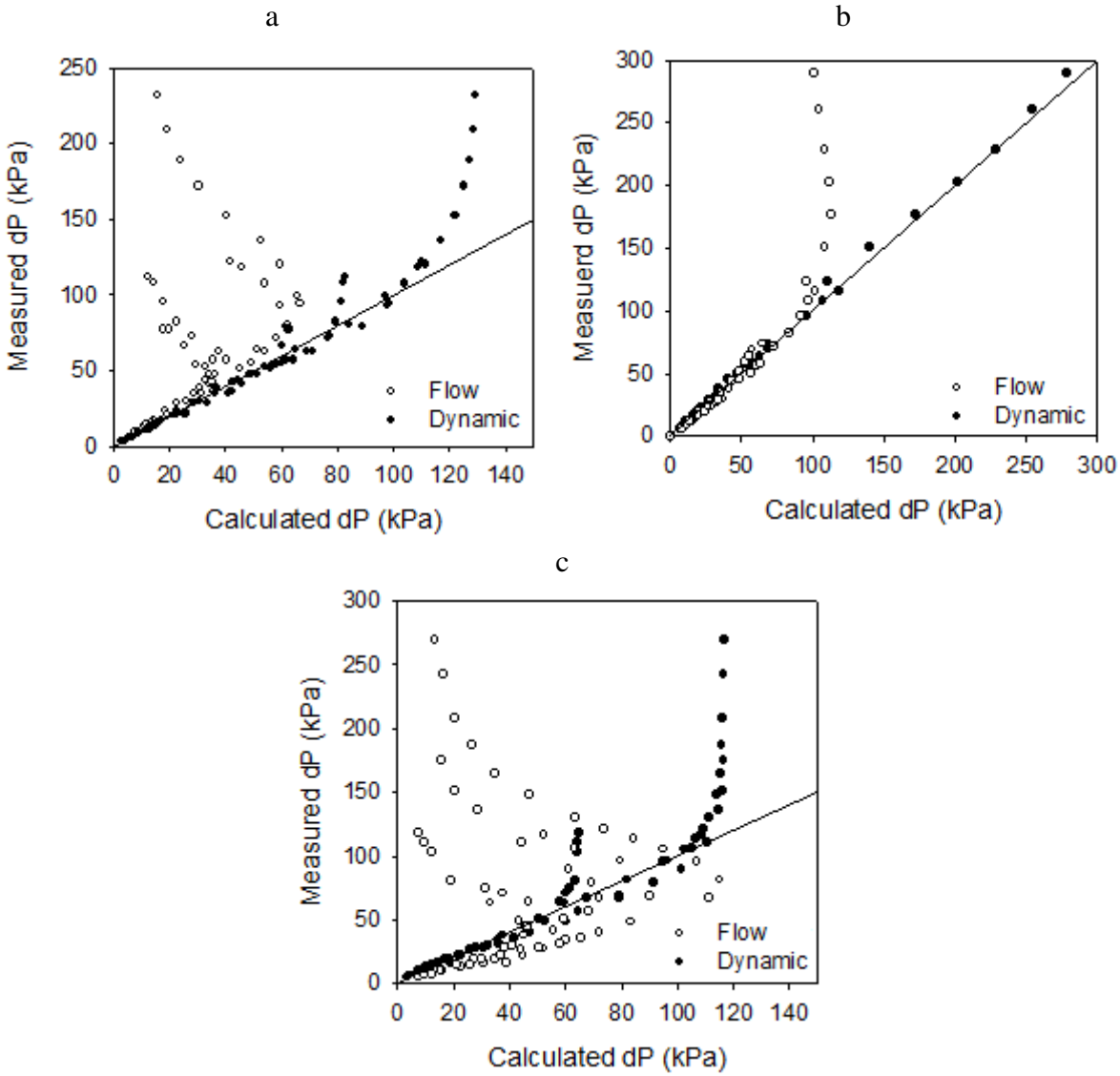

Figure 6.4. Measured pressure drop against pressure drop calculated based on the fluid models for (a) fluid A, (b) fluid B and (c) fluid C.

6.5 CONCLUSIONS

Pilot plant trials were carried out in order to develop a better understanding of pressure drop of complex fluids inside SMX mixers. Three fluids that follow the Carreau-Yasuda fluid model were used, as well as glycerol, for methodology verification. SMX mixers of 3 diameters, 15, 25 and 40 mm were used, with either 10 or 18 elements.

Apparent viscosities of fluids within the SMX mixers were possible to estimate based on the apparent shear rate and recorded pressure drop across the mixer assembly, under the assumption that inside the mixer all fluids behave as a Newtonian fluid. For all fluids the apparent viscosity closely matched that predicted by rheological models based on offline oscillatory rheological measurements.

The fluid models were then in turn used to predict the pressure drop across the mixer assemblies under the same conditions as those in the pilot plant study. It was found, that while the predictions deviated from the observed values at higher shear rates, the proposed approach delivered accurate predictions within the standard equipment operating range. This approach also illustrates that within the SMX mixer shar banding does not occur, with the fluid flowing the rheological behaviour described by oscillatory measurements.

6.6 REFERENCES

Cates, M.E., Fielding, S.M. (2006) 'Rheology of giant micelles', *Advances In Physics*, 55(7–8), 799–879.

Cox, W.P., Merz, E.H. (1958) 'Correlation of dynamic and steady flow viscosities', *Journal of Polymer Science*, 28(118), 619–622.

Helgeson, M.E., Reichert, M.D., Hu, Y.T., Wagner, N.J. (2009) 'Relating shear banding, structure, and phase behavior in wormlike micellar solutions', *Soft Matter*, 5(20), 3858.

Li, H.Z.Z., Fasol, C., Choplin, L. (1997) 'Pressure Drop of Newtonian and Non-Newtonian Fluids Across a Sulzer SMX Static Mixer', *Chemical Engineering Research and Design*, 75(8), 792–796.

Liu, S., Hrymak, A., Wood, P. (2006) 'Laminar mixing of shear thinning fluids in a SMX static mixer', *Chemical Engineering Science*, 61, 1753–1759.

Menon, E.S. (2005) *Piping Calculations Manual*, McGraw-Hill Education: New York.

Mihailova, O., O'Sullivan, D., Ingram, A., Bakalis, S. (2016) 'Velocity Field Characterisation of Newtonian and Non-Newtonian Fluids in SMX Mixers Using PEPT', *Chemical Engineering Research and Design*, 108, 126–138.

Mütze, A., Heunemann, P., Fischer, P. (2014) 'On the appearance of vorticity and gradient shear bands in wormlike micellar solutions of different CPCl/salt systems', *Journal of Rheology*, 58(6).

Parker, A., Fieber, W. (2013) 'Viscoelasticity of anionic wormlike micelles: effects of ionic strength and small hydrophobic molecules', *Soft Matter*, 9(4), 1203.

Sankar, D.S., Hemalatha, K. (2007) 'A non-Newtonian fluid flow model for blood flow through a catheterized artery—Steady flow', *Applied Mathematical Modelling*, 31(9), 1847–1864.

Spenley, N.A., Cates, M.E., McLeish, T.C.B. (1993) 'Nonlinear Rheology of Wormlike Micelles', *Physical Review Letters*, 71(6), 939–942.

Streiff, F.A., Jaffer, S., Schneider, G. (1999) 'Design and application of motionless mixer technology', in *ISMIP3, Osaka*, 107–114.

Yesilata, B. (2002) 'Nonlinear dynamics of a highly viscous and elastic fluid in pipe flow', *Fluid dynamics research*, 31, 41–64.

CHAPTER 7. CONCLUSIONS AND FUTURE WORK

The aim of the work described in this thesis was to evaluate and apply a range of novel techniques in the pursuit of advancing the understanding of fluid dynamics within SMX static mixers. Static mixers were studied due to their popularity in continuous processing across a wide range of industries and poor degrees of understanding available to date. Understanding the fluid flow dynamics within static mixers allows for designing manufacturing processes in a way that ensures high product quality and consistency, as well as reducing processing time, energy and waste. The study is particularly relevant to P&G as being one of the industries leaders, their products are always becoming more complex, leading to increased intricacy of their processes, which requires advanced understanding of employed processing equipment.

To carry out this study a number of techniques were used to assess the dynamics of Newtonian and non-Newtonian model fluids, as well as industrially relevant fluids, such as P&G products, inside DN25 SMX static mixers. High speed image capture combined with fluids stained with a dye was applied for mixing and changeover studies, where the flow patterns of the clear and dye fluids provided an insight into the dynamics of the flow. Pilot plant pressure drop studies were then conducted in order to correlate the pressure drop across the mixer with the properties of the fluids and mixer geometry, such as number of mixer elements and mixer diameter.

Due to limitations of the aforementioned data acquisition approaches, the majority of the results were derived from the Positron Emission Particle Tracking (PEPT) data, which provides detailed information on the path of individual tracers through the mixer, detailing the tracers position in 3D space and time. The tracer path information can be processed in a number of ways, resulting in the derivation of various system properties. Local velocity fields were acquired based on the rate of particle displacement over time. Occupancy data was derived based on the length of time taken by particles to travel through the system.

The degree of mixing was defined by the flux weighted intensity of segregation, combining local velocities and local concentrations, derived by labelling the individual particle passes at the mixer entrance based on their feed location. Finally, changeover was assessed by labelling the individual tracer particles differently based on the time stamp associated with a defined mixer cross-section, where the particles with a time stamp higher than a defined threshold were defined as the fluid originally present in the system and the particles with a lower time stamp as those belonging to the new fluid. A model was subsequently derived to correlate fluid and system properties to the time required to achieve a desired level of changeover. In addition, PEPT data was successfully combined with Magnetic Resonance Imaging (MRI) providing an alternative approach to mixing characterisation.

The results of the studies conducted using the techniques described are summarised below, followed by recommendations for future research.

7.1 RESULTS OBTAINED FROM PEPT DATA ANALYSIS USING VARIOUS TECHNIQUES

7.1.1 MRI AND PEPT PROOF OF PRINCIPLE AND MIXING CHARACTERISATION

Mixing patterns within SMX mixer obtained using PEPT were contrasted against those attained using MRI for Newtonian fluids, where MRI provides imaging data of fluid with different levels of contrast material and allows for higher resolution compared to PEPT, to reveal that both techniques can be used to characterise mixing on the macroscopic level. The PEPT velocity data was then combined with the MRI concentration data to attain the flux weighted intensity of segregation, I_f, which is

conventionally used as a measure of the degree of mixing. The technique was, however, limited by the inability to tag non-Newtonian fluids used in the study with the magnetic contrast material.

7.1.2 LOCAL VELOCITY FILED ESTIMATION

The local velocity fields obtained based on the tracer particle location changes over time were compared across Newton and non-Newtonian fluids at different flowrates. Consistency with theoretical velocity profiles within empty circular pipes was illustrated for all fluids, suggesting accurate velocity tracking can be achieved using the proposed technique. Within the mixer the velocity distribution in the axial direction showed that no back mixing for all fluids and flowrates considered, as U_z is consistently positive. Radial velocity values, U_x and U_y for both Newtonian and non-Newtonian fluids were shown to be statistically indistinguishable at a constant flowrate, suggesting that within the mixer rheology of the fluids has insignificant effects on the axial velocity distribution, under Laminar conditions. However, it was also observed that the U_z velocity component still retained a degree of dependency on the fluid rheology, even though the effects were significantly less pronounced than in empty pipes.

7.1.3 MIXING

Building on the proof of principle demonstrated using MRI, mixing was further assessed using PEPT concentration and local velocity data. One of the key conclusions from the comparison of mixing patterns in glycerol, guar gum and CMC solutions is that the concentric feed of the two species to the mixer results in the highest mixing efficiency, compared to variations of side-by-side feeds. Furthermore, it was observed that for the side-by-side fluid feed scenarios the first mixer element induced little to no mixing if the feed was oriented unfavourably, emphasising the importance of equipment design. It was

also noted that for Newtonian fluids the flowrate did not appear to affect the mixing efficiency for a given feed orientation, however, for shear thinning fluids the mixing efficiency decreased with increasing flowrate. This phenomenon is difficult to explain, as it can be expected that with an increase in velocity and decrease in viscosity mixing would improve due to the magnification of any local flow instabilities. Further work is required to address this observation, as PEPT does not provide velocity distribution maps detailed enough for local phenomena differentiation. Residence time and Occupancy

Glycerol and guar gum solutions were compared on the basis of the residence time distribution across 10 SMX mixer elements. The average distance travelled by the tracers for the two fluids was found to be constant, allowing for measurement errors. A significant difference was observed between the time to breakthrough between 10 SMX mixers and an equivalent length of empty pipe, with a much sharper gradient for the SMX case, which further illustrates the plug flow behaviour within the mixer observed using optical methods.

7.1.4 CHANGEOVER

The changeover patterns reflected the efficiency of displacing fluids within the mixer. The changeover patterns for all fluids within the SMX mixer were demonstrated to closely resemble plug flow, and deliver significantly higher efficiency cleaning, than that in an empty pipe of equivalent length. However, it was further noted, that the fluids properties and flowrates have an effect on the rate of changeover. A universal model was developed which allows to predict the time required to achieve the desired level of changeover/cleaning, for a system with a known number of SMX elements, where fluids with known rheological properties are flowing at a constant flowrate. It was concluded that for a system containing an SMX mixer empty pipe sections would pose a significantly

higher challenge than the mixer sections. In fact, having several mixer elements in-line can enhance the changeover/cleaning, due to the plug flow nature of the concentration field at mixer outlet.

7.2 RESULTS OBTAINED USING ALTERNATIVE TECHNIQUES

7.2.1 HIGH SPEED IMAGE CAPTURE

Changeover in pipes that did not contain any SMX mixer elements was shown to take a significantly longer amount of time to clear out the original fluid contained in the system. The changeover/concentration pattern for the empty pipe is dependent on the parabolic velocity profile characteristic for such flows, the pattern for the SMX mixer containing pipe, on the other hand, closely resembles that observed in a fluid flowing under plug flow conditions. This is due to the flow inside the mixer being governed by its geometry, leading to the fluid exiting the mixer in multiple locations across the pipe cross-section. The technique was limited by the requirement for the transparency of the original fluid.

7.2.2 PIV

Using transparent 3D printed SMX mixer elements and fluorescent tracer particles it was demonstrated that the PIV technique can be applied to obtain 2D velocity maps comparable to the 3D velocity fields derived from PEPT data. While the technique is limited by the planar nature of the laser illumination, it provides a much more efficient approach to velocity field acquisition, compared to PEPT data collection and analysis.

7.2.3 PRESSURE DROP

Analysis of pressure drop across various SMX mixer configurations, including different number of elements and diameters revealed that for industrially relevant fluids

which follow the Carreau-Yasuda model the pressure drop can be predicted based on the apparent viscosity of the fluid. The apparent viscosity is defined by the apparent shear rate for the system, based on the Streiff-Jaffer correlation. The predicted pressure drop closely correlates with the experimentally observed pressure drop within the standard equipment operating range. This allows to accurately predict the pressure drop within the mixer when designing a manufacturing processes, which in turn allows to size ancillary equipment, such as pumps. The fluid behaviour is closely correlated to with the rheological models obtained using oscillatory, as opposed to rotational, rheological measurements, suggesting that no shear banding takes place inside SMX mixers at standard process conditions.

7.3 FUTURE RECOMMENDATIONS

7.3.1 PEPT

Positron Emission Particle Tracking can be applied once more to further develop the understanding of the dynamics within static mixers. The following work would be of interest

- To develop a better understanding of the effects of the SMX mixer geometry on the mixer performance, PEPT work on a range of mixer diameters would be a valuable addition to the understanding of SMX mixer dynamics.
- A modification of the SMX mixer design has been developed by Sulzer, SMX+, which claims reduced pressure drop without compromising mixing quality. PEPT can be used to compare the performance of the two mixer models.
- All work presented in this thesis was carried out under laminar flow conditions, with no evidence to suggest any change in performance with variation of the flowrate. Further work in the transitional and turbulent regimes can provide information on the

optimal operating regime, and whether higher Re numbers inside the mixer should be avoided or encouraged.

- Other models of static mixers are used in industry, such as plate static mixers. Building on the experience of the current research, investigation into the dynamics of such equipment can be carried out, as well as dynamics of other systems which involve in-line equipment.

7.3.2 OPTICAL TECHNIQUES

The main challenges of the work carried out using optical techniques in this work was the matte surface finish of the transparent 3D printed models, as well as visible interfaces where the layers of resin were fused, causing light scattering and refractive index inconsistencies. With the development of 3D printing technology and materials used it is becoming easier to print elements which have a smooth finish and do not have visible layer fusion points, making parts which are better suited for optical techniques. Therefore, the following work can now be carried out

- PIV allows for a higher resolution velocity field acquisition and can be used to investigate any local effects which could be responsible for the reduction in mixer efficiency with increased flowrate for non-Newtonian fluids.
- 3D PIV technology builds on traditional PIV, however, through application of multiple lasers and cameras it is possible to capture the fluid dynamics inside the entire equipment volume, instead of a single plane. 3D PIV technology can be applied to study velocity fields inside a range of equipment manufactured using improved 3D printing technology.
- PLIF, or planar laser-induced fluorescence, allows tracking the mixing and changeover dynamics across a laser illuminated plane between fluids containing

different levels of fluorescent dye. In a fashion similar to PIV, PLIF can be utilised for mixing and changeover dynamics studies for a wide range of equipment.

7.3.3 PRESSURE DROP

- Further work on the pressure drop across different mixer elements can be expanded upon by using fluids which follow other rheological models, e.g. Power law fluids and Hershel-Bulkley fluids, which are also often found in industry.
- In addition, work on other mixer geometries, such as SMX+ can be conducted, which in conjunction with some of the other methods described above would provide sufficient information to pick the in-line mixers best suited for specific product manufacture.

APPENDIX: PIV FOR 3D PRINTED MIXER ELEMENTS

A.1 INTRODUCTION

This short investigation was carried out as a proof of principle for using transparent 3D printed geometries, in this case SMX mixers, for applications in optical studies, such as Particle Image Velocimetry.

Traditionally, if a complex transparent structure is required for optical work it is constructed of either glass or Perspex by workshops, as bespoke kit, which can be both time consuming and expensive. Furthermore, such pieces can deviate from the original design or if several are manufactured, inconsistencies can arise due to the manual or semi-automated nature of the piece manufacturing. 3D printing offers a much more time and cost effective alternative, with a higher level of fidelity to the original CAD models and consistency between multiple pieces based on the same model.

However, transparent materials are not yet widely available in 3D printing applications, with some materials which claim to be transparent still retaining a certain level of opacity. This work aims to assess the quality of the data collected when using a transparent SMX mixer printed using one of these materials.

A.2 MATERIALS AND METHODS

The experimental set up shown in Figure 5.2 was used for PIV, where the Nd:YAG double pulse laser emitting source was introduced outside the field of view of the 1000×1016 pixel^2 frame-straddling charge coupled device (CCD) camera (TSI PIVCAM 10-30, TSI Inc.) and perpendicular to it, Figure A.1a shows the orientation of the mixer in the camera field of view. The laser sheet was adjusted to illuminate the mixer structure at cross-sections which correspond to radial flowrates in different directions, where Figure A.1b identifies the positions where the laser sheet was focused. This allowed the laser

sheet to illuminate a thin layer of the fluid in the mixer which was consequently captured by the camera.

Figure A.1. a. camera field of view, illuminated by the laser (green), b. laser sheet focus on the different channels within the SMX geometry.

Glycerol and CMC were used for this work, as the technique requires the fluid to be transparent, hence Guar gum solution was not applicable due to its opacity. The recirculating fluid was seeded with 10 µm silver coated hollow glass spheres (Dantec Dynamics, Denmark), which scatter the light when illuminated as they enter the sheet of light generated by the laser source, enabling the PIV technique. The high speed camera is set up to capture an image pair in rapid succession, with a time delay of 10 milliseconds. The time delay is inferred from the expected average velocity of the tracers, based on flowrate (~0.12 m/s) and the size of the interrogation window, based on the size of the section of interest in the field of view (1" SMX mixer element) and the grid size. The field of view area was broken down into a grid, where each square on the grid is 32×32 pixels in size, which a typical grid size used in PIV (Grue et al., 2004), with a total of 40 grid elements along both the x and the y axis of the field of view. This means that the physical size of a grid element is approximately 0.6×0.6 mm. The size of the grid used is similar to that applied when analysing PEPT data, allowing for easy comparison between the results of the two techniques.

Here an average tracer is expected to travel the distance equal to half of the grid size between images in a pair, ensuring that a large portion of the tracers remain within the

frame between images for correlation, and at the same time, the slower moving tracers travel a detectable distance (Grant, 1997; Lehwald et al., 2008). Based on the size of the grid and the average velocity as well as the average particle displacement between images in a pair, the required time delay can be calculated, as shown in the equation below. Here U is the average velocity (m/s), d_{int} is characteristic dimension of a grid element (m) and M is the magnification of the image, which for the current work was kept at 1.

$$\Delta t = \frac{d_{int} \times U}{4M} \quad \text{A.1}$$

After processing an image pair each grid element yields a velocity vector based on the average particle displacement, as shown in Figure A.2**Error! Reference source not found.**. Hundreds of such image pairs are captured during the experiment. Processing the data from multiple image pairs allows reducing the random error and invalid tracer pairings to provide an estimation of the local velocity fields across camera field of view.

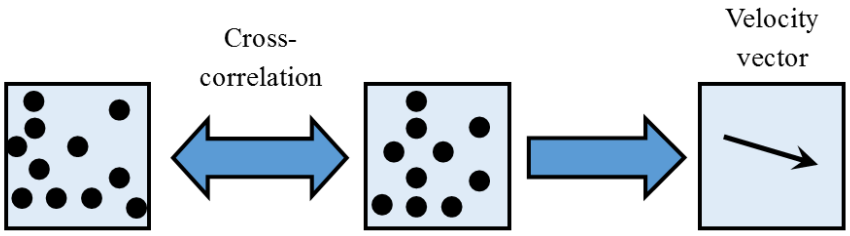

Figure A.2. PIV particle location interrogation in a single grid element and velocity vector calculation schematic (Adrian and Westerweel, 2011)

The advantage of using transparent 3D printed mixer elements for the PIV work was the ability to capture image pairs within the mixers as well as outside in the empty pipe region, which has never been attempted previously.

A.3 FLUID VELOCITY ESTIMATION USING PIV

Transparent 3D printed SMX elements were used to assess the velocity profile within the SMX mixer using PIV. The approach was tested on glycerol, which is a fully transparent fluid, allowing unobstructed passage of the laser pulse required for a good performance of the technique.

Figure A.3 illustrates an example of the velocity field across the 2D x-z plane as recorded using the PIV technique at 200L/h and 300 L/h flowrate and the same velocity field reconstructed from PEPT data, as described in Chapter 4. It can be clearly seen that at both flowrates the velocity field magnitudes and overall appearance agrees between the two techniques. However, it can also be noted that the results from the PIV study display concentrated areas of high velocity, which are less pronounced in the PEPT data. The maximum velocities recorded using PIV are also noticeably higher than those reconstructed from the PEPT tracer data. Several factors could be contributing to such inconsistencies, with the majority arising from the mixer construction material. While visibly transparent to the naked eye, when immersed in glycerol, certain artefacts can arise when transitioning between the edge of the mixer and the empty space occupied only by the fluid, such as shape deformation. When captured by the high speed camera, such deformations can lead to a perception of a tracer particle moving faster than it is in reality, leading to localised apparent high velocity pockets. This is further illustrated by the fact that in the spaces which were fully transparent, i.e. lacked any mixer presence, the velocity fields obtained using the two techniques can be shown to belong to the population with the same means using Students t-test ($P > 0.05$).

In addition, as several slices across a mixer element were captured using PIV at different y-dimension planes, it was noted that while the mixer elements were transparent,

the quality of the images captured degraded when a plane was further removed from the camera, with more mixer structure in the way. This is due to the fact that the refractive index of the plastic used for element construction is not consistent, as the 3D printing process involves the fusion of very thin layers of the construction material, meaning that the internal structure is not as uniform as, for example, if the mixer elements were cast from a resin using a mould. Due to these imperfections the light is scattered unpredictably whenever passing through an element wall, an effect which only gets more pronounced with increased wall thickness, i.e. when considering planes further removed from the camera. However, with the ever improving 3D printing technology it can be expected that in the near future this obstacle will be overcome, using continuous UV cured 3D printers, for example, which do not suffer from the same manufacturing flaws (Orange Maker LLC, 2016).

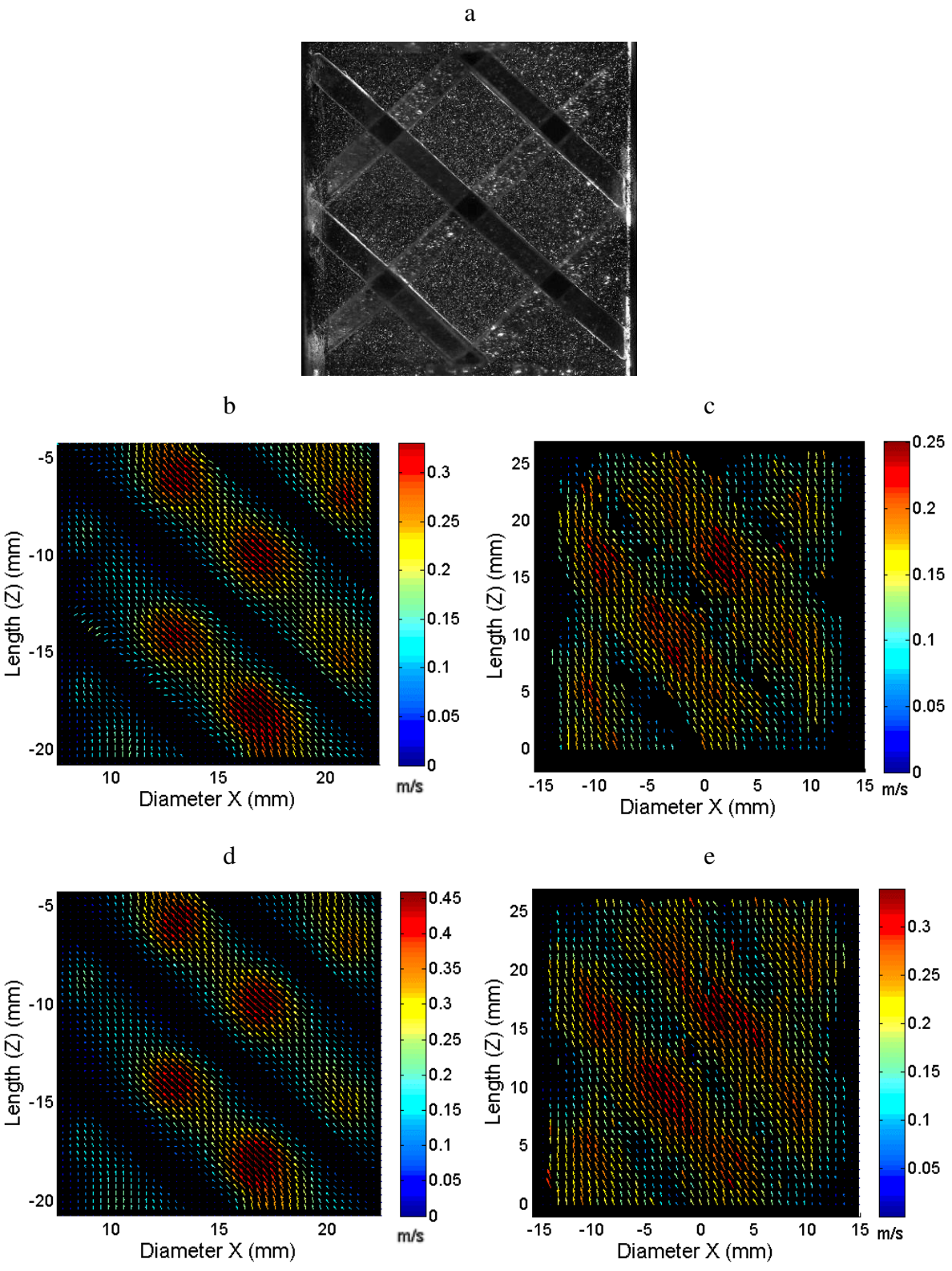

Figure A.3. a. SMX element orientation as seen by the PIV high speed camera. Side by side comparison between the velocity fields obtained using PIV (b,d) and PEPT (c,e) for glycerol flowing at 200 L/h (b,c) and 300 L/h (d,e) inside an SMX mixer element.

A.4 REFERENCES

Adrian, R.J., Westerweel, J. (2011) Particle Image Velocimetry, Cambridge University Press.

Grant, I. (1997) 'Particle image velocimetry: a review', Proceedings of the Institution of Mechanical Engineers, Part C: Journal of Mechanical Engineering Science, 211(1), 55–76.

Grue, J., Liu, P.L.-F., Pedersen, G.K. (2004) PIV and Water Waves, World Scientific Publishing: Sinagapore.

Lehwald, A., Leschka, S., Zähringer, K., Thévenin, D. (2008) 'Fluid dynamics and mixing behavior of a static mixer using simultaneously Particle Image Velocimetry and Planar Laser-Induced Fluorescence measurements Experimental set-up and measurement methods', in 14th Int Symp on Applications of Laser Techniques to Fluid Mechanics, 7–10.

Orange Maker LLC (2016) '3D printing using spiral buildup'. http://www.orangemaker.com/